



UNIONE EUROPEA
Fondo Sociale Europeo



UNIVERSITY OF MESSINA
DEPARTMENT OF CHEMICAL, BIOLOGICAL, PHARMACEUTICAL AND
ENVIRONMENTAL SCIENCES
PHD IN CHEMICAL SCIENCES
XXXVI CYCLE
S.S.D. CHIM/03

DESIGN AND DEVELOPMENT OF
SMART ADVANCED MATERIALS AND SUSTAINABLE
TECHNOLOGIES FOR WATER TREATMENT

PH.D. THESIS OF:
GIULIA RANDO

TUTOR:
DR. MARIA ROSARIA PLUTINO

CO-TUTOR:
PROF. KAREN DE CLERCK
DR. GIUSEPPE TOCCAGNI
PROF. ANNA NOTTI

HEAD OF THE PH.D. COURSE:
PROF. CONCETTA DE STEFANO

2020-2023



UNIONE EUROPEA
Fondo Sociale Europeo



**design and development of
smARt advancEd materials and Sustainable Technologies
for wAteR Treatment**

RESTART

PON-MIUR 2014-2020

TABLE OF CONTENTS

SPECIAL THANKS

PREFACE

ABSTRACT

PUBLICATIONS LIST

1. ADVANCED SMART MATERIALS AND SUSTAINABLE TECHNOLOGIES FOR INNOVATIVE WATER TREATMENT CHALLENGE: AN OVERVIEW	1
1.1 Water contamination and common treatment approaches	2
1.2 Functional nanohybrids and nanocomposites for environmental remediation	5
1.2.1 Metal nanoparticle-based composites and hybrids	7
1.2.2 Metal oxide nanoparticle-based materials	10
1.2.3 Carbon-based nanomaterials	13
1.2.4 Sol-gel based nanostructured materials	16
1.3 Membrane-based filtration techniques: limits and future perspectives	21
1.4 The aim of this PhD thesis	25
1.4.1 Limits and research gaps of water filtration technologies	25
1.4.2 Innovative approaches, methods and solutions explored in this thesis	26
2. BIOPOLYMER BASED ELECTROSPUN NANOFIBER MEMBRANES DOPED WITH FUNCTIONAL HALLOYSITE DERIVATIVES	36
2.1 Advanced and sustainable water filtration membranes	37
2.1.1 Natural-derived polymers for the development of sustainable membranes	37
2.1.2 Hybrid/mixed-matrix water filtration membranes	38
2.1.3 Functional bio-based coatings for filtration membranes	41
2.1.4 Electrospun nanofiber-based membranes	43
2.2 Sustainable bio-based PA11 electrospun nanofiber membranes doped with hybrid HNT derivatives for the removal of organic dyes from water	48
2.2.1 Abstract	48
2.2.2 Results and discussion	49
2.2.3 Conclusions	64
2.3 PA11 and chitosan blends doped with functional halloysite derivatives for the preparation of electrospun nanofiber composite membranes	65
2.2.1 Abstract	65
2.2.2 Results and discussion	66
2.2.3 Conclusions	78
3. FUNCTIONAL CELLULOSIC WATER-BASED BLEND MATERIALS FOR ELECTROSPUN NANOFIBER MEMBRANES AND HYBRID MAGNETIC COMPOSITES PREPARATION	85
3.1 Secondary raw and natural-derived cellulose-based materials in environmental remediation	86
3.1.1 Plant-based cellulose derivatives in advanced materials development	86
3.1.2 Functionalization of cellulose derivatives for environmental remediation	87

3.2	Microcrystalline cellulose and biochar from Spanish broom for eco-friendly PVA-based electrospun nanofiber composite membranes	91
3.2.1	Abstract	91
3.2.2	Results and discussion	92
3.2.3	Conclusions.....	112
4.	SMART POLYMERIC BLENDS AND BEADS AS INNOVATIVE ADSORBENT SYSTEMS..	118
4.1	Smart polymers and systems for water purification.....	119
4.1.1	Polyether sulfone based blends.....	119
4.1.2	PDMAEMA stimuli-responsive polymer	119
4.1.3	Pillar[n]arene-based adsorbent materials	121
4.2	Smart pillararene-based PES/PDMAEMA blends and beads for selective water contaminant adsorption	123
4.2.1	Abstract	123
4.2.2	Results and discussion	125
4.2.3	Conclusions.....	141
5.	CONCLUSIONS AND FINAL REMARKS	148
6.	MATERIALS AND METHODS	154
6.1	Chapter 2: Experimental section ¹	154
6.1.1	Materials.....	154
6.1.2	Synthetic procedures	154
6.1.3	Chemical-physical measurement and characterization.....	156
6.1.4	Filtration studies	157
6.2	Chapter 2: Experimental section ²	158
6.2.1	Materials.....	158
6.2.2	Synthetic procedures	158
6.2.3	Chemical-physical measurement and characterization.....	158
6.3	Chapter 3: Experimental section	159
6.3.1	Materials.....	159
6.3.2	Synthetic procedures	159
6.3.3	Chemical-physical measurement and characterization.....	163
6.3.4	Filtration studies	164
6.3.5	Adsorption isotherm calculations.....	165
6.4	Chapter 4: Experimental section	166
6.4.1	Materials.....	166
6.4.2	Synthetic procedures	166
6.4.3	Beads preparation.....	167
6.4.4	Chemical-physical measurement and characterization.....	167
6.4.5	Adsorption kinetic studies and isotherm calculations.....	168

GLOSSARY

Special thanks

First of all, I would like to express my gratitude to my supervisor Dr. Maria Rosaria Plutino of ISMN-CNR (Palermo, URT of Messina, Italy), tutor of this PhD project but above all mentor who accompanied, supported and inspired me during the last years. I would like to thank her for allowing me to be part of FunHyMat4Eco (Development of FUNctional Hybrid and bio-Inorganic MATerials FOR sustainable and low Environmental impact applicatiOns) research group and for having involved me in all the related initiatives and opportunities. I would particularly acknowledge her for having placed her trust in me, by following me in my growth and giving me the opportunity to learn and work with her in a stimulating and serene environment surrounded by fascinating, innovative materials and approaches for a greener and smarter future.

I would acknowledge my co-tutor Prof. Karen De Clerck and also Dr. Jozefien Geltemeyer and all the people that I met at the “Department of Materials, Textiles and Chemical Engineering, Faculty of Engineering and Architecture - Centre for Textile Science and Engineering” of the Ghent University (Belgium), for their hospitality, precious support and advice on the research activity carried out in my stay there during which I had the opportunity to interface with new amazing techniques and approaches such as electrospinning.

I also thank my co-tutor Dr. Giuseppe Toccagni of EuroD company (Scanzorosciate, BG, Italy) as well as Dr. Roberta Salvetti and Dr. Matteo Comi for their technical and practical advice facing with the real challenges of wastewater treatment plants which have been very important for the development of the research activity.

Sincere thanks also go to my co-tutor Prof. Anna Notti of the “Department of Chemical, Biological, Pharmaceutical and Environmental Sciences” of the University of Messina (Italy), for having hosted me in her laboratory for carrying out part of the research activity, but also for her precious advice and suggestions, allowing me to explore some of the possibilities of the world of supramolecular chemistry.

Special thanks go to Dr. Dario Drommi of the “Department of Chemical, Biological, Pharmaceutical and Environmental Sciences” of the University of Messina (Italy), who hosted and supported me in his laboratory with his helpful advice and suggestions.

I would like to express my gratitude to Dr. Maurilio Galletta and Dr. Giuseppe Sabatino of the University of Messina (Italy), for their technical assistance and support in carrying out some experimental procedures.

I cannot fail to thank all my colleagues who I prefer to define as fellow adventurers who have been close to me during this fantastic journey and continue to support me, wishing for them only the best for the future. Especially my grateful thanks go to Dr. Silvia Sfameni, smart, joyful and special adventure companion who supports me at 360 degrees and helped me in carrying out the research activities.

Alessio Mezzi and Marco Brucale of ISMN-CNR are acknowledged for performing the SEM and XPS analyses described in Chapter 4, respectively as well as their helpful comment.

Finally, PON-MIUR “Ricerca e Innovazione 2014-2020” funded “Design and Development of SmaRt AdvancEd MaterialS and SusTainable Technologies for WAtEr Treatment – RESTART” industrial PhD project is gratefully acknowledged for the financial support.

Preface

The present manuscript is structured in six chapters. The first chapter describes the state of the art of the topics giving the essential basis for a better and more complete understanding of the subsequent main sections. In the next 3 chapters (i.e., from chapter 2 to chapter 4), the overall main results obtained during this three years research activity will be presented. In the fifth chapter, the conclusions and remarks of the overall PhD thesis work will be presented, outlining the final analysis of the experimental results, and the possible future perspectives, as starting point for applications in basic and industrial research fields. Finally, in the sixth and final chapter, the materials used in this work, together with the adopted synthetic methods and characterizations techniques, will be described.

For all the presented material, submitted for the assessment on the course of PhD in Chemical Sciences (XXXVI cycle), to the best of my knowledge, I have taken reasonable care to ensure that the work is original, does not violate any copyright laws, and it has not been derived from the work of others to the extent that such work has been cited and acknowledged within the text.

The research activity reported within this whole PhD thesis was carried out within the Industrial PhD project “Design and Development of SmaRt AdvancEd MaterialS and SusTainable Technologies for WAtER Treatment – RESTART”, as funded by the PON-MIUR “Ricerca e Innovazione 2014-2020” that is gratefully acknowledged.

These studies have been carried out at the ISMN-CNR FunHyMat4Eco lab, c/o the Dep. ChiBioFarAm, Univ. of Messina, at the “Centre for Textile Science and Engineering” of the “Department of Materials, Textiles and Chemical Engineering, Faculty of Engineering and Architecture” of Ghent University (Belgium), at EuroD Company, Scanzorosciate (BG, Italy), and at the Dep. ChiBioFarAm, Univ. of Messina.

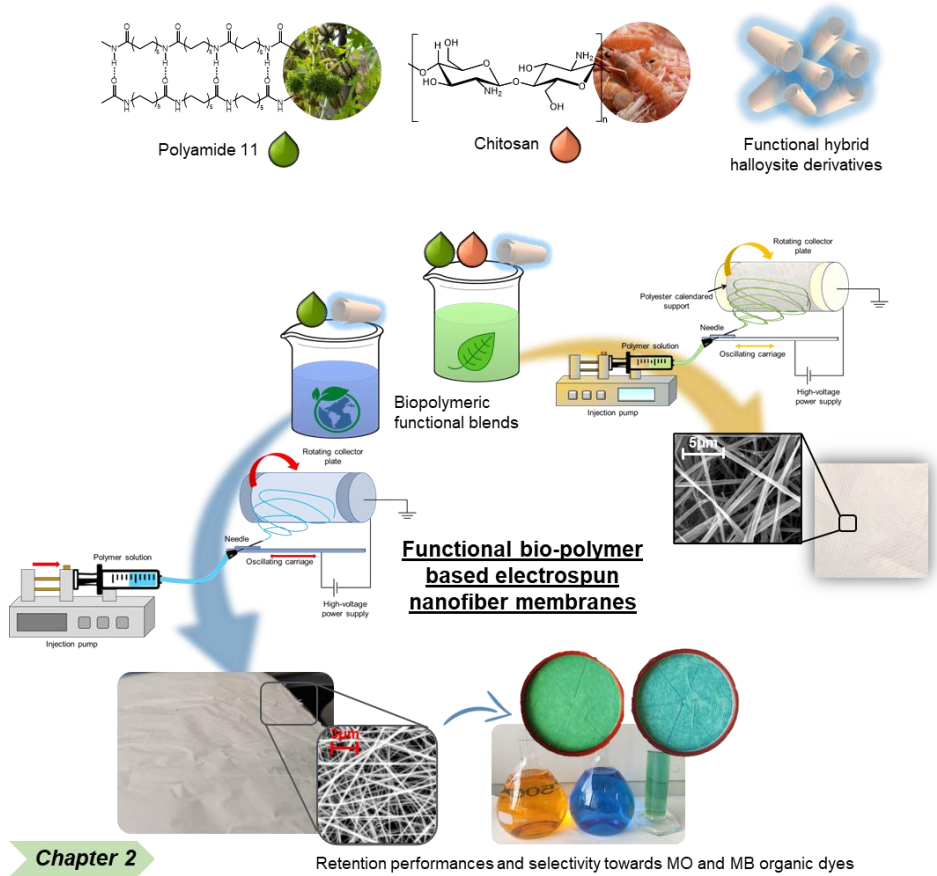
Abstract

Within the actual “One Health” perspective, the health and well-being of humans and other living species, together with the Earth ecosystems protection, are inextricably linked to clean water sources preservation. Unfortunately, because of anthropogenic activities, urbanization, expanding global population and climate changes, sources of safe and potable water are becoming less safe and more and more limited. In this scenario, significant attention has to be paid to more efficient and sustainable treatment/recycling/recovery of water (wastewater and underground water) for its reclamation and (re)use, in order to manage a global water shortage and the development of “water-smart” cities. Unfortunately, today conventional methods of wastewater treatment still lack in the removal of the so-called “emerging contaminants”, such as pharmaceuticals, cosmetics, pesticides, personal and home care products, organic dyes, etc.; actually, there is not a real and defined European legislation fixing their acceptable and allowed concentration limits in the environment. One of the most challenging tasks of the 21st century is therefore to develop new eco-friendly, sustainable, and economically-sound technologies to remediate the water from the presence of contaminants.

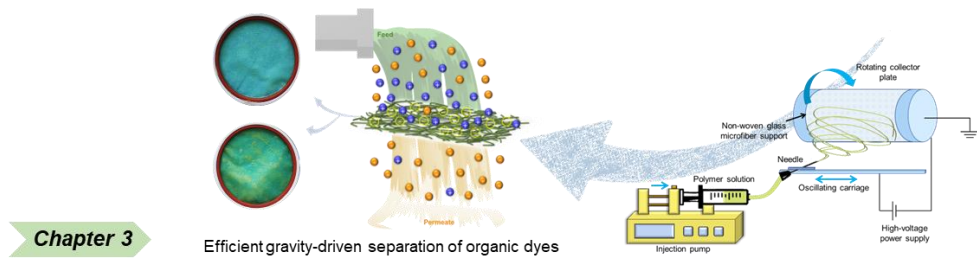
In this regard, as discussed in the First Chapter, nanotechnologies and new advanced nanostructured materials represent the potential for the development of green and smart products/techniques for a wide series of sustainable applications, as well as environmental remediation and waste/underground water treatment.

The research activity of this PhD thesis aims to explore the design and synthesis of smart, nano/micro-structured hybrid materials opportunely functionalized and blended with suitable (bio)polymers with the aim to develop by means of different synthetic and deposition techniques, new sustainable solutions and technologies useful in the landscape of the water remediation from emerging contaminants. The main goal of these studies, as described in the three Chapters 2–4, is to investigate and evaluate the effect of different hybrid, polymeric and organic additives to implement and tune the properties of the final systems, obtained as powders, beads and membranes. In particular, this thesis explores the proper design and synthesis of the functional additives, the final adsorbent/filtering material preparation, the chemical-physical-mechanical-morphological characterization techniques and, in particular, their application and test, as systems for the treatment of contaminated water.

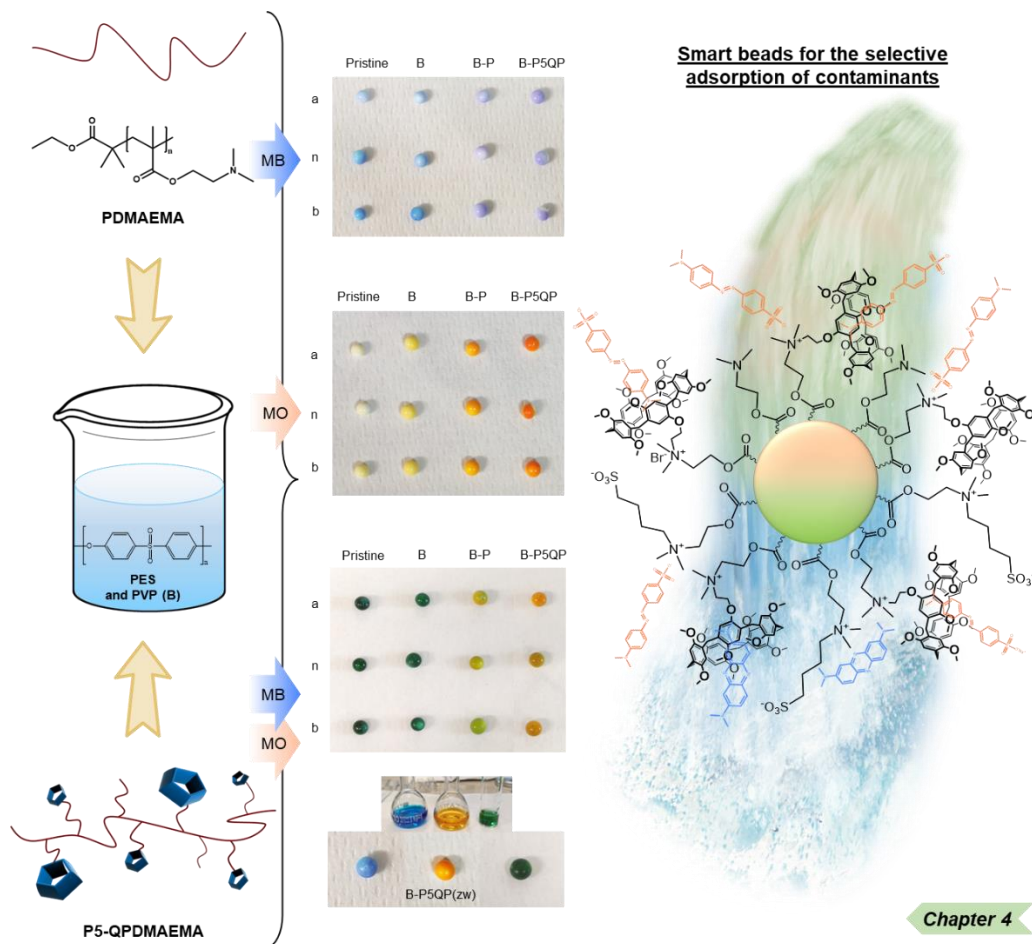
In particular, the Second Chapter concerns the design and development of sustainable biopolymeric blends based on polyamide 11 and chitosan biopolymers and doped with functional hybrid halloysite derivatives, employed to produce different electrospun nanofiber membranes and composite membranes through electrospinning technique. Their retention performances towards two model organic dyes are investigated through a dead-end filtration cell.



The Third Chapter focuses on the use of secondary-raw bio-based materials and natural waterborne sources for the development of innovative cellulose-derived opportunely functionalized products, which are employed as dopant agents for water-based polyvinyl alcohol solutions and to obtain different electrospun nanofiber composite membranes. The developed bio-based and eco-friendly membranes are tested in a dead-end filtration cell for the gravity-driven removal of two model organic dyes.



The Fourth Chapter refers to the design and development of new polyether sulfone smart blends by its combination with new innovative smart polymers combining the responsiveness of poly[2-(dimethylamino)ethyl methacrylate] polymer and the host-guest properties of the covalently linked pillararene macrocycles. The systems in the form of functional beads are tested towards the selective adsorption of two model organic dyes, i.e. MO and MB, whose kinetics and performances were studied.



The described results (see Chapter 5) emphasize how important it is to develop materials with implemented mechanical, thermal, and different pollutant retention properties, through the rational design of the starting polymeric blends with appropriate nano, micro-fillers, or functional doping agents.

The bio-based or water-based formulations, obtained within this PhD thesis, could open the way to the employment of innovative and sustainable nanotechnological approaches for the development of proof-of-concept, PoC, filtration membranes to be employed for real-case treatment and commitment of industrial, municipal, agriculture and other wastewaters, as well as contaminated groundwater reserves, thus rationally and more efficiently substituting the traditional fossil-based filtration technologies.

Finally, thanks to the presence of the Industrial Supervisor EuroD, and the interest of stakeholder and startup¹ belonging to the Environmental Technology sector, these advanced products and technologies could be scale-up into large-scale industrial applications framework.

¹ATHENA Green Solutions S.r.l., startup and spin-off of the CNR (ISMN, IRBIM) and University of Messina (see more details at the link www.athenagreenolutions.com).

INTERNATIONAL PEER-REVIEW PUBLICATIONS

1. G. Rando, J. Geltmeyer, S. Sfameni, K. De Clerck, M. R. Plutino
Advanced PVA-based electrospun nanofiber composite membranes: from functionalization of Spanish broom-derived microcrystalline cellulose and biochar to smart and sustainable water filtration.
Sustainable Materials and Technologies **2023**, in preparation.
2. G. Rando, J. Geltmeyer, S. Sfameni, K. De Clerck, M. R. Plutino
Sustainable bio-based polyamide 11 electrospun nanofiber membranes doped with functional hybrid halloysite derivatives for the removal of organic dyes from (waste)water.
ACS Sustainable Chemistry & Engineering **2023**, in preparation.
3. G. Rando, J. Geltmeyer, S. Sfameni, K. De Clerck, M. R. Plutino
Design, development and characterization of eco-friendly electrospun nanofiber composite membranes based on biopolymeric polyamide 11 and chitosan blends doped with functional hybrid halloysite derivatives.
Polymers **2023**, in preparation.
4. G. Rando, S. Sfameni, M. Milone, A. Mezzi, M. Brucale, A. Notti, M. R. Plutino
Smart pillar[5]arene-based PDMAEMA/PES beads for selective dye pollutants removal: design, synthesis, chemical-physical characterization, and adsorption kinetic studies.
ChemSusChem **2023**, Accepted.
5. S. Sfameni, M. Hadhri, G. Rando, A. Mezzi, M. Brucale, G. De Luca, E. Piperopolus, C. Milone, D. Drommi, V. Trovato, G. Rosace, M. R. Plutino
Sol-Gel Assisted Immobilization of Methyl Red-functionalized Halloysite nanotubes on polyester fabrics for the development of durable dyeing coatings.
Journal of Colloid and Interface Science **2023**, in preparation.
6. V. Trovato, S. Sfameni, R. Ben Debabis, G. Rando, G. Rosace, G. Malucelli, M.R. Plutino
How to Address Flame-Retardant Technology on Cotton Fabrics by Using Functional Inorganic Sol-Gel Precursors and Nanofillers: Flammability Insights, Research Advances, and Sustainability Challenges.
Inorganics **2023**, 11(7), 306; <https://doi.org/10.3390/inorganics11070306>
7. S. Sfameni, G. Rando, M.R. Plutino
Sustainable Secondary-Raw Materials, Natural Substances and Eco-Friendly Nanomaterial-Based Approaches for Improved Surface Performances: An Overview of What They Are and How They Work.
Int. J. Mol. Sci. **2023**, 24(6), 5472; <https://doi.org/10.3390/ijms24065472> (First co-author).
8. G. Rando, S. Sfameni, M. R. Plutino
Development of Functional Hybrid Polymers and Gel Materials for Sustainable Membrane-Based Water Treatment Technology: How to Combine Greener and Cleaner Approaches.
Gels **2023**, 9, 1, 9; <https://doi.org/10.3390/gels9010009>
9. S. Sfameni, M. Hadhri, G. Rando, D. Drommi, G. Rosace, V. Trovato, M. R. Plutino
Inorganic Finishing for Textile Fabrics: Recent Advances in Wear-Resistant, UV Protection and Antimicrobial Treatments.

- Inorganics* **2023**, *11*, 1, 19; <https://doi.org/10.3390/inorganics11010019> (First co-author).
10. S. Sfameni, T. Lawnick, G. Rando, A. Visco, T. Textor, M. R. Plutino
Super-Hydrophobicity of Polyester Fabrics Driven by Functional Sustainable Fluorine-Free Silane-Based Coatings.
Gels **2023**, *9*, 2, 109; <https://doi.org/10.3390/gels9020109>
 11. Sfameni, A. Del Tedesco, G. Rando, F. Truant, A. Visco, M. R. Plutino
Waterborne Eco-Sustainable Sol–Gel Coatings Based on Phytic Acid Intercalated Graphene Oxide for Corrosion Protection of Metallic Surfaces.
International Journal of Molecular Sciences **2022**, *23*, 19, 12021; <https://doi.org/10.3390/ijms231912021>
 12. S. Sfameni, T. Lawnick, G. Rando, A. Visco, T. Textor, M. R. Plutino
Functional Silane-Based Nanohybrid Materials for the Development of Hydrophobic and Water-Based Stain Resistant Cotton Fabrics Coatings.
Nanomaterials **2022**, *12*, 19, 3404; <https://doi.org/10.3390/nano12193404>
 13. V. Trovato, S. Sfameni, G. Rando, G. Rosace, S. Libertino, A. Ferri, M.R. Plutino
A review on stimuli-responsive smart materials for wearable health technology: retrospective, perspective and prospective.
Molecules **2022**, *27*, 17, 5709; <https://doi.org/10.3390/molecules27175709> (First co-author).
 14. S. Sfameni, G. Rando, M. Galletta, I. Ielo, M. Brucale, F. De Leo, P. Cardiano, S. Cappello, A. Visco, V. Trovato, C. Urzì, M.R. Plutino
Design and Development of Fluorinated and Biocide-Free Sol–Gel Based Hybrid Functional Coatings for Anti-Biofouling/Foul-Release Activity.
Gels **2022**, *8*, 538; <https://doi.org/10.3390/gels8090538>
 15. S. Sfameni, G. Rando, A. Marchetta, C. Scolaro, S. Cappello, C. Urzì, A. Visco, M.R. Plutino
Development of Eco-Friendly Hydrophobic and Fouling-Release Coatings for Blue-Growth Environmental Applications: Synthesis, Mechanical Characterization and Biological Activity.
Gels **2022**, *8*, 528; <https://doi.org/10.3390/gels8090528>
 16. G. Rando, S. Sfameni, M. Galletta, D. Drommi, S. Cappello, M.R. Plutino
Functional Nanohybrids and Nanocomposites Development for the Removal of Environmental Pollutants and Bioremediation.
Molecules **2022**, *27*, 4856; <https://doi.org/10.3390/molecules27154856>
 17. I. Ielo, F. Giacobello, A. Castellano, S. Sfameni, G. Rando and M. Rosaria Plutino
Development of Antibacterial and Antifouling Innovative and Eco-Sustainable Sol–Gel Based Materials: From Marine Areas Protection to Healthcare Applications.
Gels **2022**, *8*, 26; doi: <https://doi.org/10.3390/gels8010026>
 18. I. Ielo, G. Rando, F. Giacobello, S. Sfameni, A. Castellano, M. Galletta, D. Drommi, G. Rosace and M. R. Plutino
Synthesis, Chemical–Physical Characterization, and Biomedical Applications of Functional Gold Nanoparticles: A Review.
Molecules **2021**, *26*, 5823; doi: [10.3390/molecules26195823](https://doi.org/10.3390/molecules26195823) (First co-author).
 19. I. Ielo, F. Giacobello, S. Sfameni, G. Rando, M. Galletta, V. Trovato, G. Rosace and M. R. Plutino

Nanostructured Surface Finishing and Coatings: Functional Properties and Applications.
Materials **2021**, *14* (11), 2733; doi: 10.3390/ma14112733

BOOK CHAPTER

1. S. Sfameni, G. Rando*, M.R. Plutino*
Perspective Chapter: Functional Sol–Gel Based Coatings for Innovative and Sustainable Applications.
IntechOpen **2023**; DOI: 10.5772/ intechopen.110514

SCOPUS-INDEXED CONFERENCE PROCEEDINGS

1. I. Ielo, M. Galletta, G. Rando, S. Sfameni, P. Cardiano, G. Sabatino, D. Drommi, G. Rosace and M. R. Plutino
Design, synthesis and characterization of hybrid coatings suitable for geopolymeric-based supports for the restoration of cultural heritage.
IOP Conf. Series: Materials Science and Engineering **2020**, 777, 012003; doi: 10.1088/1757-899X/ 777/1/012003

PATENT

1. M.R. Plutino, S. Cappello, G. Sabatino, G. Rando
Multi-functional hybrid material based on natural clays for environmental recovery and bio-remediation.
International patent publication number: WO2021124103 (A1) of 2021-06-24; also published with number: IT201900024802 (A1); EP4076729 (A1); US20230034883 (A1).
Sources: <https://patentscope.wipo.int/search/en/search.jsf>
Publication date: EN **2021** (Source of the Document Patent Cooperation Treaty Application), **2022** (European Patent Application), **2023** (United States Patent and Trademark Office Pre-Granted Publication).

CHAPTER 1

ADVANCED SMART MATERIALS AND SUSTAINABLE TECHNOLOGIES FOR INNOVATIVE WATER TREATMENT CHALLENGE: AN OVERVIEW

In this first Chapter, an overview on nanotechnologies and new advanced nanostructured materials for the development of green and smart products/technologies for a wide series of sustainable applications, as well as environmental remediation and waste/groundwater treatment, is given. After highlighting the importance of water as a fundamental asset for life and ecosystems and the types of contaminating, the traditional methods of wastewater purification are also explained, together with their main criticisms. In this regard, the peculiar and innovative properties of new classes of nanomaterials are emphasized, including those based on metal nanoparticles, nanoparticles of metal oxides, carbon derivatives, and silica sol-gel, as well as their applications in the field of environmental remediation and protection. Various examples on the use of such nanomaterials as functional doping agents of opportune polymeric blends are reported, and therefore the preparation of sustainable advanced nanohybrid or nanocomposite materials for the removal of emerging contaminants from water. The advantages of water filtration technology using polymeric membranes and their functionalization possibilities for optimizing filtration ability and properties are also shown.

1.1 Water contamination and common treatment approaches

Three-quarters of the earth surface is covered by water, one of the most abundant resources on our planet. However, only 3% of water volume is fresh water that is good for people, plants, and animals, making up the remaining 97% to the sea and ocean waters. Moreover, nearly 2.5% of fresh water is locked up in glaciers, atmosphere, and polar ice caps, leaving only 0.5–1% available to living organisms from rivers and groundwater [1–3].

This valuable resource is essential to human and ecological health and well-being, as well as social and economic development [4–6]. Water is used by humans for drinking, industrial purposes, agricultural irrigation, hydropower, waste disposal, and recreation. Water supplies, which are reduced in many locations due to population increase, pollution, and industrialization, must be protected for both human and environment health reasons. Recent continuous climate variability changes and factors that alter the hydrologic cycle have exacerbated these challenges.

Nowadays under the One Health perspectives and with the aim to move more and more towards a global sustainable lifestyle, in order to conserve and safeguard the environment, the need of preserving, reusing, and recycling products at the end of their lives, hence minimizing the waste of primary resources [7–9], as water itself, is increasingly necessary.

In order to handle a global water crisis, a great deal of emphasis has been given to the creation of “water-smart” communities, leading innovative treatment, recycling, and recovery processes of ground and wastewater [10–13].

Due to manmade activities a lot of physical, chemical, or biological elements, generally referred to as a “water pollutant”, are found in groundwater, oceans, as well as employed drinking water with potential negative effects on individuals who consume it, as well as aquatic and land species. However, the majority of water pollutants are found as dissolved or suspended compounds [14]. In particular, through the water cycle, all water travels around the Earth in various phases, as liquid water in the oceans, rivers, lakes, and even underground, as solid ice in glaciers, snow, and the North and South Poles, as well as water vapour in the Earth's atmosphere. Water may pick up pollutants at any point in the cycle and transport them to the next stage. During a heavy rain or snowmelt, litter, silt, and invisible contaminants (such as fertilizers, lubricants, pesticides, and other chemicals) are carried across land and downstream to aquatic ecosystem and lands.

Environmental pollutants and contaminants that result from human activity associated with industries, agriculture, waste handling facilities, and urban/industrial wastewater treatment are unfortunately dangerously rising, with a negative impact on both human health and all earth ecosystems. In this regard, due to the presence of common (heavy metals, oils and hydrocarbons, bacteria, etc.) and emerging pollutants (i.e., pharmaceuticals, cosmetics, pesticides, personal and home care products, organic dyes, etc., see Figure 1.1), continuously released into the environment by numerous anthropogenic activities since the last century, modern society needs to face with their filtration and remediation [15–17].

It has been established that between 1930 and 2000, man-made chemical production increased from 1 million to 400 million tons per year.

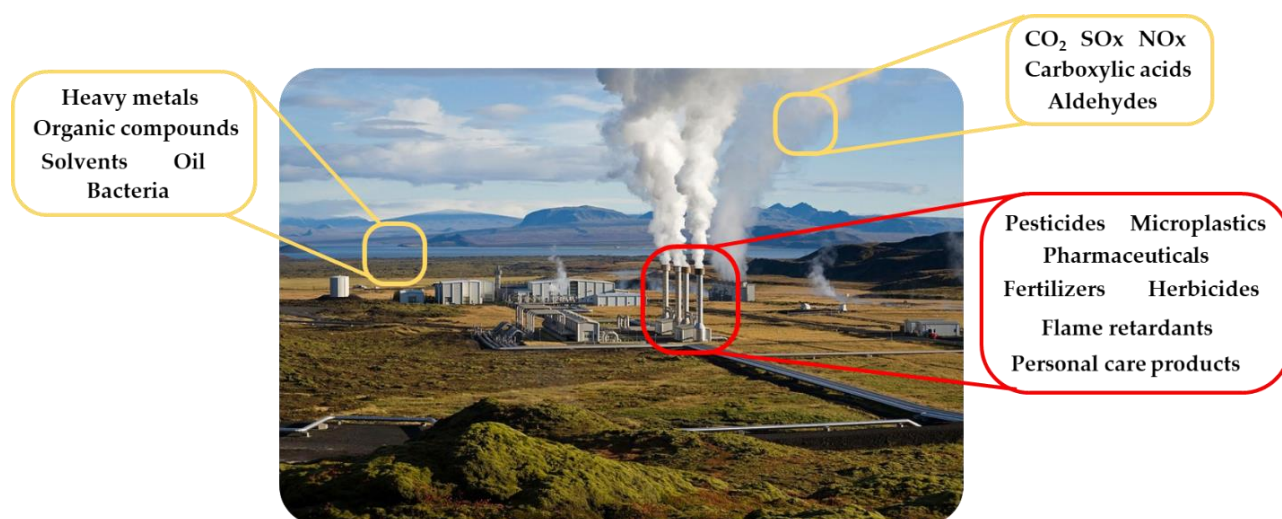


Figure 1.1. Common (yellow) and emerging (red) environmental pollutants [18].

According to data from EUROSTAT released in 2013, between the years of 2002 and 2011, compounds that are detrimental to the environment accounted for over 50% of the total chemical production, and over 70% of these chemicals have a major negative impact on the environment [19].

Table 1.1 provides a summary of some environmentally dangerous contaminants negatively affecting human health and ecosystem and that need to be cleaned up and treated to protect the environment.

Table 1.1. List of some environmentally dangerous compounds [18].

Type of substance	Pollutant	Ref.
Heavy metal	As, Cd, Cr, Cu, Pb, Hg, Ni, Zn	[20]
Radionuclide	^3H , ^{14}C , ^{90}Sr , ^{99}Tc , ^{129}I , ^{137}Cs , ^{237}Np , ^{241}Am	[21]
Fertilizer	Ammonium nitrate, phosphate	[22]
Mono- and bicyclic aromatic hydrocarbon	Benzene, toluene, xylenes, styrene, naphthalene, biphenyl	[23]
Polycyclic aromatic hydrocarbon	Benzo(a)pyrene, benz(a)anthracene, indeno(1,2,3-cd)pyrene	[24]
Halogenated aromatic (and polycyclic) hydrocarbon	Chlorobenzene, dichlorobenzene, 4-chloropyrene, 2-bromofluorene, 2,3,7,8-tetrachlorodibenzo- <i>p</i> -dioxin	[25,26]
Nitrogen-containing	Nitrobenzene, caffeine	[27,28]
Phenol	Phenol, 4-nitrophenol, 2-chlorophenol, bisphenol A	[29,30]
Ether	Diphenyl ether, dibenzofuran	[31]
Aliphatic hydrocarbon	<i>n</i> -alkanes	[32]
Insecticide	Acetamiprid, deltamethrin, endosulfan, malathion	[33]
Herbicide	Atrazine, prometryn	[34]
Organic dye	Methylene blue, rhodamine B, congo red, acid Red 88, methyl orange	[35]
Pharmaceutical	Amoxicillin, ibuprofen, ciprofloxacin, omeprazole	[36]
Perfluoroalkyl substance	Perfluorooctanoic acid, perfluorooctane sulfonate	[37]
Microplastic	Polyvinylchloride, polyethylene, polypropylene	[38]

In this sense, the search for innovative and sustainable wastewater treatment methods may represent a significant key-step for the reduction of numerous classes of emerging compounds in addition to the common classes of pollutants.

The three primary categories of common wastewater treatment techniques are based on physical, chemical, and biological processes. More specifically, the physical processes allow the elimination of contaminants without significantly affecting the biological or chemical forms of the pollutants present in the treated water.

Chemical methods, on the other hand, also defined as additive methods, may use reagents for the elimination of polluting species; for this reason, they are unattractive environmental processes compared to other techniques, since they may increase the substances dissolved in wastewater and they are not regenerable for other subsequent employment. The biological methods (classified as aerobic, in the presence of dissolved oxygen, and anaerobic, in the absence of dissolved oxygen) are based on the use of microorganisms for the biodegradation of pollutants in wastewater with the main objective of reducing nutrients and organic pollutants content.

Conventional methods used in wastewater treatment plants, apt to the specific adopted physical, chemical, biological method (as reported in parenthesis), may also be classified as [39]:

- Preliminary:
 - physical/mechanical (settling, desanding and deoiling);
- Primary:
 - physical/mechanical (flocculation and sedimentation);
 - chemical (neutralization, chemical precipitation);
- Secondary:
 - biological (aeration, activated sludge, rotating biological contactors, dripping filters, anaerobic digestion, biological nutrient removal, stabilization);
- Tertiary or advanced:
 - physical (ion exchange, absorption with activated carbon, reverse osmosis, extraction with gas, filtration with membranes);
 - chemical (chlorination, advanced oxidation, UV irradiation, ozonation).

In order to contemporary get rid of different types of contaminants, a standard wastewater treatment plant should combine all three physical, chemical, biological processes [39,40].

Unfortunately, until now the employed traditional methods of wastewater treatment and water purification occasionally lack of eliminating emerging contaminants, for which there is not yet a clear adopted European legislation that also establishes the legal limits with which they must be present in the environment; as a result, more cutting-edge ways are being researched and developed [40].

Moreover, most of the waste management and remediation methods currently in use require still large amounts of energy and chemicals that, for instance, in the case of wastewater treatment plants or polymeric absorbers/filters for pollutants and hydrocarbons, may feature themselves as secondary pollution sources [41].

1.2 Functional nanohybrids and nanocomposites for environmental remediation

Thanks to characteristics including high surface area (surface/volume ratio), size effects, catalytic capability, and reactivity, nanotechnological solutions and novel hybrid and composite nanomaterials are being used in a wide range of industrial sectors. In particular, nanoparticles may be chemically synthesized, modified and functionalized through various approaches obtaining different nanomaterials (some examples are shown in Figure 1.2) with specific properties.

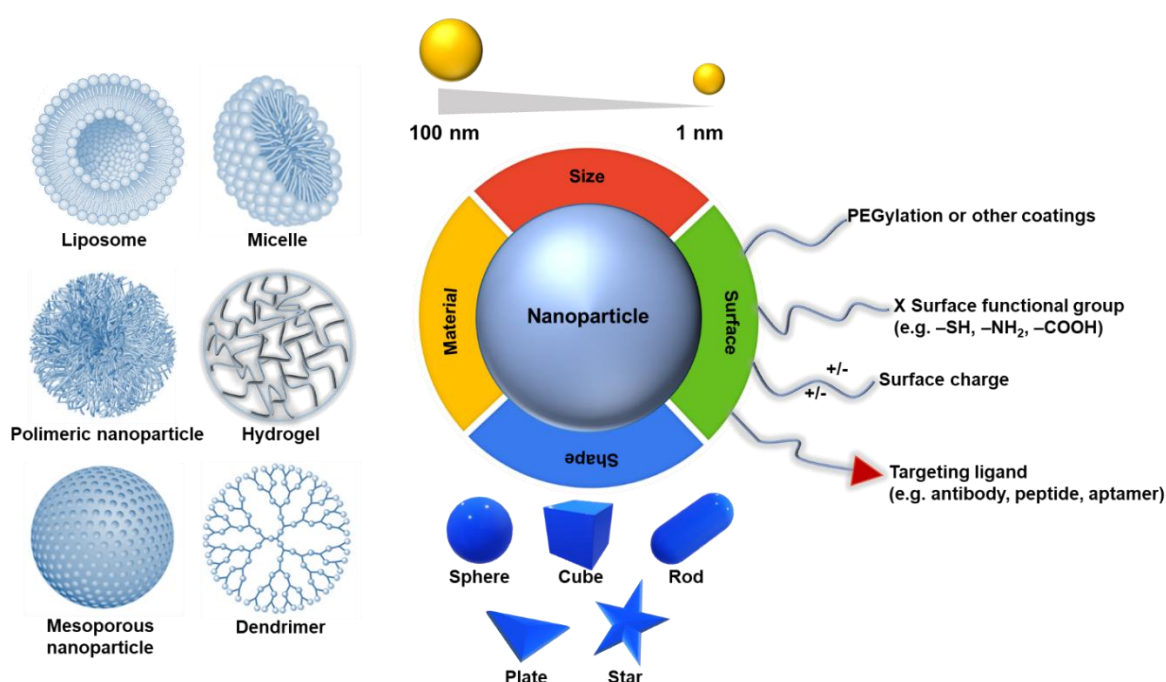


Figure 1.2. Graphical schematization of some possible modifications of nanoparticles to obtain different functional nanomaterials.

The developed functional nanomaterials may be also embedded in polymers and matrices to obtain functional organic and inorganic, hybrid materials or nanocomposites, featuring new chemical, physical, and mechanical properties, which are usually different and implemented from both the starting components (i.e. fillers and hosting polymers) thus being suitable for the development of sustainable, cutting-edge, and innovative products/technologies useful in a wide range of sustainable applications [42–44].

Useful nanomaterials, suitable as functional nanofillers, are as following [45]:

- metal nanomaterials (i.e., nanoparticles, NPs, of Pt, Pd, Ni, Ru, Al, Ag, Au, Cu) with characteristic optical, chemical, and electrical properties;
- metal oxide nanomaterials (i.e., Fe_2O_3 , ZnO, TiO_2 , Al_2O_3 , and SiO_2), either obtained from sol-gel synthesis or hydrothermal reactions;
- carbon-based nanomaterials (i.e., fullerene, carbon nanotubes CNT, graphene sheets);
- zeolite and silica-based nanomaterials with a mesoporous structure;

- ceramic nanomaterials;
- bimetallic nanomaterials;
- polymeric nanomaterials;
- bio-nanomaterials;
- metal–organic frameworks;
- core–shell nanomaterials.

Hybrid organic-inorganic materials [46], obtainable by various synthetic routes, and coming from a mixture of two amorphous or crystalline organic and inorganic phases [47], may be usually classified as:

- composites, i.e., mixtures of substances or materials made up of a matrix with micrometric dispersion;
- nanocomposites, i.e., sub-micrometric (1–100 nm) combinations of materials connected by physical interactions;
- hybrids, i.e., micrometric matrices based on covalently bonded substances with different nature;
- nanohybrids, atomic, molecular mixtures of several materials connected by chemical bonds.

A general nanostructured material, featuring organic and inorganic building blocks with nanometric dimensions, is also referred to as a nano-composite, when based on physical interactions, or as nanohybrid or hybrid materials, when the two components are covalently bonded [48].

Reversely, another classification categorize hybrid materials, basing on how the two phases interact; in particular [49]:

- class I hybrids: these are distinguished by the presence of weak electrostatic contacts, hydrogen bonds, or van der Waals forces between the phases;
- class II hybrids: displaying strong (first order) interactions between the phases (covalent, ionic bonds).

It is possible to have, as shown in Figure 1.3, a continuous phase that “traps” one dispersed phase (a) or two continuous interpenetrated phases (b) if the chemical interactions between the organic and inorganic phases are weak (Class I hybrids).

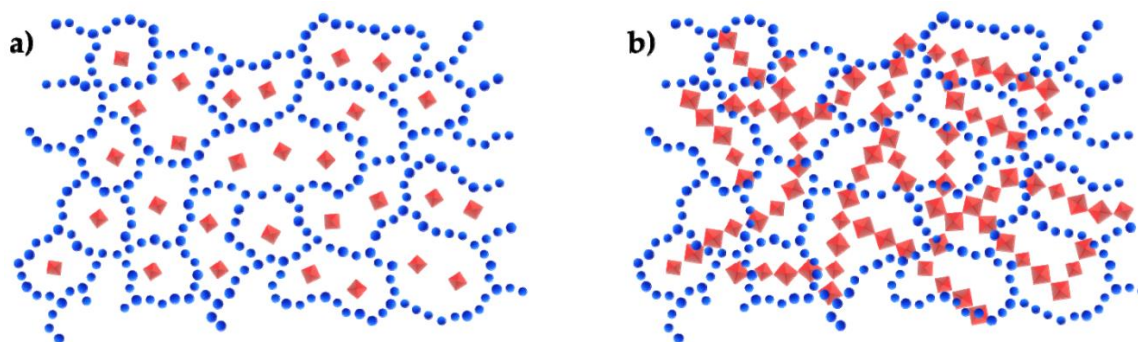


Figure 1.3. Graphical illustration of hybrid materials (Class I) with an organic continuous phase (blue line) that “traps” one dispersed inorganic phase (red cubes) (a) or two continuous interpenetrated phases (b) [18].

As shown in Figure 1.4, discrete inorganic units may exist if the chemical interactions between the organic and inorganic phases are strong (Class II hybrids). These units may take the form of clusters that are covalently linked to a continuous organic phase or vice versa (a'), or two continuous phases that are covalently linked (b') [50].

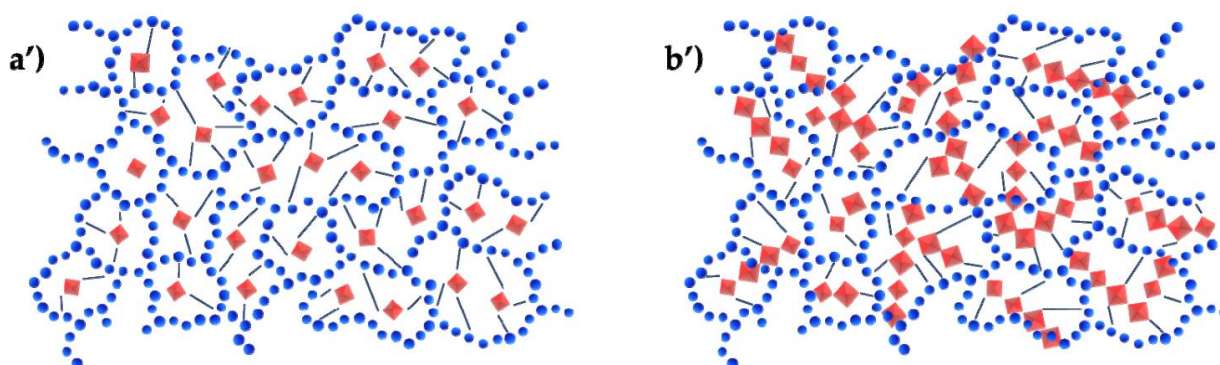


Figure 1.4. Graphical illustration of hybrid materials (Class II) with the inorganic phases in the form of clusters (red cubes) covalently linked (black lines) to a continuous organic phase (blue line) (a') or two continuous phases that are covalently linked (b') [18].

These classes of nanocomposites and nanohybrids based on some of the functional nanomaterials (nano-fillers) mentioned above in combination with organic/inorganic polymeric matrices (obtained either by sol-gel techniques [51], or derived from synthetic or natural organic polymers), due to their mechanical, physical, and adsorption properties, may be effectively used also for the treatment and remediation of wastewater, or polluted waters, soils, and air [18,52].

In addition to their catalytic or photocatalytic ability to degrade pollutants, as for example in the case of TiO_2 -based nanocomposites [53], these materials also have the potential to be used for bioremediation. They may even serve as substrates for bacterial development and as stimulants for microorganisms growth to allow and speed up the elimination of pollutants from the environment [18].

Today, due to the development of tunable characteristics and the adaptability of various nanomaterials and embedding polymers, wide examples of innovative functional nanohybrids and nanocomposites for removing pollutants are being produced. In this context, different types of nanomaterials will be explored in the next paragraphs.

1.2.1. Metal nanoparticle-based composites and hybrids

Due to their small size and high surface-to-volume ratio, metal nanoparticles (MNPs; related to metals or noble metals such as $M = \text{Pt}, \text{Pd}, \text{Ni}, \text{Ru}, \text{Al}, \text{Ag}, \text{Au}, \text{Cu}$) are nanomaterials having physical and chemical properties that are peculiarly different from the corresponding bulk materials. The ability of MNPs to kill bacteria by several processes, including the generation of reactive oxygen species, ATP depletion, harm to biomolecules, cation release, and membrane contact, is one of their most significant traits [54].

Additionally, MNPs may exhibit important optical and electrical properties, such as Rayleigh scattering, Raman scattering, and Plasmon resonances [55,56], as well as catalytic properties,

with reactivity related on their particle size, geometry, composition, oxidation state, and the surrounding chemical and physical conditions. [57].

Due to their unique properties, nanomaterials may be used in a variety of fields, including biomedicine (molecular diagnostics, imaging, drug delivery, and therapeutics), nano-catalysis, sensing and biosensing, smart textiles [58], and environmental remediation [59]. Chemical (e.g., chemical reduction, chemical vapor deposition, photochemical reduction, co-precipitation, thermal decomposition, hydrolysis) and physical processes (e.g., mechanical milling, laser ablation, vapor deposition, ion sputtering, grinding, flame pyrolysis) have both been developed as ways to synthesize MNPs. These techniques fall under the top-down or bottom-up preparation strategies [60]. Moreover, green methods for the synthesis of MNPs have also been most recently reported [61].

MNPs with very intriguing and useful characteristics may be combined with polymeric matrices to give raise to functional nanocomposites or nanohybrids, with a fine control of the chemical-physical qualities of the finished material.

In this regard, they may enable the formation of various nanocomposites, including core/shell nanoparticles, surface-modified nanoparticles, and microsphere composite nanoparticles, which are larger nanocomposite spheres, as well as polymer-matrix composites, which are made of isolated nanoparticles that have been finely dispersed in a polymer [64].

Various examples of the use of these materials for pollutant detection, treatment and remediation are shown in the following Table 1.2 [62].

Table 1.2. Some remediation methods based on MNPs [18].

Nanomaterial-based system	Remediation approach	Pollutant treated	Ref.
AgNPs-PCBMA nanocomposite	Membrane filtration	Protein/Bio-fouling	[63]
Osmium NPs on polypropylene hollow fiber membranes	Membrane filtration/redox	p-nitrophenol and 10-undecylenic acid	[64]
Au/Bi ₂ WO ₆ nanocomposite	Photocatalysis	Benzylic alcohols and Cr(VI)	[65]
Pd-Ag (NPs)/macroPSi heterostructure	Photocatalysis	Methylene blue	[66]
amid-p(Mac-co-AN)-M (M: Cu, Co) microgel	Catalysis	Nitrophenols and cationic and anionic organic dyes	[67]
PHNA vesicle/AuNPs	Catalysis	4-nitrophenol	[68]
Cellulose-AgNPs composite	Photocatalysis	Bio-fouling and methylene blue	[69]
Cu-Ni hybrid NPs	Photocatalysis	Crystal violet dye	[70]
Karaya gum crosslink poly(acrylamide-co-acrylonitrile)@AgNP hydrogel	Adsorption	Crystal violet	[71]
Ag-Cellulose Acetate impregnated on polypropylene fibers membranes	Membrane filtration	H ₂ S and C ₂ H ₅ SH	[72]
PU micelle/Ag NP clusters	<i>In-situ</i> extraction and detection (SERS)	Thiabendazole, phosmet and acetamiprid	[73]
rGO@AuNPs nanocomposite	<i>In-situ</i> detection and bioremediation	Cd ²⁺ , Pb ²⁺ , Cu ²⁺ and Hg ²⁺	[74]
FeNiNPs@corncob-activated carbon	Photo-Fenton catalysis	Rhodamine B	[75]

PdNPs embedded over chitosan/ γ MnO ₂ microspheres	Catalysis	2-nitroaniline, 4-nitrophenol, 4-nitroaniline, 4-nitro-o-phenylenediamine, congo red, methylene blue, methyl orange, methyl red, and rhodamine B	[78]
--	-----------	--	------

The field of environmental remediation may also benefit from MNPs (photo)catalytic properties.

Another instance is the employment of MNPs for the selective oxidation and reduction of certain contaminants under UV/visible light. As visible-light selective photocatalysts in water, several Au/Bi₂WO₆ nanocomposites may be made using a hydrothermal process in conjunction with a fast reduction-deposition technique and different Au weight ratios. In particular, under visible light and aerobic circumstances, this hybrid nanostructure shows a significant capacity for benzylic alcohols oxidation and Cr(VI) reduction in water. For this oxidation/reduction process, 2.0 wt.% and 1.0 wt.% Au/Bi₂WO₆ are the ideal catalyst concentrations, respectively. The initial purpose of this research is to identify a catalyst for specific redox processes in water within the context of green chemistry and environmental remediation [65].

Additionally, the use of photocatalysts in water makes it possible to oxidize harmful chemical molecules like methylene blue. For instance, to increase the activity of the methylene blue degradation in water under UV light, a heterostructure based on a plasmonic bimetallic photocatalyst based on Pd-AgNPs/macro porous silicon (macroPSi) may be used. This heterostructure was obtained by depositing monometallic and bimetallic NPs of Ag and Pd on macroporous silicon using a straightforward immersion method. Although monometallic photocatalysts such as AgNPs/macroPSi and PdNPs/macroPSi may be developed, bimetallic photocatalysts act better due to their larger specific surface area and plasmonic effect, which result in a greater efficiency (98.8%) and methylene blue degradation rate (0.033 min⁻¹) [66].

Other aggregates and composite structures incorporating MNPs could take advantage of their catalytic properties, include gels, micelles, and vesicles. Inverse suspension polymerization may be used to create microgels made of poly(methacrylic acid-co-acrylonitrile), and the amidoxime groups could be then added to create a more hydrophilic amidoximated microgel. The aqueous metal salt solutions of Cu(II) and Co(II) ions are added to amid-microgels to create MNPs based on Cu and Co, which are then processed with sodium borohydride (NaBH₄). For the simultaneous degradation of nitrophenols and cationic and anionic organic dyes (eosin Y, methylene blue, and methyl orange), which may be found in contaminated aquatic sites, the produced microgel composites (amid-p(Mac-co-AN)-M, M: Cu, Co) show significant catalytic effectiveness. It is also noted that such systems may be recycled for other catalytic cycles. In particular, amid-p(Mac-co-AN)-Cu composites appear to be more stable than Cu composites in similar aquatic environments because they might be used up to four times as sacrificial catalyst systems. Amid-p(Mac-co-AN)-Co composites do not exhibit any loss in catalytic activity for up to seven cycles. All these experimental findings may be related to a strong coordinating interaction between CoNPs and amidoxime groups [67].

A pH-responsive multifunctional homopolymer vesicle made of poly[2-hydroxy-3-(naphthalen-1-ylamino) propyl methacrylate] (PHNA), which supports AuNPs, may also aid in the reduction reaction of 4-nitrophenol. In this arrangement, the AuNPs and the supporter (PHNA vesicle) exhibits synergistic behavior. The polycyclic aromatic hydrocarbons (less than 0.876 ppb within 1 h) engage with the naphthalene pendants in PHNA vesicles via a π - π interaction, making these homopolymer vesicles effective as adsorbents of these pollutants in contaminated aquatic environments. This pH-responsive absorbent PHNA vesicles coated with AuNPs, in addition to being recyclable, also function as a nanoreactor for the reduction of 4-nitrophenol in water when NaBH_4 is added [68].

Additionally, there are many examples of useful nanotechnologies based on nanocomposites that combine the mechanical capabilities of natural polymers like cellulose with the antibacterial and catalytic properties of particular MNPs. A functional composite material may be prepared using cellulose and AgNPs. Firstly, AgNPs were simply impregnated into citrus waste-derived cellulose to create a composite nanomaterial with antibacterial, antioxidant, and photodegradation characteristics. Particularly, discs made by the composite substance cellulose-AgNPs exhibit over 90% reduction of *Staphylococcus aureus* culture within 150 min, a moderate total antioxidant potential, minor 2,2-diphenyl 1-picryl-hydrazyl (DPPH) radical scavenging activity, and a moderate photodegradation capacity of up to 63.16% (time of 60 min) of methylene blue dye under sunlight [69].

1.2.2. Metal oxide nanoparticle-based materials

Metal Oxide NPs (MONPs) are widely used in the field of environmental remediation due to their intrinsic and peculiar sorption/desorption, redox, acid-base, photocatalytic (i.e., TiO_2 nanoparticles, see Figure 1.5), and magnetic characteristics [76,77].

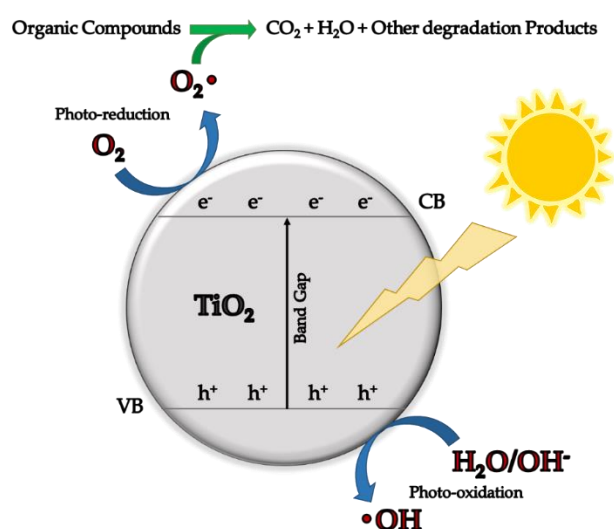


Figure 1.5. Illustration of the photocatalytic properties of TiO_2 nanoparticles [18].

These features enhance the mechanical strength, longevity, and hydraulic capabilities of materials in filtration systems, when combined with polymeric supports. There are various MONP composites, including polymer-supported NPs distributed in polymeric matrices,

which may be used to remove heavy metals from contaminated water, and magnetically active polymeric particles, which behave also very significantly and may be recycled [78].

Additionally, the magnetic properties of some MONPs, like Fe oxide NPs, are extensively used for the recovery of nanocomposite materials based on various organic, inorganic, and polymeric matrices after their use for various remediation purposes, like oil/water separation and the removal of harmful organic and inorganic substances. Several already published literature works describe a number of ways to make iron oxide nanoparticles, including hydrothermal/solvothermal synthesis, thermal breakdown, micro-emulsion, and co-precipitation technique [79].

Different methods, including complexation, electrostatic attraction, and ion-exchange, are used to absorb contaminants from MONP composites. Many MONP-based systems, as reported in Table 1.3, and further discussed below, could take advantages of these properties.

Table 1.3. Some remediation methods based on MONPs, together with the corresponding treated environmental pollutants [18].

Nanomaterial-based system	Remediation approach	Pollutant treated	Ref.
Fe-Ti-Mn composite oxide	Photocatalysis	As(V) and As(III)	[80]
ZnO@TiCN nano-urchin	Thermochemical	Cr(VI)	[81]
PAMAM dendrimers with G ₄ -OH cores immobilized on TiO ₂	Chelation	Cr (III), Cu(II) and Ni(II)	[82]
GO-MO nanocomposite	Inner-sphere complexation	Cd(II) and Cu(II)	[83]
Fe ₃ O ₄ @GOCMC core-shell structured composite bead	Adsorption	Phosphate and nitrate ions	[84]
PSB/Fe ₃ O ₄ /biochar composite	Removal and biodegradation	COD, phosphate and nitrate ions Rhodamine B, Methylene blue, Congo Red and Cr(VI)	[85]
TiO ₂ -OP@Fe ₃ O ₄ composite	Photocatalysis		[86]
n-decanol membrane-10-undecylenic acid-iron oxide NPs	Liquid membrane	Silver and lead ions	[87]
Ethylene propylene diene monomer sulfonate impregnated membranes with propylene hollow fiber impregnated magnetic particles	Membrane filtration	Aluminum ions	[88]
Magnetite NPs, biochar and graphite alginate beads	Adsorption/bioremediation	Azo blue dye	[89]
Magnetic shell cross-linked knedel-like NPs	Adsorption	Crude oil	[90]
MNP-PEA-OmpA and MNP-PEA-OmpA-Laccase bionanocompounds	Bioremediation	Oil/water emulsions and crude oil	[91]
PET and sugarcane bagasse ash/Fe ³⁺	Adsorption	Naproxen	[92]
Chitosan/Fe ₂ O ₃ /NiFe ₂ O ₄	Adsorption	Methyl green	[93]
Chitosan/hydroxyethyl cellulose gel immobilized polyaniline/CuO/ZnO	Adsorptive-Photocatalytic	Congo red	[94]

Composites based on porous granular materials with outstanding hydraulic characteristics are an example of systems that represents a potential solution to the technical issues with direct

NP application in large-scale water treatment and purification. In this context, graphene oxide (GO), a layered hydrophilic carbon material that is nonconductive and has a very high concentration of charged oxygen-containing groups (epoxides, alcohols, ketone carbonyls, and carboxylic groups) [102], makes the perfect support for metal nanoparticles (MONPs) [95]. On the other hand, Mn oxide NPs exhibit a high capacity for heavy metal retention, a negative surface charge, a wide pH range, and support the formation of a sizable porous composite when combined with GO.

Due to electrostatic attraction between negatively charged oxygen-containing groups of GO at high pH values, the negative surface of GO promotes the folding of GO nanosheets, which leads to the formation of a porous composite material with high hydraulic conductivity and low diffusion restriction. An illustration of their combination is provided by the development of Mn oxide NP-impregnated graphene oxide aggregate (GO-MONPs) nanocomposite, which was tested using samples containing the representative metals Cd(II) and Cu(II). The GO-MONPs composite may absorb Cd(II) and Cu(II) with an incredibly high absorption rate (> 99.9%) in column experiment thanks to an inner-sphere complexation mechanism. For the desorption of more than 97% of the preloaded Cu(II) and Cd(II), the exhausted material may be regenerated by flushing with a 10 BV acid-salt binary solution made of 0.2 M HCl and 4 wt% CaCl₂ [83].

Additionally, GO may be usefully employed in conjunction with Fe₃O₄ magnetic particles. Fe₃O₄ NPs adorned with graphene oxide and carboxymethylcellulose (Fe₃O₄@GOCMC) core-shell structured composite beads, produced using a one-pot synthesis, are employed for the remediation of phosphate and nitrate ions from an aqueous medium. For the purpose of removing the adsorbed anions, the nanocomposite material was regenerated using a 0.1 N NaOH solution. The dried, renewing Fe₃O₄@GOCMC systems may be subsequently used for up to four more adsorption-desorption cycles [84].

Other porous and environmentally friendly plant-based materials, such as biochar, may be employed as absorbents and matrices for MONPs. Biochar is a carbonaceous material formed by pyrolysis of biomasses such as corncob waste at low temperatures and low oxygen levels. It is utilized as a soil conditioner in agriculture, due to its huge surface area and porous structure. Because of its high carbon content and cation exchange capacity, it is utilized in carbon sequestration, organic solid waste composting, water and wastewater purification, as a catalyst and activator, as an electrode material, and as an electrode modifier [96].

Biochar may be also used in the remediation of heavy metals and organic compounds in the environment when combined with NPs (and sometimes stabilizers for example carboxymethyl cellulose) such as FeNPs for the production of nanocomposites (i.e., nano zero-valent iron (nZVI)/biochar, iron sulfide/biochar, and iron oxide/biochar). Due to their redox, catalytic, and magnetic capabilities, Fe and Fe oxide NP features improve biochar characteristics with a greater surface area, higher electron transfer efficiency, and numerous functional groups [97–99].

There are various methods for preparing Fe/biochar composites, such as pyrolysis, which produces materials with good ability for contaminant extraction from aqueous solutions and soils, hydrothermal carbonization, which uses relatively low temperatures and has fewer drawbacks than direct pyrolysis technology, ball milling with low energy consumption, and fractional precipitation (i.e., iron oxide precipitation and the liquid phase reduction method).

This last process consists in a first step of pristine biochar preparation at normal pyrolysis temperature, followed by a second step of Fe precipitation on the surface and inside the biochar pores. The remediation procedures involving these composite materials include absorption of metals, radionuclides, oxyanions, and organic compounds, reduction of organic compounds and heavy metals, and advanced oxidation processes of organic dyes, nitroresorcinol, bisphenol A, and tetracycline [100].

Alginate is another natural polymer often employed as an embedding matrix for functional NPs. Magnetic NPs of Fe_3O_4 are synthesized via a reverse co-precipitation process and encapsulated in alginate to make alginate magnetic nanostructured beads for the removal of textile blue dyes from water, with potential applications in nano-bioremediation. Different forms of magnetite NPs were used to obtain various composite beads based on sodium alginate. As a result, one form of bead is made with ferrous sulphate, another with ferrous sulphate and biochar, and a third with ferrous sulphate, biochar, and graphite. After 3 hours of equilibrium time, the ferrous sulphate, biochar, and graphite alginate bead removed (at pH 8) 82.4% of the azo blue dye from the starting concentration of 25 ppm, and the 55.22% from the starting dye concentration of 100 ppm [89].

1.2.3. Carbon-based nanomaterials

Carbon-based nanomaterials have generally piqued the scientific community interest due to their unique chemical and physical capabilities, including as superior electrical and heat conductivity, enhanced optical qualities, chemical stability, and great mechanical strength. They are composed of solid-state carbon allotropes made up of sp^3 and/or sp^2 hybridized carbon atoms with varying nanoscale dimensions, such as zero-dimensional (0D) fullerenes, nanodiamonds, and graphene quantum dots, one-dimensional (1D) single walled or multiwalled carbon nanotubes (SWCNTs and MWCNTs), and two-dimensional (2D) graphene and graphene oxide.

These nanomaterials may be produced using various techniques, such as: (i) bottom-up methods, i.e., chemical vapor deposition (CVD) on a substrate as for SWCNTs, MWCNTs and graphene; (ii) synthesis approaches from aromatic benzene derivatives; (iii) top-down approaches, such as sonication, liquid phase exfoliation, and ionic-liquid assisted electrochemical exfoliation for graphene [101]. Carbon-based nanomaterials have applications in a variety of fields, including biomedicine [102], theranostic and tissue and cell imaging based on one-photon and two-photon fluorescence properties [103], energy storage and conversion, catalysis [104], development of materials for environmental remediation (i.e., for the removal of organic molecules, heavy metals, and oil/water separation).

Several already published research are conducted in order to investigate the use of these nanomaterials in environmental remediation, including the use of these composites to improve water pollutants absorption capacity and regenerability. Porous graphene materials exhibiting improved mechanical, physical, and chemical (hydrophilic-lipophilic) characteristics, such as foams, sponges, and aerogels, are developed for these latter objectives [105]. The cellular ecotoxicity of some carbon-based nanomaterials has been investigated [106]. A size-dependent hazards and cytotoxicity is demonstrated enhanced after surface functionalization with acid treatments, due to the presence of carbonyl, carboxyl, and/or hydroxyl groups in those materials

[107]. As a result, in the light of a safe-by-design composite functional materials [108] incorporating these nanoparticles, it is even more critical to avoid dispersion in the environment.

Table 1.4 lists some uses of carbon-based nanomaterial composites and hybrids in the field of pollution remediation.

Table 1.4. Remediation approaches for carbon-based nanocomposites and hybrids [18].

Nanomaterial-based system	Remediation approach	Pollutant treated	Ref.
CNTs, nanofibers and vermiculite based nanosponge	Absorption	Oil	[109]
PANi/CNT composite	Microbial fuel cell	COD	[110]
MWCNT/Ppy composite	Microbial fuel cell	Phenol and COD	[111]
AQS/Fe ₃ O ₄ /CNTs and HA/Fe ₃ O ₄ /CNTs composite	Biocatalysis	Cr(VI) and methyl orange	[112]
Graphene aerogel/Fe ₃ O ₄ /polystyrene composite	Absorption	Crude oil	[113]
L-GO/ZnO NPs composite	Microbial fuel cell	Pb ²⁺	[114]
Graphenized sand-based composite	Absorption	Hg ²⁺	[115]
Ni-BDC@GO nanocomposite	Adsorption	Methylene blue	[116]
TZB-Gr composite nanofiber	Photocatalysis	Methylene blue and rhodamine B	[117]
P25-GR composite	Photocatalysis	Phenanthrene, fluoranthene, and benzo[a]pyrene	[118]
TiO ₂ composite based on zinc porphyrin-covalently functionalized fullerene [C60]	Photocatalysis	Phenol and methylene blue	[119]
ZrO ₂ NPs on GO supported peptide/cellulose binary nanofibrous membrane	Membrane filtration	Fluoride ions	[120]
Cyclodextrin modified GO@FeNP composite	Adsorption	Oxytetracycline	[121]
CNTs/carbon xerogel hybrid loaded Fe–Ni	Adsorption	RY160 dye	[122]
Activated carbon based on shea residue (<i>Vitellaria paradoxa</i>)	Adsorption	Hydroquinone and resorcinol	[123]

Because of their absorption, photocatalytic, and electrocatalytic properties, carbon nanotube composites enable the development of remediation technologies for environmental pollutants such as heavy metals, organic dyes, and other organic substances, including hydrocarbons. On the other hand, there are numerous examples of the use of other carbon-based nanomaterials in this sector, such as graphene and its derivative graphene oxide, as mentioned before. GO is commonly formed by the oxidation and exfoliation of graphite using oxidant agents (Hummer's method KMnO₄, NaNO₃, H₂SO₄ [124]), and it is distinguished by a high density of charged oxygen-containing groups (epoxides, alcohols, ketone carbonyls, and carboxylic groups).

Because of its negatively charged surface, GO has a high adsorption capacity for various molecules via physical and/or chemical forces such as electrostatic, π - π and hydrophobic interactions, and may be also an optimal candidate for the development of advanced membrane filtration coatings and processes for the removal of common and emerging contaminants from water (see Figure 1.6).

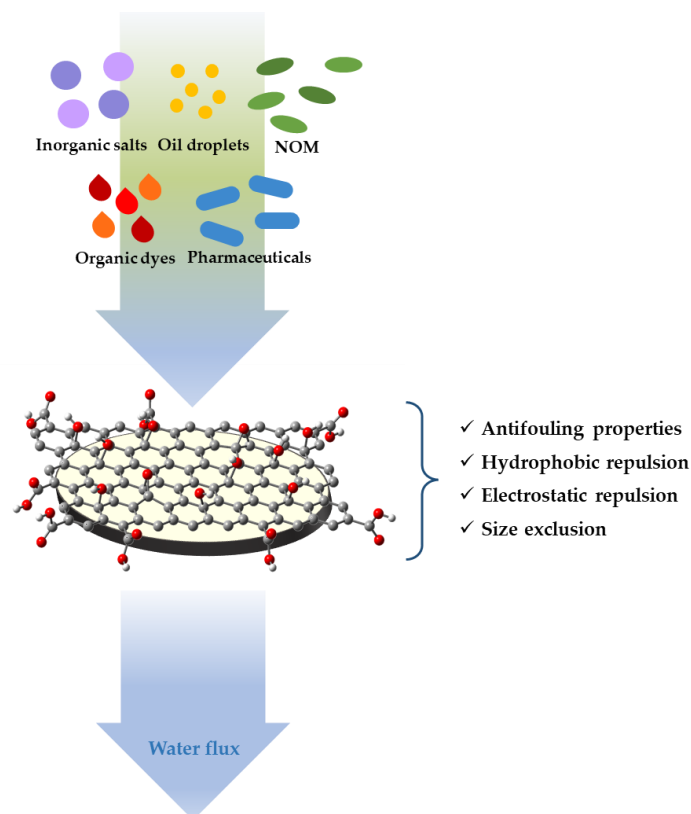


Figure 1.6. Illustration of the advantages in the use of GO for the development of functional membrane coatings for water filtration [125].

There are two ways to functionalize GO and generate nanocomposites, i.e., using GO as a host material or in host materials. In the first instance, multiple techniques are shown to be used to functionalize the GO surface. The second way consists to crosslink GO with a polymeric matrix using simple and non-toxic syntheses to create nanocomposites with a stable structural configuration, high absorption capacity, and quick recovery and regeneration after use [126].

Composite aerogels are porous materials with adsorption capabilities that have applications in water remediation.

In particular, aerogels with high hydrophobicity that float in aquatic environments may be developed for their easy use and recovery. A unique graphene aerogel/ Fe_3O_4 /polystyrene composite created by an environmentally friendly and cost-effective solvothermal process is one example. This aerogel is distinguished by the presence of porous Fe_3O_4 -NPs, which act as cross-linkers for graphene oxide plates (made using a modified Hummer process), and polystyrene, which allows the production of a porous structure with enhanced hydrophobicity of the composite aerogel in conjunction with Fe_3O_4 -NPs. After 10 water-oil separation cycles, the ultralow density aerogel composite has a crude oil absorption capacity of 40 times its own mass

and is easily recovered due to its floating capacity. Because of the presence of Fe_3O_4 -NPs, it also exhibits magnetic characteristics, allowing for the collecting of the exhausted aerogel using a magnet. Aerogel regeneration is accomplished through a simple squeezing method [113].

Methylene blue and other organic dyes may be degraded using metal oxide NPs, such as TiO_2 , ZnO , and Bi_2O_3 . In this context, graphene, a nanomaterial easily generated from GO via reduction procedures, may be used for photocatalytic activity in pollutants removal and in combination with metal oxide nanoparticles.

It is discovered that graphene, embedded with composite nanofibers (titanium dioxide-zinc oxide-bismuth oxide-graphene, TZB-Gr), as prepared by a sol-gel based nozzle-less electrospinning process, improves the removal capacity of organic dyes due to the synergic coupling of 2D graphene with photoactive semiconductor nanofibers. When exposed to visible and UV light, the TZB-Gr composite nanofibers may activate organic dyes, producing $\cdot\text{O}_2$ and $\cdot\text{OH}$ radicals, which are potent oxidizing species for the degradation of different organic pollutants [117].

A TiO_2 -graphene (P25-GR) composite generated by a hydrothermal reaction of GO with TiO_2 (P25), by varying the graphene ratios, is another example of a nanocomposite combining graphene and metal oxide NP characteristics. This composite material has been investigated for polycyclic aromatic hydrocarbon (PAH) absorption and photodegradation (phenanthrene, fluoranthene, and benzo[a]pyrene as models). At high PAH concentrations ($2.0\text{--}4.0\text{ g}\cdot\text{mL}^{-1}$) under alkaline circumstances, the P25-GR with 2.5% graphene demonstrate the highest results for absorption, charge transfer, and photocatalytic efficacy (80% of PAHs eliminated after 2 h) [118].

1.2.4. Sol-gel based nanostructured materials

Silica NPs may be synthesized using an easy sol-gel method. This is a two-step synthesis that begins with aqueous alcohol solutions of silicon alkoxides, and ends with monodisperse silica NPs, using ammonia as a catalyst. The first step in the sol-gel process is a hydrolysis reaction to generate silanol groups, and the second step is a condensation polymerization reaction to form siloxane bridges [127]. These reactions may take place in an acidic (Figure 1.7 a,b) or alkaline (Figure 1.7 c,d) catalytic environment.

The sol-gel technique is also widely used to functionalize and modify the surfaces of various materials with the goal of producing advanced and multifunctional materials with properties such as UV radiation protection, antimicrobial finishing, water repellency, bio-molecule or functional-molecule immobilization, flame retardancy, chemical resistance, and self-cleaning properties [128–130].

On the other hand, because of their extensive surface area and the presence of large holes that act as hosts for diverse molecules, porous silica nanoparticles perform better in a variety of industries.

Nanomaterials with well-defined pore network, such as zeolites and mesoporous silica NPs, may be defined in two categories of porous silica materials, i.e. as silicate or aluminosilicate (namely, minerals composed of aluminum, silicon, and oxygen, plus counteractions).

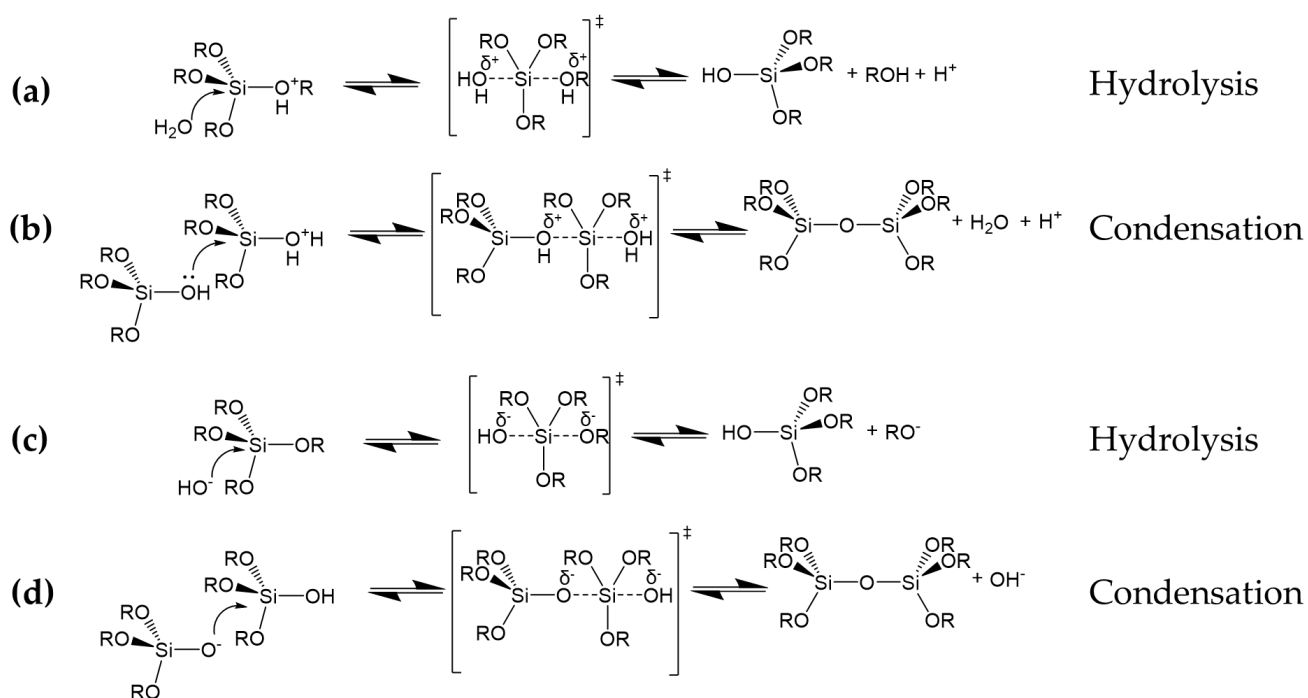


Figure 1.7. Sol-gel synthesis in acidic (a,b) or alkaline (c,d) catalytic environment [128].

Mesoporous silica NPs are highly versatile nanomaterials derived from silicate gels and quaternary ammonium surfactants of varying chain lengths, with applications in drug delivery, nanomedicine, theranostics, and photodynamic therapy due to their high surface area, large pore volumes, tunable pore size, and easy surface modification properties [131].

Because of the absorption capabilities of mesoporous silica NPs and their composites, they may be used in environmental remediation to adsorb different pollutants from aqueous or gaseous environments [132,133].

In this regard, zeolites are crystalline aluminosilicates (or silicates) with a regular spatial arrangement of homogeneous cages, cavities, or channels of molecular dimensions, a high surface area, and cation exchange characteristics that are often formed under hydrothermal conditions using organic templates.

Because of their high selectivity for inorganic cations (zinc, lead, cadmium, copper, nickel) and anions, and organic compounds (such as pesticides and phenols), zeolites have applications in a variety of sectors, including catalysis and renewable energy applications [134,135].

Clays are nanostructured fine-grained minerals that are based on aluminosilicates. Because of differences in mineral content, size, and layered structure, they are classified as montmorillonite, kaolinite, illite, bentonite, and chlorite (Figure 1.8).

Moreover, they are characterized by a negatively charged surface, large surface area, swelling capacity (especially montmorillonite and bentonite clays), cation exchange capacity, and significant adsorption/absorption capabilities [136].

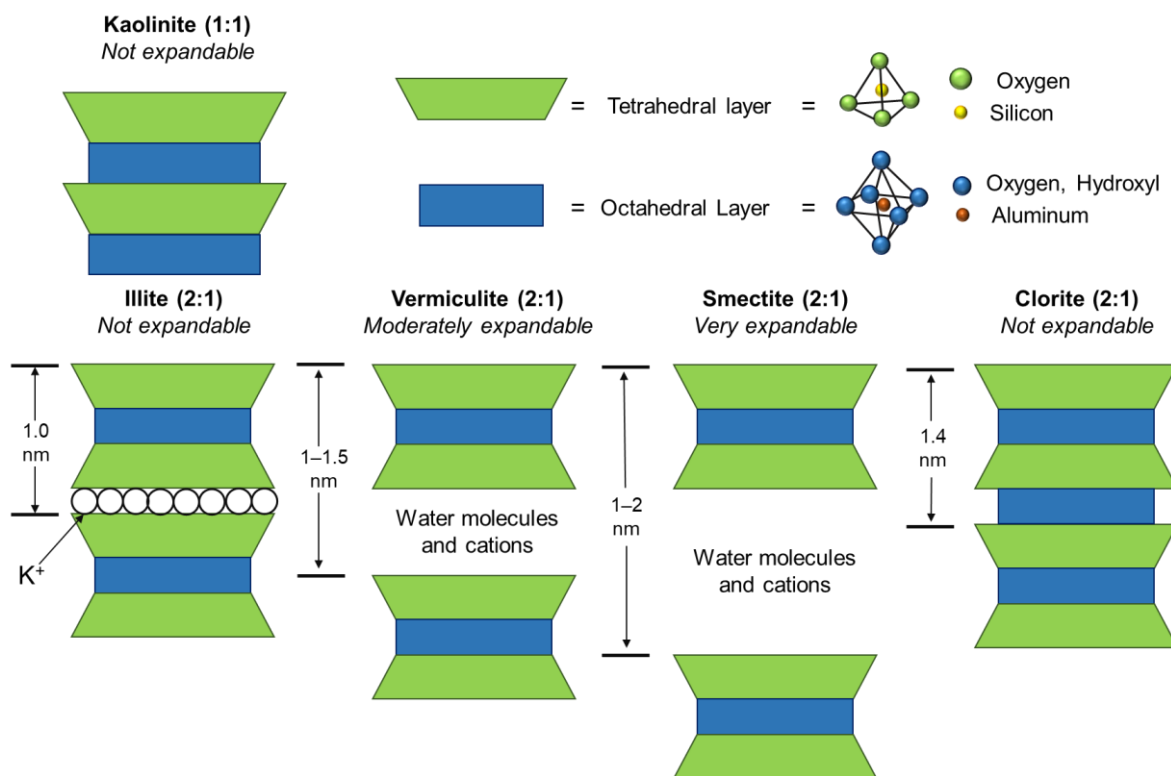


Figure 1.8. Graphical classification of some types of clays.

They may be also easily functionalized by modifying their hydrophilicity/hydrophobicity surface and adsorption capabilities to produce functional clays or composites [137,138](Figure 1.9) for environmental remediation applications [139,140].

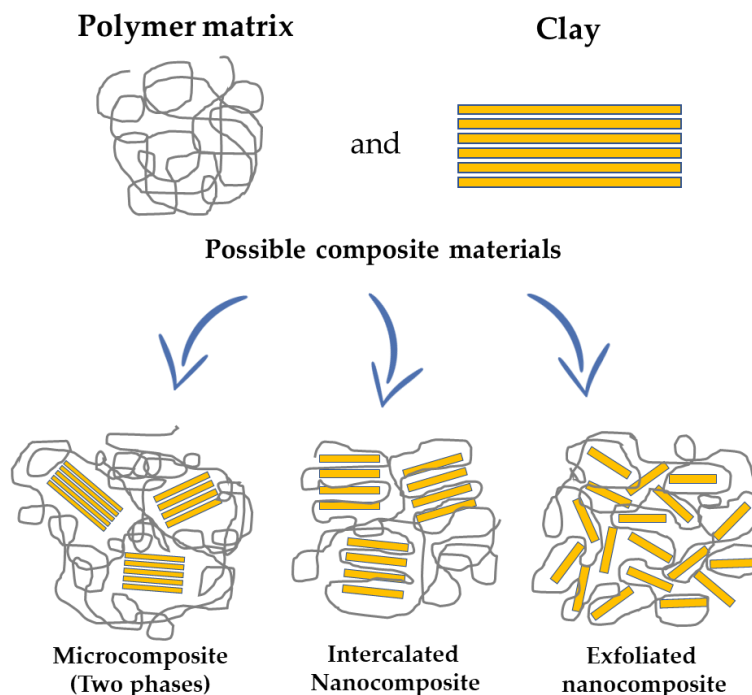


Figure 1.9. Illustration of clay-based composite materials [18].

Silica-based nanomaterial composites and hybrids offer enormous potential for environmental remediation and bioremediation applications, as shown in Table 1.5.

Table 1.5. Approaches for remediation based on silica-based nanocomposites and hybrids [18].

Nanomaterial-based system	Remediation approach	Pollutant treated	Ref.
Ppy/HMSNs hybrid	Adsorption	Cr(VI)	[141]
Pd@h-mSiO ₂ nanotubes	Catalysis	4-nitrophenol and 4-chlorophenol	[142]
Mesoporous silica NPs and magnetic GO	Adsorption	Sulfamethoxazole antibiotic	[143]
Fe ₃ O ₄ -MWCNTs@SiO ₂ nanocomposite and laccase	Biocatalysis	Eriochrome Black T, Acid Red 88, and Reactive Black 5	[144]
SBA-15 mesoporous silica and laccase	Biocatalysis	Protocatechuic acid, ferulic acid, sinapic acid and caffeic acid	[145]
Fe ₃ O ₄ @SiO ₂ @Ru hybrid magnetic composite	Photocatalysis	Methyl orange and methyl red	[146]
Cu-Z-GO-M composite	Adsorption	Methylene blue	[147]
nZVI/Ni@FZA composite	Adsorption	Cr(VI) and Cu(II)	[148]
T/MZ composite	Photocatalysis	Metoprolol	[149]
Zeolite, GO and laccase bio-nanocompound	Biocatalysis	Direct Red 23	[150]
Zeolite coated by <i>Pseudomonas veronii</i> cells on xanthan gum-based biopolymer	Biocatalysis	Hg ²⁺	[151]
Cellulose fibers/zeolite-A nanocomposite	Adsorption	Organic and inorganic Se ions	[152]
ODTMS modified halloysite	Bioremediation	Crude oil	[153]
Sodium alginate/halloysite/hemp hurd	Adsorption	Methylene blue	[154]
PU foam coated with POS@HNT	Absorption	Chloroform and dichloroethane	[155]
Iron-clay-cyclodextrin composite	Catalysis	Bisphenol A, carbamazepine and perfluorooctanoic acid	[156]
Chitosan-clay and laccase nano-biocomposite bead	Biocatalysis	Anthrax quinone dye, azo dye of and diazodye	[157]
Biocomposite membranes of chitosan with montmorillonite and kaolin	Adsorption	Cu(II)	[158]

Nanocomposites based on various clays (such as montmorillonite, kaolinite, and halloysite) are shown to be interesting and useful systems for environmental remediation purposes. Halloysite is a natural tubular clay that has been extensively explored owing to its biocompatibility (low in vivo and in vitro toxicity) and peculiar mechanical, physical, and chemical characteristics (simple inner/outer surface functionalization).

Because of its tubular shape, it may also be loaded with various species for the release of active molecules, such as antioxidants [159], flame retardants, corrosion inhibitors [160], biocides, and drugs [161]. There are numerous examples of halloysite loaded or functionalized with various nanomaterials, such as metal or magnetic NPs, for environmental remediation approaches that may perform pollutant degradation and catalytic reactions or may be used as reusable absorbent systems. Halloysite may be functionalized with organo-silanes, using simple sol-gel processes, to increase dispersibility into polymer matrices, improve thermal stability and tensile characteristics, and give rise to hydrophobic nanohybrids suitable for various applications [162].

The inner layer of halloysite may also be hydrophobized with surfactants, like octadecyl phosphonic acid, to provide more binding sites for MNP, thus neutralizing the positive charge in the inner alumina layer, as well as loading hydrophobic molecules, like oil and organic pollutants. In contrast, halloysite may form stable oil-water emulsions and encapsulate water droplets inside the clay shell to form liquid marbles. These liquid marbles may be then used for the encapsulation of biomaterials or biofilms of selected bacterial species, such as the hydrocarbonoclastic bacteria *Alcanivorax borkumensis*, featuring a mechanical reinforcement and oil-spill bioremediation activity [163].

Other clays, due to their absorption and mechanical characteristics, may be utilized to obtain functional nanocomposites for remediation processes. The incorporation of clays in composite materials, such as membranes, reduces the harmful effects of certain nanomaterials, such as GO nanoplates, due to clay/NP aggregation, which weakens their possible dispersion into the environment [164].

Furthermore, catalytic nanocomposites based on clays and metal oxide NPs may be employed in conjunction with macrocycles, such as cyclodextrin, to increase their affinity and degradation for organic contaminants. By covering montmorillonite clay with iron-oxide and further modifying the resulting composite with cyclodextrin monomers and polymers, cross-linked with polyfluorinated aromatic molecules, an iron-clay-cyclodextrin composite absorbent catalyst was developed.

This material demonstrate high absorption of the model pollutants bisphenol A (BPA), carbamazepine (CBZ), and perfluorooctanoic acid (PFOA), as well as excellent degradation efficiency by H_2O_2 (over 90% in 1 h for BPA and CBZ, and 80% for PFOA), which remained constant after five consecutive cycles of absorption and degradation [156].

Laccase enzyme may catalyze the decomposition of organic contaminants. Chitosan-clay composite beads could be used to immobilize laccase from the *Alcaligenes faecalis XFI* strain, thus demonstrating a higher efficiency in enzyme immobilization than simple chitosan beads, due to the synergetic effect of clay (mechanical strength) and chitosan (porous nature), and their better biocompatibility with the laccase enzyme. The chitosan-clay-laccase nano-biocomposite is further examined for the degradation of three synthetic dyes, with a maximum decolorization percentage of 85% for anthrax quinone dye, 82% for azo dye, and 69% for diazo dye, and high reusability [157].

1.3 Membrane-based filtration techniques: limits and future perspectives

One of the most common wastewater treatment approaches include the use of filtering systems [165–167].

They are procedures that mostly rely on ceramic or polymeric membranes and take use of pressure to remove various contaminants and/or desalinate water [168,169].

Since the pressure may be applied perpendicularly (Figure 1.10 a) or tangentially (Figure 1.10 b) to the membrane, it is possible to distinguish primarily two membrane-based filtration techniques [170,171], i.e. dead-end or cross-flow filtration processes, respectively.

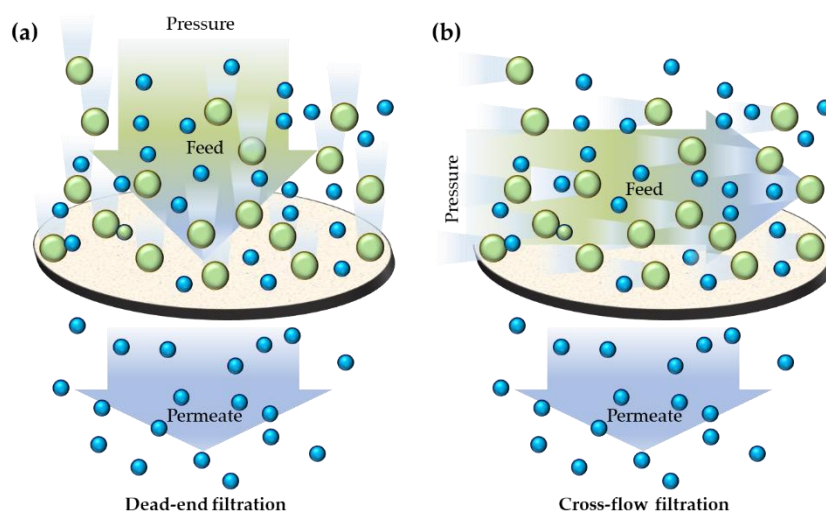


Figure 1.10. Graphical schematization of dead-end (a) and cross-flow (b) filtration approaches [172].

Additionally, it is feasible to distinguish between four major kinds of membranes with various capacities for removing pollutants, which is mostly related to the size of the membrane pores (Figure 1.11):

- membranes for microfiltration (0.1–5 μm pore size range), which may hold onto organisms including bacteria, algae, suspended particles, and sediments;
- ultrafiltration membranes that retain proteins and viruses and have pores between 0.01–0.1 μm in size;
- membranes for nanofiltration that capture dissolved organic compounds and divalent cations and have pores that range from 0.001–0.01 μm in size;
- reverse osmosis membranes operate on the theory of solvent diffusion across the membrane (pore sizes ranging from 0.0001–0.001 μm).

Membrane technology presents different benefits and advantages, such as scalability, relatively low power usage, lack of need for chemicals like other wastewater treatment methods, and low temperatures of operation [41].

Despite this, the common polymers summarized in Table 1.6 and used to prepare polymeric filtration membranes came from non-renewable and petroleum resources [173,174] or toxic substances [175], representing themselves as sources of secondary contamination.

Therefore, combining greener and cleaner ways to produce environmentally friendly processes in wastewater and water purification is the key challenge facing research and industries.

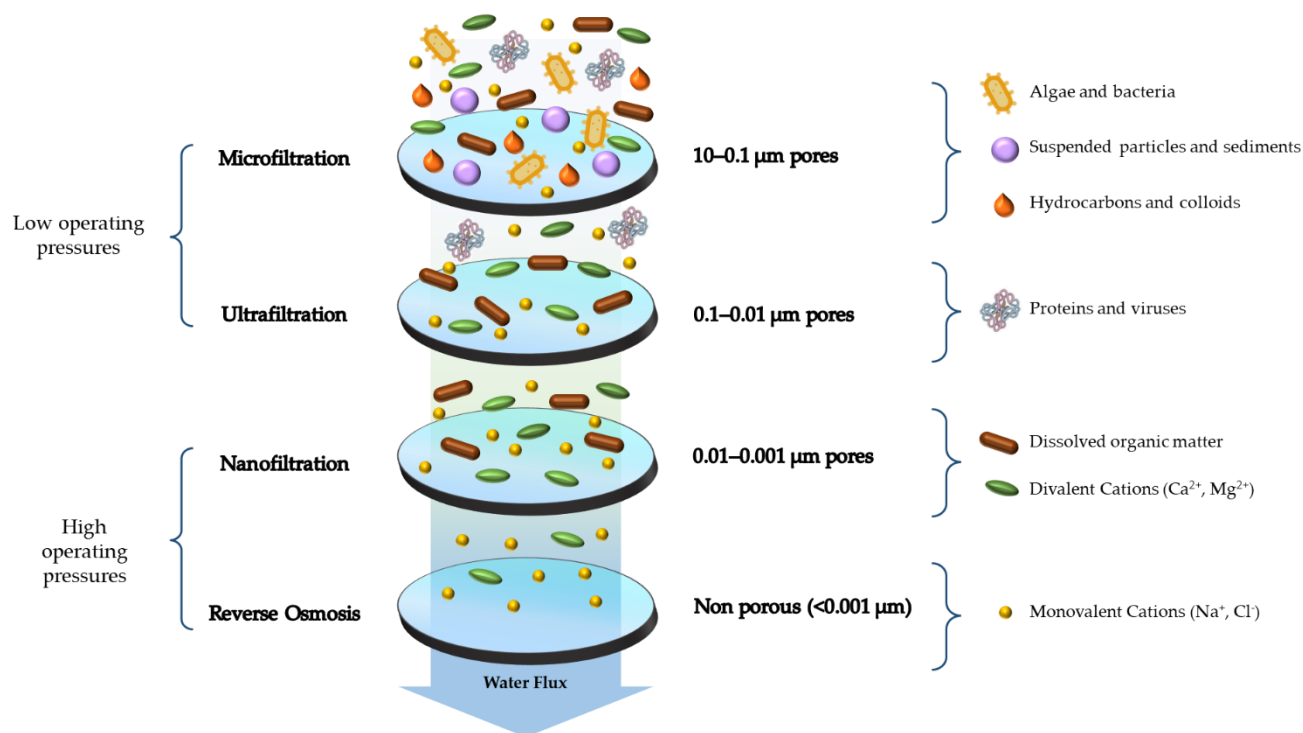


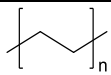
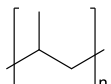
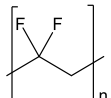
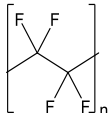
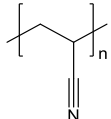
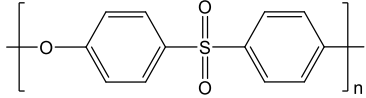
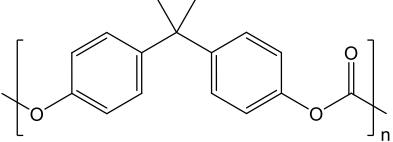
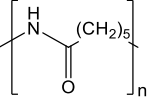
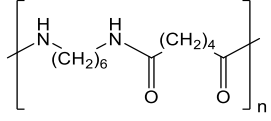
Figure 1.11. An illustration of the relative pollutant retention abilities of various membrane-based filtration techniques [172].

As a matter of fact, a distinction has to be remarked between the so-far employed and complementary “green”, “sustainable”, and “eco-friendly” terms that reflect different aspects of environmentally conscious practices. “Green” is a broad term that generally refers to practices, processes or products that are environmentally friendly with no negative impact on the environment, so far contributing to the conservation of resources, to the reduction of pollution, or to the overall environmental preservation. Likewise, “Eco-friendly” describes products, or processes that are not anymore harmful to the environment, even if they come by the employment of synthetic and harmful reagents. It implies a minimal impact on ecosystems, human health, and the planet, thus contributing to an overall maintaining of a healthy environment, on a local or global scale, and sustainable living practices like recycling. Finally, “Sustainable” refers to something that widely and positively affect the environment, the economy and the society. A sustainable product is one that may be regarded not destructive or detrimental to the environment from the extraction of raw materials required for its manufacturing all the way to the product's end of life. In this regard, sustainable products/processes will not deplete natural resources over the long term, thus emphasizing the balance between present needs of the society and the respect of the environment, without compromising the ability of future generations to safely meet their own needs [176,177].

As a result, most recently researchers are focusing on creating novel membrane filtration techniques that employ biopolymers or eco-friendly gel mix polymers [178–181]. Additionally, it

is now possible to modify the performance of these sustainable membranes, which may differ in some ways from membranes made from fossil-derived polymers in terms of mechanical properties, thermal resistance, and chemical resistance [180,182] thanks to the knowledge of nanotechnology and molecular functionalization [125,183,184].

Table 1.6. Fossil-derived common polymers for usual water filtration membranes [172].

Polymer	Abbreviation	Chemical Structure
Polyethylene	UPE, HDPE	
Polypropylene	PP	
Polyvinylidene fluoride	PVDF	
Polytetrafluoroethylene	PTFE	
Polyacrylonitrile	PAN	
Polyethersulfone	PES	
Polycarbonate	PC	
Nylon 6	Ny6	
Nylon 6,6	Ny6,6	

In this regard, carbon-based, silica-based, or metal-based nanomaterials or sol-gels, as well as nanohybrids and nanocomposites based on various compounds, such as metal or metal oxide nanoparticles, represent a crucial component in the rational design of adsorbent materials or membranes with implemented features and functionality for water remediation and bioremediation [18]. These materials are also helpful in reducing membrane fouling; as a matter of fact, one of the biggest problems in membrane technology efficiency is the fouling [185], caused by substances like bacteria, proteins, inorganic compounds, and other organic molecules [186,187].

In particular, it may be distinguished into reversible and irreversible fouling, which decreases the effectiveness and longevity of membranes in water and wastewater treatment processes and necessitates the use of higher pressures, raising the cost of the filtration process

and consuming more energy [188,189]. Membrane fouling may be identified in a variety of ways, as depicted in Figure 1.12 [190,191].

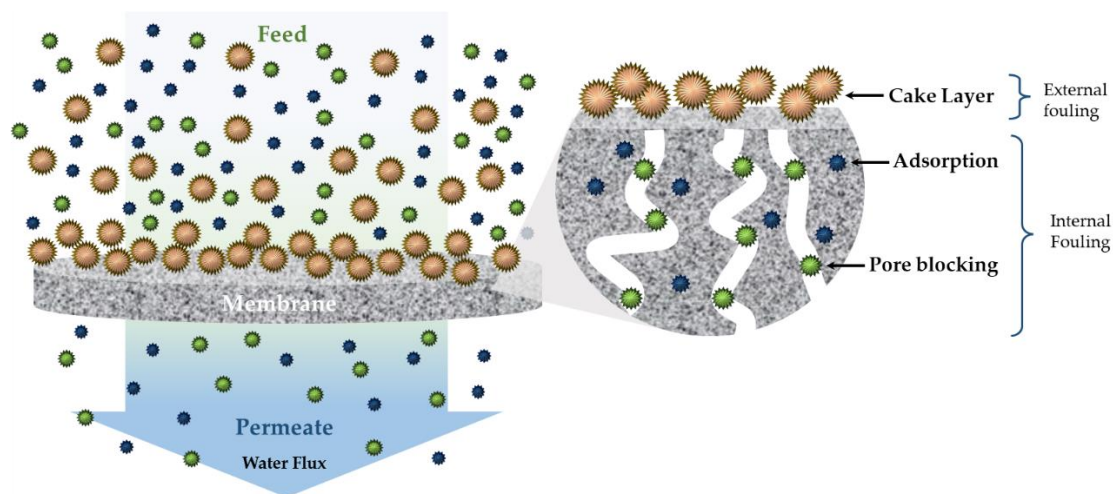


Figure 1.12. Graphical schematization of several membrane fouling types [172].

Smaller-pored membranes, such as those used in reverse osmosis and nanofiltration, are more susceptible to exterior fouling than larger-pored membranes, which are primarily concerned with interior fouling [192,193].

The employment of appropriate antifouling additives for membrane coatings (Figure 1.13) or as useful antifouling/antibacterial fillers, to be added to the blend mixture before the production processes, are some of the developed approaches to contrast fouling [185,194].

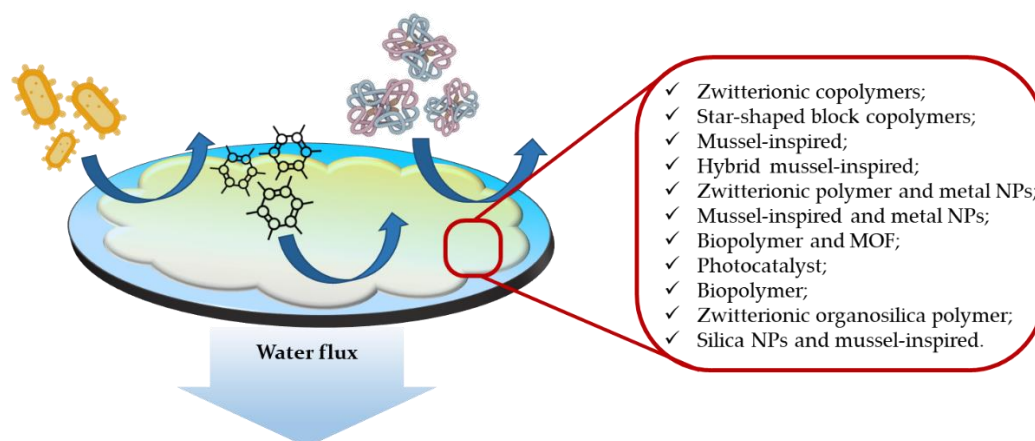


Figure 1.13. Graphical representation of a general antifouling coated membrane for typical water foulants (bacteria, proteins, and other organic molecules), as well as some antifouling functional agents [18,185].

Methods that could aid in finding long-term answers to the challenge mentioned above may take into account the design and the development of advanced sustainable natural/bio-based polymeric blends, doped with opportune active molecules, nanofillers or stimuli-responsive polymers, useful as functional hybrid/mixed matrix (MM) membranes, hybrid/functional coatings or electrospun nanofiber membranes (Figure 1.14).

Some of these approaches are at the basis of the next PhD Thesis Chapters.

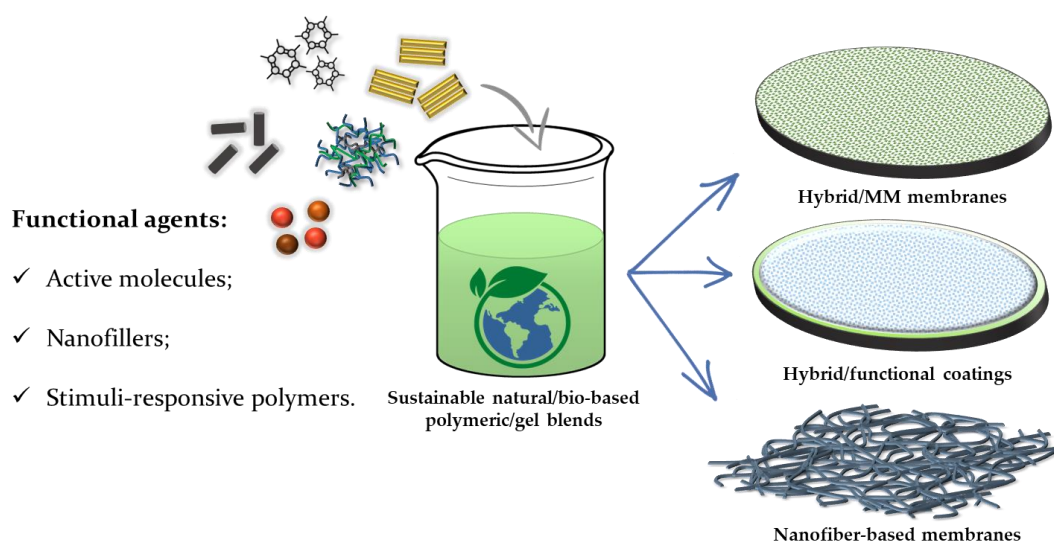


Figure 1.14. Illustration of innovative and environmentally friendly methods for modifying water filtration membranes [172].

1.4. The aim of this PhD thesis

1.4.1 Limits and research gaps of water filtration technologies

Wastewater treatment faces several challenges in dealing with emerging contaminants that are not typically addressed by conventional wastewater treatment processes. Some of the key challenges associated with emerging contaminants in wastewater treatment includes: (i) limited regulatory framework; (ii) analytical detection and monitoring; (iii) treatment technologies; (iv) transformation products; (v) mixtures and synergistic effects between contaminants; (vi) resilience to climate change; (vii) lack of public awareness; (viii) urbanization and population growth.

Addressing these challenges requires a multi-faceted approach involving research, regulatory action, technological innovation, and public awareness. Collaboration between researchers, policymakers, water utilities, and the public is essential to develop sustainable solutions for managing emerging contaminants in wastewater.

On these regards, membrane filtration is a widely used technology for wastewater remediation, but it does have certain limitations and research gaps, whose understanding and identifying is crucial for advancing in this field. Just to mention some, these can be represented by: (i) membrane fouling; (ii) selectivity and flux trade-off; (iii) chemical and biological stability; (iv) energy consumption; (v) costs and scale-up challenges; (vi) membrane material sustainability; (vii) emerging contaminants treatment; (viii) life cycle assessment and cost-benefit.

Moreover, membrane material optimization involves a nuanced understanding of contaminant characteristics, a focus on selectivity and durability, and the development of cost-effective solutions. This comprehensive approach is essential for advancing membrane filtration technologies and making significant strides in the removal of emerging contaminants from water sources, as well as of the so-called “common” pollutants. Closing these research gaps would not only improve the efficiency and effectiveness of membrane filtration for wastewater remediation, but it may also definitely open the way to the development of more sustainable, less expensive and innovative solutions for more inclusive and efficient water treatment.

1.4.2 Innovative approaches, methods and solutions explored in this thesis

On the light of the current wastewater treatment issues and limitations, the continuous advancements in the field of nanotechnology and material sciences represent the necessary skills to maintain a cutting edge in the design and development of environmentally friendly nanostructured membranes for water filtration and smart technologies, bearing enhanced functionalities, specific porosity, selectivity towards water contaminants and recyclability, as reported in this PhD thesis. In particular, since it is possible to combine the properties of nanomaterials with eco-friendly approaches for environmental remediation, new research advances in this field are represented by the development of new innovative nanocomposites and hybrids featuring different functional properties, which can be also easily regenerated and reused so that they do not become a source of waste or secondary pollution.

With this in mind, the rational design of the filtering functional materials led to an implementation of the synthetic procedures that are carried out starting from a selection of (blended) polymeric matrices, such as natural polymers (obtained from renewable sources) or synthetically polymerized engineered (namely, organic, inorganic, hybrid, and composite) materials.

Specific doping nano and micro fillers (inorganic/organic nanoparticles/nanofibers, layered or porous nanomaterials, such as e.g., nanostructured clays) and functional molecules (hydrophobic or hydrophilic compounds, chelating or complexing ligands, catalysts, host/guest macrocyclic systems such as pillararenes) are opportunely selected and stably embedded into the 3D polymeric matrices through chemical-physical interactions.

Finally, the nanostructured porous functional and nanocomposite membranes may be obtained in various shapes through various deposition and synthetic approaches, and fully characterized by a wide series of chemical, physical, mechanical, and morphological techniques. The electrospinning technique is also studied and employed as useful approach to overcome the limits of membrane filtration technology. The use of an innovative electrospinning setup based on a large rotating drum equipped with oscillating carriages, allow to the production of large electrospun nanofiber (composite) membranes eligible as systems to be employed for prototypes development, in view of large-scale applications in real wastewater filtration processes.

The filtration (dead-end), retention and adsorption capabilities of the developed porous functional hybrid materials are tested and studied, in order to assess their potential use for the development of more environmentally friendly and advanced filtering systems, obtained through safe-by-design and rational processes, thus reducing or replacing the traditional non-

renewable water and wastewater filtration devices and overcoming the overmentioned research gaps and limits of wastewater filtration. As a matter of fact, all the developed systems may be suitable for their possible regeneration and reuse for various cycle of filtration/sorption. This feature will be explored in future studies.

More in detail, **Chapter 2, 3 and 4**, respectively, deeply describe the following research studies focused on the development of innovative adsorbent systems, such as:

- Biopolymer based electrospun nanofiber membranes, doped with functional halloysite derivatives;
- Functional waterborne cellulosic-based blends for electrospun nanofiber composite membranes and hybrid magnetic composites;
- Smart host-guest polymeric blend membranes and beads.

This three years' research activity was carried out within the “design and development of smaRt advancEd materials and Sustainable Technologies for wAteR Treatment – RESTART” Industrial PhD project, funded by PON-MIUR “Ricerca e Innovazione 2014-2020”.

Part of the research activities have been performed at the “Centre for Textile Science and Engineering” of the “Department of Materials, Textiles and Chemical Engineering, Faculty of Engineering and Architecture” of Ghent University (Belgium). In particular, this six-month activity involved the development of electrospun nanofiber membranes starting from polymeric blends based on natural or water-soluble polymers, suitably doped with functional and smart organic/inorganic fillers, such as nanostructured clays or micro-structured cellulosic derivatives developed at the ISMN-CNR FunHyMat4Eco lab, c/o the Dep. ChiBioFarAm, Univ. of Messina.

Another part of this research activity, related to the study of advanced filtration techniques for the removal of emerging contaminants from wastewater, including PFAS, has been carried out at EuroD company, Scanzorosciate (BG, Italy). This six-month study was preparatory to the development of filtration membranes functionalized with suitable hybrid organic/inorganic dopants within the RESTART project.

The research activity related to pillar[5]arene-based PDMAEMA/PES blend polymers were carried out at the Dep. ChiBioFarAm, Univ. of Messina, and at the ISMN-CNR FunHyMat4Eco lab.

References

1. Gude, V.G. Desalination and Water Reuse to Address Global Water Scarcity. *Rev. Environ. Sci. Bio/Technology* **2017**, *16*, 591–609, doi:10.1007/s1157-017-9449-7.
2. Ahmed, S.S.; Bali, R.; Khan, H.; Mohamed, H.I.; Sharma, S.K. Improved Water Resource Management Framework for Water Sustainability and Security. *Environ. Res.* **2021**, *201*, 11527, doi:https://doi.org/10.1016/j.envres.2021.11527.
3. Peeters, R.; Vanderschaeghe, H.; Rongé, J.; Martens, J.A. Energy Performance and Climate Dependency of Technologies for Fresh Water Production from Atmospheric Water Vapour. *Environ. Sci. Water Res. Technol.* **2020**, *6*, 2016–2034, doi:10.1039/DoEW00128G.
4. Yang, Z.; Song, J.; Cheng, D.; Xia, J.; Li, Q.; Ahamad, M.I. Comprehensive Evaluation and Scenario Simulation for the Water Resources Carrying Capacity in Xi'an City, China. *J. Environ. Manage.* **2019**, *230*, 221–233, doi:https://doi.org/10.1016/j.jenvman.2018.09.085.
5. Li, P.; Qian, H. Water Resources Research to Support a Sustainable China. *Int. J. Water Resour. Dev.* **2018**, *34*, 327–336, doi:10.1080/07900627.2018.1452723.
6. Wei, J.; Wei, Y.; Western, A. Evolution of the Societal Value of Water Resources for Economic Development versus Environmental Sustainability in Australia from 1843 to 2011. *Glob. Environ. Chang.* **2017**, *42*, 82–92, doi:https://doi.org/10.1016/j.gloenvcha.2016.12.005.
7. Abdel-Shafy, H.I.; Mansour, M.S.M. Solid Waste Issue: Sources, Composition, Disposal, Recycling, and Valorization. *Egypt. J. Pet.* **2018**, *27*, 1275–1290, doi:https://doi.org/10.1016/j.ejpe.2018.07.003.
8. Wu, C.-Y.; Hu, M.-C.; Ni, F.-C. Supporting a Circular Economy: Insights from Taiwan's Plastic Waste Sector and Lessons for Developing Countries. *Sustain. Prod. Consum.* **2021**, *26*, 228–238, doi:https://doi.org/10.1016/j.spc.2020.10.009.
9. Sverko Grdic, Z.; Krstinic Nizic, M.; Rudan, E. Circular Economy Concept in the Context of Economic Development in EU Countries. *Sustainability* **2020**, *12*.
10. Anderson, J. The Environmental Benefits of Water Recycling and Reuse. *Water Supply* **2003**, *3*, 1–10, doi:10.2166/ws.2003.0041.
11. Jia, Z.; Cai, Y.; Chen, Y.; Zeng, W. Regionalization of Water Environmental Carrying Capacity for Supporting the Sustainable Water Resources Management and Development in China. *Resour. Conserv. Recycl.* **2018**, *134*, 282–293, doi:https://doi.org/10.1016/j.resconrec.2018.03.030.
12. Howe, C.W. The Effects of Water Resource Development on Economic Growth: The Conditions for Success. In *Water in a Developing World*; Routledge, 2019; pp. 202–218 ISBN 0429267274.
13. Del Borghi, A.; Moreschi, L.; Gallo, M. Circular Economy Approach to Reduce Water–Energy–Food Nexus. *Curr. Opin. Environ. Sci. Heal.* **2020**, *13*, 23–28, doi:https://doi.org/10.1016/j.coesh.2019.10.002.
14. Goel, P.K. *Water Pollution: Causes, Effects and Control*; New age international, 2006; ISBN 8122418392.
15. Rathi, B.S.; Kumar, P.S.; Show, P.-L. A Review on Effective Removal of Emerging Contaminants from Aquatic Systems: Current Trends and Scope for Further Research. *J. Hazard. Mater.* **2021**, *409*, 124413.
16. Morin-Crini, N.; Lichtfouse, E.; Fourmentin, M.; Ribeiro, A.R.L.; Noutsopoulos, C.; Mapelli, F.; Fenyvesi, É.; Vieira, M.G.A.; Picos-Corrales, L.A.; Moreno-Piraján, J.C.; et al. Removal of Emerging Contaminants from Wastewater Using Advanced Treatments. A Review. *Environ. Chem. Lett.* **2022**, *20*, 1333–1375, doi:10.1007/s10311-021-01379-5.
17. Valdez-Carrillo, M.; Abrell, L.; Ramírez-Hernández, J.; Reyes-López, J.A.; Carreón-Diazconti, C. Pharmaceuticals as Emerging Contaminants in the Aquatic Environment of Latin America: A Review. *Environ. Sci. Pollut. Res.* **2020**, *27*, 44863–44891.
18. Rando, G.; Sfamini, S.; Galletta, M.; Drommi, D.; Cappello, S.; Plutino, M.R. Functional Nanohybrids and Nanocomposites Development for the Removal of Environmental Pollutants and Bioremediation. *Mol.* **2022**, *27*.
19. Gavrilesco, M.; Demnerová, K.; Aamand, J.; Agathos, S.; Fava, F. Emerging Pollutants in the Environment: Present and Future Challenges in Biomonitoring, Ecological Risks and Bioremediation. *N. Biotechnol.* **2015**, *32*, 147–156, doi:10.1016/j.nbt.2014.01.001.
20. Vareda, J.P.; Valente, A.J.M.; Durães, L. Assessment of Heavy Metal Pollution from Anthropogenic Activities and Remediation Strategies: A Review. *J. Environ. Manage.* **2019**, *246*, 101–118, doi:https://doi.org/10.1016/j.jenvman.2019.05.126.
21. Hu, Q.-H.; Weng, J.-Q.; Wang, J.-S. Sources of Anthropogenic Radionuclides in the Environment: A Review. *J. Environ. Radioact.* **2010**, *101*, 426–437, doi:https://doi.org/10.1016/j.jenvrad.2008.08.004.
22. Bungau, S.; Behl, T.; Aleya, L.; Bourgeade, P.; Aloui-Sossé, B.; Purza, A.L.; Abid, A.; Samuel, A.D. Expatriating the Impact of Anthropogenic Aspects and Climatic Factors on Long-Term Soil Monitoring and Management. *Environ. Sci. Pollut. Res.* **2021**, *28*, 30528–30550, doi:10.1007/s11356-021-14127-7.
23. Paxéus, N.; Robinson, P.; Balmér, P. Study of Organic Pollutants in Municipal Wastewater in Göteborg, Sweden. *Water Sci. Technol.* **1992**, *25*, 249–256, doi:10.2166/wst.1992.0299.
24. Mastrangelo, G.; Fadda, E.; Marzia, V. Polycyclic Aromatic Hydrocarbons and Cancer in Man. *Environ. Health Perspect.* **1996**, *104*, 1166–1170, doi:10.1289/ehp.961041166.
25. Sun, J.-L.; Zeng, H.; Ni, H.-G. Halogenated Polycyclic Aromatic Hydrocarbons in the Environment. *Chemosphere* **2013**, *90*, 1751–1759, doi:https://doi.org/10.1016/j.chemosphere.2012.10.094.
26. Hites, R.A. Dioxins: An Overview and History. *Environ. Sci. Technol.* **2011**, *45*, 16–20, doi:10.1021/es1013664.
27. Zhao, Y.; Lin, S.; Choi, J.-W.; Bediako, J.K.; Song, M.-H.; Kim, J.-A.; Cho, C.-W.; Yun, Y.-S. Prediction of Adsorption Properties for Ionic and Neutral Pharmaceuticals and Pharmaceutical Intermediates on Activated Charcoal from Aqueous Solution via LFER Model. *Chem. Eng. J.* **2019**, *362*, 199–206, doi:https://doi.org/10.1016/j.cej.2019.01.031.

28. Sun, B.; Guan, X.; Fang, J.; Tratnyek, P.G. Activation of Manganese Oxidants with Bisulfite for Enhanced Oxidation of Organic Contaminants: The Involvement of Mn(III). *Environ. Sci. Technol.* **2015**, *49*, 12414–12421, doi:10.1021/acs.est.5b03111.
29. Eriksson, J.; Rahm, S.; Green, N.; Bergman, Å.; Jakobsson, E. Photochemical Transformations of Tetrabromobisphenol A and Related Phenols in Water. *Chemosphere* **2004**, *54*, 117–126, doi:https://doi.org/10.1016/S0045-6535(03)00704-5.
30. Idowu, G.A.; David, T.L.; Idowu, A.M. Polycarbonate Plastic Monomer (Bisphenol-A) as Emerging Contaminant in Nigeria: Levels in Selected Rivers, Sediments, Well Waters and Dumpsites. *Mar. Pollut. Bull.* **2022**, *176*, 113444, doi:https://doi.org/10.1016/j.marpolbul.2022.113444.
31. Motamedi, M.; Yerushalmi, L.; Haghghat, F.; Chen, Z. A Critical Review of Water Contamination by Polybrominated Diphenyl Ethers (PBDE) and Main Degradation Techniques. *J. Environ. Chem. Eng.* **2022**, *10*, 108196, doi:https://doi.org/10.1016/j.jece.2022.108196.
32. Gaskin, S.; Soole, K.; Bentham, R. Screening of Australian Native Grasses for Rhizoremediation of Aliphatic Hydrocarbon-Contaminated Soil. *Int. J. Phytoremediation* **2008**, *10*, 378–389, doi:10.1080/15226510802100465.
33. Rana, A.K.; Mishra, Y.K.; Gupta, V.K.; Thakur, V.K. Sustainable Materials in the Removal of Pesticides from Contaminated Water: Perspective on Macro to Nanoscale Cellulose. *Sci. Total Environ.* **2021**, *797*, 149129, doi:https://doi.org/10.1016/j.scitotenv.2021.149129.
34. Bonora, S.; Benassi, E.; Maris, A.; Tugnoli, V.; Ottani, S.; Di Foggia, M. Raman and SERS Study on Atrazine, Prometryn and Simetryn Triazine Herbicides. *J. Mol. Struct.* **2013**, *1040*, 139–148, doi:https://doi.org/10.1016/j.molstruc.2013.02.025.
35. Tkaczyk, A.; Mitrowska, K.; Posyniak, A. Synthetic Organic Dyes as Contaminants of the Aquatic Environment and Their Implications for Ecosystems: A Review. *Sci. Total Environ.* **2020**, *717*.
36. Zuccato, E.; Castiglioni, S.; Fanelli, R. Identification of the Pharmaceuticals for Human Use Contaminating the Italian Aquatic Environment. *J. Hazard. Mater.* **2005**, *122*, 205–209, doi:https://doi.org/10.1016/j.jhazmat.2005.03.001.
37. Zhang, W.; Zhang, D.; Liang, Y. Nanotechnology in Remediation of Water Contaminated by Poly- and Perfluoroalkyl Substances: A Review. *Environ. Pollut.* **2019**, *247*, 266–276, doi:https://doi.org/10.1016/j.envpol.2019.01.045.
38. Xiang, Y.; Jiang, L.; Zhou, Y.; Luo, Z.; Zhi, D.; Yang, J.; Lam, S.S. Microplastics and Environmental Pollutants: Key Interaction and Toxicology in Aquatic and Soil Environments. *J. Hazard. Mater.* **2022**, *422*, 126843, doi:https://doi.org/10.1016/j.jhazmat.2021.126843.
39. Shahedi, A.; Darban, A.K.; Taghipour, F.; Jamshidi-Zanjani, A. A Review on Industrial Wastewater Treatment via Electrocoagulation Processes. *Curr. Opin. Electrochem.* **2020**, *22*, 154–169, doi:https://doi.org/10.1016/j.coelec.2020.05.009.
40. Badawi, A.K.; Abd Elkodous, M.; Ali, G.A.M. Recent Advances in Dye and Metal Ion Removal Using Efficient Adsorbents and Novel Nano-Based Materials: An Overview. *RSC Adv.* **2021**, *11*, 36528–36553, doi:10.1039/D1RA06892J.
41. Lemming, G.; Chambon, J.C.; Binning, P.J.; Bjerg, P.L. Is There an Environmental Benefit from Remediation of a Contaminated Site? Combined Assessments of the Risk Reduction and Life Cycle Impact of Remediation. *J. Environ. Manage.* **2012**, *112*, 392–403, doi:https://doi.org/10.1016/j.jenvman.2012.08.002.
42. Lu, H.; Wang, J.; Stoller, M.; Wang, T.; Bao, Y.; Hao, H. An Overview of Nanomaterials for Water and Wastewater Treatment. *Adv. Mater. Sci. Eng.* **2016**, *2016*.
43. Santhosh, C.; Velmurugan, V.; Jacob, G.; Jeong, S.K.; Grace, A.N.; Bhatnagar, A. Role of Nanomaterials in Water Treatment Applications: A Review. *Chem. Eng. J.* **2016**, *306*, 1116–1137.
44. Dontsova, T.A.; Nahiriak, S. V; Astrelin, I.M. Metaloxide Nanomaterials and Nanocomposites of Ecological Purpose. *J. Nanomater.* **2019**, *2019*, 1–31.
45. Saleh, T.A. Nanomaterials: Classification, Properties, and Environmental Toxicities. *Environ. Technol. Innov.* **2020**, *20*, 101067, doi:https://doi.org/10.1016/j.eti.2020.101067.
46. Descalzo, A.B.; Martínez-Máñez, R.; Sancenón, F.; Hoffmann, K.; Rurack, K. The Supramolecular Chemistry of Organic-Inorganic Hybrid Materials. *Angew. Chemie Int. Ed.* **2006**, *45*, 5924–5948, doi:https://doi.org/10.1002/anie.200600734.
47. Kicelbick, G. *Hybrid Materials: Synthesis, Characterization, and Applications*; John Wiley & Sons, 2007; ISBN 3527610480.
48. Makisima, A. Possibility of Hybrids Materials, Ceramic Japan. **2004**.
49. Iurzhenko, M. Electrical, Thermomechanical and Sorption Properties of Hybrid Organic-Inorganic Systems Based on Urethane Oligomers and Silicates 2009.
50. García-Martínez, J.-M.; Collar, E.P. Organic-Inorganic Hybrid Materials. *Polymers (Basel)*. **2020**, *13*, 86.
51. Trovato, V.; Colleoni, C.; Castellano, A.; Plutino, M.R. The Key Role of 3-Glycidoxypropyltrimethoxysilane Sol-Gel Precursor in the Development of Wearable Sensors for Health Monitoring. *J. Sol-Gel Sci. Technol.* **2018**, *87*, 27–40, doi:10.1007/s10971-018-4695-x.
52. Ucanus, G.; Ercan, M.; Uzunoglu, D.; Culha, M. Methods for Preparation of Nanocomposites in Environmental Remediation. In *New Polymer Nanocomposites for Environmental Remediation*; Elsevier, 2018; pp. 1–28.
53. Szczepek, B. Photocatalytic Degradation of Organic Contaminants over Clay-TiO₂ Nanocomposites: A Review. *Appl. Clay Sci.* **2017**, *141*, 227–239.
54. Slavin, Y.N.; Asnis, J.; Hñfeli, U.O.; Bach, H. Metal Nanoparticles: Understanding the Mechanisms behind Antibacterial Activity. *J. Nanobiotechnology* **2017**, *15*, 1–20.
55. Kelly, K.L.; Coronado, E.; Zhao, L.L.; Schatz, G.C. The Optical Properties of Metal Nanoparticles: The Influence of Size, Shape, and Dielectric Environment. *J. Phys. Chem. B* **2003**, *107*, 668–677, doi:10.1021/jp026731y.
56. Doria, G.; Conde, J.; Veigas, B.; Giestas, L.; Almeida, C.; Assunção, M.; Rosa, J.; Baptista, P. V Noble Metal Nanoparticles for Biosensing Applications. *Sensors* **2012**, *12*, 1657–1687.
57. Cuenya, B.R. Synthesis and Catalytic Properties of Metal Nanoparticles: Size, Shape, Support, Composition, and

- Oxidation State Effects. *Thin Solid Films* **2010**, *518*, 3127–3150.
58. AbouElmaaty, T.; Abdeldayem, S.A.; Ramadan, S.M.; Sayed-Ahmed, K.; Plutino, M.R. Coloration and Multi-Functionalization of Polypropylene Fabrics with Selenium Nanoparticles. *Polymers (Basel)*. **2021**, *13*.
 59. Cook, S.M. Assessing the Use and Application of Zero-Valent Iron Nanoparticle Technology for Remediation at Contaminated Sites. *Jackson State Univ.* **2009**.
 60. Jamkhande, P.G.; Ghule, N.W.; Bamer, A.H.; Kalaskar, M.G. Metal Nanoparticles Synthesis: An Overview on Methods of Preparation, Advantages and Disadvantages, and Applications. *J. Drug Deliv. Sci. Technol.* **2019**, *53*, 101174, doi:10.1016/j.jddst.2019.101174.
 61. Annamalai, A.; Christina, V.L.P.; Sudha, D.; Kalpana, M.; Lakshmi, P.T. V Green Synthesis, Characterization and Antimicrobial Activity of Au NPs Using Euphorbia Hirta L. Leaf Extract. *Colloids Surfaces B Biointerfaces* **2013**, *108*, 60–65.
 62. Hanemann, T.; Szabó, D.V. Polymer-Nanoparticle Composites: From Synthesis to Modern Applications. *Materials (Basel)*. **2010**, *3*, 3468–3517.
 63. Li, J.; Zhang, D.; Ni, X.; Zheng, H.; Zhang, Q. Excellent Hydrophilic and Anti-Bacterial Fouling PVDF Membrane Based on Ag Nanoparticle Self-Assembled PCBMA Polymer Brush. *Chinese J. Polym. Sci.* **2017**, *35*, 809–822.
 64. Nechifor, G.; Păncescu, F.M.; Grosu, A.R.; Albu, P.C.; Oprea, O.; Tanczos, S.-K.; Bungău, C.; Grosu, V.-A.; Pîrțac, A.; Nechifor, A.C. Osmium Nanoparticles-Polypropylene Hollow Fiber Membranes Applied in Redox Processes. *Nanomaterials* **2021**, *11*, 2526.
 65. Yang, J.; Wang, X.; Chen, Y.; Dai, J.; Sun, S. Enhanced Photocatalytic Activities of Visible-Light Driven Green Synthesis in Water and Environmental Remediation on Au/Bi₂WO₆ Hybrid Nanostructures. *RSC Adv.* **2015**, *5*, 9771–9782.
 66. Wali, L.A.; Alwan, A.M.; Dheyab, A.B.; Hashim, D.A. Excellent Fabrication of Pd-Ag NPs/PSi Photocatalyst Based on Bimetallic Nanoparticles for Improving Methylene Blue Photocatalytic Degradation. *Optik (Stuttg)*. **2019**, *179*, 708–717.
 67. Ajmal, M.; Demirci, S.; Siddiq, M.; Aktas, N.; Sahiner, N. Simultaneous Catalytic Degradation/Reduction of Multiple Organic Compounds by Modifiable p (Methacrylic Acid-Co-Acrylonitrile)-M (M: Cu, Co) Microgel Catalyst Composites. *New J. Chem.* **2016**, *40*, 1485–1496.
 68. Zhu, Y.; Fan, L.; Yang, B.; Du, J. Multifunctional Homopolymer Vesicles for Facile Immobilization of Gold Nanoparticles and Effective Water Remediation. *ACS Nano* **2014**, *8*, 5022–5031.
 69. Ali, A.; Haq, I.U.; Akhtar, J.; Sher, M.; Ahmed, N.; Zia, M. Synthesis of Ag-NPs Impregnated Cellulose Composite Material: Its Possible Role in Wound Healing and Photocatalysis. *IET nanobiotechnology* **2017**, *11*, 477–484.
 70. Abdullah; Hussain, T.; Faisal, S.; Rizwan, M.; Saira; Zaman, N.; Iqbal, M.; Iqbal, A.; Ali, Z. Green Synthesis and Characterization of Copper and Nickel Hybrid Nanomaterials: Investigation of Their Biological and Photocatalytic Potential for the Removal of Organic Crystal Violet Dye. *J. Saudi Chem. Soc.* **2022**, *26*, 101486, doi:https://doi.org/10.1016/j.jscs.2022.101486.
 71. Pandey, S.; Son, N.; Kang, M. Synergistic Sorption Performance of Karaya Gum Crosslink Poly(Acrylamide-Co-Acrylonitrile) @ Metal Nanoparticle for Organic Pollutants. *Int. J. Biol. Macromol.* **2022**, *210*, 300–314, doi:https://doi.org/10.1016/j.ijbiomac.2022.05.019.
 72. Nechifor, A.C.; Cotorcea, S.; Bungău, C.; Albu, P.C.; Pașcu, D.; Oprea, O.; Grosu, A.R.; Pîrțac, A.; Nechifor, G. Removing of the Sulfur Compounds by Impregnated Polypropylene Fibers with Silver Nanoparticles-Cellulose Derivatives for Air Odor Correction. *Membranes (Basel)*. **2021**, *11*, 256.
 73. Kang, Y.; Li, L.; Chen, W.; Zhang, F.; Du, Y.; Wu, T. Rapid in Situ SERS Analysis of Pesticide Residues on Plant Surfaces Based on Micelle Extraction of Targets and Stabilization of Ag Nanoparticle Aggregates. *Food Anal. Methods* **2018**, *11*, 3161–3169.
 74. Gnanaprakasam, P.; Jeena, S.E.; Premnath, D.; Selvaraju, T. Simple and Robust Green Synthesis of Au NPs on Reduced Graphene Oxide for the Simultaneous Detection of Toxic Heavy Metal Ions and Bioremediation Using Bacterium as the Scavenger. *Electroanalysis* **2016**, *28*, 1885–1893.
 75. Sun, Z.; Zhang, Y.; Guo, S.; Shi, J.; Shi, C.; Qu, K.; Qi, H.; Huang, Z.; Murugadoss, V.; Huang, M.; et al. Confining FeNi Nanoparticles in Biomass-Derived Carbon for Effectively Photo-Fenton Catalytic Reaction for Polluted Water Treatment. *Adv. Compos. Hybrid Mater.* **2022**, doi:10.1007/s42114-022-00477-4.
 76. Boruah, P.K.; Yadav, A.; Das, M.R. Magnetic Mixed Metal Oxide Nanomaterials Derived from Industrial Waste and Its Photocatalytic Applications in Environmental Remediation. *J. Environ. Chem. Eng.* **2020**, *8*, 104297.
 77. Theerthagiri, J.; Chandrasekaran, S.; Salla, S.; Elakkiya, V.; Senthil, R.A.; Nithyadharseni, P.; Maiyalagan, T.; Micheal, K.; Ayeshamariam, A.; Arasu, M.V. Recent Developments of Metal Oxide Based Heterostructures for Photocatalytic Applications towards Environmental Remediation. *J. Solid State Chem.* **2018**, *267*, 35–52.
 78. Cumbal, L.; Greenleaf, J.; Leun, D.; SenGupta, A.K. Polymer Supported Inorganic Nanoparticles: Characterization and Environmental Applications. *React. Funct. Polym.* **2003**, *54*, 167–180, doi:https://doi.org/10.1016/S1381-5148(02)00192-X.
 79. Ali, N.; Zaman, H.; Bilal, M.; Shah, A.-H.A.; Nazir, M.S.; Iqbal, H.M.N. Environmental Perspectives of Interfacially Active and Magnetically Recoverable Composite Materials – A Review. *Sci. Total Environ.* **2019**, *670*, 523–538, doi:https://doi.org/10.1016/j.scitotenv.2019.03.209.
 80. Zhang, W.; Zhang, G.; Liu, C.; Li, J.; Zheng, T.; Ma, J.; Wang, L.; Jiang, J.; Zhai, X. Enhanced Removal of Arsenite and Arsenate by a Multifunctional Fe-Ti-Mn Composite Oxide: Photooxidation, Oxidation and Adsorption. *Water Res.* **2018**, *147*, 264–275, doi:https://doi.org/10.1016/j.watres.2018.10.001.
 81. Rasaki, S.A.; Zhang, B.; Liu, S.; Thomas, T.; Yang, M. Nanourchin ZnO@TiCN Composites for Cr (VI) Adsorption and Thermochemical Remediation. *J. Environ. Chem. Eng.* **2018**, *6*, 3837–3848, doi:https://doi.org/10.1016/j.jece.2018.05.040.
 82. Barakat, M.A.; Ramadan, M.H.; Alghamdi, M.A.; Algarny, S.S.; Woodcock, H.L.; Kuhn, J.N. Remediation of Cu(II), Ni(II), and Cr(III) Ions from Simulated Wastewater by Dendrimer/Titania Composites. *J. Environ. Manage.* **2013**, *117*, 50–57,

- doi:<https://doi.org/10.1016/j.jenvman.2012.12.025>.
83. Wan, S.; Ding, W.; Wang, Y.; Wu, J.; Gu, Y.; He, F. Manganese Oxide Nanoparticles Impregnated Graphene Oxide Aggregates for Cadmium and Copper Remediation. *Chem. Eng. J.* **2018**, *350*, 1135–1143, doi:<https://doi.org/10.1016/j.cej.2018.06.068>.
84. Karthikeyan, P.; Meenakshi, S. In Situ Fabrication of Magnetic Particles Decorated Biopolymeric Composite Beads for the Selective Remediation of Phosphate and Nitrate from Aqueous Medium. *J. Environ. Chem. Eng.* **2020**, *8*, 103530, doi:<https://doi.org/10.1016/j.jece.2019.103530>.
85. He, S.; Zhong, L.; Duan, J.; Feng, Y.; Yang, B.; Yang, L. Bioremediation of Wastewater by Iron Oxide-Biochar Nanocomposites Loaded with Photosynthetic Bacteria. *Front. Microbiol.* **2017**, *8*.
86. Djellabi, R.; Yang, B.; Adeel Sharif, H.M.; Zhang, J.; Ali, J.; Zhao, X. Sustainable and Easy Recoverable Magnetic TiO₂-Lignocellulosic Biomass@Fe₃O₄ for Solar Photocatalytic Water Remediation. *J. Clean. Prod.* **2019**, *233*, 841–847, doi:<https://doi.org/10.1016/j.jclepro.2019.06.125>.
87. Nechifor, G.; Păncescu, F.M.; Albu, P.C.; Grosu, A.R.; Oprea, O.; Tanczos, S.-K.; Bungău, C.; Grosu, V.-A.; Ioan, M.-R.; Nechifor, A.C. Transport and Separation of the Silver Ion with Decanol Liquid Membranes Based on Undecylenic Acid, Undecenol and Magnetic Nanoparticles. *Membranes (Basel)* **2021**, *11*.
88. Nechifor, A.C.; Goran, A.; Grosu, V.-A.; Bungău, C.; Albu, P.C.; Grosu, A.R.; Oprea, O.; Păncescu, F.M.; Nechifor, G. Improving the Performance of Composite Hollow Fiber Membranes with Magnetic Field Generated Convection Application on PH Correction. *Membranes (Basel)* **2021**, *11*.
89. Lincy, A.; Jegathambal, P.; Mkandawire, M.; MacQuarrie, S. Nano Bioremediation of Textile Dye Effluent Using Magnetite Nanoparticles Encapsulated Alginate Beads. *J. Environ. Treat. Tech* **2020**, *8*, 936–946.
90. Pavia-Sanders, A.; Zhang, S.; Flores, J.A.; Sanders, J.E.; Raymond, J.E.; Wooley, K.L. Robust Magnetic/Polymer Hybrid Nanoparticles Designed for Crude Oil Entrapment and Recovery in Aqueous Environments. *ACS Nano* **2013**, *7*, 7552–7561, doi:[10.1021/nn401541e](https://doi.org/10.1021/nn401541e).
91. Rangel-Muñoz, N.; González-Barríos, A.F.; Pradilla, D.; Osmá, J.F.; Cruz, J.C. Novel Bionanocompounds: Outer Membrane Protein A and Laccase Co-Immobilized on Magnetite Nanoparticles for Produced Water Treatment. *Nanomaterials* **2020**, *10*.
92. Américo-Pinheiro, J.H.P.; Paschoa, C.V.M.; Salomão, G.R.; Cruz, I.A.; Isique, W.D.; Ferreira, L.F.R.; Sher, F.; Torres, N.H.; Kumar, V.; Pinheiro, R.S.B. Adsorptive Remediation of Naproxen from Water Using In-House Developed Hybrid Material Functionalized with Iron Oxide. *Chemosphere* **2022**, *289*, 133222, doi:<https://doi.org/10.1016/j.chemosphere.2021.133222>.
93. Ansari, M.J.; Jasim, S.A.; Bokov, D.O.; Thangavelu, L.; Yasin, G.; Khalaji, A.D. Preparation of New Bio-Based Chitosan/Fe₂O₃/NiFe₂O₄ as an Efficient Removal of Methyl Green from Aqueous Solution. *Int. J. Biol. Macromol.* **2022**, *198*, 128–134, doi:<https://doi.org/10.1016/j.ijbiomac.2021.12.082>.
94. Gelaw, T.B.; Sarojini, B.K.; Kodoth, A.K. Chitosan/Hydroxyethyl Cellulose Gel Immobilized Polyaniline/CuO/ZnO Adsorptive-Photocatalytic Hybrid Nanocomposite for Congo Red Removal. *J. Polym. Environ.* **2022**, doi:[10.1007/s10924-022-02492-4](https://doi.org/10.1007/s10924-022-02492-4).
95. He, Y.; Zhang, N.; Gong, Q.; Li, Z.; Gao, J.; Qiu, H. Metal Nanoparticles Supported Graphene Oxide 3D Porous Monoliths and Their Excellent Catalytic Activity. *Mater. Chem. Phys.* **2012**, *134*, 585–589.
96. Wang, J.; Wang, S. Preparation, Modification and Environmental Application of Biochar: A Review. *J. Clean. Prod.* **2019**, *227*, 1002–1022.
97. Zhu, K.; Chen, C. Chapter 6 - Application of NZVI and Its Composites into the Treatment of Toxic/Radioactive Metal Ions. In *Emerging Natural and Tailored Nanomaterials for Radioactive Waste Treatment and Environmental Remediation*; Chen, C.B.T.-I.S. and T., Ed.; Elsevier, 2019; Vol. 29, pp. 281–330 ISBN 1573-4285.
98. Lv, Y.; Huang, S.; Huang, G.; Liu, Y.; Yang, G.; Lin, C.; Xiao, G.; Wang, Y.; Liu, M. Remediation of Organic Arsenic Contaminants with Heterogeneous Fenton Process Mediated by SiO₂-Coated Nano Zero-Valent Iron. *Environ. Sci. Pollut. Res.* **2020**, *27*, 12017–12029, doi:[10.1007/s11356-020-07808-2](https://doi.org/10.1007/s11356-020-07808-2).
99. Yıldırım, G.M.; Bayrak, B. The Synthesis of Biochar-Supported Nano Zero-Valent Iron Composite and Its Adsorption Performance in Removal of Malachite Green. *Biomass Convers. Biorefinery* **2022**, *12*, 4785–4797, doi:[10.1007/s13399-021-01501-1](https://doi.org/10.1007/s13399-021-01501-1).
100. Lyu, H.; Tang, J.; Cui, M.; Gao, B.; Shen, B. Biochar/Iron (BC/Fe) Composites for Soil and Groundwater Remediation: Synthesis, Applications, and Mechanisms. *Chemosphere* **2020**, *246*, 125609.
101. Li, Z.; Wang, L.; Li, Y.; Feng, Y.; Feng, W. Carbon-Based Functional Nanomaterials: Preparation, Properties and Applications. *Compos. Sci. Technol.* **2019**, *179*, 10–40.
102. Xin, Q.; Shah, H.; Nawaz, A.; Xie, W.; Akram, M.Z.; Batool, A.; Tian, L.; Jan, S.U.; Boddula, R.; Guo, B. Antibacterial Carbon-based Nanomaterials. *Adv. Mater.* **2019**, *31*, 1804838.
103. Patel, K.D.; Singh, R.K.; Kim, H.-W. Carbon-Based Nanomaterials as an Emerging Platform for Theranostics. *Mater. Horizons* **2019**, *6*, 434–469.
104. Bayatsarmadi, B.; Zheng, Y.; Vasileff, A.; Qiao, S. Recent Advances in Atomic Metal Doping of Carbon-based Nanomaterials for Energy Conversion. *Small* **2017**, *13*, 1700191.
105. Niu, Z.; Liu, L.; Zhang, L.; Chen, X. Porous Graphene Materials for Water Remediation. *Small* **2014**, *10*, 3434–3441.
106. Weijie, M.; Chongnv, W.; Xuming, P.; Weixin, J.; Yuhang, W.; Benhui, S. TiO₂ Nanoparticles and Multi-Walled Carbon Nanotubes Monitoring and Bioremediation Potential Using Ciliates *Pseudocohnilembus Persalinus*. *Ecotoxicol. Environ. Saf.* **2020**, *187*, 109825.
107. Magrez, A.; Kasas, S.; Salicio, V.; Pasquier, N.; Seo, J.W.; Celio, M.; Catsicas, S.; Schwaller, B.; Forró, L. Cellular Toxicity

- of Carbon-Based Nanomaterials. *Nano Lett.* **2006**, *6*, 1121–1125.
108. Bhattacharya, K.; Mukherjee, S.P.; Gallud, A.; Burkert, S.C.; Bistarelli, S.; Bellucci, S.; Bottini, M.; Star, A.; Fadeel, B. Biological Interactions of Carbon-Based Nanomaterials: From Coronation to Degradation. *Nanomedicine Nanotechnology, Biol. Med.* **2016**, *12*, 333–351.
109. Moura, F.C.C.; Lago, R.M. Catalytic Growth of Carbon Nanotubes and Nanofibers on Vermiculite to Produce Floatable Hydrophobic “Nanosponges” for Oil Spill Remediation. *Appl. Catal. B Environ.* **2009**, *90*, 436–440.
110. Yellappa, M.; Srajan, J.S.; Sarkar, O.; Reddy, Y.V.R.; Mohan, S.V. Modified Conductive Polyaniline–Carbon Nanotube Composite Electrodes for Bioelectricity Generation and Waste Remediation. *Bioresour. Technol.* **2019**, *284*, 148–154.
111. Khan, N.; Anwer, A.H.; Ahmad, A.; Sabir, S.; Sevda, S.; Khan, M.Z. Investigation of CNT/PPy-Modified Carbon Paper Electrodes under Anaerobic and Aerobic Conditions for Phenol Bioremediation in Microbial Fuel Cells. *ACS omega* **2019**, *5*, 471–480.
112. He, C.; Gu, L.; He, H.; Zhang, Z.; Wang, X.; Han, F.; Huang, B.; Pan, X. Dissolved Organic Matter Modified Magnetic Carbon Nanotubes Enhance the Bioremediation of Azo Dyes and Cr (VI). *Environ. Sci. Water Res. Technol.* **2020**, *6*, 1804–1815.
113. Zhou, S.; Jiang, W.; Wang, T.; Lu, Y. Highly Hydrophobic, Compressible, and Magnetic Polystyrene/Fe₃O₄/Graphene Aerogel Composite for Oil–Water Separation. *Ind. Eng. Chem. Res.* **2015**, *54*, 5460–5467.
114. Yaqoob, A.A.; Ibrahim, M.N.M.; Yaakop, A.S.; Umar, K.; Ahmad, A. Modified Graphene Oxide Anode: A Bioinspired Waste Material for Bioremediation of Pb²⁺ with Energy Generation through Microbial Fuel Cells. *Chem. Eng. J.* **2021**, *417*, 128052.
115. Bajpai, A.K.; Dubey, R.; Bajpai, J. Synthesis, Characterization, and Adsorption Properties of a Graphene Composite Sand (GCS) and Its Application in Remediation of Hg (II) Ions. *Water, Air, Soil Pollut.* **2017**, *228*, 1–19.
116. Ahsan, M.A.; Jabbari, V.; Imam, M.A.; Castro, E.; Kim, H.; Curry, M.L.; Valles-Rosales, D.J.; Noveron, J.C. Nanoscale Nickel Metal Organic Framework Decorated over Graphene Oxide and Carbon Nanotubes for Water Remediation. *Sci. Total Environ.* **2020**, *698*, 134214.
117. Kanjwal, M.A.; Lo, K.K.S.; Leung, W.W.-F. Graphene Composite Nanofibers as a High-Performance Photocatalyst for Environmental Remediation. *Sep. Purif. Technol.* **2019**, *215*, 602–611.
118. Bai, H.; Zhou, J.; Zhang, H.; Tang, G. Enhanced Adsorbability and Photocatalytic Activity of TiO₂-Graphene Composite for Polycyclic Aromatic Hydrocarbons Removal in Aqueous Phase. *Colloids Surfaces B Biointerfaces* **2017**, *150*, 68–77.
119. Regulska, E.; Rivera-Nazario, D.M.; Karpinska, J.; Plonska-Brzezinska, M.E.; Echegoyen, L. Zinc Porphyrin-Functionalized Fullerenes for the Sensitization of Titania as a Visible-Light Active Photocatalyst: River Waters and Wastewaters Remediation. *Molecules* **2019**, *24*, 1118.
120. Chen, Y.; Yang, G.; Liu, B.; Kong, H.; Xiong, Z.; Guo, L.; Wei, G. Biomineralization of ZrO₂ Nanoparticles on Graphene Oxide-Supported Peptide/Cellulose Binary Nanofibrous Membranes for High-Performance Removal of Fluoride Ions. *Chem. Eng. J.* **2022**, *430*, 132721, doi:https://doi.org/10.1016/j.cej.2021.132721.
121. Lin, X.; Xu, Q.; Gan, L.; Owens, G.; Chen, Z. Cyclodextrin Modified Green Synthesized Graphene Oxide@iron Nanoparticle Composites for Enhanced Removal of Oxytetracycline. *J. Colloid Interface Sci.* **2022**, *608*, 3159–3167, doi:https://doi.org/10.1016/j.jcis.2021.11.049.
122. Fathy, N.A.; El-Shafey, S. Carbon-Based Nanohybrid Fabricated in-Situ and Boosted the Adsorption of Anionic Reactive Yellow Dye. *Int. J. Environ. Sci. Technol.* **2022**, doi:10.1007/s13762-022-04061-7.
123. Amola, L.A.; Kamgaing, T.; Tiegam Tagne, R.F.; Atemkeng, C.D.; Kuethe, I.-H.T.; Anagho, S.G. Optimized Removal of Hydroquinone and Resorcinol by Activated Carbon Based on Shea Residue (*Vitellaria Paradoxa*): Thermodynamics, Adsorption Mechanism, Nonlinear Kinetics, and Isotherms. *J. Chem.* **2022**, *2022*, 1125877, doi:10.1155/2022/1125877.
124. Razaq, A.; Bibi, F.; Zheng, X.; Papadakis, R.; Jafri, S.H.M.; Li, H. Review on Graphene-, Graphene Oxide-, Reduced Graphene Oxide-Based Flexible Composites: From Fabrication to Applications. *Materials (Basel)*. **2022**, *15*, 1012.
125. Ielo, I.; Giacobello, F.; Sfameni, S.; Rando, G.; Galletta, M.; Trovato, V.; Rosace, G.; Plutino, M.R. Nanostructured Surface Finishing and Coatings with Functional Properties and Applications. *Materials (Basel)*. **2021**, *14*, 1–41, doi:10.3390/ma1412733.
126. Wang, Y.; Pan, C.; Chu, W.; Vipin, A.K.; Sun, L. Environmental Remediation Applications of Carbon Nanotubes and Graphene Oxide: Adsorption and Catalysis. *Nanomaterials* **2019**, *9*, 439.
127. Rao, K.S.; El-Hami, K.; Kodaki, T.; Matsushige, K.; Makino, K. A Novel Method for Synthesis of Silica Nanoparticles. *J. Colloid Interface Sci.* **2005**, *289*, 125–131, doi:https://doi.org/10.1016/j.jcis.2005.02.019.
128. Sfameni, S.; Hadhri, M.; Rando, G.; Drommi, D.; Rosace, G.; Trovato, V.; Plutino, M.R. Inorganic Finishing for Textile Fabrics: Recent Advances in Wear-Resistant, UV Protection and Antimicrobial Treatments. *Inorganics* **2023**, *11*.
129. Trovato, V.; Sfameni, S.; Rando, G.; Rosace, G.; Libertino, S.; Ferri, A.; Plutino, M.R. A Review of Stimuli-Responsive Smart Materials for Wearable Technology in Healthcare: Retrospective, Perspective, and Prospective. *Molecules* **2022**, *27*.
130. Sfameni, S.; Rando, G.; Plutino, M.R. Perspective Chapter: Functional Sol–Gel Based Coatings for Innovative and Sustainable Applications. In: Singh, D.J.P., Acharya, D.S.S., Kumar, D.S., Dixit, D.S.K., Eds.; IntechOpen: Rijeka, 2023; p. Ch. 3 ISBN 978-1-80355-415-0.
131. Möller, K.; Bein, T. Talented Mesoporous Silica Nanoparticles. *Chem. Mater.* **2017**, *29*, 371–388.
132. Guerra, F.D.; Attia, M.F.; Whitehead, D.C.; Alexis, F. Nanotechnology for Environmental Remediation: Materials and Applications. *Molecules* **2018**, *23*, 1760.
133. Singh, B.; Na, J.; Konarova, M.; Wakihara, T.; Yamauchi, Y.; Salomon, C.; Gawande, M.B. Functional Mesoporous Silica Nanomaterials for Catalysis and Environmental Applications. *Bull. Chem. Soc. Jpn.* **2020**, *93*, 1459–1496.
134. Lehman, S.E.; Larsen, S.C. Zeolite and Mesoporous Silica Nanomaterials: Greener Syntheses, Environmental Applications and Biological Toxicity. *Environ. Sci. Nano* **2014**, *1*, 200–213.

135. Boros-Lajszner, E.; Wyszowska, J.; Kucharski, J. Use of Zeolite to Neutralise Nickel in a Soil Environment. *Environ. Monit. Assess.* **2018**, *190*, 1–13.
136. Bergaya, F.; Lagaly, G. Chapter 1 General Introduction: Clays, Clay Minerals, and Clay Science. In: 2006; pp. 1–18.
137. Arora, A.; Padua, G.W. Nanocomposites in Food Packaging. *J. Food Sci.* **2010**, *75*, R43–R49.
138. Raja Beryl, J.; Xavier, J.R. Influence of Silane Functionalized Nanoclay on the Barrier, Mechanical and Hydrophobic Properties by Clay Nanocomposite Films in an Aggressive Chloride Medium. *Colloids Surfaces A Physicochem. Eng. Asp.* **2021**, *630*, 127625, doi:<https://doi.org/10.1016/j.colsurfa.2021.127625>.
139. Kausar, A.; Iqbal, M.; Javed, A.; Aftab, K.; Bhatti, H.N.; Nouren, S. Dyes Adsorption Using Clay and Modified Clay: A Review. *J. Mol. Liq.* **2018**, *256*, 395–407.
140. Carmody, O.; Frost, R.; Xi, Y.; Kokot, S. Adsorption of Hydrocarbons on Organo-Clays—Implications for Oil Spill Remediation. *J. Colloid Interface Sci.* **2007**, *305*, 17–24.
141. Du, L.; Gao, P.; Liu, Y.; Minami, T.; Yu, C. Removal of Cr (VI) from Aqueous Solution by Polypyrrole/Hollow Mesoporous Silica Particles. *Nanomaterials* **2020**, *10*, 686.
142. Tian, M.; Long, Y.; Xu, D.; Wei, S.; Dong, Z. Hollow Mesoporous Silica Nanotubes Modified with Palladium Nanoparticles for Environmental Catalytic Applications. *J. Colloid Interface Sci.* **2018**, *521*, 132–140.
143. Ninwiwek, N.; Hongsawat, P.; Punyapalakul, P.; Prarat, P. Removal of the Antibiotic Sulfamethoxazole from Environmental Water by Mesoporous Silica-Magnetic Graphene Oxide Nanocomposite Technology: Adsorption Characteristics, Coadsorption and Uptake Mechanism. *Colloids Surfaces A Physicochem. Eng. Asp.* **2019**, *580*, 123716.
144. Habimana, P.; Gao, J.; Mwizerwa, J.P.; Ndayambaje, J.B.; Liu, H.; Luan, P.; Ma, L.; Jiang, Y. Improvement of Laccase Activity via Covalent Immobilization over Mesoporous Silica Coated Magnetic Multiwalled Carbon Nanotubes for the Discoloration of Synthetic Dyes. *ACS omega* **2021**, *6*, 2777–2789.
145. Salis, A.; Pisano, M.; Monduzzi, M.; Solinas, V.; Sanjust, E. Laccase from *Pleurotus Sajor-Caju* on Functionalised SBA-15 Mesoporous Silica: Immobilisation and Use for the Oxidation of Phenolic Compounds. *J. Mol. Catal. B Enzym.* **2009**, *58*, 175–180.
146. Kumar, A.P.; Bilehal, D.; Desalegn, T.; Kumar, S.; Ahmed, F.; Murthy, H.C.A.; Kumar, D.; Gupta, G.; Chellappan, D.K.; Singh, S.K. Studies on Synthesis and Characterization of Fe₃O₄@ SiO₂@ Ru Hybrid Magnetic Composites for Reusable Photocatalytic Application. *Adsorpt. Sci. Technol.* **2022**, *2022*, 1–18.
147. Huang, T.; Yan, M.; He, K.; Huang, Z.; Zeng, G.; Chen, A.; Peng, M.; Li, H.; Yuan, L.; Chen, G. Efficient Removal of Methylene Blue from Aqueous Solutions Using Magnetic Graphene Oxide Modified Zeolite. *J. Colloid Interface Sci.* **2019**, *543*, 43–51.
148. Angaru, G.K.R.; Choi, Y.-L.; Lingamdinne, L.P.; Choi, J.-S.; Kim, D.-S.; Koduru, J.R.; Yang, J.-K.; Chang, Y.-Y. Facile Synthesis of Economical Feasible Fly Ash–Based Zeolite–Supported Nano Zerovalent Iron and Nickel Bimetallic Composite for the Potential Removal of Heavy Metals from Industrial Effluents. *Chemosphere* **2021**, *267*, 128889.
149. López, J.G.P.; Pichardo, O.H.G.; Escobar, J.A.P.; del Río, D.A. de H.; Méndez, H.I.; Rodríguez, L.M.G. Photocatalytic Degradation of Metoprolol in Aqueous Medium Using a TiO₂/Natural Zeolite Composite. *Fuel* **2021**, *284*, 119030.
150. Mahmoodi, N.M.; Saffar-Dastgerdi, M.H. Clean Laccase Immobilized Nanobiocatalysts (Graphene Oxide-Zeolite Nanocomposites): From Production to Detailed Biocatalytic Degradation of Organic Pollutant. *Appl. Catal. B Environ.* **2020**, *268*, 118443.
151. McCarthy, D.; Edwards, G.C.; Gustin, M.S.; Care, A.; Miller, M.B.; Sunna, A. An Innovative Approach to Bioremediation of Mercury Contaminated Soils from Industrial Mining Operations. *Chemosphere* **2017**, *184*, 694–699.
152. Ashraf, M.-T.; AlHammadi, A.A.; El-Sherbeeney, A.M.; Alhammadi, S.; Al Zoubi, W.; Ko, Y.G.; Abukhadra, M.R. Synthesis of Cellulose Fibers/Zeolite-A Nanocomposite as an Environmental Adsorbent for Organic and Inorganic Selenium Ions; Characterization and Advanced Equilibrium Studies. *J. Mol. Liq.* **2022**, *360*, 119573, doi:<https://doi.org/10.1016/j.molliq.2022.119573>.
153. Panchal, A.; Swientoniewski, L.T.; Omarova, M.; Yu, T.; Zhang, D.; Blake, D.A.; John, V.; Lvov, Y.M. Bacterial Proliferation on Clay Nanotube Pickering Emulsions for Oil Spill Bioremediation. *Colloids Surfaces B Biointerfaces* **2018**, *164*, 27–33.
154. Viscusi, G.; Lamberti, E.; Gorrasi, G. Design of a Hybrid Bio-Adsorbent Based on Sodium Alginate/Halloysite/Hemp Hurd for Methylene Blue Dye Removal: Kinetic Studies and Mathematical Modeling. *Colloids Surfaces A Physicochem. Eng. Asp.* **2022**, *633*, 127925, doi:<https://doi.org/10.1016/j.colsurfa.2021.127925>.
155. Wu, F.; Pickett, K.; Panchal, A.; Liu, M.; Lvov, Y. Superhydrophobic Polyurethane Foam Coated with Polysiloxane-Modified Clay Nanotubes for Efficient and Recyclable Oil Absorption. *ACS Appl. Mater. Interfaces* **2019**, *11*, 25445–25456.
156. Kundu, S.; Korin Manor, N.; Radian, A. Iron–Montmorillonite–Cyclodextrin Composites as Recyclable Sorbent Catalysts for the Adsorption and Surface Oxidation of Organic Pollutants. *ACS Appl. Mater. Interfaces* **2020**, *12*, 52873–52887.
157. Mehandia, S.; Sharma, S.C.; Arya, S.K. Immobilization of Laccase on Chitosan-Clay Composite Beads to Improve Its Catalytic Efficiency to Degrade Industrial Dyes. *Mater. Today Commun.* **2020**, *25*, 101513.
158. VEDULA, S.S.; YADAV, G.D. Superior Efficacy of Biocomposite Membranes of Chitosan with Montmorillonite and Kaolin vs Pure Chitosan for Removal of Cu(II) from Wastewater. *J. Chem. Sci.* **2022**, *134*, 55, doi:[10.1007/s12039-022-02051-3](https://doi.org/10.1007/s12039-022-02051-3).
159. de Abreu Pereira, V.; dos Santos Paz, I.; Gomes, A.L.; Leite, L.A.; Fechine, P.B.A. Effects of Acid Activation on the Halloysite Nanotubes for Curcumin Incorporation and Release. *Appl. Clay Sci.* **2021**, *200*, 105953.
160. Gkouma, E.; Gianni, E.; Avgoustakis, K.; Papoulis, D. Applications of Halloysite in Tissue Engineering. *Appl. Clay Sci.* **2021**, *214*, 106291.
161. Persano, F.; Gigli, G.; Leporatti, S. Halloysite-Based Nanosystems for Biomedical Applications. *Clays Clay Miner.* **2021**, 1–21.
162. Lazzara, G.; Cavallaro, G.; Panchal, A.; Fakhruddin, R.; Stavitskaya, A.; Vinokurov, V.; Lvov, Y. An Assembly of Organic-

- Inorganic Composites Using Halloysite Clay Nanotubes. *Curr. Opin. Colloid Interface Sci.* **2018**, *35*, 42–50, doi:<https://doi.org/10.1016/j.cocis.2018.01.002>.
163. Lvov, Y.; Panchal, A.; Fu, Y.; Fakhrullin, R.; Kryuchkova, M.; Batasheva, S.; Stavitskaya, A.; Glotov, A.; Vinokurov, V. Interfacial Self-Assembly in Halloysite Nanotube Composites. *Langmuir* **2019**, *35*, 8646–8657.
164. Cavallaro, G.; Lazzara, G.; Rozhina, E.; Konnova, S.; Kryuchkova, M.; Khaertdinov, N.; Fakhrullin, R. Organic-Nanoclay Composite Materials as Removal Agents for Environmental Decontamination. *RSC Adv.* **2019**, *9*, 40553–40564.
165. Al-Tohamy, R.; Ali, S.S.; Li, F.; Okasha, K.M.; Mahmoud, Y.A.-G.; Elsamahy, T.; Jiao, H.; Fu, Y.; Sun, J. A Critical Review on the Treatment of Dye-Containing Wastewater: Ecotoxicological and Health Concerns of Textile Dyes and Possible Remediation Approaches for Environmental Safety. *Ecotoxicol. Environ. Saf.* **2022**, *231*, 113160, doi:<https://doi.org/10.1016/j.ecoenv.2021.113160>.
166. Crini, G.; Lichtfouse, E. Advantages and Disadvantages of Techniques Used for Wastewater Treatment. *Environ. Chem. Lett.* **2019**, *17*, 145–155, doi:[10.1007/s10311-018-0785-9](https://doi.org/10.1007/s10311-018-0785-9).
167. Rout, P.R.; Zhang, T.C.; Bhunia, P.; Surampalli, R.Y. Treatment Technologies for Emerging Contaminants in Wastewater Treatment Plants: A Review. *Sci. Total Environ.* **2021**, *753*, 141990, doi:<https://doi.org/10.1016/j.scitotenv.2020.141990>.
168. Hofs, B.; Ogier, J.; Vries, D.; Beerendonk, E.F.; Cornelissen, E.R. Comparison of Ceramic and Polymeric Membrane Permeability and Fouling Using Surface Water. *Sep. Purif. Technol.* **2011**, *79*, 365–374, doi:<https://doi.org/10.1016/j.seppur.2011.03.025>.
169. Katheresan, V.; Kansedo, J.; Lau, S.Y. Efficiency of Various Recent Wastewater Dye Removal Methods: A Review. *J. Environ. Chem. Eng.* **2018**, *6*, 4676–4697, doi:<https://doi.org/10.1016/j.jece.2018.06.060>.
170. Imbrogno, A.; Schäfer, A.I. Comparative Study of Nanofiltration Membrane Characterization Devices of Different Dimension and Configuration (Cross Flow and Dead End). *J. Memb. Sci.* **2019**, *585*, 67–80, doi:<https://doi.org/10.1016/j.memsci.2019.04.035>.
171. Wang, Q.; Tang, X.; Liang, H.; Cheng, W.; Li, G.; Zhang, Q.; Chen, J.; Chen, K.; Wang, J. Effects of Filtration Mode on the Performance of Gravity-Driven Membrane (GDM) Filtration: Cross-Flow Filtration and Dead-End Filtration. *Water* **2022**, *14*.
172. Rando, G.; Sfameni, S.; Plutino, M.R. Development of Functional Hybrid Polymers and Gel Materials for Sustainable Membrane-Based Water Treatment Technology: How to Combine Greener and Cleaner Approaches. *Gels* **2023**, *9*.
173. Zhang, H.; Wu, A.; Wei, J.; Buschjost, R. Effect of Nanofiltration on Photochemical Integrity. In Proceedings of the Proc.SPIE; April 3 2008; Vol. 6923, p. 69233H.
174. Someya, M.; Higashino, K.; Imoto, Y.; Sakanakura, H.; Yasutaka, T. Effects of Membrane Filter Material and Pore Size on Turbidity and Hazardous Element Concentrations in Soil Batch Leaching Tests. *Chemosphere* **2021**, *265*, 128981, doi:<https://doi.org/10.1016/j.chemosphere.2020.128981>.
175. Galiano, F.; Briceño, K.; Marino, T.; Molino, A.; Christensen, K.V.; Figoli, A. Advances in Biopolymer-Based Membrane Preparation and Applications. *J. Memb. Sci.* **2018**, *564*, 562–586, doi:<https://doi.org/10.1016/j.memsci.2018.07.059>.
176. <https://Sundayandlola.Com/Blogs/News/Whats-the-Difference-between-Green-Sustainable-and-Eco-Friendly>.
177. Rangappa, S.M.; Siengchin, S.; Dhakal, H.N. Green-Composites: Ecofriendly and Sustainability. *Appl. Sci. Eng. Prog.* **2020**, *13*, 183–184.
178. Hardian, R.; Alammar, A.; Holtzl, T.; Szekely, G. Fabrication of Sustainable Organic Solvent Nanofiltration Membranes Using Cellulose–Chitosan Biopolymer Blends. *J. Memb. Sci.* **2022**, *658*, 120743, doi:<https://doi.org/10.1016/j.memsci.2022.120743>.
179. Aji, M.M.; Narendren, S.; Purkait, M.K.; Katiyar, V. Biopolymer (Gum Arabic) Incorporation in Waste Polyvinylchloride Membrane for the Enhancement of Hydrophilicity and Natural Organic Matter Removal in Water. *J. Water Process Eng.* **2020**, *38*, 101569, doi:<https://doi.org/10.1016/j.jwpe.2020.101569>.
180. Udayakumar, G.P.; Muthusamy, S.; Selvaganesh, B.; Sivarajasekar, N.; Rambabu, K.; Sivamani, S.; Sivakumar, N.; Maran, J.P.; Hosseini-Bandegharaei, A. Ecofriendly Biopolymers and Composites: Preparation and Their Applications in Water-Treatment. *Biotechnol. Adv.* **2021**, *52*, 107815, doi:<https://doi.org/10.1016/j.biotechadv.2021.107815>.
181. Dassanayake, R.S.; Acharya, S.; Abidi, N. Recent Advances in Biopolymer-Based Dye Removal Technologies. *Molecules* **2021**, *26*.
182. Mansoori, S.; Davarnejad, R.; Matsuura, T.; Ismail, A.F. Membranes Based on Non-Synthetic (Natural) Polymers for Wastewater Treatment. *Polym. Test.* **2020**, *84*, 106381, doi:<https://doi.org/10.1016/j.polymertesting.2020.106381>.
183. Libertino, S.; Plutino, M.R.; Rosace, G. Design and Development of Wearable Sensing Nanomaterials for Smart Textiles. *AIP Conf. Proc.* **2018**, *1990*, doi:[10.1063/1.5047770](https://doi.org/10.1063/1.5047770).
184. Puoci, F.; Saturnino, C.; Trovato, V.; Iacopetta, D.; Piperopoulos, E.; Triolo, C.; Bonomo, M.G.; Drommi, D.; Parisi, O.I.; Milone, C.; et al. Sol-Gel Treatment of Textiles for the Entrapping of an Antioxidant/Anti-Inflammatory Molecule: Functional Coating Morphological Characterization and Drug Release Evaluation. *Appl. Sci.* **2020**, *10*, doi:[10.3390/app10072287](https://doi.org/10.3390/app10072287).
185. Ielo, I.; Giacobello, F.; Castellano, A.; Sfameni, S.; Rando, G.; Plutino, M.R. Development of Antibacterial and Antifouling Innovative and Eco-Sustainable Sol–Gel Based Materials: From Marine Areas Protection to Healthcare Applications. *Gels* **2022**, *8*.
186. Sfameni, S.; Rando, G.; Marchetta, A.; Scolaro, C.; Cappello, S.; Urzì, C.; Visco, A.; Plutino, M.R. Development of Eco-Friendly Hydrophobic and Fouling-Release Coatings for Blue-Growth Environmental Applications: Synthesis, Mechanical Characterization and Biological Activity. *Gels* **2022**, *8*.
187. Sfameni, S.; Rando, G.; Galletta, M.; Ielo, I.; Brucale, M.; De Leo, F.; Cardiano, P.; Cappello, S.; Visco, A.; Trovato, V.; et al. Design and Development of Fluorinated and Biocide-Free Sol–Gel Based Hybrid Functional Coatings for Anti-Biofouling/Foul-Release Activity. *Gels* **2022**, *8*.

188. Li, C.; Sun, W.; Lu, Z.; Ao, X.; Li, S. Ceramic Nanocomposite Membranes and Membrane Fouling: A Review. *Water Res.* **2020**, *175*, 115674, doi:<https://doi.org/10.1016/j.watres.2020.115674>.
189. Du, X.; Shi, Y.; Jegatheesan, V.; Haq, I.U. A Review on the Mechanism, Impacts and Control Methods of Membrane Fouling in MBR System. *Membranes (Basel)*. **2020**, *10*.
190. Enfrin, M.; Lee, J.; Le-Clech, P.; Dumée, L.F. Kinetic and Mechanistic Aspects of Ultrafiltration Membrane Fouling by Nano- and Microplastics. *J. Memb. Sci.* **2020**, *601*, 117890, doi:<https://doi.org/10.1016/j.memsci.2020.117890>.
191. Meng, X.; Luosang, D.; Meng, S.; Wang, R.; Fan, W.; Liang, D.; Li, X.; Zhao, Q.; Yang, L. The Structural and Functional Properties of Polysaccharide Foulants in Membrane Fouling. *Chemosphere* **2021**, *268*, 129364, doi:<https://doi.org/10.1016/j.chemosphere.2020.129364>.
192. Tanudjaja, H.J.; Anantharaman, A.; Ng, A.Q.Q.; Ma, Y.; Tanis-Kanbur, M.B.; Zydney, A.L.; Chew, J.W. A Review of Membrane Fouling by Proteins in Ultrafiltration and Microfiltration. *J. Water Process Eng.* **2022**, *50*, 103294, doi:<https://doi.org/10.1016/j.jwpe.2022.103294>.
193. Muhamad, N.A.S.; Mokhtar, N.M.; Lau, W.J.; Ismail, A.F.; Naim, R. Fouling Studies on Hydrophobic PVDF-Bentonite Hollow Fiber Membrane during Membrane Distillation of Palm Oil Mill Effluent. *J. Water Process Eng.* **2022**, *49*, 102969, doi:<https://doi.org/10.1016/j.jwpe.2022.102969>.
194. Mohammad, A.W.; Teow, Y.H.; Ang, W.L.; Chung, Y.T.; Oatley-Radcliffe, D.L.; Hilal, N. Nanofiltration Membranes Review: Recent Advances and Future Prospects. *Desalination* **2015**, *356*, 226–254, doi:[10.1016/j.desal.2014.10.043](https://doi.org/10.1016/j.desal.2014.10.043).

CHAPTER 2

BIOPOLYMER BASED ELECTROSPUN NANOFIBER MEMBRANES DOPED WITH FUNCTIONAL HALLOYSITE DERIVATIVES

The Second Chapter concerns the design and development of sustainable and functional membranes for advanced and smart water filtration. In particular, paragraph 2.1, will give an overview of the most recent advances regarding functional membranes as obtained through various synthetic approaches (i.e., production of mixed blend polymeric membranes, employment of functional coatings and use of advanced techniques such as electrospinning). In the light of such improvements, the research activity, performed in the framework of this PhD project, is then described, focusing on the design and development of bio-polymeric blends based on polyamide 11 (paragraph 2.2) and polyamide 11 and chitosan biopolymers (paragraph 2.3) and doped with functional hybrid halloysite derivatives, employed to produce different electrospun nanofiber membranes and composite membranes through electrospinning technique. Their retention performances towards two model organic dyes are also investigated through a dead-end filtration cell.

2.1. Advanced and sustainable water filtration membranes

2.1.1. Natural-derived polymers for the development of sustainable membranes

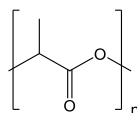
Researchers must face with different limits to find more sustainable alternatives to fossil-derived polymers. One of the challenges with biopolymer-based membranes might be a lack of suitable mechanical, thermal, and chemical resistance [1,2]. As a result, combining them with other polymers, gels, functional nanofillers, or reinforcing agents is a critical step. As described in Chapter 1, new nanotechnologies and nanomaterials are currently being used in a wide range of applications due to their qualities, such as a large surface area (surface/volume ratio), size effects, reactivity, and catalytic capabilities, presenting themselves as suitable candidates to tackle these challenges [3–6]. In this context, nanomaterials may be easily chemically altered, functionalized, and embedded in different polymers and matrices using various and simple synthetic techniques to generate hybrid materials or nanocomposites with specific and desired chemical, physical, and mechanical characteristics [7–10].

As a result, they may be employed to create advanced, sustainable, stimuli-responsive, and unique materials and technologies for a variety of industries, including blue-growth, smart and technical textiles, biomedicine, construction, cultural heritages, and environmental remediation [11–13].

The most recent examples of state-of-the-art water filtration membranes based on sustainable or renewable materials include the use of various natural-derived polymers and gels [14–16]. Table 2.1 lists some of the most frequent polymers employed for these objectives.

Table 2.1. Common natural-derived and renewable polymers used for the development of water filtration membranes [17].

Polymer	Chemical Structure	Derivation	Ref.
Cellulose acetate ¹		Wood pulp	[18]
Alginate ²		Brown algae	[19]
Chitosan ³		Crustacean shells	[20]
Pectin		Dried citrus peels or apple pomace	[21]
Carrageenan ⁴		Red seaweed	[22]

Polylactic acid ⁵Corn starch, sugarcane,
and other biomasses [23]

¹Cellulose acetate = CA; ² the chemical structure is referred to sodium alginate = NaAlg; ³ chitosan = CS; ⁴ the chemical structure is referred to lambda carrageenan = λ -Cg; ⁵ polylactic acid = PLA.

2.1.2. Hybrid/mixed-matrix water filtration membranes

The blending of bio-based polymeric solutions with different functional compounds and nanofillers lead to the production of the so called “mixed-matrix membranes” (MMM).

An overview of the most recent sustainable nano-hybrid and mixed-matrix membranes based on different biopolymers, is given in Table 2.2 that also includes a comparison of their preparation techniques, performances, and retention qualities against various water common and emerging contaminants.

Chitosan is a natural amino polysaccharide derived from chitin deacetylation. It is derived from the shells of crustaceans, and it is the second most common biopolymer in nature after cellulose. It is distinguished by a high concentration of amine and hydroxyl functionalities and has attracted increasing interest in a variety of applications, including (waste)water treatment and purification [24,25].

Table 2.2. Descriptive table presenting a comparison of the most recently developed sustainable hybrid mixed-matrix membranes.

System	Preparation Method	Filtration Process	Pollutant Treated	Filtration Performances ¹	Ref.
CS/PVA/MMT ²	Non-solvent-induced phase inversion	Dead-end	Chromium	<ul style="list-style-type: none"> • 50 mg·L⁻¹ feed • pH = 7 • 100 kPa • 84–88.34% removal efficiency 	[26]
Fe–Al–Mn@CS CA-based	Phase inversion	Cross-flow	Fluoride anions	<ul style="list-style-type: none"> • 3.8 mg·L⁻¹ feed • pH = 6–9 • 6–8 bar • Treatment capacity of 4000 L·m⁻² 	[27]
CS/GO ³	Casting and solvent evaporation	Pervaporation	High-salinity water	<ul style="list-style-type: none"> • 5 wt.% aqueous NaCl feed • 81 °C • 30.0 kg·m⁻²·h⁻¹ permeate flux • 99.99% of salt rejection 	[28]
TiO ₂ -COOH/CaAlg	Non-solvent-induced phase inversion	Cross-flow	Organic dyes	<ul style="list-style-type: none"> • 100 mg·L⁻¹ of each dye feed • 14.1 L·m⁻²·h⁻¹·bar⁻¹ flux • 0.1 MPa • Brilliant blue G250 (98.4%) and Congo Red (95.9%) removal rates 	[29]
PES blended PVA-GO-NaAlg	Phase inversion by immersion precipitation	Dead-end	Organic dyes	<ul style="list-style-type: none"> • 100 mg·L⁻¹ Lanazol Blue 3R • pH = 4.76 • 3 bar 	[30]

MWCNTs/chitosan-carrageenan ⁴	Vacuum filtration	Dead-end	<ul style="list-style-type: none"> • Up to 88.9% dye rejection • 2 mg·L⁻¹ heavy metals mixture • pH = 7 • 1–6 bar • Up to 90% removal 	[31]
			Heavy metals (Cu ²⁺ , Cd ²⁺ , Co ²⁺ , Ni ²⁺ , Ba ²⁺ , and Pb ²⁺)	

¹ Referred to optimized feed concentration, working pH and pressure, permeation flux, removal capabilities, and parameters; ² MMT = montmorillonite; ³ GO = graphene oxide; ⁴ MWCNTs = multiwalled carbon nanotubes.

In this regard, its properties make it a potentially effective adsorbent system for a variety of common and novel pollutants, such as heavy metals, anionic organic dyes, and macromolecules [32,33]. Thin films for ultra-nanofiltration technologies, based on chitosan and other polymeric functional blends, may be produced using simple casting or non-solvent-induced phase inversion processes [34,35].

Furthermore, clays have a wide range of applications in environmental remediation due to their negatively charged surfaces, high surface area, swelling capacity (particularly bentonite and montmorillonite clays), cation exchange capacity, and strong adsorption/absorption properties [36,37]. They may also be easily functionalized by changing the surface hydrophilicity/hydrophobicity and adsorption characteristics [38].

A unique organic-inorganic hybrid thin sheet membrane generated by a non-solvent-induced phase inversion approach from a chitosan/polyvinyl alcohol and montmorillonite clay mix (CS/PVA/MMT) is an example of how these two materials have been combined. The resulting hybrid clay-polymeric nanofiltration membrane demonstrated good chromium rejection rate as well as excellent overall performances, including increased hydrophilicity and anti-biofouling capabilities [26].

Mixed-matrix membranes, as previously mentioned, are membranes that comprise polymeric matrixes in which inorganic/organic fillers are uniformly dispersed [39,40]. In another work, a metal oxide nanofiller was used to make a regenerable MMM based on cellulose acetate obtained via a phase inversion approach. To create the final MMM, the Fe-Al-Mn@chitosan nanocomposite was evenly dispersed in a cellulose acetate solution after being prepared by a simple co-precipitation process from a Mn-slag waste resource. This was tested in a cross-flow arrangement to remove fluoride anions. The experimental results indicate that 1 m² of this MMM can treat 4000 L of fluoride-spiked synthetic water by using adsorption and electrostatic repulsion phenomena (thanks to the F⁻ cake layers generated on the membrane). Furthermore, adsorption isotherm tests reveal that the membrane have a maximum adsorption capacity of 2.3 mg·g⁻¹. Finally, the membrane was regenerated with 0.01 M NaOH and used for three cycles of filtering [27].

Gel materials are well-known adsorbent systems for several environmental contaminants [41]. Microgels, in particular, are an important class of reusable smart materials that are temperature and pH sensitive, making them appropriate for the effective removal of heavy metal ions [42] and herbicides [43], as well as the removal and degradation of organic dyes [44].

Alginate is a heteropolysaccharide derived from brown seaweed and the capsules of certain bacteria that, due to its gel-forming ability, is widely employed in the paper, textile, food, and environmental remediation sectors [45,46].

An appropriate nanofiller can be used to improve its mechanical properties. In this regard, an organo-modification was performed in order to promote nano-filler dispersibility and interfacial adhesion with the substrate or polymeric matrix, hence reducing agglomeration phenomena. For example, by carboxylating TiO_2 nanoparticles, this organo-modified nanofiller might be used as an appropriate reinforcing agent in the creation of a hybrid hydrogel membrane based on sodium alginate ($\text{TiO}_2\text{-COOH/CaAlg}$). The mixture was then cast using a film-casting process and crosslinked in a 2.5 wt.% CaCl_2 aqueous solution. Following that, the generated negatively charged nanofiltration hydrogel membrane was used to reject several organic dyes such as Brilliant blue G250, Direct black 38, and Congo red, with rejection ratios of 98.4%, 96.8%, and 95.9%, respectively. This hybrid membrane have also higher tensile strength than the pristine sodium alginate crosslinked membrane and low rejection rates for the various inorganic salts tested [29].

Thanks to their capacity to be regenerated and reused, alginate hydrogels may also be used to combine petroleum-derived polymers to lessen the environmental impact of the resulting membranes. An immersion precipitation process was used to create a new asymmetric microporous membrane based on a nanocomposite hydrogel of polyvinyl alcohol-graphene oxide-sodium alginate (PVA-GO-NaAlg) combined with PES. The membrane demonstrate adequate antifouling capabilities and organic dye rejection performances, particularly for the tested Lanazol Blue 3R dye [30].

Carrageenan is not only used as a surfactant in the creation of stable dispersions. Indeed, because of its propensity to create solid gels, it finds uses in a variety of fields, including pharmacology, industry, and biology [47,48]. Furthermore, it finds applications as an adsorbent system in environmental remediation, because of the presence of sulphate, hydroxyl, and carboxyl groups on its polysaccharide structure, which may serve as potential reactive and coordinating sites for the adsorption of different pollutants [49,50].

This biopolymer is classified into three categories based on the number of sulfated groups: lambda carrageenan, which includes three of them, iota, which contains two, and kappa, which has a single sulphate group per disaccharide unit [51].

It can also be used to increase membrane hydrophilicity in membrane production. For example, kappa-Cg is combined with PVDF to produce asymmetric membrane structures with greater dye retention and water permeability than pristine PVDF [52].

A dry casting approach was employed to create an ecofriendly composite membrane based on a chitosan/ κ -carrageenan/acid-activated bentonite mix that is effectively used for methylene blue (MB) removal in a batch system. The 98% removal rate is attained after 200 minutes at pH=4 and 50 °C with an adsorbent dosage of 0.05 g/10 mL MB solution. The adsorption capacity of MB is 18.80 $\text{mg}\cdot\text{g}^{-1}$ at 50 °C, fitting the pseudo-second-order kinetic model and the Freundlich isotherm model [53].

As a result, various examples of sustainable mixed-matrix, composite, and hybrid membranes were described; however, despite the fact that they can be prepared using simple procedures, the employed starting materials and polymers have a not-treasurable economic impact when applied on a large scale.

2.1.3. Functional bio-based coatings for filtration membranes

The combination of commonly used polymers with natural or more sustainable ones can represent a solution for the development of more ecofriendly and less expensive systems; however, applying functional coatings is a more economical and effective approach to improve the selectivity and durability of the actual petroleum-derived membranes.

Coating polymeric membranes with functional polymeric gels and blends is a simple and sustainable strategy to improve the performance of currently used polymeric membranes, which can also lead to an increase in their lifespan while minimizing fouling [54,55].

Table 2.3 lists some employed coatings, comparing some of the most current techniques and coating solutions in terms of preparation process and filtering performance.

It is possible to develop functional gel coatings for commercial membranes to provide them the potential to retain numerous contaminants through rational design [56–58].

For example, a hydrolyzed-PAN membrane was coated layer by layer with a polymeric blend prepared from naturally obtained κ -carrageenan and nanoclay-laponite to create an efficient self-cleaning and antifouling membrane with superoleophobicity properties.

Table 2.3. Comparison of the most recently produced sustainable and functional coatings for filtration membranes given together with preparation methods and filtration performances data [17].

System	Coated Membrane	Preparation Method	Filtration Process	Pollutant Treated	Filtration Performances ¹	Ref.
κ -carrageenan/laponite	h-PAN	Layer-by-layer	Dead-end	Motor oil, metal ions, BB, RB ²	<ul style="list-style-type: none"> • 200 mg·L⁻¹ BB, 100 mg·L⁻¹ RB feed • 100 L·m⁻²·h⁻¹ flux • 0.1 MPa, 27 °C • >99% Hexadecane (1:30 v/v), 98% RB, 99% BB, >99% NaCl, MgSO₄ rejection 	[59]
CS, polyethyleneimine, GO	Cellulose	Dip-Coating	Batch filtration	Cr(VI) and Cu(II)	<ul style="list-style-type: none"> • 5 mL·min⁻¹ feed rate • 20 mL of 10 mg·L⁻¹ feed • ≈90% and ≈30% Cr(VI) and Cu(II) respectively 	[60]
Chitosan-AlFu MOF ³	Cellulose acetate	Film coating	Forward osmosis cross-flow filtration	COD, NH ₄ -N, NO ₃ -N and PO ₄	<ul style="list-style-type: none"> • 18 L·m⁻²·h⁻¹ flux for synthetic wastewater • 8.75 L·m⁻²·h⁻¹ flux for real wastewater • Over 80% water recovery 	[61]
CS-NaAlg Fe ₀ @WO ₃ NPs	PES	Layer-by-layer	Cross-flow	Cr(VI)	<ul style="list-style-type: none"> • 5, 25, and 50 mg·L⁻¹ feed • 1 bar • Irradiation chamber with visible light • 99.2%, 92.1%, and 78.1% rejection, respectively 	[62]
k-Cg/GO	UA-60	Film coating	Dead-end	Divalent ions	<ul style="list-style-type: none"> • 2000 mg·L⁻¹ feed 	[63]

				<ul style="list-style-type: none"> • 5 bar • 94.86% and 23.6% rejection for MgSO_4 and NaCl, respectively
Catechol/CS	PVDF	Oxidant-induced ultrafast co-deposition	Dead-end	<ul style="list-style-type: none"> • 0.45 $\text{g}\cdot\text{L}^{-1}$ of each oil and Tween 20 feed • pH range 2–11 • $\approx 428 \text{ L}\cdot\text{m}^{-2}\cdot\text{h}^{-1}\cdot\text{bar}^{-1}$ flux • Up to 90% removal efficiencies of O/W emulsions

[64]

¹ Referred to optimized feed concentration, working pH and pressure, permeation flux, removal capabilities, and parameters; ² BB = brilliant blue, RB = rhodamine-B; ³ MOF = metal organic framework.

The modified laponite/ κ -carrageenan membrane demonstrates high water-soluble dye adsorption, particularly of brilliant blue (BB) and rhodamine-B (RB), as well as high stability and flexibility, demonstrating the efficient underwater superoleophobicity and water filtration capabilities of organic contaminants. In addition to removing oil emulsions and water-soluble pigments, the filtrate is almost entirely free of metal ions (NaCl, MgSO_4) [59].

The negatively charged structure of κ -carrageenan improves not only membrane wettability, but also salt rejection and antifouling performances. A crosslinked kappa-carrageenan (κ -CGN) and GO coating on a commercial UA-60 loose nanofiltration membrane is one example. In particular, glycerol was used as an ecologically friendly cross-linker for κ -carrageenan. Furthermore, the concentration of GO nanosheets was varied to tune the surface charge, hydrophilicity, and antifouling features of the membrane in order to develop an ideal coating. Finally, the coated membrane was examined for water recovery ratio and divalent ion rejection of landfill leachate wastewater [63].

A response surface approach may be used to improve performance and optimize the formulation of a functional coating. In this case, a cellulose membrane was dip-coated with chitosan, polyethyleneimine (PEI), GO, and glutaraldehyde as a cross-linker. The concentration of the nanofiller and biopolymeric blend components was successfully optimized using response surface methodology to produce a multifunctional nanocomposite coating of cellulose and glass nanofiber membrane capable of removing both positively and negatively charged heavy metals such as Cr(VI) and Cu (II) [60].

Other naturally available biopolymer/gel precursors can be used to give rise to improved membrane antifouling, hydrophilicity, and chelation properties [133-136]. Their inclusion in biopolymeric blends can involve one-step procedures to produce functional gel-based coatings. By using an oxidant-induced ultrafast co-deposition on PVDF membranes, a catechol/chitosan coating was easily developed in a green way. The resulting membrane demonstrates high water permeability and chemical stability in severe pH conditions. Furthermore, the membrane surface hydrophilic coating serves as an energy barrier for oil droplets, minimizing oil adherence on the surface and allowing the modified membrane to be used for cyclic oil-in-water (O/W) emulsion separation operations. Furthermore, a 70% greater water flux is attained than with pristine PVDF

membranes, and three filtering cycles are performed on a cross-flow cell, each time cleaning the membrane with DI water [64].

Despite chemical modulation and functionalization of membranes, innovative approaches to their preparation can include a variety of methodologies to achieve, for example, micro-/nano-architecture morphologies to improve the membrane active surface and various other aspects [65,66]. A basic example is a PLA membrane with a hierarchical surface to replicate the predatory behavior of coral tentacles for the effective deposition of a functional nanoparticle-based coating, resulting in resilient and superwetting properties. The micro-/nano-architecture preparation procedure comprised the spreading and film casting of a PLA and β -cyclodextrin (β -CD) solution over a PET non-woven fabric. Following that, the ultrafiltration membrane generated by the NIPS method was dried and peeled off the support, resulting in the hierarchical surface resembling coral tentacles [67].

Furthermore, innovative and scalable technologies that are already used in industry may be employed to create high homogenous systems at the nanoscale level, such as nanofibers.

2.1.4. Electrospun nanofiber-based membranes

Nanofibers, i.e. fibers with a diameter smaller between 1-100 nm, are progressively being reported in the literature for the development of water filtration membranes with specified features [68–70] (Figure 2.1). Nanofibers have a high surface-to-volume ratio and have emerged as an intriguing new class of materials used to prepare a wide range of systems in different application fields such as energy storage, healthcare, environmental technologies, biotechnology, catalysis, air/water filtration, and information technology [71–74].

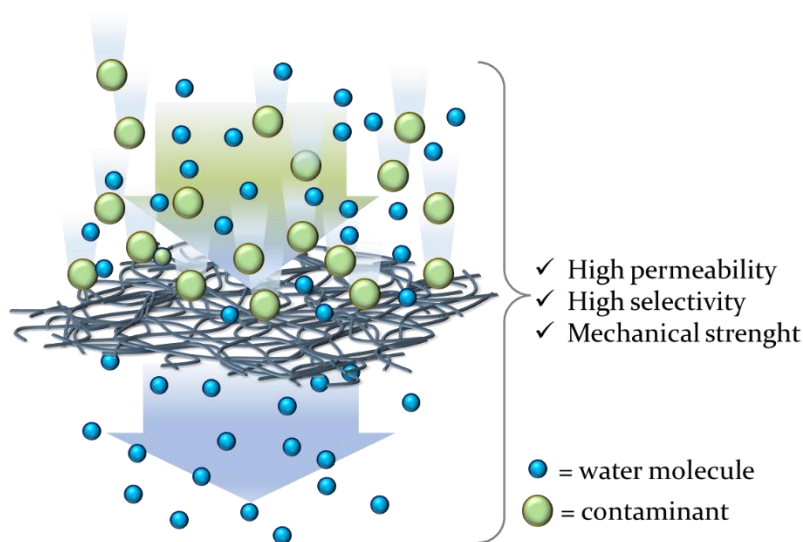


Figure 2.1. Illustration of nanofiber-based water filtration membranes together with their benefits [17].

Drawing, self-assembly, phase separation, template synthesis, and, most recently, electrospinning [75] (Figure 2.2) are examples of polymeric nanofiber processing methods already documented in the literature.

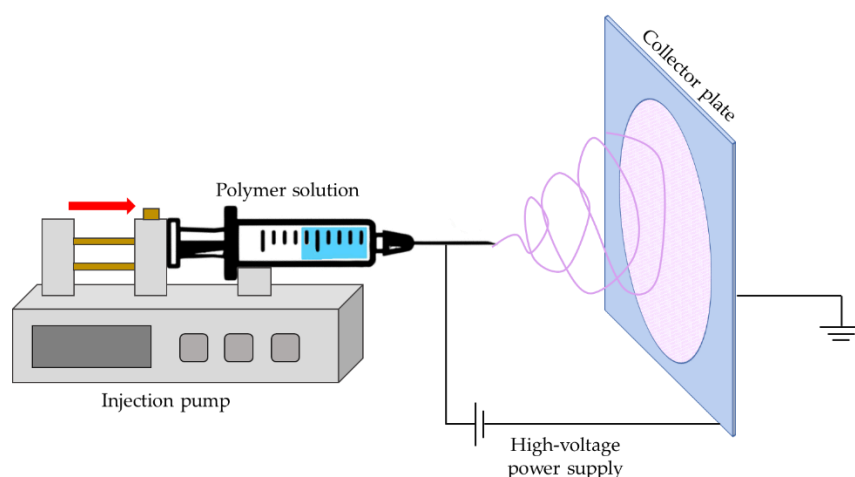


Figure 2.2. Schematic representation of the electrospinning technology employed for producing nanofibers [17].

In particular, electrospinning technology allows for the easy production of nanofibers for a variety of applications, starting from polymeric solutions or mixtures, and using a high voltage power supply and a collector plate, without the use of coagulating agents or high temperatures[76–78].

Some examples are provided in this paragraph to highlight some of the functionalization options, benefits, and variety of possibilities available in this process for producing functional doped sustainable nanofibers for water filtration.

Table 2.4 summarizes the main characteristics of recent sustainable nanofiber-based and composite membranes, as well as the biopolymers, gels, and functional agents used in their manufacture.

Table 2.4. Detailed table presenting a comparison of the most recently produced sustainable and functional nanofiber-based filtration membranes [17].

Polymers	Doping Agent	Support	Filtration Process	Pollutant Treated	Filtration Performances ¹	Ref.
CS/PEO ²	Cu ²⁺	TEMPO-oxidized cellulose	Dead-end	<i>Escherichia coli</i> and <i>Bacillus subtilis</i>	<ul style="list-style-type: none"> • 104 CFU·mL⁻¹ <i>E. coli</i> and <i>B. subtilis</i> feed • 1600 L·m⁻²·h⁻¹·MPa⁻¹ flux • 100% microfiltration efficiency 	[79]
CS	FeOOH/g-C ₃ N ₄ particles	PAN	Dead-end	MB, ERY ³	<ul style="list-style-type: none"> • 50 mg·L⁻¹ MB, 20 mg·L⁻¹ ERY feed • 15 psi • 35.6 L·m⁻²·h⁻¹·psi⁻¹ • FRR 89.4% (30 min, Vis + 50 mM H₂O₂) 	[80]
CS/PAN	UiO-66-NH ₂	PVDF nanofibrous sublayer	Cross-flow	Pb ²⁺ , Cd ²⁺ , Cr ⁶⁺	<ul style="list-style-type: none"> • 20 mg·L⁻¹ feed of metal ion • 1 bar, 30 °C 	[81]

					<ul style="list-style-type: none"> • 452, 463, 479 L·m⁻²·h⁻¹ flux, respectively • 94%, 89%, 85.5% removal, respectively 	
CaAlg	CNTs	Polyhydroxy butyrate nanofibers	Custom filtration device	BB, DOS, PR, HY, and SY ⁴	<ul style="list-style-type: none"> • 0.1 g·L⁻¹ feed of each dye • 0.1 to 0.7 MPa • 130 and 109.5 L·m⁻²·h⁻¹ flux, BB and PR, respectively • 99.1% and 97.6%, BB and PR, respectively 	[82]
CS/PVP	CNTs	CS/PVP/PVA	Laboratory-scale pressure-driven membrane filtration system	Cu ²⁺ , Ni ²⁺ , Cd ²⁺ , Pb ²⁺ , MG, MB and CV ⁵	<ul style="list-style-type: none"> • 30 mg·L⁻¹ feed • 1 bar, 25 °C • 1533.26 L·m⁻²·h⁻¹ flux • 95.68 %, 93.86 %, 88.52 %, 80.41%, 87.20 %, 76.33 %, 63.39 % rejection of Cu²⁺, Ni²⁺, Cd²⁺, Pb²⁺, MG, MB, CV, respectively 	[83]
PLA	β-cyclodextrin	-	Dead-end	Toluene-in-water emulsions, MB, OG ⁶	<ul style="list-style-type: none"> • Toluene-in-water emulsions of 3 wt.%, 3 mg·L⁻¹ MB, OG feed • >1500 L·m⁻²·h⁻¹ flux • >95% oil/water separation efficiency 	[84]

¹ Referred to optimized feed concentration, working pH and pressure, permeation flux, removal capabilities, and parameters; ² PEO = polyethylene oxide; ³ MB = methylene blue, ERY = erythromycin; ⁴ DOS = direct orange S, PR = procion red mx-5B, HY = hydrazine yellow, SY = stilbene yellow; ⁵ MG = malachite green, CV = crystal violet; ⁶ OG = methyl orange.

Multiple examples in literature already report on the usage of various supports on which the nanofibers are electrospun in order to increase the efficiency and durability of the final composite membrane [85–88]. The outer layers of a TEMPO-oxidized cellulose core-shell fiber support were covered on both sides with electrospun nanofibers generated from a chitosan-polyethylene oxide solution to create a “sandwich-like” composite membrane. To improve antibacterial performances, electrospun nanofibers were doped with copper ions by soaking in a CuSO₄ solution. In fact, the membrane was evaluated for microfiltration of *Escherichia coli* and *Bacillus subtilis*, demonstrating 100% removal of both bacteria without a substantial decrease in permeability and reusability [79].

In this regard, the Fenton reaction has piqued the interest of researchers due to its capacity to convert dangerous organic pollutants into low-molecular-weight inorganic molecules [89–91]. It is a chemical oxidation technique that uses iron salt-based systems or, more recently, heterogeneous Fenton-like procedures using diverse iron-containing materials or nano zero-valent iron to execute catalytic degradation processes in the presence of H₂O₂ [92–94]. Such specific materials can be incorporated into polymeric and gel blends to give functionality at the final system of performing Fenton-like degrading processes of various water contaminants. Some

FeOOH/g-C₃N₄ submicron particles sensitive to visible light were used to dope a PAN solution and an electrospun nanofiber membrane. The membrane was treated with chitosan to increase its antifouling and hydrophilicity. The system was tested for the removal of methylene blue and erythromycin from water. The photo-Fenton reaction mediated by the nanofiber doped catalyst in the presence of visible light and H₂O₂ results in excellent antifouling and pollutant removal. The degradation of organic pollutants on the membrane surface and pores, in particular, enabled fouling elimination, constant water flow, and high oxidation resistance, allowing it to be used for up to ten filtration cycles [80].

Using nanofibrous supports for the deposition of another layer of nanofibers or a coating allows for the creation of membranes with improved tensile properties. In this regard, they can also be coated with bio-polymeric hydrogels to increase the composite filtration system barrier, hydrophilic, and adsorption properties. A polyhydroxybutyrate/carbon nanotubes (PHB/CNT) electrospun nanofibrous membrane, for example, with high tensile mechanical properties and porosity due to CNT nanofillers, was coated with sodium alginate via simple film casting and immersion in a 1.5 wt.% NaAlg solution. The membrane is then immersed in CaCl₂ water solution to induce biopolymer crosslinking and the formation of the hydrogel.

Filtration experiments using brilliant blue G, direct orange S, procion red mx-5B, hydrazine yellow, and stilbene yellow dyes were performed to assess the adsorption and filtration characteristics of the composite membrane. According to these findings, the composite nanofiber membrane might be employed as a highly effective nanofiltration membrane with acceptable oil and protein antifouling capabilities for wastewater dye removal with high flux and removal rates [82]. CNTs in nanofibers not only functioned as reinforcing agents, but they also resulted in the formation of nanochannels in functional coatings, which improved water permeability and, therefore, the flow of the final membrane.

This was also proven in the study of a chitosan/polyvinylpyrrolidone/polyvinyl alcohol (CS/PVP/PVA) nanofiber membrane generated using electrospinning and subsequently coated with a CS, PVP, and single-walled CNTs mix using the electrospray technique. The aligned CS/PVP/PVA electrospun membranes demonstrate excellent pure water permeate flow, a smooth surface with linked pore topologies, and good antifouling, dye rejection, and heavy metals removal capabilities. Batch adsorption studies revealed that the maximum adsorption capacitance for Cu²⁺, Ni²⁺, Cd²⁺, Pb²⁺, MG, MB, and CV are 54.32, 53.16, 52.06, 48.19, 49.31, 44.13, and 37.76 mg·g⁻¹, respectively. Adsorption isotherm computations validate the Langmuir model as the model that best matches the results, although the adsorption data for Cu²⁺ and Ni²⁺ are more consistent with the Freundlich model [83].

Some recent examples of electrospun nanofiber sustainable membranes in composite systems are shown, either prepared on supports or used as supports for the deposition of additional functional nanofibers or coatings. Nonetheless, it is possible to develop totally bio-based systems for multiple pollutant filtering that are not as well supported as the preceding ones.

Some PLA nanofibers were electrospun and functionalized with polydopamine (PDA) and mono-6-deoxy-6-ethylenediamine-β-cyclodextrin. In order to achieve the nanofiber coating, the PLA membrane is first functionalized with PDA and then with the functional β-CDs. The final

β -CD-PDA@PLA nanofiltration (NF) membrane was evaluated for separation of toluene-in-water emulsions as well as removal of methylene blue and methyl orange. Because of the negatively charged surface and the presence of host-guest complexation functional agents like β -CDs, the NF membrane demonstrate superhydrophilicity and high underwater oleophobicity, with an absorbability of >95% of positively charged water-soluble organic dyes. Gravity-driven filtration was used to examine the membrane separation efficiency of 100 mL of green MB/MO solution ($3 \text{ mg}\cdot\text{L}^{-1}$ MO and MB). The MB content is reduced from $3 \text{ mg}\cdot\text{L}^{-1}$ of feed to $0.009 \text{ mg}\cdot\text{L}^{-1}$ of filtrate, whereas the MO concentration showed only a little decrease after filtering, resulting in a separation efficiency of 99.70% with a flow of $1770 \text{ L}\cdot\text{m}^{-2}\cdot\text{h}^{-1}$. Furthermore, it has great durability to efficiently purify wastewater including both toluene emulsion and MB for at least 30 cycles since the membrane can be easily recovered by washing with a small quantity of solvents and reusing for the next filtration cycle [84]. A chitosan/poly(vinyl alcohol)/amino-functionalized montmorillonite nanocomposite electrospun membrane with improved adsorption capacity and thermomechanical properties was also developed. These membranes were used to remove a model cationic dye (Basic Blue 41) with a nanofiller loading of up to 3 wt.%. In adsorption tests, the nanofibrous membrane with 2% nanofiller loading exhibit the greatest and quickest dye removal, with roughly 80% of the cationic dye removed within 15 minutes, at least 20% better than the pristine chitosan/poly(vinyl alcohol) membrane [95].

Electrospinning was also employed to create a water-based poly(vinyl alcohol) (PVA)/starch hydrogel nanofiber membrane with a high surface area and three-dimensional structure. Following the thermal cross-linking procedure, the membrane was evaluated for filtration of 100 mL of MB/MO solution with concentrations of $5 \text{ mg}\cdot\text{L}^{-1}$ for MB and $18.1 \text{ mg}\cdot\text{L}^{-1}$ for MO. Using a vacuum pump and a flow rate of $180 \text{ mg}\cdot\text{min}^{-1}$, the solution was fed over the PVA/starch nanofiber membrane. The MB adsorbs on the membrane after 54 seconds, and the MO flows through. With a dye separation efficiency of 99.6%, the MB content in the filtrate decreased from 5 to $0.065 \text{ mg}\cdot\text{L}^{-1}$, and the MO concentration decreased from 18.1 to $17.5 \text{ mg}\cdot\text{L}^{-1}$ [96].

Finally, the described most recent examples of sustainable electrospun nanofiber membranes already reported in literature can be classified into:

- Double deposited as “sandwich-like” composites;
- Deposited on commercial supports;
- Deposited on nanofibrous sublayers;
- Coated with hydrogels or functional gels;
- Coated with electrospray processes;
- Not supported.

Therefore, several recent approaches were evaluated for the employment of sustainable bio-based and hybrid/doped blends to produce electrospun nanofiber membranes for the removal of various pollutants from water, thus demonstrating the feasibility of designing and easily obtaining membranes with implemented separation features starting from bio-polymeric blends. In Paragraph 2.2 the production of such electrospun nanofiber membranes based on polyamide 11 bio-polymer will be detailed, meanwhile in Paragraph 2.3 the preparation of a blend of polyamide 11 and chitosan, as applied for the production of electrospun nanofiber composite membranes, will be described.

2.2. Sustainable bio-based PA₁₁ electrospun nanofiber membranes doped with hybrid HNT derivatives for the removal of organic dyes from water

2.2.1. Abstract

Polyamide 11 (PA₁₁) is a semi-crystalline, thermoplastic polymer produced from castor oil. When compared to petroleum-based nylons and other conventional polymers, it has low net CO₂ emissions and global warming potential. Moreover, negative charged polyamides can react with cationic dyes above the isoelectric point [97]. There are some reports of PA₁₁ polymer electrospinning on literature [98–100]. PA₁₁ is distinguished by enhanced features such as strong chemical resistance, high impact and abrasion resistance, low specific gravity, high thermal stability, and the ability to be treated over a wide temperature range [98]; these properties may be implemented by the use of opportune functional nanofillers.

In this regard Halloysite (HNT), an aluminosilicate with the empirical formula Al₂Si₂O₅(OH)₄, is used as a reinforcing nanomaterial for composites, as well as for drug delivery, anticorrosive and flame retardant coatings, catalysis, and, ultimately, in the removal of impurities from water [101,102]. It is composed mostly of oxygen (55.78%), silicon (21.76%), aluminum (20.90%), and hydrogen (1.56%), and it is distinguished by an exterior surface decorated with silanol and siloxane groups and an interior lumen composed of alumina, having a variety of easily functionalizable exposed hydroxyl groups.

The present study focused on the design and development of sustainable bio-polymeric blends based on hybrid polyamide 11 (PA₁₁) that are used to produce different electrospun nanofiber membranes (ENMs) through the electrospinning technology (Figure 2.3).

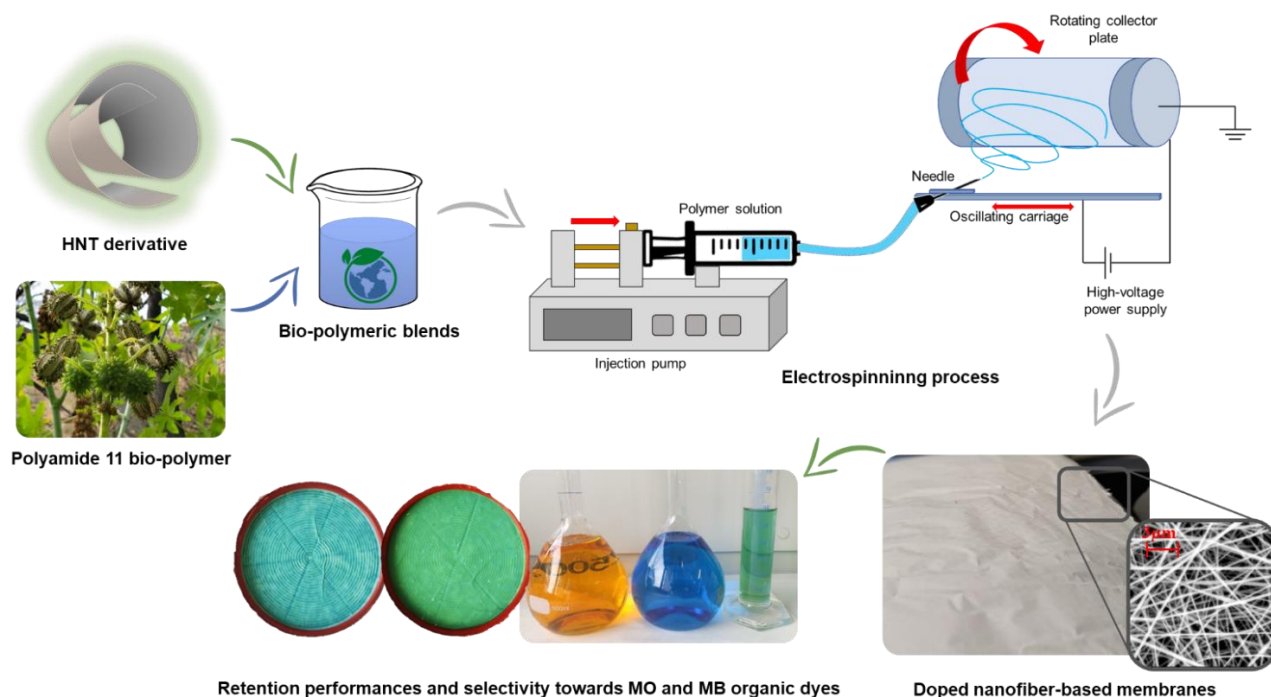


Figure 2.3. Schematic representation of the preparation of advanced ENMs starting from PA₁₁ bio-polymeric solutions doped with functional halloysite derivatives for selective dye removal.

Furthermore, different eco-friendly functional nanofillers based on hybrid halloysite (HNT) derivatives were used as dopant agents of the starting polymeric blends in a ratio of 1, 2, and 5 wt.% of PA11 to achieve better mechanical, thermal, and retention performances of specific wastewater organic contaminants. Chemical-physical and structural-morphological characterizations of all nanofillers and the resulting sustainable hybrid polymeric membranes are presented, as the removal and separation studies of two selected anionic and cationic dyes, methyl orange (MO) and methylene blue (MB), in a dead-end filtration apparatus. In comparison to pristine PA11 ENMs, the newly created composite ENMs demonstrate good tensile mechanical and thermal characteristics, as well as higher MO and MB removal rates, which are managed by the different HNT derivatives used. Dead-end filtration studies were carried out with 1 and 3 layers of each kind of ENM, indicating a selectivity towards the removal of the cationic dye MB with good separation efficiencies and MO and MB retention rates.

The whole research activity described in this paragraph 2.2 refers to the content outlined in the article n.2 of the publication list.

2.2.2. Results and discussions

2.2.2.1 Synthetic approaches

Sustainable and environmentally friendly methodologies were used, including sol-gel processes and water/ethanol as solvents, for the production of the hybrid halloysite derivatives. The sol-gel technique is gaining popularity due to its advantages, which include low process temperature, high product uniformity, lack of cytotoxicity, and high adaptability of appropriate silane precursors in stable binding to functional molecules or surfaces [3].

As a result, five different halloysite hybrid nanofillers, as showed in Figure 2.4, were developed.

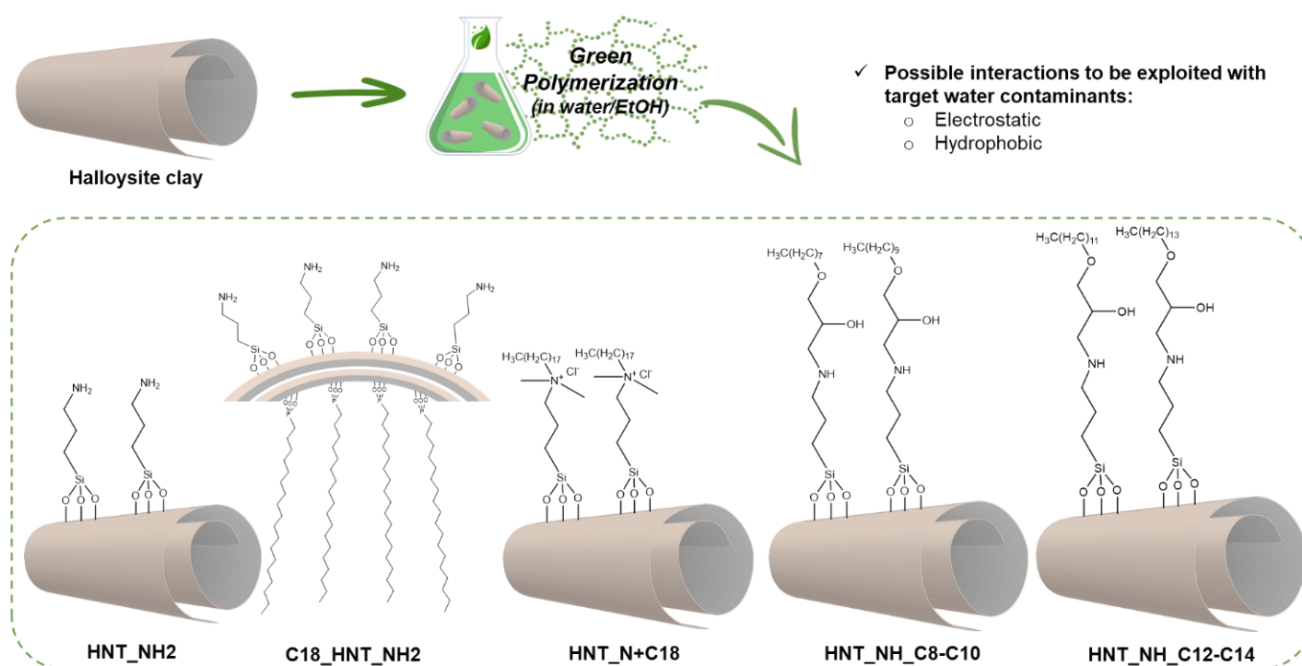


Figure 2.4. Graphical schematization of the synthesized halloysite eco-friendly hybrid derivatives for the development of functional polymeric blends for the membrane production.

The adopted synthetic approach is based on the choice of appropriate alkoxy silane precursors, focusing on their functionalities in order to promote different possible interactions (i.e., electrostatic and hydrophobic) with target wastewater pollutants and to increase the affinity of the inorganic halloysite nanotubes with the organic polymeric matrix in which they are dispersed to obtain the final blends for membrane production.

2.2.2.2 ATR-FTIR and XRD characterizations of the hybrid halloysite derivatives

ATR-FTIR analysis was used to study the chemical composition of the developed hybrid nanofillers. Each derivative exhibits H–C–H asymmetric stretching and H–C–H symmetric stretching.

These IR vibrations are linked to the alkyl chains inserted into the halloysite structure by functionalization, as reported in Table 2.5 and illustrated in Figure 2.5 a,b, indicating their successful synthesis.

HNT_NH₂, HNT_NH_C8-C₁₀ and HNT_NH_C12-C₁₄ derivatives display N–H scissoring signals. However, C–O–C vibration related to the aliphatic ether functional group characterizing HNT_NH_C8-C₁₀ and HNT_NH_C12-C₁₄ that has to appear around 1100 cm⁻¹, is not clearly evident and they are most probably hidden under the strong Si–O stretching vibration band [103].

Table 2.5. Table summarizing the main IR vibrations of pristine and functionalized halloysite derivatives.

	HNT	HNT_NH ₂	HNT_NH_C8-C ₁₀	HNT_NH_C12-C ₁₄	Ref.
	<i>Wavenumber/cm⁻¹</i>				
Inner-surface O–H stretching	3693	-	-	-	[104,105]
Inner O–H stretching	3624	-	-	-	[104–106]
O–H stretching of water	3548	-	-	-	[104–106]
N–H ₂ Asymmetric stretching	n.r.	3273	3270	3269	[104]
C–H ₂ Asymmetric stretching	n.r.	2927	2925	2922	[104,105]
C–H ₂ Symmetric stretching	n.r.	n.r.	2855	2852	[105]
O–H deformation of water	1651	1642	1650	1650	[104,106,107]
N–H scissoring	n.r.	1556	1555	1554	[104]

C-H Bending vibration	n.r.	1407	1464-1377	1463-1375	[104,105]
C-N stretching	n.r.	1221	1237	1238	[108]
Si-O asymmetric stretching	1118, 1002, 906	-	-	-	[104,106]
Si-O stretching	793,750	-	-	-	[104-106,109]
Al-O-Si bending	679, 521	-	-	-	[104,110]
Si-O-Si bending	458	-	-	-	[104,106]
		C18_HNT_NH2		HNT_N+C18	Ref.
Inner-surface O-H stretching		-		-	[104,105]
Inner O-H stretching		-		-	[104-106]
O-H stretching of water		-		-	[104-106]
C-H ₂ Asymmetric stretching		2919		2924	[104,105]
C-H ₂ Symmetric stretching		2850		2853	[105]
O-H deformation of water		1649		1651	[104,106,107]
N-H scissoring		1531		n.r.	[104]
C-H Bending vibration		1467,1410		1469	[104,105]
Si-O asymmetric stretching		-		-	[104,106]
Si-O stretching		-		-	[104-106,109]
Al-O-Si bending		-		-	[104,110]
Si-O-Si bending		-		-	[104,106]

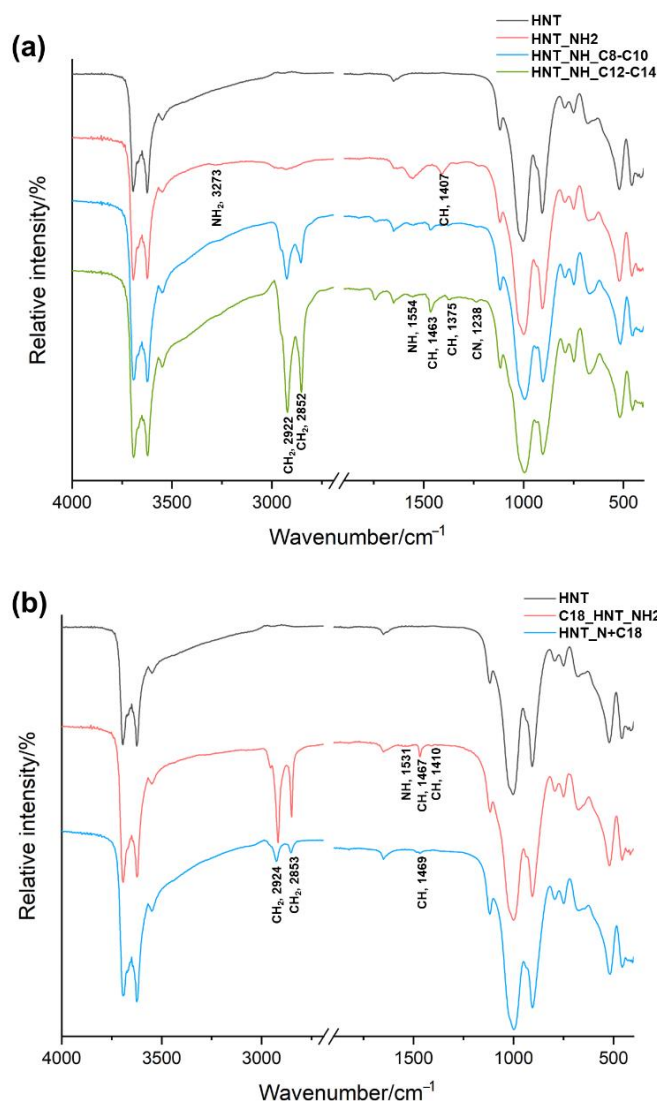


Figure 2.5. ATR-FT-IR spectra of pristine and functional HNT_{NH₂}, HNT_{NH_C8-C10}, HNT_{NH_C12-C14} (a) and C18_{HNT_NH₂}, HNT_{N+C18} (b) halloysite derivatives.

XRD diffractograms were recorded in order to detect halloysite characteristic peaks (Figure 2.6 a-c) in the different derivatives C18_{HNT}, C18_{HNT_NH₂}, HNT_{N+C18}, HNT_{NH₂}, HNT_{NH_C8-C10} and HNT_{NH_C12-C14}.

The XRD patterns of all samples are comparable, demonstrating that the crystalline structure of HNTs remains nearly intact after functionalization [111,112]. The pristine halloysite XRD diffractograms shows a sharp peak at 11.21° with a basal spacing of 0.79 nm for the (001) plane of halloysite, identifying the HNT samples as halloysite-(7 Å). The appearance of the (020) reflection at $2\theta = 19.78^\circ$ (0.45 nm) further indicates the tubular halloysite dehydrated condition [113]. The halloysite 001 peak has changed to a higher 2θ value for HNT_{NH₂} ($2\theta = 11.97^\circ$, d-spacing of 0.74 nm), and for HNT_{NH_C8-C10} and HNT_{NH_C12-C14} ($2\theta = 11.71^\circ$, d-spacing of 0.76 nm). Meanwhile for C18_{HNT} and C18_{HNT_NH₂} a $2\theta = 11.79^\circ$, d-spacing of 0.75 nm and $2\theta = 11.67^\circ$, d-spacing of 0.76 nm are detected respectively. HNT_{N+C18} showed a $2\theta = 11.76^\circ$, d-spacing of 0.75 nm.

This increase in d-spacing is attributable to silane molecules functionalizing halloysite [114]. Changes in the (002) plane ($2\theta = 24.68^\circ$) after silylation are also observed.

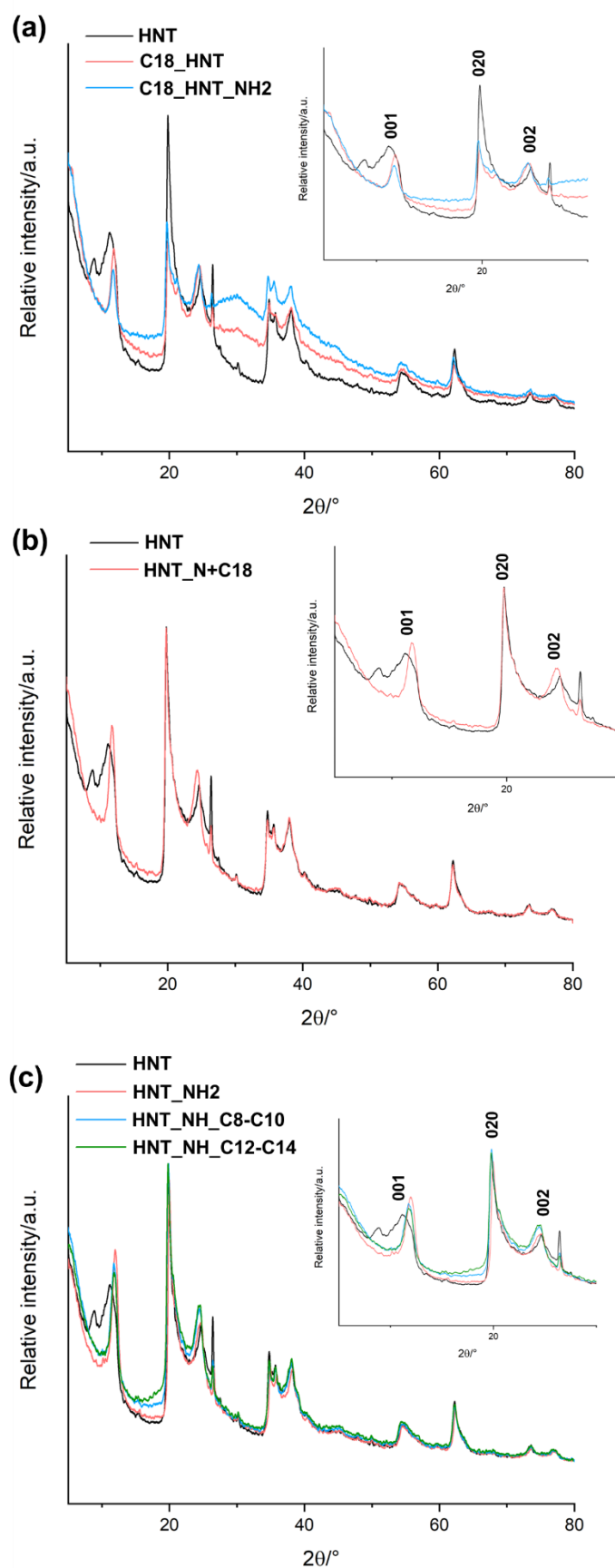


Figure 2.6. XRD patterns of pristine and functional C18_HNT, C18_HNT_NH₂ (a), HNT_N+C18 (b), HNT_NH₂, HNT_NH_C8-C10 and HNT_NH_C12-C14 (c) halloysite derivatives.

2.2.2.3 Morphological study of the hybrid halloysite derivatives

Figure 2.7 a–f depicts SEM images of pristine and functionalized HNT. Because of the strong physical, hydrogen, and van der Waals bonding connections between their hydroxyl groups, HNTs have a characteristic aggregated morphology [115]. Furthermore, after the interaction with the various functional molecules, pristine HNT retains its long fibrous and tubular shape, as well as its aggregate property. The normal proportions of HNT nanotubes are preserved when the outer surface is functionalized [116]. Furthermore, the hybrid derivatives displayed an exceptionally dense structure in which the nanotubes appear to be connected together with a rough surface, indicating the presence of an organic domain [117] and electrostatic interactions between them.

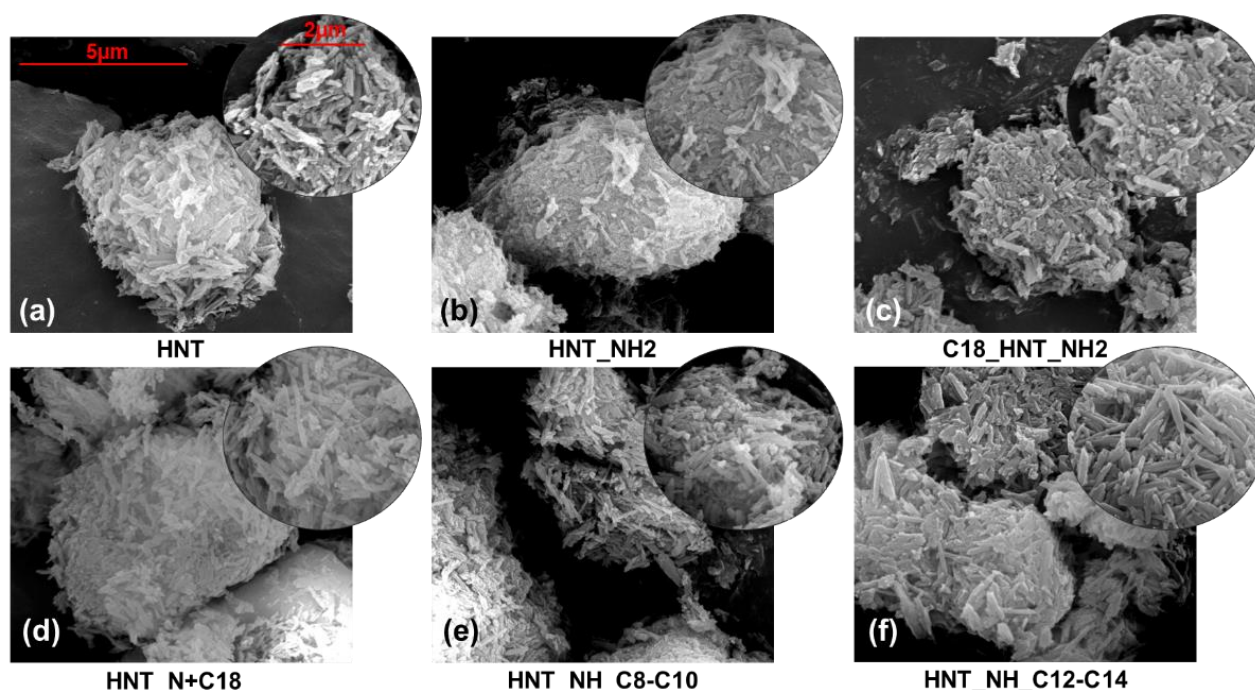


Figure 2.7. SEM images of pristine (a) and functional HNT_NH₂ (b), C18_HNT_NH₂ (c), HNT_N+C18 (d), HNT_NH_C8-C10 (e), HNT_NH_C12-C14 (f) halloysite samples.

2.2.2.4 PA11 doped solutions preparation and ENMs preparation

A solvent solution of formic acid/anisole (60:40 v/v) was used to produce PA11 bio-polymeric solutions (12% wt.% g·mL⁻¹). Each nanofiller was individually added in the PA11 solution in amounts of 1, 2, and 5% (w/w nanofiller and PA11).

The mixture was left to stir in an oil bath at 40°C for 1 hour before cooling to room temperature and electrospinning.

Then, each electrospun membrane was produced (at room temperature) by collecting nanofibers on a large rotating drum (at a speed of 200 rpm) coated with aluminum foil, with a voltage of 30 kV, a distance of 6 cm between the syringe needle tip and a metal collector, and a solution flow rate of 0.5 mL·h⁻¹.

Six syringes were simultaneously employed, and the nanofibers were collected for a total of 5 hours for each membrane. The characteristics of the obtained membranes are showed in Table 2.6.

Table 2.6. Characteristics of the obtained ENMs, in term of average weight and thickness.

Name	Average weight/ $\text{mg}\cdot\text{cm}^{-2}$	Average thickness/ μm
PA11	0.95 ± 0.01	78 ± 7
PA11@HNT 1%	1.55 ± 0.03	
PA11@HNT 2%	1.21 ± 0.9	
PA11@HNT 5%	0.86 ± 0.03	60 ± 8
PA11@HNT_NH ₂ 1%	0.82 ± 0.01	
PA11@HNT_NH ₂ 2%	1.21 ± 0.5	
PA11@HNT_NH ₂ 5%	1.29 ± 0.03	83 ± 3
PA11@C18_HNT_NH ₂ 1%	1.08 ± 0.01	
PA11@C18_HNT_NH ₂ 2%	1.33 ± 0.03	
PA11@C18_HNT_NH ₂ 5%	1.24 ± 0.06	80 ± 2
PA11@HNT_N ⁺ C ₁₈ 1%	1.16 ± 0.04	
PA11@HNT_N ⁺ C ₁₈ 2%	1.27 ± 0.04	
PA11@HNT_N ⁺ C ₁₈ 5%	1.20 ± 0.04	82 ± 1
PA11@HNT_NH_C ₈ -C ₁₀ 1%	1.03 ± 0.06	
PA11@HNT_NH_C ₈ -C ₁₀ 2%	1.16 ± 0.07	
PA11@HNT_NH_C ₈ -C ₁₀ 5%	0.94 ± 0.02	66 ± 5
PA11@HNT_NH_C ₁₂ -C ₁₄ 1%	1.16 ± 0.01	
PA11@HNT_NH_C ₁₂ -C ₁₄ 2%	0.76 ± 0.07	
PA11@HNT_NH_C ₁₂ -C ₁₄ 5%	1.36 ± 0.11	84 ± 4

2.2.2.5 Morphological study of the electrospun nanofiber membranes

Figure 2.8 and Figure 2.9 a–g' depict the nanofiber average diameters of the 5% loaded hybrid electrospun PA11 nanofiber membranes together with the corresponding SEM images.

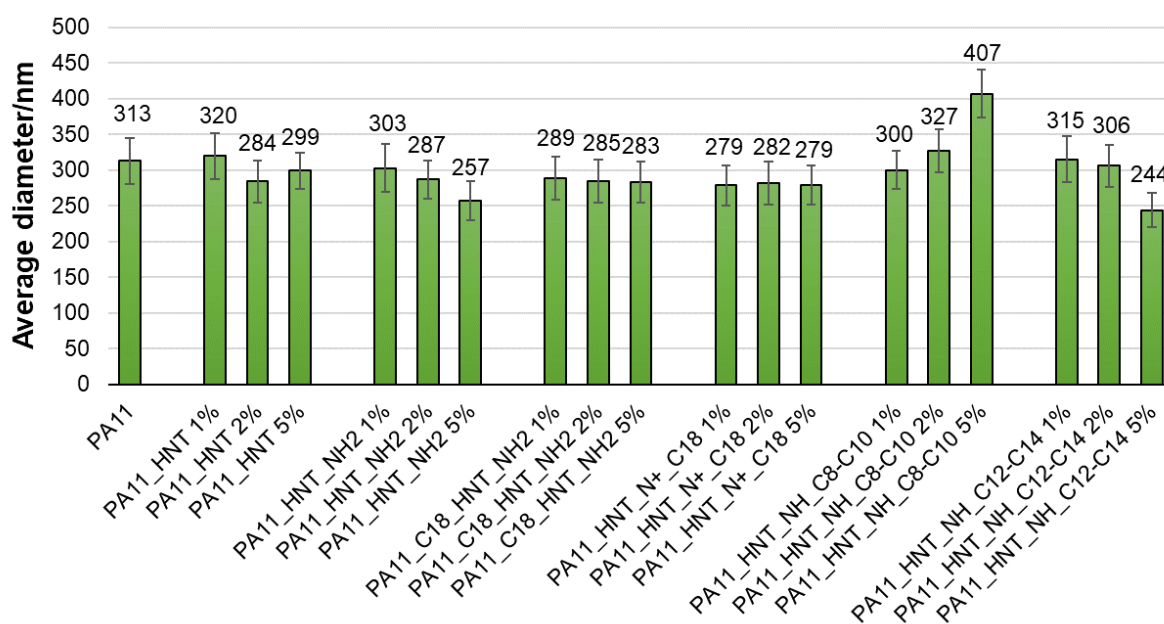


Figure 2.8. Histogram reporting the average diameter of the electrospun nanofibers produced with different functional nanofiller loading percentages.

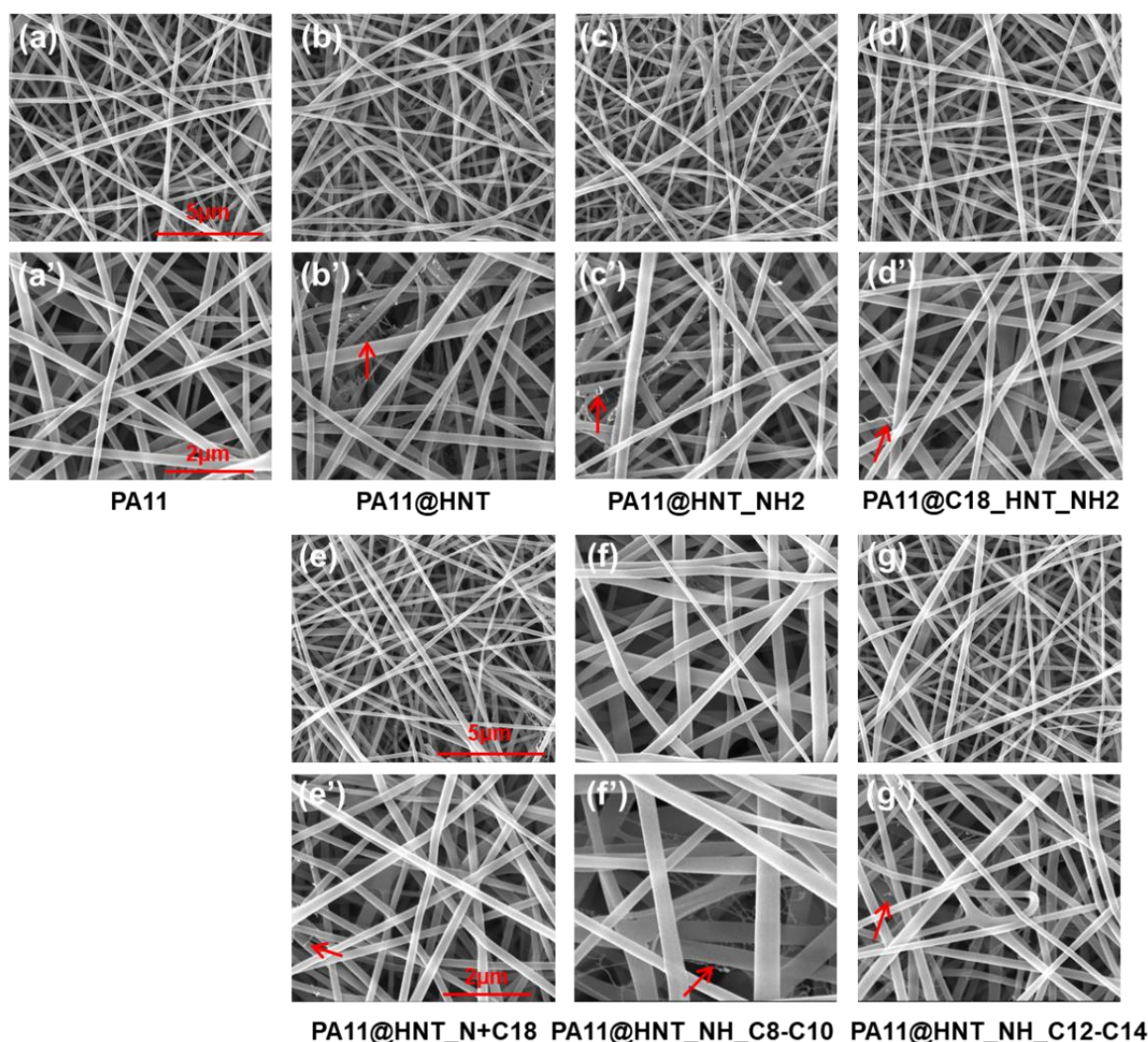


Figure 2.9. SEM images at two different magnifications (a–g and a'–g') of PA₁₁ ENMs doped with a 5% loading of the different HNT_NH₂, C18_HNT_NH₂, HNT_N+C18, HNT_NH_C8-C10 and HNT_NH_C12-C14 halloysite hybrid derivatives.

The figures show a characteristic distribution of thin mesh-like nanofibers with a high surface area-to-volume ratio. The morphology of the PA₁₁ nanofibers remains unchanged following the addition of functional nanofillers. The nanofibers produced have a uniform diameter and a smooth surface. This last element of evidence implies that the HNTs nanotubes are embedded within the produced PA₁₁ nanofibers and oriented co-axially along the nanofiber direction [118].

Despite this, a very fine 'secondary' mesh composed of finer fibers of PA₁₁ is observable, as illustrated by the arrows in Figure 2.9, most likely due to the enhanced conductivity of the initial polymeric mix and charge density variations after HNT nanofiller addition [119]. The average diameter range of all the nanofiber samples with the different loading values of halloysite derivatives is comprised in 244–327 nm as illustrated in Figure 2.8.

All the nanofiber samples are characterized by similar diameters compared to the pristine PA₁₁, thus evidencing that the hybrid halloysite derivatives do not affect only the obtaining of

excellent and uniformly distributed nanofibers, but also slight differences in their dimension. Furthermore, PA₁₁@HNT_NH_C8-C10 5% nanofibers have an average diameter of 407 ± 67 nm, which may be attributed to an increase in solution viscosity [119,120] due to the interactions between the organophilic HNT derivatives and the polymeric solution [121].

2.2.2.6 Electrospun nanofiber membrane static water contact angle measurement

Further characterizations were carried out in order to comprehend the influence of the HNT loading value and functionalization in the various polymeric blends. The water drop method was used to study the wetting behavior of the produced nanofibers. Figure 2.10 and Table 2.7 show the static water contact angle histogram and values, respectively, determined to better assess the surface wettability.

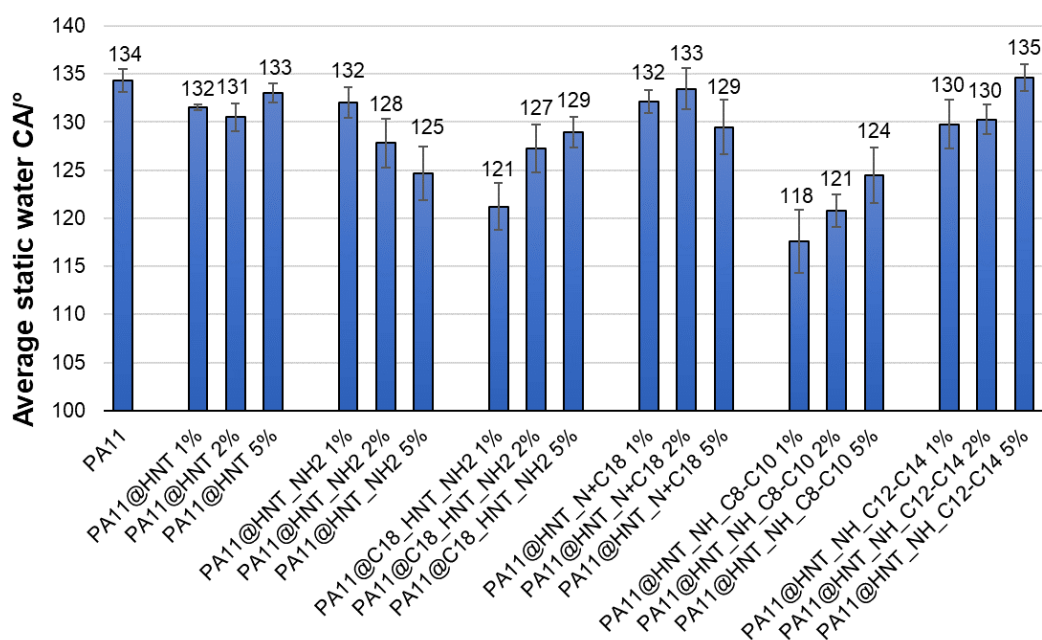


Figure 2.10. Histogram reporting the static water contact angle value of ENMs.

Table 2.7. Static water contact angle value results.

Name	WCA/°
PA ₁₁	134.3 ± 1.2
PA ₁₁ @HNT 1%	131.5 ± 0.3
PA ₁₁ @HNT 2%	130.5 ± 1.5
PA ₁₁ @HNT 5%	133.0 ± 1.0
PA ₁₁ @HNT_NH ₂ 1%	132.1 ± 1.6
PA ₁₁ @HNT_NH ₂ 2%	127.9 ± 2.5
PA ₁₁ @HNT_NH ₂ 5%	124.7 ± 2.8
PA ₁₁ @C18_HNT_NH ₂ 1%	121.2 ± 2.4
PA ₁₁ @C18_HNT_NH ₂ 2%	127.3 ± 2.5
PA ₁₁ @C18_HNT_NH ₂ 5%	128.9 ± 1.6
PA ₁₁ @HNT_N+C18 1%	132.2 ± 1.2
PA ₁₁ @HNT_N+C18 2%	133.5 ± 2.2
PA ₁₁ @HNT_N+C18 5%	129.5 ± 2.8

PA ₁₁ @HNT_NH_C8-C ₁₀ 1%	117.6 ± 3.3
PA ₁₁ @HNT_NH_C8-C ₁₀ 2%	120.7 ± 1.7
PA ₁₁ @HNT_NH_C8-C ₁₀ 5%	124.5 ± 2.9
PA ₁₁ @HNT_NH_C12-C ₁₄ 1%	129.8 ± 2.6
PA ₁₁ @HNT_NH_C12-C ₁₄ 2%	130.3 ± 1.6
PA ₁₁ @HNT_NH_C12-C ₁₄ 5%	134.6 ± 1.4

As indicated by the experimental results, the wetting behavior of the various doped ENMs shows to be moderately affected by the hybrid HNT derivative employed. Only the PA₁₁@HNT and PA₁₁@HNT_N+C₁₈ membranes do not exhibit a significant shift in static water contact angle values. Meanwhile, the PA₁₁@HNT_NH₂ shows a decrease in surface hydrophobicity from $132 \pm 3^\circ$ to $125 \pm 5^\circ$ proportional to the increasing of the nanofiller loading value, due to an increase in surface energy caused by the hydroxyl and amino groups present in the hybrid HNT derivatives [122]. Furthermore, PA₁₁@C₁₈_HNT_NH₂, PA₁₁@HNT_NH_C8-C₁₀, and PA₁₁@HNT_NH_C12-C₁₄ samples have higher hydrophilicity than pure PA₁₁ membrane. The WCA values for these samples slightly increase as the amount of doping nanofiller rise.

All the observed results may be explained in the distribution of the nanofiller into the polymeric nanofibers, together with that of the functional groups, and the hydrophobicity of the long alkyl chains of the employed functional molecules [123,124].

2.2.2.7 Tensile mechanical analysis

In Figure 2.11 a–c the tensile stress-strain graphs of the 5% loaded ENM samples doped with all the HNT derivatives are showed, together with the related average maximum stress and elongation at break values. All of the sample data exhibit the typical thermoplastic polymer behavior. The rigid morphology of the HNT nanotubes has been observed to reduce the rigidity and stiffness of polyamide 6,6 polymeric composite nanofibers (5, 10, 15, and 30 wt.% HNT load) [119].

The obtained results reveal moderate increase in tensile strength, which can be attributed to effective stress transfer from the PA₁₁ polymeric matrix to the hybrid nanofillers, as a result of good affinity and interfacial bonding between them, which causes a decrease in polymer chain mobility [115]. A slight increase of the average max strength is observed compared to pristine PA₁₁ for the PA₁₁@HNT, PA₁₁@HNT_NH₂, PA₁₁@C₁₈_HNT_NH₂, PA₁₁@HNT_N+C₁₈, and PA₁₁@HNT_NH_C12-C₁₄ doped ENMs (see Table 2.8).

Table 2.8. Average maximum tensile strength and elongation at break values of the tested electrospun nanofiber membranes.

Name	Average max tensile strength/MPa	Average elongation at break/%
PA ₁₁	3.04 ± 0.21	40.91 ± 5.00
PA ₁₁ @HNT 5%	3.81 ± 0.31	65.14 ± 6.77
PA ₁₁ @HNT_NH ₂ 5%	5.03 ± 0.09	73.09 ± 4.05
PA ₁₁ @C ₁₈ _HNT_NH ₂ 5%	4.26 ± 0.26	51.64 ± 3.19
PA ₁₁ @HNT_N+C ₁₈ 5%	4.36 ± 0.21	69.78 ± 4.52
PA ₁₁ @HNT_NH_C8-C ₁₀ 5%	3.07 ± 0.22	58.60 ± 5.21
PA ₁₁ @HNT_NH_C12-C ₁₄ 5%	4.42 ± 0.36	47.23 ± 5.84

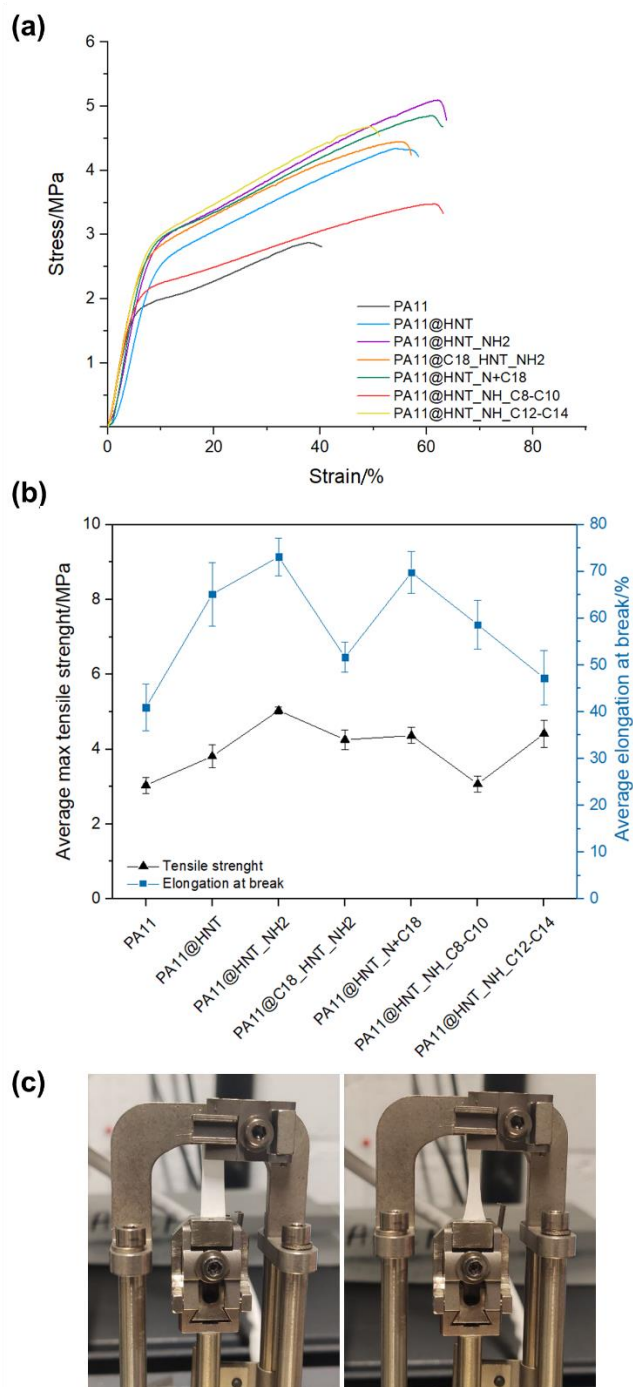


Figure 2.11. Plots showing the tensile stress-strain curves of the investigated materials (a), and average maximum tensile strength and elongation at break (b), together with the instrumental setup (c).

Only the PA11@HNT_NH_C8-C10 sample show a 3.07 ± 0.22 Mpa average maximum strength, which is not relevant in comparison to PA11 pristine ENM, but this result is consistent with the differences observed in the morphology and surface wettability analyses, confirming that there is a correlation between nanofiber diameter, wettability, and tensile strength.

Therefore, the effective transfer of stress to the HNT derivatives demonstrate again their well incorporation into the nanofibers, but also the achievement of ENMs with quite good mechanical features, making them suitable for possible applications in filtration devices.

2.2.2.8 Differential scanning calorimetry study

A study on the crystallinity changes upon a thermal treatment of the developed PA11 5% doped ENMs was performed and investigated with a DSC instrument. The results of the first heating, cooling and second heating measurements are showed in Figure 12 a–f and Figure 13 a–c, also showing the comparison between the melting and crystallization temperatures and the related enthalpy.

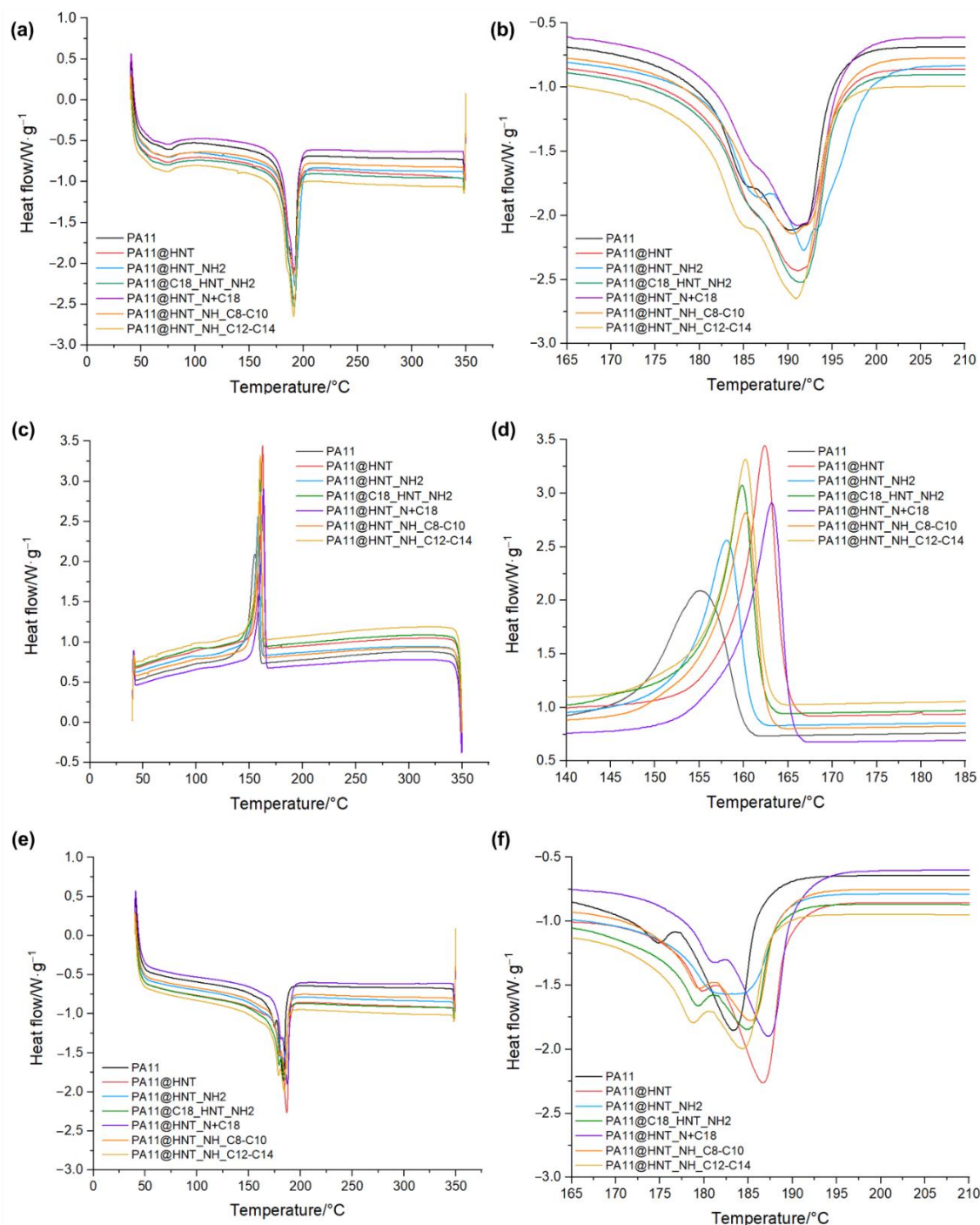


Figure 2.12. Plots showing the DSC data with magnification of the obtained results and elaboration of the average temperatures and enthalpies associated to the first heating run (a,b), second cooling run (c,d), and third heating run (e,f) of all the pristine PA11 ENMs and the 5% loaded ENMs.

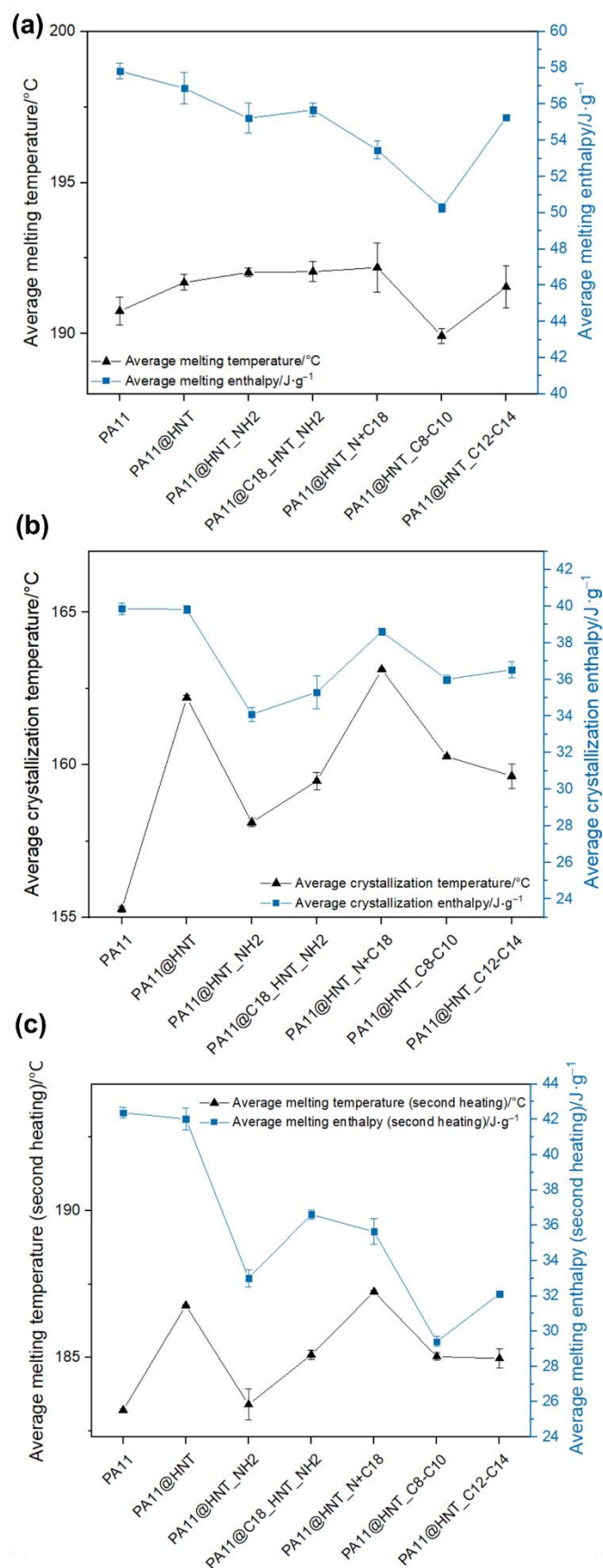


Figure 2.13. Plots reporting the average temperatures and enthalpies based on DSC data of the first heating run (a), second cooling run (b), and third heating run (c) of all the pristine PA11 ENMs and the 5% loaded ENMs.

The pristine PA11 and the doped ENMs show a melting peak comprised from 189 and 192 °C, revealing slight differences in this values and the related melting enthalpies due to the presence of the hybrid HNT nanofillers.

Meanwhile, the crystallization temperatures for the pristine PA11 ENM vary from 155.27 ± 0.09 °C to 163.13 ± 0.03 °C for the PA11@HNT_N+C18 ENM. These moderate variations might be explained by distinct forms of nucleation and crystallization growth taking place in composite ENMs featuring HNT derivatives [125]. After the second heating, the endothermic peak structures of all samples have small differences, suggesting a change in the crystal structure of the composite nanofibers probably as a consequence of the loosing of the intrinsic nanofiber morphology [126,127].

2.2.2.9 Organic dyes filtration experiments

Various separation tests were carried out in order to correlate the functionalities of the resulting doped nanofibers, as well as their removal capacity and selectivity towards anionic and cationic organic dyes. The model cationic and anionic molecules, MB and MO, respectively, were chosen to investigate the influence of the 5% loaded ENMs on the retention of two different types of organic dyes. A mixture of MO and MB ($V_{\text{tot}} = 50$ mL; $[\text{MO}] = [\text{MB}] = 2.5$ mg·L⁻¹) was then filtered in a dead-end filtration cell with a constant flux of 209 L·m⁻²·h⁻¹ under nitrogen flow and testing 1 and 3 layers of the same functional ENM for retention rate and separation efficiency determination.

As shown in Figure 2.14, 3 layers of ENMs are more effective than 1 layer in the retention of the two organic dyes, although in certain situations, they are less selective towards one of the two tested dyes.

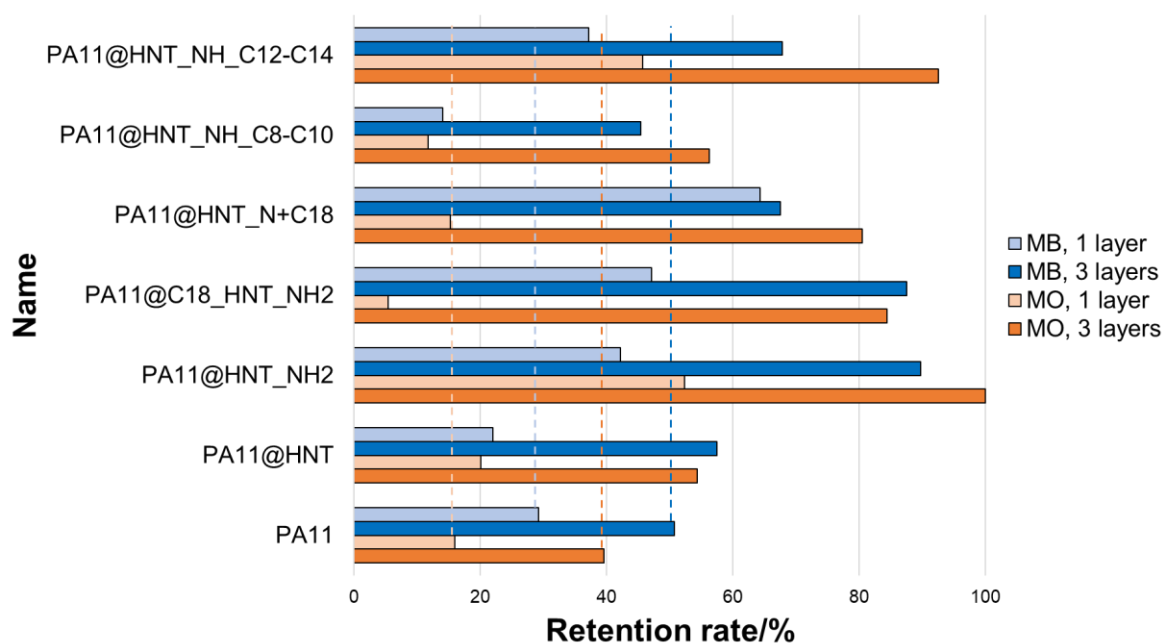


Figure 2.14. Retention rates for a MO and MB solution filtration in a dead-end filtration cell with 1 and 3 layers of 5% loaded ENMs.

Particularly, the 1-layer PA₁₁@C₁₈_HNT_NH₂ and PA₁₁@HNT_N+C₁₈ ENMs (Figure 15 a–d) demonstrate selectivity for the removal of the cationic dye MB, with retention rates of 47.1 and 64.3% and separation efficiencies of 69.8 and 73.3%, respectively.

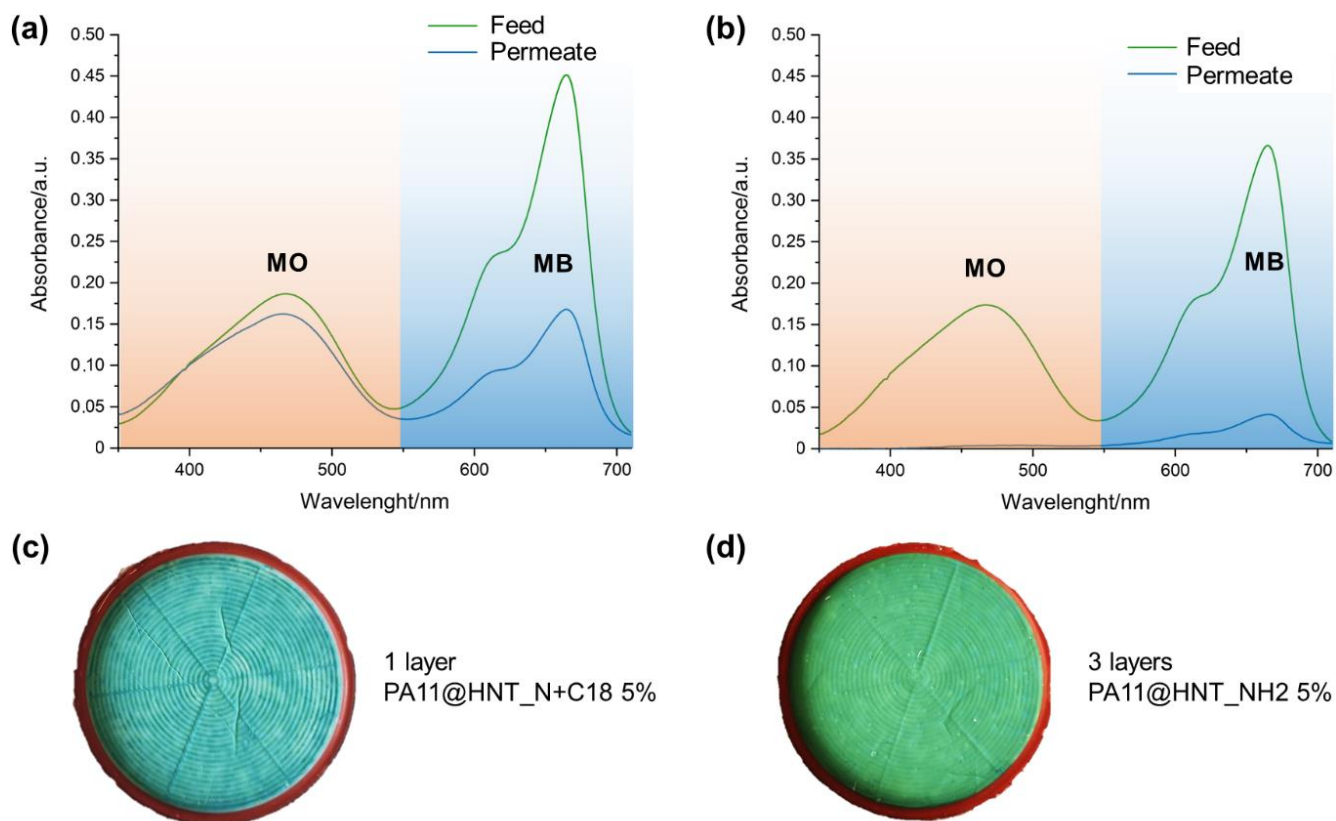


Figure 2.15. UV-Vis spectra of the MO/MB solution filtration experiment carried out via one layer of the PA₁₁@HNT_N+C₁₈ 5% ENM (a) and three layers of the PA₁₁@HNT_NH₂ 5% ENM (b), with corresponding pictures of their appearance after the filtration experiment (c, d).

This can be explained by the presence of cationic or cationizable groups (i.e., quaternary ammonium groups of N+C₁₈ functional molecule and APTES amino groups) in the hybrid HNT derivatives employed which allow the retention of MB according to the process depicted in Figure 16 a [128].

However, the extremely porous character of the developed ENMs may allow for enhanced interactions between anionic and cationic MO and MB dyes and hybrid HNT nanofillers [129], which promotes the production of fouling on the membrane surface resulting in higher retention rates of both the organic dyes as revealed from the 3 layer ENMs experiments (Figure 16 b) [130].

As a result, 3-layer PA₁₁@HNT_NH₂ ENMs show the highest MO and MB retention rates of 100 and 89.8%, respectively, followed by 3-layer PA₁₁@HNT_NH_C₁₂-C₁₄ (92.5 and 67.8%) > 3 layer PA₁₁@C₁₈_HNT_NH₂ (84.4 and 87.5%) > 3 layer PA₁₁@HNT_N+C₁₈ (80.4 and 67.5%).

The amorphous nature of PA₁₁ may also contribute in the retention of organic dyes [97], but more tests are needed to explain this phenomenon.

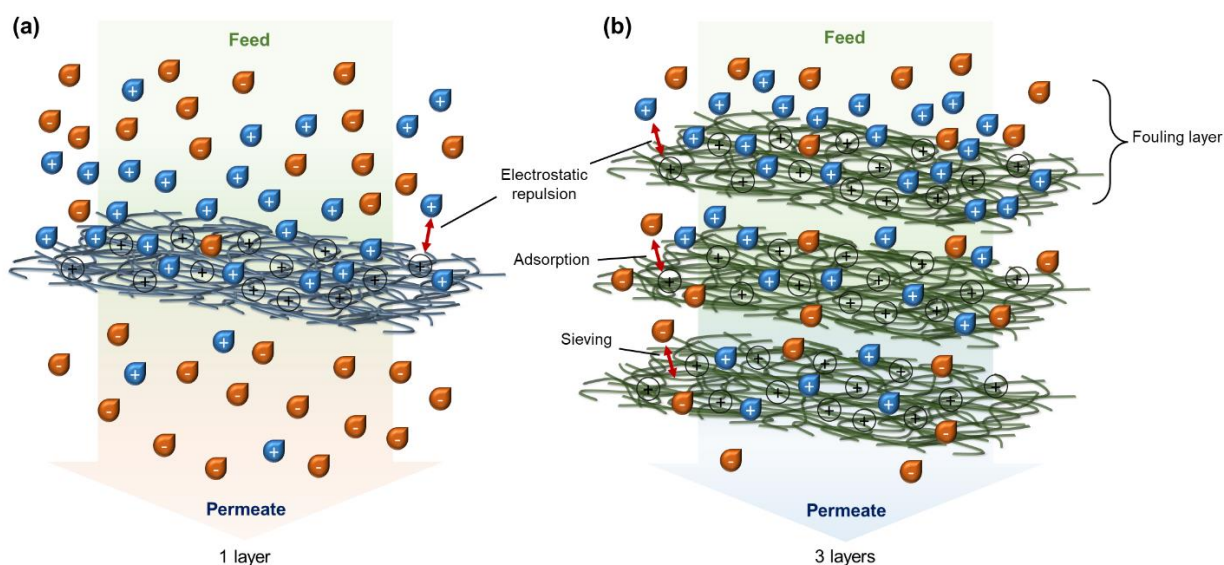


Figure 2.16. Illustration of sieving, adsorption, electrostatic repulsion, and fouling layer formation as possible processes responsible for the MO/MB retention and separation performances of the 1-layer (a) and 3-layer (b) ENMs.

2.2.3. Conclusions

Through a green sol-gel polymerization process, five distinct eco-friendly functional nanofillers based on halloysite clay were effectively synthesized. ATR-FTIR, XRD, and SEM investigations were used to examine the associated chemical-physical, crystalline, and morphological features. The electrospinning technology and a rotating collector were used to create new nanofiber-based membranes from polymer blends based on the embedding of these functional derivatives and the polyamide 11 biopolymer, while different concentrations of nanofillers (1, 2, and 5 wt.%) and process parameters were tested. The nanofiber shape, water wettability behavior, tensile and thermal characteristics of the produced ENMs were investigated. The separation efficiency and retention performances of the two model organic dyes, MO and MB, were researched using a dead-end filtering cell with one and three layers of each type of ENM. PA₁₁@C₁₈_HNT_NH₂ and PA₁₁@HNT_N+C₁₈ 1-layer ENMs demonstrate a selectivity towards the removal of the cationic dye MB with a separation efficiency of 69.8 and 73.3 % respectively, at a constant flux of 10 mL·min⁻¹ (209 L·m⁻²·h⁻¹). Hence, PA₁₁@HNT_NH₂ 3-layer ENMs display the highest retention rate for MO and MB of 100 and 89.8%, respectively.

In conclusion, the preliminary results achieved by these filtration experiments permits to affirm that, despite the hydrophobicity and poor adsorption properties of PA₁₁ polymer, the chemical, thermal and mechanical resistance of this material, when combined with synthetic functional HNT nanofillers, allow the production through the electrospinning process of nanofibers with quite good thermal and tensile properties, as well as retention and separation features towards cationic and anionic organic dyes. As a result, a fully bio-based, sustainable, and economically scalable approach for the production of new functional ENMs with potential applications in wastewater filtration was described, employing simple, low-impact, one-step synthesis protocols and procedures, with the goal of greener remediation technologies and future.

2.3. PA₁₁ and chitosan blends doped with functional halloysite derivatives for the preparation of electrospun nanofiber composite membranes

2.3.1. Abstract

Chitosan is a natural cationic polysaccharide generated from the deacetylation of chitin that has been extensively researched in a variety of applications. It is a biocompatible, biodegradable, and nontoxic copolymer of (1 → 4)-2-acetamido-2-deoxy-β-d-glucan and (1 → 4)-2-amino-2-deoxy-β-d-glucan. Because of its extraordinary qualities, such as antimicrobial, bioadhesive, coagulant, antibacterial properties, and wound healing ability, chitosan is an optimal candidate for applications in various sectors such as medicinal, cosmetics, and pharmaceutical, as well as agricultural product preservation [131].

Chitosan composites are widely employed in the food industry and (waste)water treatment, in addition to a variety of other industrial applications [132].

Although chitosan electrospinning has already been examined, particularly viscous polymer solutions such as alginate and carboxymethylcellulose are frequently difficult to electrospun due to their high surface tension and lack of chain entanglement [133]. As a result, current research has focused on electrospinning chitosan blends with other appropriate polymers such as polyethylene oxide [134], poly(vinyl alcohol) [135], polyamide-6 [136], polyamide-6,6 [137] and biopolymers such as gum Arabic [138] and cellulose acetate [139].

As explained before, halloysite nanotubes (HNT) are clay minerals from the layered aluminosilicate (1:1) family that are abundantly available, cheap, and have great mechanical and thermal stability [140]; thanks to its intriguing properties it is widely used as functional nanofiller in various applicative sectors. Other interesting aspects of this kind of nanoclay include good biodegradability, minimal cytotoxicity at higher HNT concentrations (up to 0.5 mg·mL⁻¹), and the ability to improve mechanical properties of reinforced polymeric electrospun mats [133].

Furthermore due to these overall properties, including a large specific area and variable surface chemistry, their usage in electrospun nanofiber membranes and composites for water purification has expanded significantly in recent years [141].

In the previous paragraph, the successful incorporation of various hybrid halloysite derivatives into PA₁₁ solution was demonstrated with the aim to prepare electrospun nanofiber membranes with quite good mechanical properties and retention performances towards two tested organic dyes (i.e., methyl orange and methylene blue) after filtration experiments performed in a dead-end filtration cell.

The synthesis of eco-friendly electrospun nanofiber composite membranes based on polyamide 11 and chitosan biopolymers in various ratios (90:10, 80:20, and 70:30 w/w PA₁₁/chitosan) is discussed in this paragraph. Three halloysite derivatives produced from (3-aminopropyl)triethoxysilane, dimethyloctadecyl[3(trimethoxysilyl)propyl]ammoniumchloride, and octyl/decyl glycidyl ether alkoxy silane precursors were used as functional additives to improve the properties of the final nanofibers.

These latter were subsequently collected on a polyester calendared substrate to produce electrospun nanofiber composite membranes that might be used in water filtration devices (Figure 2.17). The morphology, wettability behaviors, mechanical tensile and thermal properties

of pristine and doped PA₁₁ and PA₁₁/chitosan membranes were investigated, thus demonstrating the efficient enhancement of characteristics through the synergistic effects of cationic and hydroxyl group rich chitosan biopolymer, mechanical properties of PA₁₁, and, ultimately, the functionalities of hybrid halloysite derivatives.

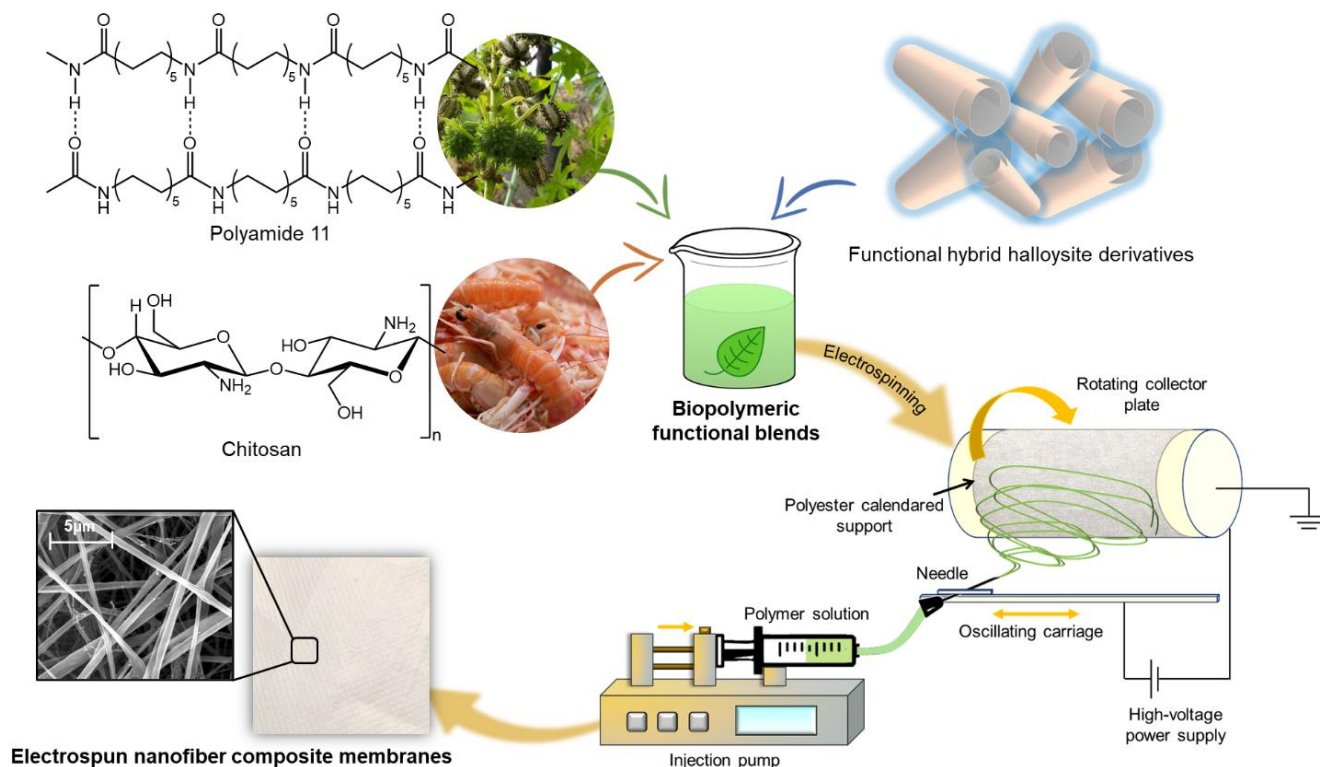


Figure 2.17. Schematic graphical representation of the preparation of advanced electrospun nanofiber composite membranes starting from PA₁₁ and chitosan bio-polymeric solutions doped with functional halloysite derivatives.

The whole research activity described in this paragraph 2.3 refers to the content outlined in the article n.3 of the publication list.

2.3.2. Results and discussions

2.3.2.1 Functionalization approaches and bio-polymeric blend preparation

The functional halloysite derivatives used in the present research were created using ecologically friendly and sustainable methods. Three hybrid derivatives were obtained using sol-gel synthesis in water and ethanol as solvents. The sol-gel approach is an interesting synthetic strategy for developing superior formulations with high structural and compositional homogeneity. It consists of a sequence of simple hydrolysis and condensation processes of metal alkoxides.

The low temperature chemistry, repeatability, lack of toxic solvents, and high surface-to-volume ratios of generated compounds differentiate this process [3,142].

As a consequence, three distinct halloysite hybrid nanofillers (Figure 2.18) were developed and named as HNT_NH₂, HNT_N+_C₁₈ and HNT_NH_C₈-C₁₀, by use respectively of the

alkoxysilane precursors (3-aminopropyl)triethoxysilane, dimethyloctadecyl[3(trimethoxysilyl)propyl]ammoniumchloride and octyl/decyl glycidyl ether.

The alkoxysilane precursors were chosen to impart diverse functionalities to halloysite nanotubes and exploit various interactions with potential target water contaminants.

Furthermore, because of the presence of the added organic functionality, the obtained hybrid materials can be easily blended with polymers to achieve better homogeneity of the final blend, as well as to promote their cross-linking and hydrogen bonding interactions with the polymeric matrix (Figure 2.19).

The ATR-FTIR, XRD and SEM characterizations of the three HNT derivatives were already reported in the previous paragraph.

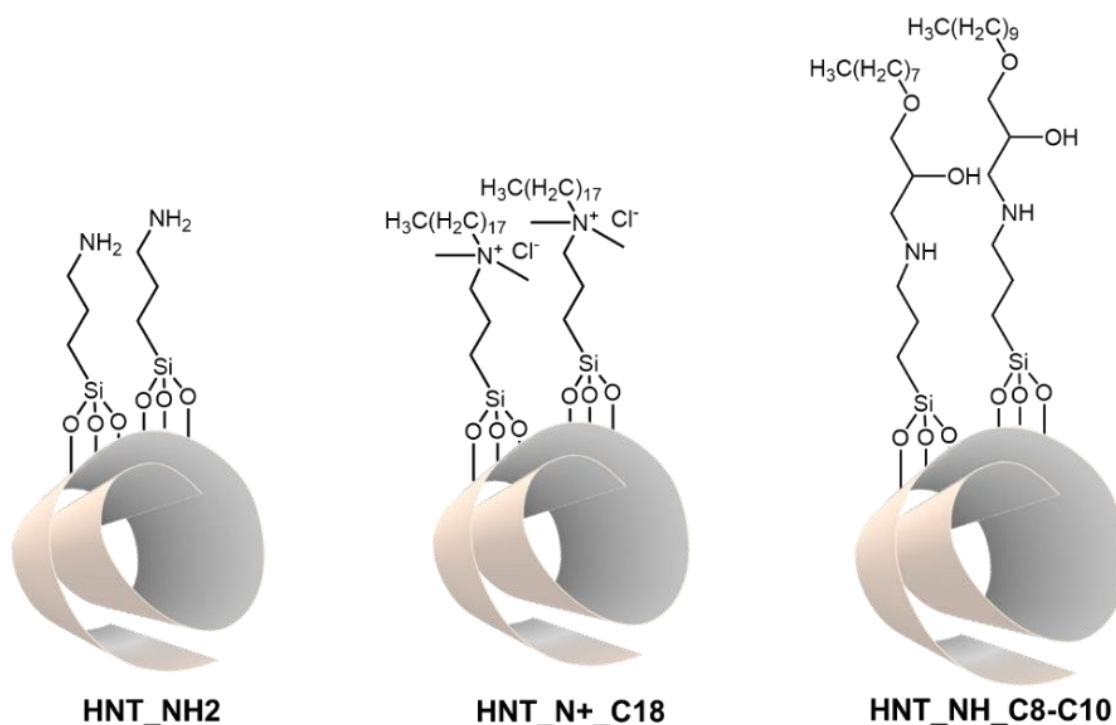


Figure 2.18. Graphical illustration of halloysite derivatives developed as functional nanofillers for the electrospun nanofiber composite membrane development.

Polyamide 11 and chitosan are used as biopolymers for electrospun nanofibers preparation doped with functional hybrid nanofillers.

The main goal of this work thus is the synergic combination of the very good mechanical and thermal properties of polyamide 11 with the functionalities of chitosan biopolymer and HNT derivatives to obtain membranes with enhanced properties that could be evaluated as eco-friendly alternatives to common fossil-based membranes for water remediation.

The thermal, mechanical, and wettability characteristics of the produced membranes with varied PA11/chitosan ratios (i.e., 90:10, 80:20, 70:30, w/w) and functional nanofillers at 3% wt. (of PA11) are thus detailed. The electrospinning technique was carried out on a polyester calendared support (PE) in order to prepare PE_PA11 and PE_PA11/Chitosan composite membranes for an easy use in water filtration processes.

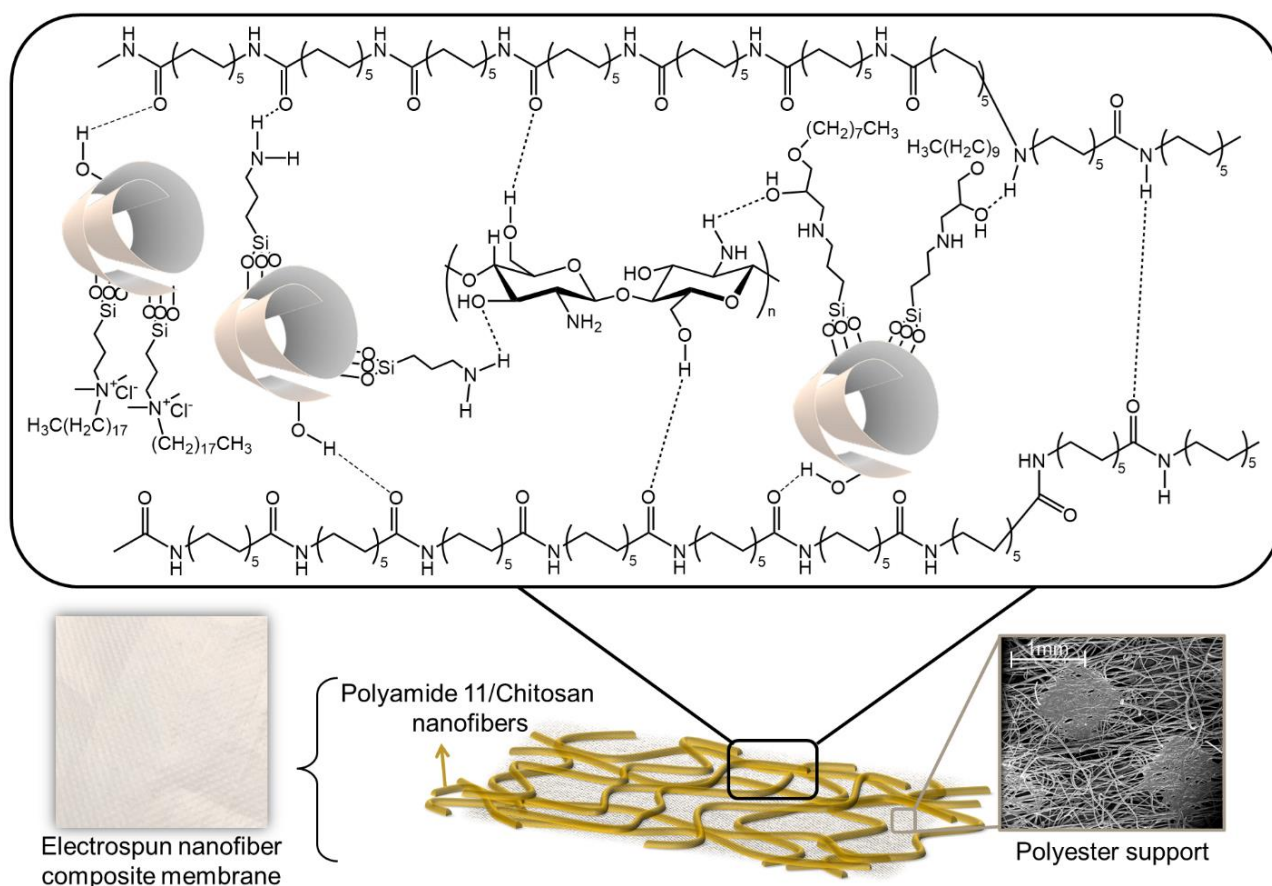


Figure 2.19. Illustration of polyamide 11/chitosan electrospun nanofibers doped with hybrid functional halloysite derivatives and spun on a polyester calendared substrate, with its SEM image, and potential interactions taking place between biopolymers and additives.

2.3.2.2 Bio-polymeric blends and electrospun nanofiber membranes preparation and characteristics

Bio-polymeric blends were developed by combining PA₁₁ with chitosan (in a total polymeric concentration of 12% wt.% g·mL⁻¹) in the following ratios: 90:10, 80:20, and 70:30 (PA₁₁/chitosan). Formic acid and anisole in a 60:40 volumetric ratio was then added as a solvent.

A 3% w/w (to total polymers) ratio of each nanofiller was added individually to the PA₁₁ or PA₁₁/Chitosan solution. The mixture was agitated in an oil bath at 40°C for one hour, before electrospinning it.

The PA₁₁ and PA₁₁/Chitosan blends (these lasts also known as PA₁₁/Chi) were electrospun at room temperature.

The nanofibers were collected using a large rotating drum (rotation speed of 200 rpm) that was covered in aluminum foil and a polyester calendared substrate. A voltage of 25 kV, a distance of 4 cm from the syringe needle tip and the collector and a solution flow rate of 1 mL·h⁻¹ was used as the electrospinning settings.

For each membrane, the nanofibers were collected for a total of one hour using four syringes operating concurrently.

Table 2.9 illustrates a list of the developed hybrid electrospun nanofiber composite membranes, together with their average weight and thickness.

Table 2.9. Properties of the developed hybrid electrospun nanofiber composite membranes.

Name	Average weight/mg·cm ⁻²	Average thickness/μm
PE Support	4.74 ± 0.08	133 ± 3
PE_PA11	5.25 ± 0.14	165 ± 6
PE_PA11@HNT	5.36 ± 0.12	149 ± 6
PE_PA11@HNT_NH ₂	5.35 ± 0.18	155 ± 7
PE_PA11@HNT_N+_C18	5.32 ± 0.07	153 ± 7
PE_PA11@HNT_NH_C8-C10	5.05 ± 0.15	153 ± 9
PE_PA11/Chi 90:10	5.00 ± 0.16	155 ± 7
PE_PA11/Chi 90:10@HNT	5.07 ± 0.04	161 ± 5
PE_PA11/Chi 90:10@HNT_NH ₂	5.99 ± 0.32	153 ± 9
PE_PA11/Chi90:10@N+_C18	5.55 ± 0.29	150 ± 8
PE_PA11/Chi 90:10@NH_C8-C10	5.36 ± 0.18	152 ± 3
PE_PA11/Chi 80:20	5.28 ± 0.07	152 ± 9
PE_PA11/Chi 80:20@HNT	5.51 ± 0.18	145 ± 4
PE_PA11/Chi 80:20@HNT_NH ₂	5.08 ± 0.17	144 ± 7
PE_PA11/Chi 80:20@N+_C18	5.10 ± 0.18	142 ± 7
PE_PA11/Chi 80:20@NH_C8-C10	5.11 ± 0.19	157 ± 2
PE_PA11/Chi 70:30	5.27 ± 0.32	144 ± 7
PE_PA11/Chi 70:30@HNT	5.14 ± 0.24	145 ± 7
PE_PA11/Chi 70:30@HNT_NH ₂	5.20 ± 0.24	156 ± 5
PE_PA11/Chi 70:30@N+_C18	6.04 ± 0.24	147 ± 5
PE_PA11/Chi 70:30@NH_C8-C10	5.07 ± 0.12	165 ± 4

2.3.2.3 Morphological analysis of the electrospun nanofiber composite membranes

Scanning electron microscopy (SEM) was used to examine the morphology of the nanofiber composite membranes. Figures 2.20 a–t and 2.21 a–t show micrographs of various pristine and doped PE_PA11 and PE_PA11/Chitosan-based nanofibers on PE support, at two different magnifications.

The images show fine mesh-like nanofibers with a high surface area-to-volume ratio and a smooth surface. The smooth surface of the nanofibers indicates that HNTs nanotubes are co-axially aligned along the nanofiber direction and are therefore incorporated within the nanofibers [118].

Figures 2.20, 2.21 and 2.22 and Table 2.10 show that the form and average diameter of the nanofibers vary with the concentration of chitosan in the starting blend solution, ranging from a maximum of 671 ± 79 nm for PE_PA11/Chi 90:10@NH_C8-C10 samples to a minimum of 388 ± 43 nm for PE_PA11/Chi 70:30@NH_C8-C10 samples.

When the chitosan content increased to 20 wt.% in PA11, the nanofiber diameter decreased, and they became progressively non uniform. In comparison to the other samples, the PA11/Chitosan 70:30 nanofibers are slightly finer.

Polymer conductivity may be increased by including cationic and anionic polyelectrolytes, resulting in finer fibers.

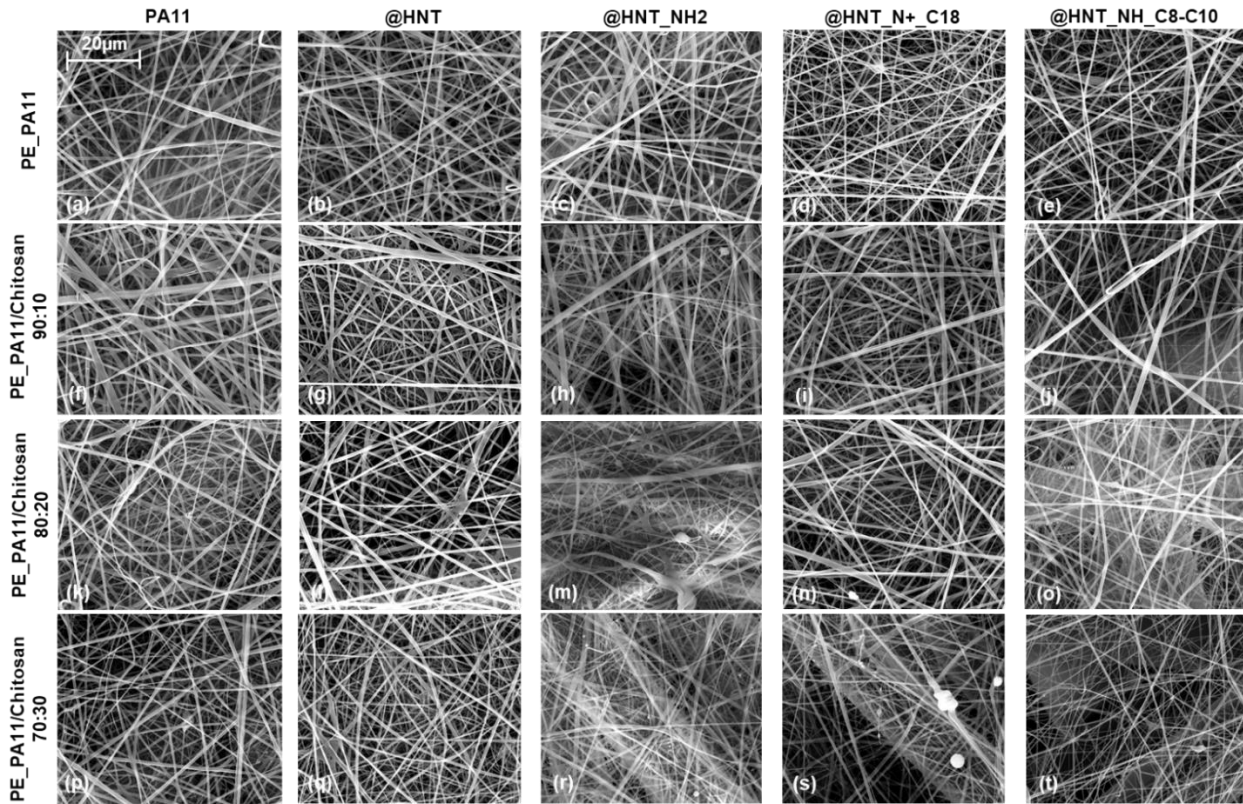


Figure 2.20. SEM images of pristine (a,f,k,p) and doped (b–e, g–j, l–o, q–t) PE_PA11 (a–e) and PE_PA11/Chitosan (f–t) electrospun nanofiber composite membranes (magnification 5,000 \times).

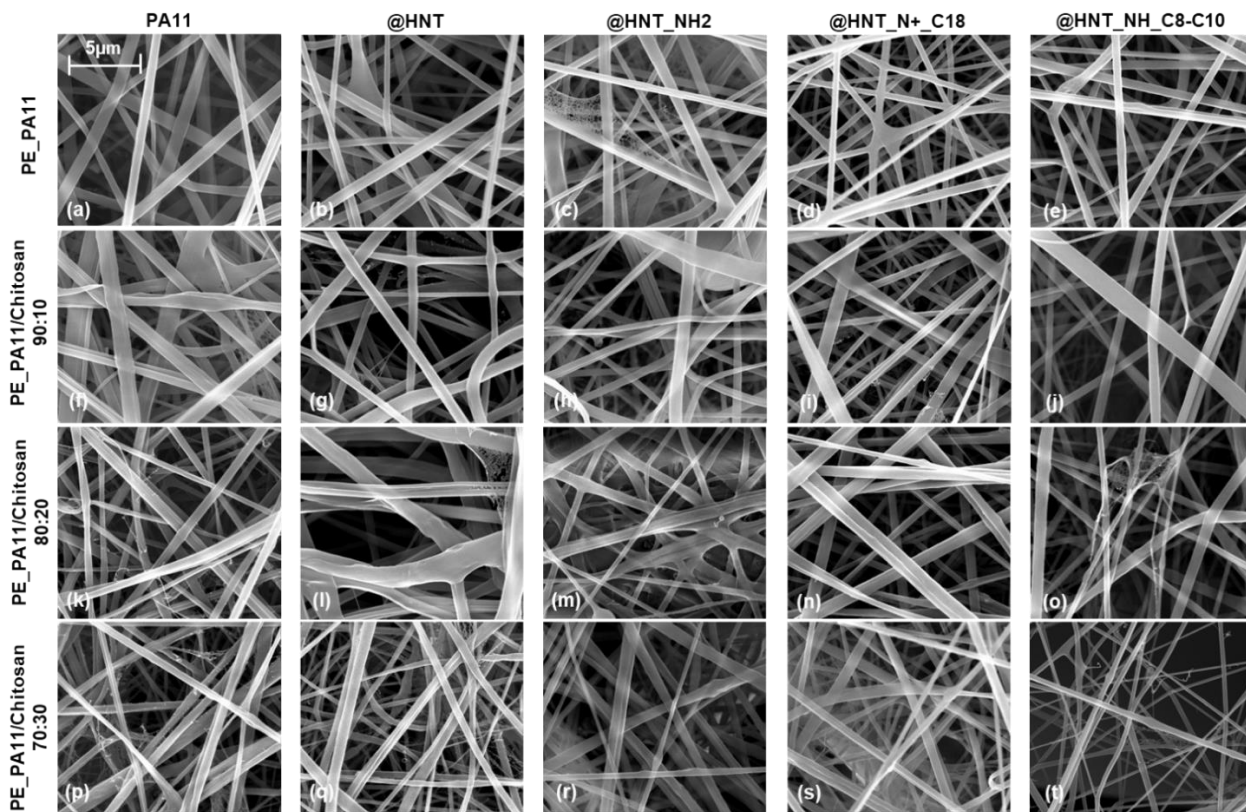
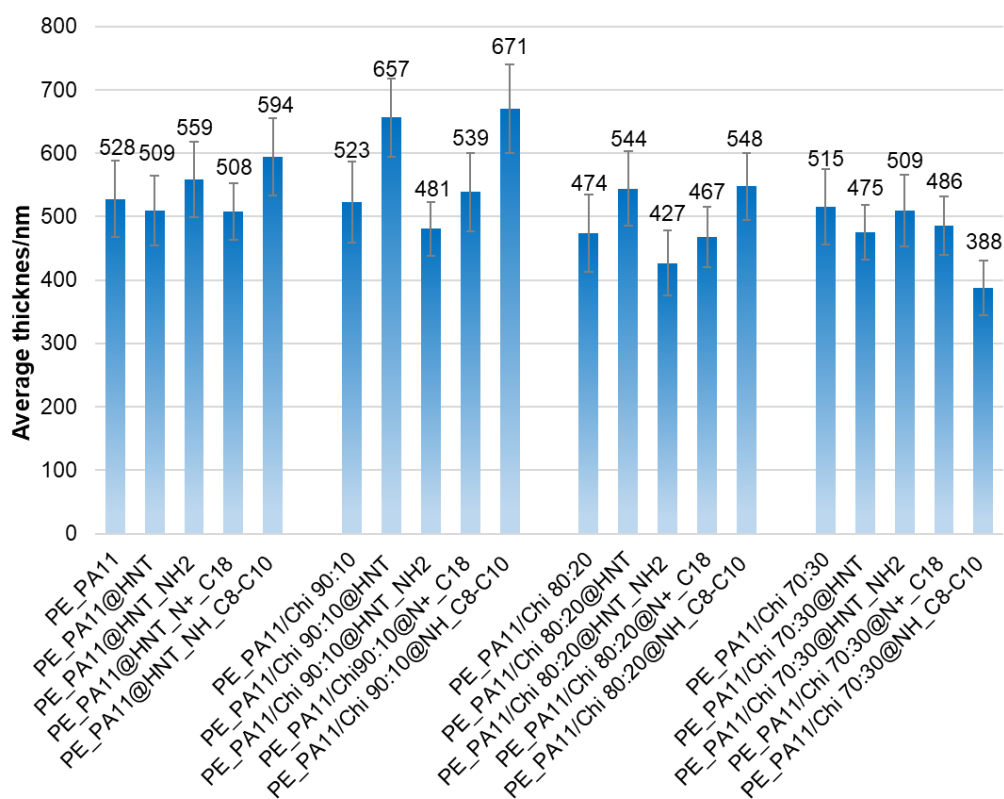


Figure 2.21. SEM images of pristine (a,f,k,p) and doped (b–e, g–j, l–o, q–t) PE_PA11 (a–e) and PE_PA11/Chitosan (f–t) electrospun nanofiber composite membranes (magnification 20,000 \times).

Table 2.10. Average thickness of pristine and doped PE_PA11 and PE_PA11/Chitosan electrospun nanofibers.

Name	Average thickness/nm
PE_PA11	528 ± 60
PE_PA11@HNT	509 ± 55
PE_PA11@HNT_NH ₂	559 ± 60
PE_PA11@HNT_N+_C18	508 ± 45
PE_PA11@HNT_NH_C8-C10	594 ± 61
PE_PA11/Chi 90:10	523 ± 64
PE_PA11/Chi 90:10@HNT	657 ± 62
PE_PA11/Chi 90:10@HNT_NH ₂	481 ± 43
PE_PA11/Chi90:10@N+_C18	539 ± 62
PE_PA11/Chi 90:10@NH_C8-C10	671 ± 79
PE_PA11/Chi 80:20	474 ± 61
PE_PA11/Chi 80:20@HNT	544 ± 59
PE_PA11/Chi 80:20@HNT_NH ₂	427 ± 51
PE_PA11/Chi 80:20@N+_C18	467 ± 48
PE_PA11/Chi 80:20@NH_C8-C10	548 ± 53
PE_PA11/Chi 70:30	515 ± 60
PE_PA11/Chi 70:30@HNT	475 ± 43
PE_PA11/Chi 70:30@HNT_NH ₂	509 ± 57
PE_PA11/Chi 70:30@N+_C18	486 ± 46
PE_PA11/Chi 70:30@NH_C8-C10	388 ± 43

**Figure 2.22.** Histogram showing the average thickness of pure and doped PE_PA11 and PE_PA11/Chitosan electrospun nanofibers.

Chitosan is a cationic polysaccharide with ionizable amino groups at acidic or neutral pH, resulting in a higher charge density on the surface of an electrospun ejected jet. As the charges carried by the jet increase, the electrical field drives the jet to elongate further, resulting in thinner fibers [137,143,144].

Furthermore, the inclusion of hybrid halloysite derivatives containing cationizable or quaternary amino groups may improve this action. The increased conductivity of the initial polymeric blend for the combined presence of chitosan and HNT derivatives also promotes the nano nailed-bat-like morphology seen in Figure 2.21 c,f,i,k,l,o,p,f [119,145].

2.3.2.4 Electrospun nanofiber mats static water contact angle measurements

Static water contact angle measurements were performed to study the surface wettability of pristine and doped PA₁₁ and PA₁₁/Chitosan nanofibers (Figure 2.23 and Table 2.11).

The wetting behavior of the as spun nanofibers was evaluated by introducing a water drop to the nanofiber mat without the PE support.

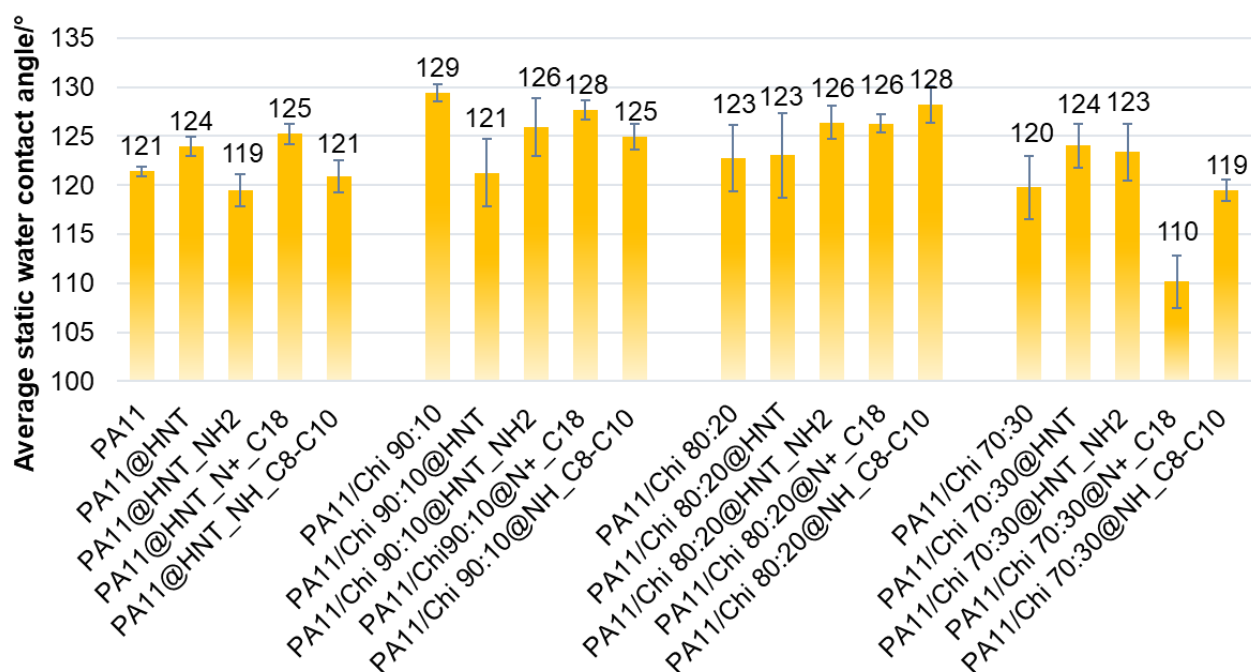


Figure 2.23. Histogram reporting the wettability data of pristine and doped PA₁₁ and PA₁₁/Chitosan nanofibers.

Table 2.11. Electrospun nanofiber static water contact angle.

Name	Average static water contact angle/°
PA ₁₁	121.4 ± 0.5
PA ₁₁ @HNT	124.0 ± 1.0
PA ₁₁ @HNT_NH ₂	119.5 ± 1.6
PA ₁₁ @HNT_N ⁺ _C18	125.2 ± 1.0
PA ₁₁ @HNT_NH_C8-C10	120.9 ± 1.7
PA ₁₁ /Chi 90:10	129.4 ± 0.9

PA ₁₁ /Chi 90:10@HNT	121.3 ± 3.5
PA ₁₁ /Chi 90:10@HNT_NH ₂	126.0 ± 2.9
PA ₁₁ /Chi 90:10@N ₊ _C18	127.7 ± 1.0
PA ₁₁ /Chi 90:10@NH_C8-C10	124.9 ± 1.3
PA ₁₁ /Chi 80:20	122.8 ± 3.4
PA ₁₁ /Chi 80:20@HNT	123.0 ± 4.3
PA ₁₁ /Chi 80:20@HNT_NH ₂	126.4 ± 1.7
PA ₁₁ /Chi 80:20@N ₊ _C18	126.3 ± 0.9
PA ₁₁ /Chi 80:20@NH_C8-C10	128.3 ± 1.9
PA ₁₁ /Chi 70:30	119.8 ± 3.2
PA ₁₁ /Chi 70:30@HNT	124.1 ± 2.2
PA ₁₁ /Chi 70:30@HNT_NH ₂	123.4 ± 2.9
PA ₁₁ /Chi 70:30@N ₊ _C18	110.2 ± 2.7
PA ₁₁ /Chi 70:30@NH_C8-C10	119.5 ± 1.1

The numerous hydroxyl and amine groups in chitosan, as well as the amide groups that are partly hydrolyzed, all contribute to the hydrophilicity of the final chitosan composites [144].

The hydrophilicity of PA₁₁/Chi 90:10, PA₁₁/Chi 80:20, and PA₁₁/Chi 70:30 mats slight increase from 129.4 ± 0.9° to 122.8 ± 3.4° and 119.8 ± 3.2°, respectively.

PA₁₁/Chi 70:30@N₊_C18 sample demonstrate the lowest water contact angle value of 110.2 ± 2.7°. In contrast, certain doped PA₁₁/Chitosan nanofibers have a moderate lower hydrophilicity than pristine ones.

This behavior may be explained by the cross-linking and interactions of the hydroxyl and amino groups of hybrid nanofillers with PA₁₁ and chitosan, resulting in an increase in the hydrophobicity of the final nanofibers [146].

Surface wettability is critical in the manufacturing of water filtration membranes. Energy consumption reduction in high-water flux processes, as well as the functional features of dopant agents, may promote economic and significant benefits in the advanced retention and adsorption of target water pollutants from wastewater treatment facilities.

2.3.2.5 Thermal properties study of the electrospun nanofiber mats

A DSC instrument was used to study the changes in crystallinity of pristine and doped PA₁₁ and PA₁₁/Chi 80:20 nanofibers after heat treatment (Figure 2.24 a–c and Figure 2.25 a–f).

Figures 2.24 a–f provides a comparison of the melting and crystallization temperatures and enthalpy, while Figures 2.25 a–c shows the results of the first heating, cooling, and second heating measurements.

The melting temperatures of pure and doped PA₁₁ and PA₁₁/Chi 80:20 nanofibers vary slightly, ranging from 173.9 ± 1.3 °C for PA₁₁/Chi 80:20 to 181.5 ± 1.4 °C for PA₁₁@HNT samples.

The PA₁₁ pristine and PA₁₁/Chi (80:20) derivative electrospun nanofiber crystallisation temperatures are 154.9 ± 0.4 °C and 149.6 ± 1.4 °C, respectively.

The moderate differences in crystallization temperature and enthalpy of the pristine and doped samples may be attributed to the various forms of nucleation and crystallization growth of the doped nanofiber additives [125]. Following the second heating, the endothermic peak structures of all samples shows slight changes, indicating the loss of morphology of the nanofibers [126,127].

More tests are needed to thoroughly study changes in the amorphous nature of PA11 nanofibers.

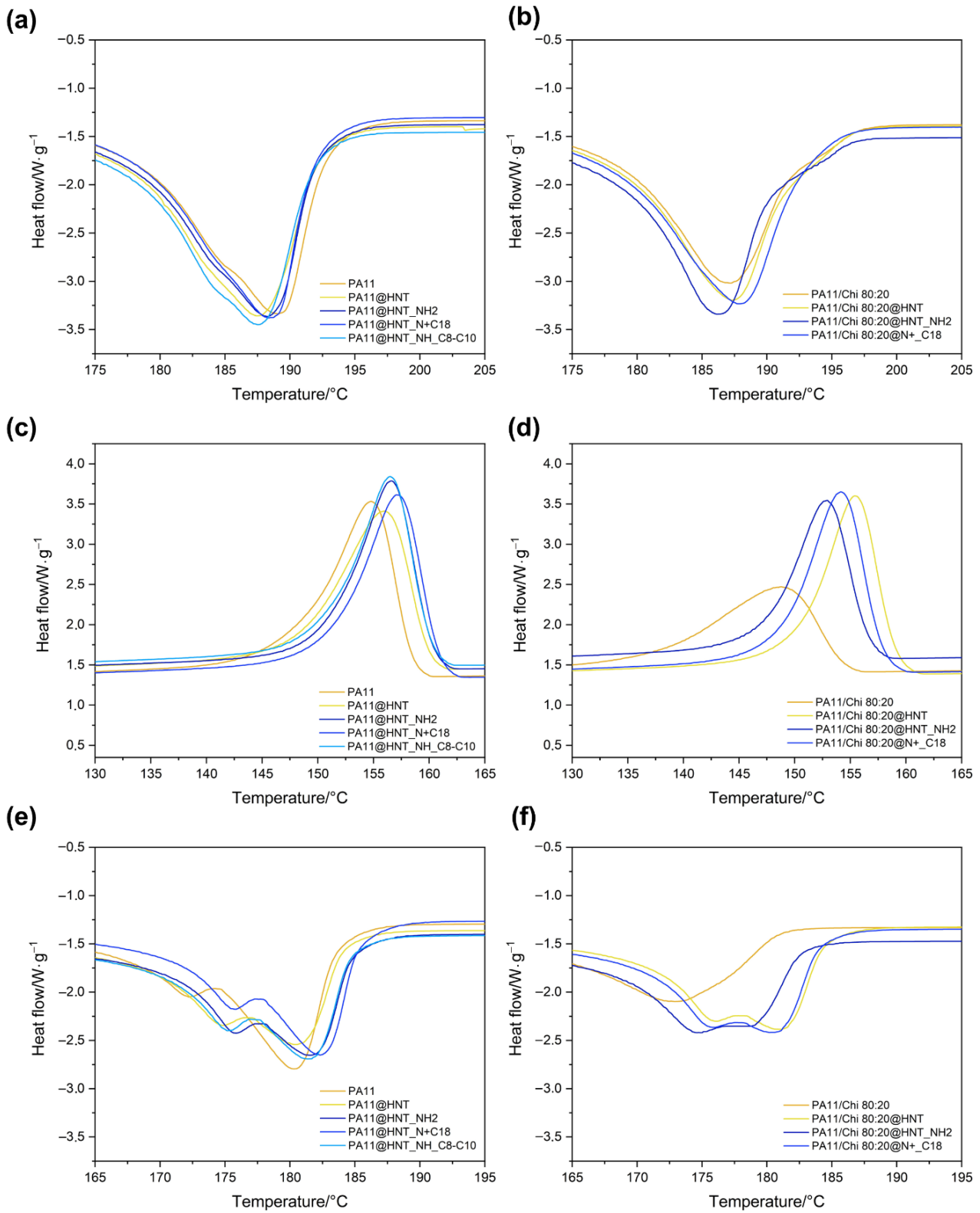


Figure 2.24. DSC data plots with magnification of the first heating run (a, b), second cooling run (c, d), and third heating run (e, f) of pristine and doped PA11 and PA11/Chit 80:20 electrospun nanofibers.

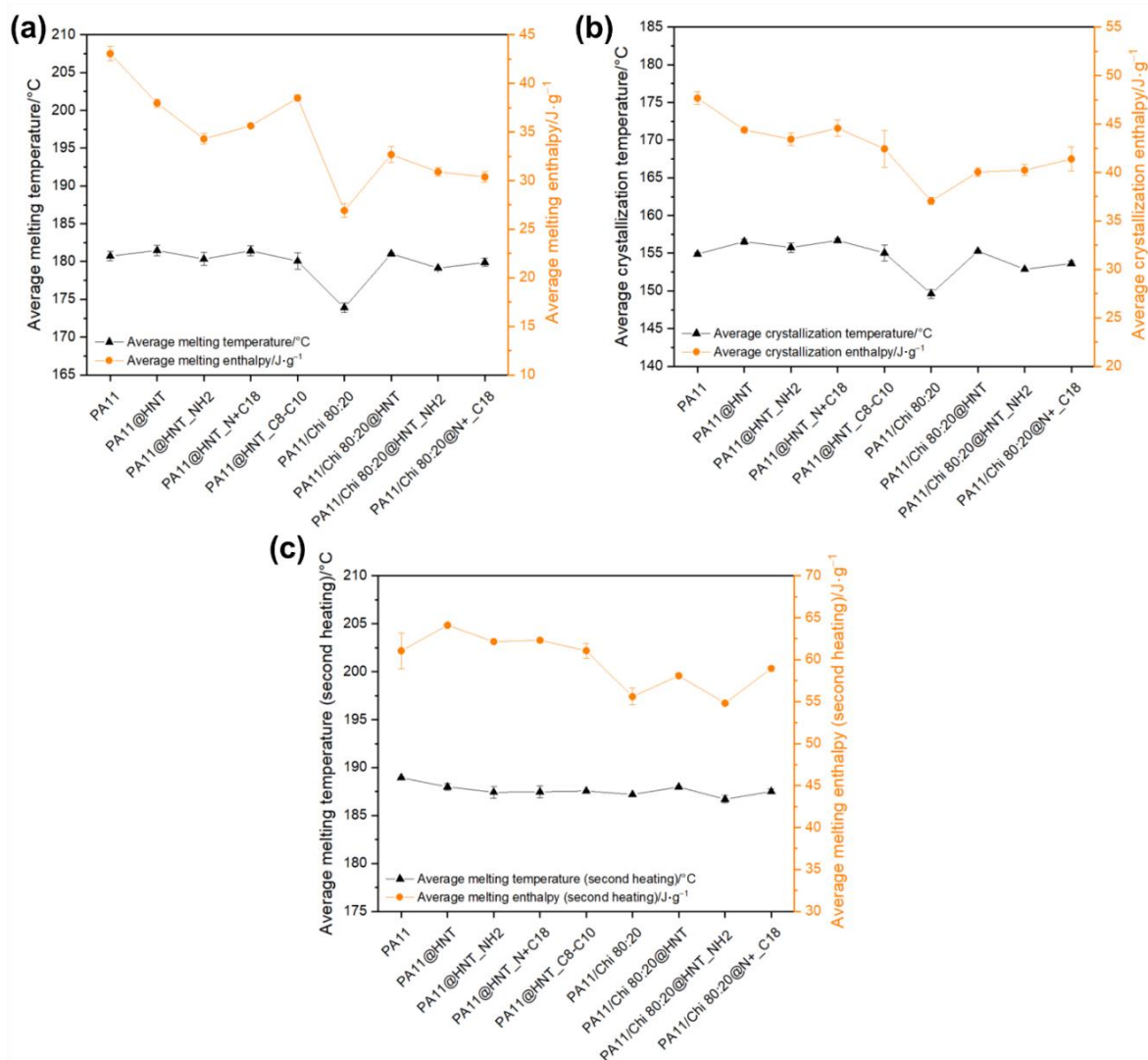


Figure 2.25. Elaboration data plots of average temperatures and enthalpies based on DSC data from the first heating run (a), second cooling run (b), and third heating run (c) of pristine and doped PA11 and PA11/Chit 80:20 electrospun nanofibers.

2.3.2.6 Tensile mechanical properties study of the electrospun nanofiber composite membranes

A DMA instrument was used to examine the tensile mechanical characteristics of the composite PE_PA11 and PE_PA11/Chitosan electrospun nanofiber membranes.

Figure 2.26 a–d displays the stress/strain graphs. Figure 2.27 illustrates the average maximum tensile strength of the tested specimens. When compared to pristine PE support and PE_PA11 nanofibers, the doped composite nanofibers exhibit enhanced strength. The effect of PE support is playing a key role, as showed in the enhancement of the mechanical tensile properties of the obtained composite membranes compared to pristine nanofibers.

Because of their rigid shape, high concentrations of HNT nanotubes reduce the rigidity and stiffness of PA 6,6 polymeric composite nanofibers [119]. Agglomeration would occur at higher levels of HNT loading, resulting in stress concentration areas and lowering mechanical strength [147]. The reported moderate increase in tensile strength can be attributed to the effective stress transfer from the PA11 polymeric matrix to the hybrid organophilic nanofillers as a result of good

affinity and interfacial bonding between them, resulting in a decrease in polymer chain mobility [115].

Other factors that possibly contribute to the increase in mechanical tensile properties are as following: (i) uniform dispersion of 3 wt.% HNT in the PA₁₁ and PA₁₁/Chitosan matrices, which prevents nanofiller agglomeration, (ii) hydrogen bonding between the functional groups on the HNT surface and PA₁₁ and chitosan, (iii) electrostatic interactions between the biopolymers and nanofiller [133], and (iv) stronger bridging interactions between the nanofibrous layer and the support.

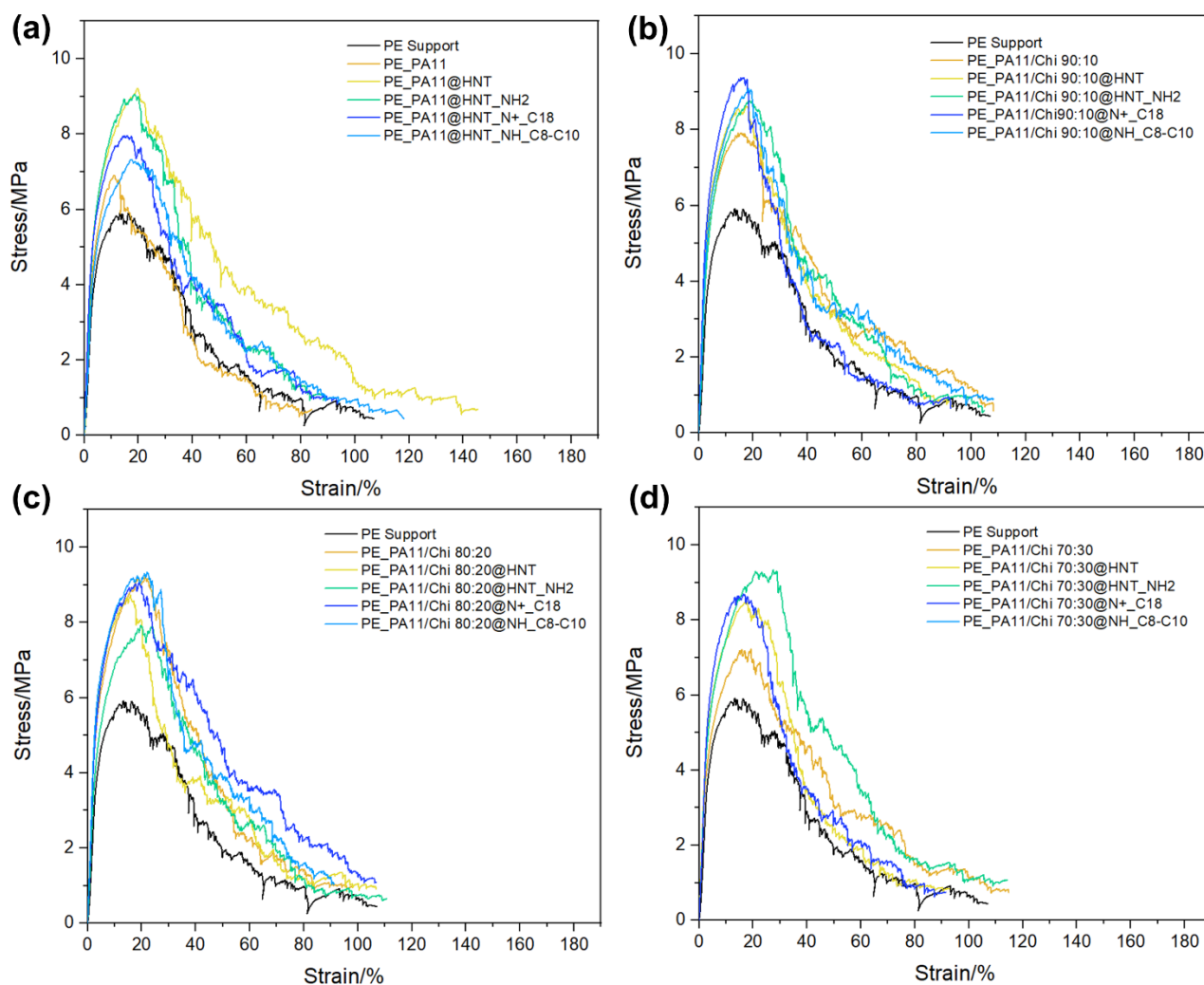


Figure 2.26. Tensile stress-strain curves for the analyzed PE_PA₁₁ samples (a), PE_PA₁₁/Chitosan 90:10 (b), PE_PA₁₁/Chitosan 80:20 (c), and PE_PA₁₁/Chitosan 70:30 (d).

The increase in chitosan weight ratio has no detrimental effect on the average maximum strength of the nanofibers when compared to PE_PA₁₁ samples. Only at high PA₁₁/Chitosan ratios (70:30 w/w PA₁₁/Chitosan) is observed a modest drop in maximum strength.

It has been proven that the addition of chitosan weakens the hydrogen bond between polyamide chains, shortening or increasing bond order and, thereby, increasing bond stiffness [148].

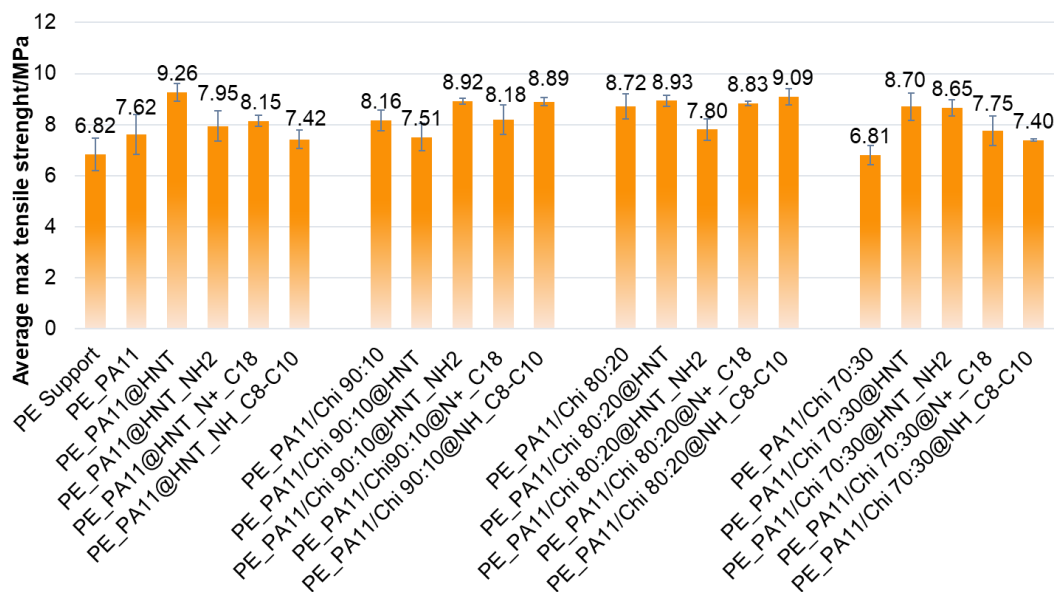


Figure 2.27. Histogram of the average maximum tensile strength of the electrospun nanofiber composite membranes.

In particular, the hydrogen link between the C=O and N-H amide planes is broken (as shown in Figure 2.28) and the dipoles shift to a different orientation to save energy and construct a new amide plane with the inserted chitosan molecules [144].

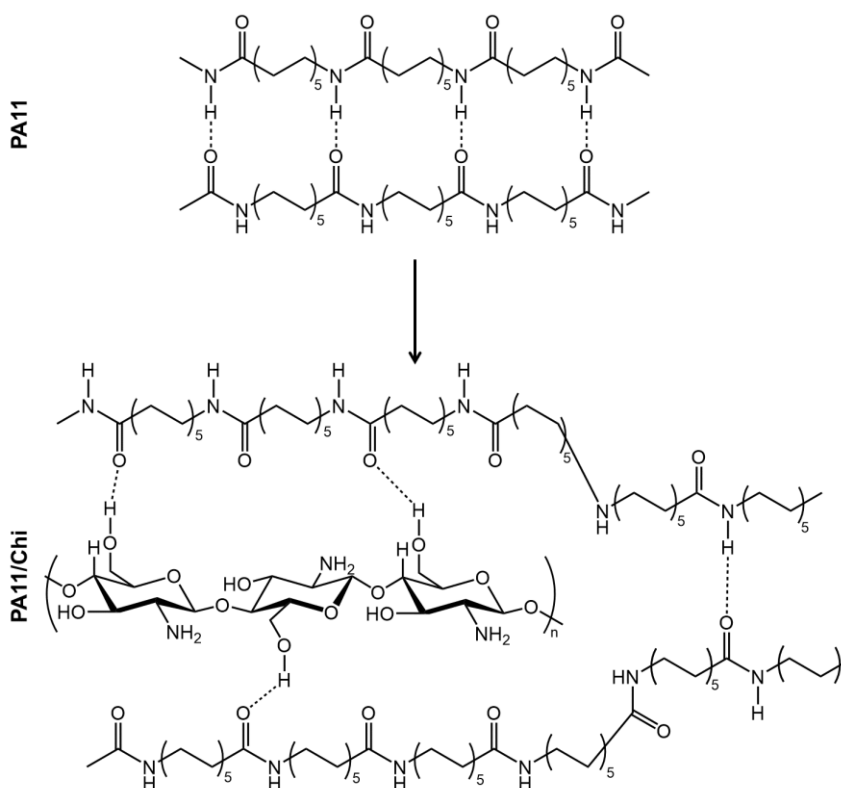


Figure 2.28. Representation of the deformation of polyamide 11 chains after blending with chitosan with the formation of new hydrogen bonds.

As a result, when chitosan is mixed with PA11, the interactions between the two components might change the hydrogen bonds and stiffness of the PA11 primary chains, hence changing their stretching properties.

A moderate improvement of the mechanical properties of the final composite membrane compared to pure PE support is therefore observed and could be attributed to the inclusion of chitosan and the hybrid HNT derivative into PA11 blends and the adhesion of the nanofibers on the support, making the obtained membranes appropriate for a prospective use in filtering technologies.

2.3.3. Conclusions

Eco-friendly electrospun nanofiber composite membranes based on PA11 and chitosan biopolymers have been developed in this study. The impact of several chitosan ratios (90:10, 80:20, and 70:30 w/w PA11/chitosan) was also studied. Three halloysite derivatives obtained from the functionalization with three alkoxy silane precursors, namely (3-aminopropyl)triethoxysilane, dimethyloctadecyl[3-(trimethoxysilyl)propyl]ammoniumchloride, and octyl/decyl glycidyl ether, were added as functional agents into the bio-polymeric blends to improve the properties of the nanofibers. The electrospinning technology was therefore used to produce electrospun nanofibers collected on a polyester calendared substrate to produce the final composite membranes.

The morphology, wettability behavior, mechanical tensile and thermal properties of pristine and doped PA11 and PA11/chitosan membranes were investigated, demonstrating a quite good improvement of characteristics via the synergistic effects of cationic and hydroxyl group rich chitosan biopolymer, good mechanical properties of PA11 and PE support, and ultimately the functionalities of hybrid halloysite derivatives. All experimental findings also demonstrate a reduction in nanofiber quality and features with a larger chitosan ratio in the biopolymeric blend (70:30). Future investigations will entail evaluating the removal characteristics of the produced membranes against specific water pollutants, using electrostatic, hydrogen bonding, and sieving effects due to the diverse functionalities of the nanofiber composite membranes.

The ability to easily manage the membranes for the creation of long-lasting filtration membranes for (waste)water treatment/remediation is also made feasible by the presence of the polyester support and the good mechanical tensile qualities of the membranes.

References

1. Mansoori, S.; Davarnejad, R.; Matsuura, T.; Ismail, A.F. Membranes Based on Non-Synthetic (Natural) Polymers for Wastewater Treatment. *Polym. Test.* **2020**, *84*, 106381, doi:https://doi.org/10.1016/j.polymertesting.2020.106381.
2. Udayakumar, G.P.; Muthusamy, S.; Selvaganesh, B.; Sivarajasekar, N.; Rambabu, K.; Sivamani, S.; Sivakumar, N.; Maran, J.P.; Hosseini-Bandegharaei, A. Ecofriendly Biopolymers and Composites: Preparation and Their Applications in Water-Treatment. *Biotechnol. Adv.* **2021**, *52*, 107815, doi:https://doi.org/10.1016/j.biotechadv.2021.107815.
3. Sfameni, S.; Lawnick, T.; Rando, G.; Visco, A.; Textor, T.; Plutino, M.R. Functional Silane-Based Nanohybrid Materials for the Development of Hydrophobic and Water-Based Stain Resistant Cotton Fabrics Coatings. *Nanomaterials* **2022**, *12*.
4. Sfameni, S.; Del Tedesco, A.; Rando, G.; Truant, F.; Visco, A.; Plutino, M.R. Waterborne Eco-Sustainable Sol-Gel Coatings Based on Phytic Acid Intercalated Graphene Oxide for Corrosion Protection of Metallic Surfaces. *Int. J. Mol. Sci.* **2022**, *23*.
5. Araby, S.; Philips, B.; Meng, Q.; Ma, J.; Laoui, T.; Wang, C.H. Recent Advances in Carbon-Based Nanomaterials for Flame Retardant Polymers and Composites. *Compos. Part B Eng.* **2021**, *212*, 108675, doi:https://doi.org/10.1016/j.compositesb.2021.108675.
6. Zhu, M.; Li, J.; Chen, J.; Song, H.; Zhang, H. Improving Thermal Conductivity of Epoxy Resin by Filling Boron Nitride Nanomaterials: A Molecular Dynamics Investigation. *Comput. Mater. Sci.* **2019**, *164*, 108–115, doi:https://doi.org/10.1016/j.commatsci.2019.04.012.
7. Banerjee, S.; Bairagi, S.; Wazed Ali, S. A Critical Review on Lead-Free Hybrid Materials for next Generation Piezoelectric Energy Harvesting and Conversion. *Ceram. Int.* **2021**, *47*, 16402–16421, doi:https://doi.org/10.1016/j.ceramint.2021.03.054.
8. Andre, R.S.; Sanfelice, R.C.; Pavinatto, A.; Mattoso, L.H.C.; Correa, D.S. Hybrid Nanomaterials Designed for Volatile Organic Compounds Sensors: A Review. *Mater. Des.* **2018**, *156*, 154–166, doi:https://doi.org/10.1016/j.matdes.2018.06.041.
9. Oun, A.A.; Shankar, S.; Rhim, J.-W. Multifunctional Nanocellulose/Metal and Metal Oxide Nanoparticle Hybrid Nanomaterials. *Crit. Rev. Food Sci. Nutr.* **2020**, *60*, 435–460, doi:10.1080/10408398.2018.1536966.
10. Stauber, J.M.; Qian, E.A.; Han, Y.; Rheingold, A.L.; Král, P.; Fujita, D.; Spokoyny, A.M. An Organometallic Strategy for Assembling Atomically Precise Hybrid Nanomaterials. *J. Am. Chem. Soc.* **2020**, *142*, 327–334, doi:10.1021/jacs.9b10770.
11. Gao, S.; Tang, G.; Hua, D.; Xiong, R.; Han, J.; Jiang, S.; Zhang, Q.; Huang, C. Stimuli-Responsive Bio-Based Polymeric Systems and Their Applications. *J. Mater. Chem. B* **2019**, *7*, 709–729, doi:10.1039/C8TB02491J.
12. Si, A.; Kyzas, G.Z.; Pal, K.; de Souza Jr., F.G. Graphene Functionalized Hybrid Nanomaterials for Industrial-Scale Applications: A Systematic Review. *J. Mol. Struct.* **2021**, *1239*, 130518, doi:https://doi.org/10.1016/j.molstruc.2021.130518.
13. Trovato, V.; Sfameni, S.; Rando, G.; Rosace, G.; Libertino, S.; Ferri, A.; Plutino, M.R. A Review of Stimuli-Responsive Smart Materials for Wearable Technology in Healthcare: Retrospective, Perspective, and Prospective. *Molecules* **2022**, *27*.
14. Nasrollahzadeh, M.; Sajjadi, M.; Irvani, S.; Varma, R.S. Starch, Cellulose, Pectin, Gum, Alginate, Chitin and Chitosan Derived (Nano)Materials for Sustainable Water Treatment: A Review. *Carbohydr. Polym.* **2021**, *251*, 116986, doi:https://doi.org/10.1016/j.carbpol.2020.116986.
15. Mittal, H.; Al Alili, A.; Alhassan, S.M.; Naushad, M. Advances in the Role of Natural Gums-Based Hydrogels in Water Purification, Desalination and Atmospheric-Water Harvesting. *Int. J. Biol. Macromol.* **2022**, doi:https://doi.org/10.1016/j.ijbiomac.2022.10.067.
16. Vinod, A.; Sanjay, M.R.; Suchart, S.; Jyotishkumar, P. Renewable and Sustainable Biobased Materials: An Assessment on Biofibers, Biofilms, Biopolymers and Biocomposites. *J. Clean. Prod.* **2020**, *258*, 120978, doi:https://doi.org/10.1016/j.jclepro.2020.120978.
17. Rando, G.; Sfameni, S.; Plutino, M.R. Development of Functional Hybrid Polymers and Gel Materials for Sustainable Membrane-Based Water Treatment Technology: How to Combine Greener and Cleaner Approaches. *Gels* **2023**, *9*.
18. Thakur, V.K.; Voicu, S.I. Recent Advances in Cellulose and Chitosan Based Membranes for Water Purification: A Concise Review. *Carbohydr. Polym.* **2016**, *146*, 148–165, doi:https://doi.org/10.1016/j.carbpol.2016.03.030.
19. Wang, Y.; He, Y.; Yan, S.; Yin, X.; Chen, J. Development of Alginate Hydrogel Modified Multifunctional Filtration Membrane with Robust Anti-Fouling Property for Efficient Water Purification. *Colloids Surfaces A Physicochem. Eng. Asp.* **2019**, *582*, 123891, doi:https://doi.org/10.1016/j.colsurfa.2019.123891.
20. Salehi, E.; Daraei, P.; Arabi Shamsabadi, A. A Review on Chitosan-Based Adsorptive Membranes. *Carbohydr. Polym.* **2016**, *152*, 419–432, doi:https://doi.org/10.1016/j.carbpol.2016.07.033.
21. Lara-Espinoza, C.; Carvajal-Millán, E.; Balandrán-Quintana, R.; López-Franco, Y.; Rascón-Chu, A. Pectin and Pectin-Based Composite Materials: Beyond Food Texture. *Molecules* **2018**, *23*.
22. Manohara, H.M.; Nayak, S.S.; Franklin, G.; Nataraj, S.K.; Mondal, D. Progress in Marine Derived Renewable Functional Materials and Biochar for Sustainable Water Purification. *Green Chem.* **2021**, *23*, 8305–8331, doi:10.1039/D1GC03054J.
23. More, N.; Avhad, M.; Utekar, S.; More, A. Polylactic Acid (PLA) Membrane—Significance, Synthesis, and Applications: A Review. *Polym. Bull.* **2022**, doi:10.1007/s00289-022-04135-z.
24. Wang, W.; Meng, Q.; Li, Q.; Liu, J.; Zhou, M.; Jin, Z.; Zhao, K. Chitosan Derivatives and Their Application in Biomedicine. *Int. J. Mol. Sci.* **2020**, *21*.
25. Negm, N.A.; Hefni, H.H.H.; Abd-Elal, A.A.A.; Badr, E.A.; Abou Kana, M.T.H. Advancement on Modification of Chitosan Biopolymer and Its Potential Applications. *Int. J. Biol. Macromol.* **2020**, *152*, 681–702, doi:https://doi.org/10.1016/j.ijbiomac.2020.02.196.
26. K., S.; P., A.V.; P.N., S.; Faleh A., A.; Sukumaran, A. Novel Chitosan Based Thin Sheet Nanofiltration Membrane for Rejection of Heavy Metal Chromium. *Int. J. Biol. Macromol.* **2019**, *132*, 939–953, doi:https://doi.org/10.1016/j.ijbiomac.2019.03.244.

27. Chaudhary, M.; Maiti, A. Fe–Al–Mn@chitosan Based Metal Oxides Blended Cellulose Acetate Mixed Matrix Membrane for Fluoride Decontamination from Water: Removal Mechanisms and Antibacterial Behavior. *J. Memb. Sci.* **2020**, *611*, 118372, doi:https://doi.org/10.1016/j.memsci.2020.118372.
28. Qian, X.; Li, N.; Wang, Q.; Ji, S. Chitosan/Graphene Oxide Mixed Matrix Membrane with Enhanced Water Permeability for High-Salinity Water Desalination by Pervaporation. *Desalination* **2018**, *438*, 83–96, doi:https://doi.org/10.1016/j.desal.2018.03.031.
29. Wang, X.; Qin, W.; Wang, L.; Zhao, K.; Wang, H.; Liu, H.; Wei, J. Desalination of Dye Utilizing Carboxylated TiO₂/Calcium Alginate Hydrogel Nanofiltration Membrane with High Salt Permeation. *Sep. Purif. Technol.* **2020**, *253*, 117475, doi:https://doi.org/10.1016/j.seppur.2020.117475.
30. Amiri, S.; Asghari, A.; Vatanpour, V.; Rajabi, M. Fabrication and Characterization of a Novel Polyvinyl Alcohol-Graphene Oxide-Sodium Alginate Nanocomposite Hydrogel Blended PES Nanofiltration Membrane for Improved Water Purification. *Sep. Purif. Technol.* **2020**, *250*, 117216, doi:https://doi.org/10.1016/j.seppur.2020.117216.
31. Alshahrani, A.; Alharbi, A.; Alnasser, S.; Almihtar, M.; Alsuhybani, M.; AlOtaibi, B. Enhanced Heavy Metals Removal by a Novel Carbon Nanotubes Buckypaper Membrane Containing a Mixture of Two Biopolymers: Chitosan and i-Carrageenan. *Sep. Purif. Technol.* **2021**, *276*, 119300, doi:https://doi.org/10.1016/j.seppur.2021.119300.
32. Mallakpour, S.; Sirous, F.; Hussain, C.M. A Journey to the World of Fascinating ZnO Nanocomposites Made of Chitosan, Starch, Cellulose, and Other Biopolymers: Progress in Recent Achievements in Eco-Friendly Food Packaging, Biomedical, and Water Remediation Technologies. *Int. J. Biol. Macromol.* **2021**, *170*, 701–716, doi:https://doi.org/10.1016/j.ijbiomac.2020.12.163.
33. Bessa, A.; Gonçalves, G.; Henriques, B.; Domingues, E.M.; Pereira, E.; Marques, P.A.A.P. Green Graphene–Chitosan Sorbent Materials for Mercury Water Remediation. *Nanomaterials* **2020**, *10*.
34. Hardian, R.; Alammari, A.; Holtzl, T.; Szekely, G. Fabrication of Sustainable Organic Solvent Nanofiltration Membranes Using Cellulose–Chitosan Biopolymer Blends. *J. Memb. Sci.* **2022**, *658*, 120743, doi:https://doi.org/10.1016/j.memsci.2022.120743.
35. Lu, Q.; Li, N. Preparation of Hydrophilic Polyvinylidene Fluoride/Polyvinyl Alcohol Ultrafiltration Membrane via Polymer/Non-Solvent Co-Induced Phase Separation Method towards Enhance Anti-Fouling Performance. *J. Environ. Chem. Eng.* **2021**, *9*, 106431, doi:https://doi.org/10.1016/j.jece.2021.106431.
36. Otunola, B.O.; Ololade, O.O. A Review on the Application of Clay Minerals as Heavy Metal Adsorbents for Remediation Purposes. *Environ. Technol. Innov.* **2020**, *18*, 100692, doi:https://doi.org/10.1016/j.eti.2020.100692.
37. Biswas, B.; Warr, L.N.; Hilder, E.F.; Goswami, N.; Rahman, M.M.; Churchman, J.G.; Vasilev, K.; Pan, G.; Naidu, R. Biocompatible Functionalisation of Nanoclays for Improved Environmental Remediation. *Chem. Soc. Rev.* **2019**, *48*, 3740–3770, doi:10.1039/C8CS01019F.
38. Malsawmdawngzela, R.; Lalhmunsiamia; Tiwari, D.; Lee, S. Synthesis of Novel Clay-Based Nanocomposite Materials and Its Application in the Remediation of Arsenic Contaminated Water. *Int. J. Environ. Sci. Technol.* **2022**, doi:10.1007/s13762-022-04506-z.
39. Nasir, R.; Mukhtar, H.; Man, Z.; Mohshim, D.F. Material Advancements in Fabrication of Mixed-Matrix Membranes. *Chem. Eng. Technol.* **2013**, *36*, 717–727, doi:https://doi.org/10.1002/ceat.201200734.
40. Qadir, D.; Mukhtar, H.; Keong, L.K. Mixed Matrix Membranes for Water Purification Applications. *Sep. Purif. Rev.* **2017**, *46*, 62–80, doi:10.1080/15422119.2016.1196460.
41. Lim, J.Y.C.; Goh, S.S.; Liow, S.S.; Xue, K.; Loh, X.J. Molecular Gel Sorbent Materials for Environmental Remediation and Wastewater Treatment. *J. Mater. Chem. A* **2019**, *7*, 18759–18791, doi:10.1039/C9TA05782J.
42. Naseem, K.; Begum, R.; Wu, W.; Usman, M.; Irfan, A.; Al-Sehemi, A.G.; Farooqi, Z.H. Adsorptive Removal of Heavy Metal Ions Using Polystyrene-Poly(N-Isopropylmethacrylamide-Acrylic Acid) Core/Shell Gel Particles: Adsorption Isotherms and Kinetic Study. *J. Mol. Liq.* **2019**, *277*, 522–531, doi:https://doi.org/10.1016/j.molliq.2018.12.054.
43. Ajmal, M.; Siddiq, M.; Aktas, N.; Sahiner, N. Magnetic Co-Fe Bimetallic Nanoparticle Containing Modifiable Microgels for the Removal of Heavy Metal Ions, Organic Dyes and Herbicides from Aqueous Media. *RSC Adv.* **2015**, *5*, 43873–43884, doi:10.1039/C5RA05785J.
44. Arif, M.; Shahid, M.; Irfan, A.; Nisar, J.; Wang, X.; Batool, N.; Ali, M.; Farooqi, Z.H.; Begum, R. Extraction of Copper Ions from Aqueous Medium by Microgel Particles for In-Situ Fabrication of Copper Nanoparticles to Degrade Toxic Dyes. **2022**, *236*, 1219–1241, doi:10.1515/zpch-2022-0038.
45. Ahmad Raus, R.; Wan Nawawi, W.M.F.; Nasaruddin, R.R. Alginate and Alginate Composites for Biomedical Applications. *Asian J. Pharm. Sci.* **2021**, *16*, 280–306, doi:https://doi.org/10.1016/j.ajps.2020.10.001.
46. Fernando, I.P.S.; Lee, W.; Han, E.J.; Ahn, G. Alginate-Based Nanomaterials: Fabrication Techniques, Properties, and Applications. *Chem. Eng. J.* **2020**, *391*, 123823, doi:https://doi.org/10.1016/j.cej.2019.123823.
47. Pacheco-Quito, E.-M.; Ruiz-Caro, R.; Veiga, M.-D. Carrageenan: Drug Delivery Systems and Other Biomedical Applications. *Mar. Drugs* **2020**, *18*.
48. Dong, Y.; Wei, Z.; Xue, C. Recent Advances in Carrageenan-Based Delivery Systems for Bioactive Ingredients: A Review. *Trends Food Sci. Technol.* **2021**, *112*, 348–361, doi:https://doi.org/10.1016/j.tifs.2021.04.012.
49. Li, W.; Qamar, S.A.; Qamar, M.; Basharat, A.; Bilal, M.; Iqbal, H.M.N. Carrageenan-Based Nano-Hybrid Materials for the Mitigation of Hazardous Environmental Pollutants. *Int. J. Biol. Macromol.* **2021**, *190*, 700–712, doi:https://doi.org/10.1016/j.ijbiomac.2021.09.039.
50. Abu-Saied, M.A.; Elnouby, M.; Taha, T.; El-shafeey, M.; G. Alshehri, A.; Alamri, S.; Alghamdi, H.; Shati, A.; Alrumman, S.; Al-Kahtani, M.; et al. Potential Decontamination of Drinking Water Pathogens through K-Carrageenan Integrated Green Bottle Fly Bio-Synthesized Silver Nanoparticles. *Molecules* **2020**, *25*.
51. Bagal-Kestwal, D.R.; Pan, M.H.; Chiang, B.-H. Properties and Applications of Gelatin, Pectin, and Carrageenan Gels. In

- Bio Monomers for Green Polymeric Composite Materials*; 2019; pp. 117–140 ISBN 9781119301714.
52. Alam, J.; Alhoshan, M.; Shukla, A.K.; Aldalbahi, A.; Ali, F.A.A. K-Carrageenan – A Versatile Biopolymer for the Preparation of a Hydrophilic PVDF Composite Membrane. *Eur. Polym. J.* **2019**, *120*, 109219, doi:https://doi.org/10.1016/j.eurpolymj.2019.109219.
 53. Ulu, A.; Alpaslan, M.; Gultek, A.; Ates, B. Eco-Friendly Chitosan/ κ -Carrageenan Membranes Reinforced with Activated Bentonite for Adsorption of Methylene Blue. *Mater. Chem. Phys.* **2022**, *278*, 125611, doi:https://doi.org/10.1016/j.matchemphys.2021.125611.
 54. Tan, H.-F.; Ooi, B.S.; Leo, C.P. Future Perspectives of Nanocellulose-Based Membrane for Water Treatment. *J. Water Process Eng.* **2020**, *37*, 101502, doi:https://doi.org/10.1016/j.jwpe.2020.101502.
 55. Mavukkandy, M.O.; McBride, S.A.; Warsinger, D.M.; Dizge, N.; Hasan, S.W.; Arafat, H.A. Thin Film Deposition Techniques for Polymeric Membranes– A Review. *J. Memb. Sci.* **2020**, *610*, 118258, doi:https://doi.org/10.1016/j.memsci.2020.118258.
 56. AlAbduljabbar, F.A.; Haider, S.; Ahmed Ali, F.A.; Alghyamah, A.A.; Almasry, W.A.; Patel, R.; Mujtaba, I.M. TiO₂ Nanostructured Coated Functionally Modified and Composite Electrospun Chitosan Nanofibers Membrane for Efficient Photocatalytic Degradation of Organic Pollutant in Wastewater. *J. Mater. Res. Technol.* **2021**, *15*, 5197–5212, doi:https://doi.org/10.1016/j.jmrt.2021.10.119.
 57. Yan, L.; Yang, X.; Zhao, Y.; Wu, Y.; Motlhaletsi Moutloali, R.; Mamba, B.B.; Sorokin, P.; Shao, L. Bio-Inspired Mineral-Hydrogel Hybrid Coating on Hydrophobic PVDF Membrane Boosting Oil/Water Emulsion Separation. *Sep. Purif. Technol.* **2022**, *285*, 120383, doi:https://doi.org/10.1016/j.seppur.2021.120383.
 58. Pan, S.; Li, J.; Noonan, O.; Fang, X.; Wan, G.; Yu, C.; Wang, L. Dual-Functional Ultrafiltration Membrane for Simultaneous Removal of Multiple Pollutants with High Performance. *Environ. Sci. Technol.* **2017**, *51*, 5098–5107, doi:10.1021/acs.est.6b05295.
 59. Prasannan, A.; Udomsin, J.; Tsai, H.-C.; Wang, C.-F.; Lai, J.-Y. Robust Underwater Superoleophobic Membranes with Bio-Inspired Carrageenan/Laponite Multilayers for the Effective Removal of Emulsions, Metal Ions, and Organic Dyes from Wastewater. *Chem. Eng. J.* **2020**, *391*, 123585, doi:https://doi.org/10.1016/j.cej.2019.123585.
 60. Bandara, P.C.; Nadres, E.T.; Rodrigues, D.F. Use of Response Surface Methodology To Develop and Optimize the Composition of a Chitosan–Polyethyleneimine–Graphene Oxide Nanocomposite Membrane Coating To More Effectively Remove Cr(VI) and Cu(II) from Water. *ACS Appl. Mater. Interfaces* **2019**, *11*, 17784–17795, doi:10.1021/acsami.9b03601.
 61. Lakra, R.; Balakrishnan, M.; Basu, S. Development of Cellulose Acetate-Chitosan-Metal Organic Framework Forward Osmosis Membrane for Recovery of Water and Nutrients from Wastewater. *J. Environ. Chem. Eng.* **2021**, *9*, 105882, doi:https://doi.org/10.1016/j.jece.2021.105882.
 62. Kazemi, M.; Jahanshahi, M.; Peyravi, M. Chitosan-Sodium Alginate Multilayer Membrane Developed by Fe₀/WO₃ Nanoparticles: Photocatalytic Removal of Hexavalent Chromium. *Carbohydr. Polym.* **2018**, *198*, 164–174, doi:https://doi.org/10.1016/j.carbpol.2018.06.069.
 63. Yadav, S.; Ibrar, I.; Altaee, A.; Samal, A.K.; Zhou, J. Surface Modification of Nanofiltration Membrane with Kappa-Carrageenan/Graphene Oxide for Leachate Wastewater Treatment. *J. Memb. Sci.* **2022**, *659*, 120776, doi:https://doi.org/10.1016/j.memsci.2022.120776.
 64. Zhao, S.; Tao, Z.; Chen, L.; Han, M.; Zhao, B.; Tian, X.; Wang, L.; Meng, F. An Antifouling Catechol/Chitosan-Modified Polyvinylidene Fluoride Membrane for Sustainable Oil-in-Water Emulsions Separation. *Front. Environ. Sci. Eng.* **2020**, *15*, 63, doi:10.1007/s11783-020-1355-5.
 65. Lee, W.J.; Bao, Y.; Guan, C.; Hu, X.; Lim, T.-T. Ce/TiO_x-Functionalized Catalytic Ceramic Membrane for Hybrid Catalytic Ozonation-Membrane Filtration Process: Fabrication, Characterization and Performance Evaluation. *Chem. Eng. J.* **2021**, *410*, 128307, doi:https://doi.org/10.1016/j.cej.2020.128307.
 66. Dlamini, D.S.; Matindi, C.; Vilakati, G.D.; Tesha, J.M.; Motsa, M.M.; Thwala, J.M.; Mamba, B.B.; Hoek, E.M. V; Li, J. Fine-Tuning the Architecture of Loose Nanofiltration Membrane for Improved Water Flux, Dye Rejection and Dye/Salt Selective Separation. *J. Memb. Sci.* **2021**, *621*, 118930, doi:https://doi.org/10.1016/j.memsci.2020.118930.
 67. Xiong, Z.; Lin, H.; Zhong, Y.; Qin, Y.; Li, T.; Liu, F. Robust Superhydrophilic Polylactide (PLA) Membranes with a TiO₂ Nano-Particle Inlaid Surface for Oil/Water Separation. *J. Mater. Chem. A* **2017**, *5*, 6538–6545, doi:10.1039/C6TA11156D.
 68. Xue, J.; Wu, T.; Dai, Y.; Xia, Y. Electrospinning and Electrospun Nanofibers: Methods, Materials, and Applications. *Chem. Rev.* **2019**, *119*, 5298–5415, doi:10.1021/acs.chemrev.8b00593.
 69. Cui, J.; Li, F.; Wang, Y.; Zhang, Q.; Ma, W.; Huang, C. Electrospun Nanofiber Membranes for Wastewater Treatment Applications. *Sep. Purif. Technol.* **2020**, *250*, 117116, doi:https://doi.org/10.1016/j.seppur.2020.117116.
 70. Tijjng, L.D.; Yao, M.; Ren, J.; Park, C.-H.; Kim, C.S.; Shon, H.K. Nanofibers for Water and Wastewater Treatment: Recent Advances and Developments BT - Water and Wastewater Treatment Technologies. In; Bui, X.-T., Chiemchaisri, C., Fujioka, T., Varjani, S., Eds.; Springer Singapore: Singapore, 2019; pp. 431–468 ISBN 978-981-13-3259-3.
 71. Wang, X.; Hsiao, B.S. Electrospun Nanofiber Membranes. *Curr. Opin. Chem. Eng.* **2016**, *12*, 62–81, doi:https://doi.org/10.1016/j.coche.2016.03.001.
 72. Liang, J.; Zhao, H.; Yue, L.; Fan, G.; Li, T.; Lu, S.; Chen, G.; Gao, S.; Asiri, A.M.; Sun, X. Recent Advances in Electrospun Nanofibers for Supercapacitors. *J. Mater. Chem. A* **2020**, *8*, 16747–16789, doi:10.1039/DoTA05100D.
 73. Rasouli, R.; Barhoum, A.; Bechelany, M.; Dufresne, A. Nanofibers for Biomedical and Healthcare Applications. *Macromol. Biosci.* **2019**, *19*, 1800256, doi:https://doi.org/10.1002/mabi.201800256.
 74. Lu, T.; Cui, J.; Qu, Q.; Wang, Y.; Zhang, J.; Xiong, R.; Ma, W.; Huang, C. Multistructured Electrospun Nanofibers for Air Filtration: A Review. *ACS Appl. Mater. Interfaces* **2021**, *13*, 23293–23313, doi:10.1021/acsami.1c06520.
 75. Zanin, M.H.A.; Cerize, N.N.P.; de Oliveira, A.M. Production of Nanofibers by Electrospinning Technology: Overview and

- Application in Cosmetics BT - Nanocosmetics and Nanomedicines: New Approaches for Skin Care. In: Beck, R., Guterres, S., Pohlmann, A., Eds.; Springer Berlin Heidelberg: Berlin, Heidelberg, 2011; pp. 311–332 ISBN 978-3-642-19792-5.
76. Rahmati, M.; Mills, D.K.; Urbanska, A.M.; Saeb, M.R.; Venugopal, J.R.; Ramakrishna, S.; Mozafari, M. Electrospinning for Tissue Engineering Applications. *Prog. Mater. Sci.* **2021**, *117*, 100721, doi:https://doi.org/10.1016/j.pmatsci.2020.100721.
 77. Li, X.; Chen, W.; Qian, Q.; Huang, H.; Chen, Y.; Wang, Z.; Chen, Q.; Yang, J.; Li, J.; Mai, Y.-W. Electrospinning-Based Strategies for Battery Materials. *Adv. Energy Mater.* **2021**, *11*, 2000845, doi:https://doi.org/10.1002/aenm.202000845.
 78. Luraghi, A.; Peri, F.; Moroni, L. Electrospinning for Drug Delivery Applications: A Review. *J. Control. Release* **2021**, *334*, 463–484, doi:https://doi.org/10.1016/j.jconrel.2021.03.033.
 79. Bates, I.I.C.; Carrillo, I.B.S.; Germain, H.; Loranger, É.; Chabot, B. Antibacterial Electrospun Chitosan-PEO/TEMPO-Oxidized Cellulose Composite for Water Filtration. *J. Environ. Chem. Eng.* **2021**, *9*, 106204, doi:https://doi.org/10.1016/j.jece.2021.106204.
 80. Zheng, S.; Chen, H.; Tong, X.; Wang, Z.; Crittenden, J.C.; Huang, M. Integration of a Photo-Fenton Reaction and a Membrane Filtration Using CS/PAN@FeOOH/g-C₃N₄ Electrospun Nanofibers: Synthesis, Characterization, Self-Cleaning Performance and Mechanism. *Appl. Catal. B Environ.* **2021**, *281*, 119519, doi:https://doi.org/10.1016/j.apcatb.2020.119519.
 81. Jamshidifard, S.; Koushkbaghi, S.; Hosseini, S.; Rezaei, S.; Karamipour, A.; Jafari rad, A.; Irani, M. Incorporation of UiO-66-NH₂ MOF into the PAN/Chitosan Nanofibers for Adsorption and Membrane Filtration of Pb(II), Cd(II) and Cr(VI) Ions from Aqueous Solutions. *J. Hazard. Mater.* **2019**, *368*, 10–20, doi:https://doi.org/10.1016/j.jhazmat.2019.01.024.
 82. Zhijiang, C.; Cong, Z.; Ping, X.; Jie, G.; Kongyin, Z. Calcium Alginate-Coated Electrospun Polyhydroxybutyrate/Carbon Nanotubes Composite Nanofibers as Nanofiltration Membrane for Dye Removal. *J. Mater. Sci.* **2018**, *53*, 14801–14820, doi:10.1007/s10853-018-2607-7.
 83. Wu, S.; Li, K.; Shi, W.; Cai, J. Chitosan/Polyvinylpyrrolidone/Polyvinyl Alcohol/Carbon Nanotubes Dual Layers Nanofibrous Membrane Constructed by Electrospinning-Electrospray for Water Purification. *Carbohydr. Polym.* **2022**, *294*, 119756, doi:https://doi.org/10.1016/j.carbpol.2022.119756.
 84. Kang, Y.-L.; Zhang, J.; Wu, G.; Zhang, M.-X.; Chen, S.-C.; Wang, Y.-Z. Full-Biobased Nanofiber Membranes toward Decontamination of Wastewater Containing Multiple Pollutants. *ACS Sustain. Chem. Eng.* **2018**, *6*, 11783–11792, doi:10.1021/acssuschemeng.8b01996.
 85. Udomluck, N.; Koh, W.-G.; Lim, D.-J.; Park, H. Recent Developments in Nanofiber Fabrication and Modification for Bone Tissue Engineering. *Int. J. Mol. Sci.* **2020**, *21*.
 86. Obaid, M.; Abdelkareem, M.A.; Kook, S.; Kim, H.-Y.; Hilal, N.; Ghaffour, N.; Kim, I.S. Breakthroughs in the Fabrication of Electrospun-Nanofiber-Supported Thin Film Composite/Nanocomposite Membranes for the Forward Osmosis Process: A Review. *Crit. Rev. Environ. Sci. Technol.* **2020**, *50*, 1727–1795, doi:10.1080/10643389.2019.1672510.
 87. Gonzales, R.R.; Park, M.J.; Tijing, L.; Han, D.S.; Phuntsho, S.; Shon, H.K. Modification of Nanofiber Support Layer for Thin Film Composite Forward Osmosis Membranes via Layer-by-Layer Polyelectrolyte Deposition. *Membranes (Basel)*. **2018**, *8*.
 88. Lei, Y.; Wang, Q.; Peng, S.; Ramakrishna, S.; Zhang, D.; Zhou, K. Electrospun Inorganic Nanofibers for Oxygen Electrocatalysis: Design, Fabrication, and Progress. *Adv. Energy Mater.* **2020**, *10*, 1902115, doi:https://doi.org/10.1002/aenm.201902115.
 89. Hammad, M.; Fortugno, P.; Hardt, S.; Kim, C.; Salamon, S.; Schmidt, T.C.; Wende, H.; Schulz, C.; Wiggers, H. Large-Scale Synthesis of Iron Oxide/Graphene Hybrid Materials as Highly Efficient Photo-Fenton Catalyst for Water Remediation. *Environ. Technol. Innov.* **2021**, *21*, 101239, doi:https://doi.org/10.1016/j.eti.2020.101239.
 90. Zhu, Y.; Fan, W.; Feng, W.; Wang, Y.; Liu, S.; Dong, Z.; Li, X. A Critical Review on Metal Complexes Removal from Water Using Methods Based on Fenton-like Reactions: Analysis and Comparison of Methods and Mechanisms. *J. Hazard. Mater.* **2021**, *414*, 125517, doi:https://doi.org/10.1016/j.jhazmat.2021.125517.
 91. Ramos, J.M.P.; Pereira-Queiroz, N.M.; Santos, D.H.S.; Nascimento, J.R.; Carvalho, C.M. de; Tonholo, J.; Zanta, C.L.P.S. Printing Ink Effluent Remediation: A Comparison between Electrochemical and Fenton Treatments. *J. Water Process Eng.* **2019**, *31*, 100803, doi:https://doi.org/10.1016/j.jwpe.2019.100803.
 92. Yang, X.; Chen, W.; Huang, J.; Zhou, Y.; Zhu, Y.; Li, C. Rapid Degradation of Methylene Blue in a Novel Heterogeneous Fe₃O₄@rGO@TiO₂-Catalyzed Photo-Fenton System. *Sci. Rep.* **2015**, *5*, 10632, doi:10.1038/srep10632.
 93. Raji, M.; Mirbagheri, S.A.; Ye, F.; Dutta, J. Nano Zero-Valent Iron on Activated Carbon Cloth Support as Fenton-like Catalyst for Efficient Color and COD Removal from Melanoidin Wastewater. *Chemosphere* **2021**, *263*, 127945, doi:https://doi.org/10.1016/j.chemosphere.2020.127945.
 94. Lv, Y.; Huang, S.; Huang, G.; Liu, Y.; Yang, G.; Lin, C.; Xiao, G.; Wang, Y.; Liu, M. Remediation of Organic Arsenic Contaminants with Heterogeneous Fenton Process Mediated by SiO₂-Coated Nano Zero-Valent Iron. *Environ. Sci. Pollut. Res.* **2020**, *27*, 12017–12029, doi:10.1007/s11356-020-07808-2.
 95. Hosseini, S.A.; Daneshvar e Asl, S.; Vossoughi, M.; Simchi, A.; Sadrzadeh, M. Green Electrospun Membranes Based on Chitosan/Amino-Functionalized Nanoclay Composite Fibers for Cationic Dye Removal: Synthesis and Kinetic Studies. *ACS Omega* **2021**, *6*, 10816–10827, doi:10.1021/acsomega.1c00480.
 96. Moradi, E.; Ebrahimzadeh, H.; Mehrani, Z.; Asgharinezhad, A.A. The Efficient Removal of Methylene Blue from Water Samples Using Three-Dimensional Poly (Vinyl Alcohol)/Starch Nanofiber Membrane as a Green Nanosorbent. *Environ. Sci. Pollut. Res.* **2019**, *26*, 35071–35081, doi:10.1007/s11356-019-06400-7.
 97. Akbari, A.; Remigy, J.C.; Aptel, P. Treatment of Textile Dye Effluent Using a Polyamide-Based Nanofiltration Membrane. *Chem. Eng. Process. Process Intensif.* **2002**, *41*, 601–609, doi:https://doi.org/10.1016/S0255-2701(01)00181-7.
 98. Bugatti, V.; Vertuccio, L.; Viscusi, G.; Gorrasi, G. Antimicrobial Membranes of Bio-Based PA 11 and HNTs Filled with Lysozyme Obtained by an Electrospinning Process. *Nanomaterials* **2018**, *8*.

99. Kabir, H.; Kamali Dehghan, H.; Mashayekhan, S.; Bagherzadeh, R.; Sorayani Bafqi, M.S. Hybrid Fibrous (PVDF-BaTiO₃)/PA-11 Piezoelectric Patch as an Energy Harvester for Pacemakers. *J. Ind. Text.* **2022**, *51*, 4698S-4719S.
100. Behler, K.; Havel, M.; Gogotsi, Y. New Solvent for Polyamides and Its Application to the Electrospinning of Polyamides 11 and 12. *Polymer (Guildf)*. **2007**, *48*, 6617-6621.
101. Danyliuk, N.; Tomaszewska, J.; Tatarchuk, T. Halloysite Nanotubes and Halloysite-Based Composites for Environmental and Biomedical Applications. *J. Mol. Liq.* **2020**, *309*, 113077. doi:https://doi.org/10.1016/j.molliq.2020.113077.
102. Massaro, M.; Noto, R.; Riela, S. Past, Present and Future Perspectives on Halloysite Clay Minerals. *Molecules* **2020**, *25*.
103. Nouailhas, H.; Aouf, C.; Le Guerneve, C.; Caillol, S.; Boutevin, B.; Fulcrand, H. Synthesis and Properties of Biobased Epoxy Resins. Part 1. Glycidylation of Flavonoids by Epichlorohydrin. *J. Polym. Sci. Part A Polym. Chem.* **2011**, *49*, 2261-2270. doi:https://doi.org/10.1002/pola.24659.
104. Krishnaiah, P.; Ratnam, C.T.; Manickam, S. Development of Silane Grafted Halloysite Nanotube Reinforced Poly lactide Nanocomposites for the Enhancement of Mechanical, Thermal and Dynamic-Mechanical Properties. *Appl. Clay Sci.* **2017**, *135*, 583-595. doi:https://doi.org/10.1016/j.clay.2016.10.046.
105. Yah, W.O.; Takahara, A.; Lvov, Y.M. Selective Modification of Halloysite Lumen with Octadecylphosphonic Acid: New Inorganic Tubular Micelle. *J. Am. Chem. Soc.* **2012**, *134*, 1853-1859. doi:10.1021/ja210258y.
106. Li, X.; Nikiforow, I.; Pohl, K.; Adams, J.; Johannsmann, D. Polyurethane Coatings Reinforced by Halloysite Nanotubes. *Coatings* **2013**, *3*, 16-25.
107. Zhu, J.; Wang, F.; Li, D.; Zhai, J.; Liu, P.; Zhang, W.; Li, Y. Amine Functionalized Graphene Oxide Stabilized Pickering Emulsion for Highly Efficient Knoevenagel Condensation in Aqueous Medium. *Catal. Letters* **2020**, *150*, 1909-1922. doi:10.1007/s10562-020-03103-4.
108. Saif, B., Wang, C., Chuan, D. and Shuang, S. Synthesis and Characterization of Fe₃O₄ Coated on APTES as Carriers for Morin-Anticancer Drug. *J. Biomater. Nanobiotechnol.* **2015**, *6*, 267-275.
109. Li, C.; Zhao, Y.; Zhu, T.; Li, Y.; Ruan, J.; Li, G. Effective Solvent-Free Oxidation of Cyclohexene to Allylic Products with Oxygen by Mesoporous Etched Halloysite Nanotube Supported Co₂+. *RSC Adv.* **2018**, *8*, 14870-14878. doi:10.1039/C7RA11245A.
110. Nohra, B.; Candy, L.; Blanco, J.-F.; Raoul, Y.; Mouloungui, Z. Synthesis of High-Molecular-Weight Multifunctional Glycerol Polyhydroxyurethanes PHUs. *Mol.* **2016**, *21*.
111. Sun, P.; Liu, G.; Lv, D.; Dong, X.; Wu, J.; Wang, D. Effective Activation of Halloysite Nanotubes by Piranha Solution for Amine Modification via Silane Coupling Chemistry. *RSC Adv.* **2015**, *5*, 52916-52925. doi:10.1039/C5RA04444H.
112. He, Y.; Xu, W.; Tang, R.; Zhang, C.; Yang, Q. PH-Responsive Nanovalves Based on Encapsulated Halloysite for the Controlled Release of a Corrosion Inhibitor in Epoxy Coating. *RSC Adv.* **2015**, *5*, 90609-90620. doi:10.1039/C5RA19296J.
113. Le Ba, T.; Alkurdi, A.Q.; Lukács, I.E.; Molnár, J.; Wongwises, S.; Gróf, G.; Szilágyi, I.M. A Novel Experimental Study on the Rheological Properties and Thermal Conductivity of Halloysite Nanofluids. *Nanomater.* **2020**, *10*.
114. Raji, M.; Mekhzoum, M.E.M.; Rodrigue, D.; Qaiss, A. el kacem; Bouhfid, R. Effect of Silane Functionalization on Properties of Polypropylene/Clay Nanocomposites. *Compos. Part B Eng.* **2018**, *146*, 106-115. doi:https://doi.org/10.1016/j.compositesb.2018.04.013.
115. Zhang, Y.; Meng, R.; Zhou, J.; Liu, X.; Guo, W. Halloysite Nanotubes-Decorated Electrospun Biobased Polyamide Scaffolds for Tissue Engineering Applications. *Colloids Surfaces A Physicochem. Eng. Asp.* **2022**, *648*, 129378. doi:https://doi.org/10.1016/j.colsurfa.2022.129378.
116. Cavallaro, G.; Lazzara, G.; Milioto, S.; Parisi, F. Hydrophobically Modified Halloysite Nanotubes as Reverse Micelles for Water-in-Oil Emulsion. *Langmuir* **2015**, *31*, 7472-7478. doi:10.1021/acs.langmuir.5b01181.
117. Massaro, M.; Colletti, C.G.; Lazzara, G.; Guernelli, S.; Noto, R.; Riela, S. Synthesis and Characterization of Halloysite-Cyclodextrin Nanosponges for Enhanced Dyes Adsorption. *ACS Sustain. Chem. Eng.* **2017**, *5*, 3346-3352. doi:10.1021/acssuschemeng.6b03191.
118. Qi, R.; Guo, R.; Shen, M.; Cao, X.; Zhang, L.; Xu, J.; Yu, J.; Shi, X. Electrospun Poly(Lactic-Co-Glycolic Acid)/Halloysite Nanotube Composite Nanofibers for Drug Encapsulation and Sustained Release. *J. Mater. Chem.* **2010**, *20*, 10622-10629. doi:10.1039/C0JM01328E.
119. Karahan Toprakci, H.A.; Turgut, A.; Toprakci, O. Nailed-Bat like Halloysite Nanotube Filled Polyamide 6,6 Nanofibers by Electrospinning. *Polym. Technol. Mater.* **2021**, *60*, 522-535. doi:10.1080/25740881.2020.1819313.
120. Stepanyan, R.; Subbotin, A. V.; Cuperus, L.; Boonen, P.; Dorschu, M.; Oosterlinck, F.; Bulters, M.J.H. Nanofiber Diameter in Electrospinning of Polymer Solutions: Model and Experiment. *Polymer (Guildf)*. **2016**, *97*, 428-439. doi:https://doi.org/10.1016/j.polymer.2016.05.045.
121. Ristolainen, N.; Heikkilä, P.; Harlin, A.; Seppälä, J. Poly(Vinyl Alcohol) and Polyamide-66 Nanocomposites Prepared by Electrospinning. *Macromol. Mater. Eng.* **2006**, *291*, 114-122. doi:https://doi.org/10.1002/mame.200500213.
122. Juang, R.-S.; Liu, C.-A.; Fu, C.-C. Polyaminated Electrospun Chitosan Fibrous Membranes for Highly Selective Removal of Anionic Organics from Aqueous Solutions in Continuous Operation. *Sep. Purif. Technol.* **2023**, *319*, 124043. doi:https://doi.org/10.1016/j.seppur.2023.124043.
123. Woo, Y.C.; Tijng, L.D.; Shim, W.-G.; Choi, J.-S.; Kim, S.-H.; He, T.; Drioli, E.; Shon, H.K. Water Desalination Using Graphene-Enhanced Electrospun Nanofiber Membrane via Air Gap Membrane Distillation. *J. Memb. Sci.* **2016**, *520*, 99-110. doi:https://doi.org/10.1016/j.memsci.2016.07.049.
124. Shanmugaraj, A.M.; Yoon, J.H.; Yang, W.J.; Ryu, S.H. Synthesis, Characterization, and Surface Wettability Properties of Amine Functionalized Graphene Oxide Films with Varying Amine Chain Lengths. *J. Colloid Interface Sci.* **2013**, *401*, 148-154. doi:https://doi.org/10.1016/j.jcis.2013.02.054.
125. Nirmala, R.; Navamathavan, R.; Kang, H.-S.; El-Newehy, M.H.; Kim, H.Y. Preparation of Polyamide-6/Chitosan Composite Nanofibers by a Single Solvent System via Electrospinning for Biomedical Applications. *Colloids Surfaces B*

- Biointerfaces* **2011**, *83*, 173–178, doi:https://doi.org/10.1016/j.colsurfb.2010.11.026.
126. Stark, W.; Jaunich, M. Investigation of Ethylene/Vinyl Acetate Copolymer (EVA) by Thermal Analysis DSC and DMA. *Polym. Test.* **2011**, *30*, 236–242, doi:https://doi.org/10.1016/j.polymertesting.2010.12.003.
127. Chien, H.-C.; Peng, W.-T.; Chiu, T.-H.; Wu, P.-H.; Liu, Y.-J.; Tu, C.-W.; Wang, C.-L.; Lu, M.-C. Heat Transfer of Semicrystalline Nylon Nanofibers. *ACS Nano* **2020**, *14*, 2939–2946, doi:10.1021/acsnano.9b07493.
128. Johari, N.A.; Yusof, N.; Lau, W.J.; Abdullah, N.; Salleh, W.N.W.; Jaafar, J.; Aziz, F.; Ismail, A.F. Polyethersulfone Ultrafiltration Membrane Incorporated with Ferric-Based Metal-Organic Framework for Textile Wastewater Treatment. *Sep. Purif. Technol.* **2021**, *270*, 118819, doi:https://doi.org/10.1016/j.seppur.2021.118819.
129. Ahmadipouya, S.; Mousavi, S.A.; Shokrgozar, A.; Mousavi, D.V. Improving Dye Removal and Antifouling Performance of Polysulfone Nanofiltration Membranes by Incorporation of UiO-66 Metal-Organic Framework. *J. Environ. Chem. Eng.* **2022**, *10*, 107535, doi:https://doi.org/10.1016/j.jece.2022.107535.
130. Zheng, J.; Li, Y.; Xu, D.; Zhao, R.; Liu, Y.; Li, G.; Gao, Q.; Zhang, X.; Volodine, A.; Van der Bruggen, B. Facile Fabrication of a Positively Charged Nanofiltration Membrane for Heavy Metal and Dye Removal. *Sep. Purif. Technol.* **2022**, *282*, 120155, doi:https://doi.org/10.1016/j.seppur.2021.120155.
131. Begum, S.; Yuhana, N.Y.; Md Saleh, N.; Kamarudin, N.H.N.; Sulong, A.B. Review of Chitosan Composite as a Heavy Metal Adsorbent: Material Preparation and Properties. *Carbohydr. Polym.* **2021**, *259*, 117613, doi:https://doi.org/10.1016/j.carbpol.2021.117613.
132. Kumar, S.; Ye, F.; Dobretsov, S.; Dutta, J. Chitosan Nanocomposite Coatings for Food, Paints, and Water Treatment Applications. *Appl. Sci.* **2019**, *9*.
133. Govindasamy, K.; Dahlan, N.A.; Janarthanan, P.; Goh, K.L.; Chai, S.-P.; Pasbakhsh, P. Electrospun Chitosan/Polyethylene-Oxide (PEO)/Haloysites (HAL) Membranes for Bone Regeneration Applications. *Appl. Clay Sci.* **2020**, *190*, doi:https://doi.org/10.1016/j.clay.2020.105601.
134. Abid, S.; Hussain, T.; Nazir, A.; Zahir, A.; Ramakrishna, S.; Hameed, M.; Khenoussi, N. Enhanced Antibacterial Activity of PEO-Chitosan Nanofibers with Potential Application in Burn Infection Management. *Int. J. Biol. Macromol.* **2019**, *135*, 1222–1236, doi:https://doi.org/10.1016/j.ijbiomac.2019.06.022.
135. Elkady, M.; Salama, E.; Amer, W.A.; Ebeid, E.-Z.M.; Ayad, M.M.; Shokry, H. Novel Eco-Friendly Electrospun Nanomagnetic Zinc Oxide Hybridized PVA/Alginate/Chitosan Nanofibers for Enhanced Phenol Decontamination. *Environ. Sci. Pollut. Res.* **2020**, *27*, 43077–43092, doi:10.1007/s11356-020-10247-8.
136. Niu, X.; Wang, L.; Xu, M.; Qin, M.; Zhao, L.; Wei, Y.; Hu, Y.; Lian, X.; Liang, Z.; Chen, S.; et al. Electrospun Polyamide-6/Chitosan Nanofibers Reinforced Nano-Hydroxyapatite/Polyamide-6 Composite Bilayered Membranes for Guided Bone Regeneration. *Carbohydr. Polym.* **2021**, *260*, 117769, doi:https://doi.org/10.1016/j.carbpol.2021.117769.
137. Shrestha, B.K.; Mousa, H.M.; Tiwari, A.P.; Ko, S.W.; Park, C.H.; Kim, C.S. Development of Polyamide-6,6/Chitosan Electrospun Hybrid Nanofibrous Scaffolds for Tissue Engineering Application. *Carbohydr. Polym.* **2016**, *148*, 107–114, doi:https://doi.org/10.1016/j.carbpol.2016.03.094.
138. Shavisi, N.; Shahbazi, Y. Chitosan-Gum Arabic Nanofiber Mats Encapsulated with PH-Sensitive Rosa Damascena Anthocyanins for Freshness Monitoring of Chicken Fillets. *Food Packag. Shelf Life* **2022**, *32*, 100827, doi:https://doi.org/10.1016/j.fpsl.2022.100827.
139. ZabihiSahebi, A.; Koushkbaghi, S.; Pishnamazi, M.; Askari, A.; Khosravi, R.; Irani, M. Synthesis of Cellulose Acetate/Chitosan/SWCNT/Fe₃O₄/TiO₂ Composite Nanofibers for the Removal of Cr(VI), As(V), Methylene Blue and Congo Red from Aqueous Solutions. *Int. J. Biol. Macromol.* **2019**, *140*, 1296–1304, doi:https://doi.org/10.1016/j.ijbiomac.2019.08.214.
140. Bertolino, V.; Cavallaro, G.; Milioto, S.; Lazzara, G. Polysaccharides/Halloysite Nanotubes for Smart Bionanocomposite Materials. *Carbohydr. Polym.* **2020**, *245*, 116502, doi:https://doi.org/10.1016/j.carbpol.2020.116502.
141. Abid, M.; Sayegh, S.; Iatsunskiy, I.; Coy, E.; Lesage, G.; Ramanavicius, A.; Ben Haj Amara, A.; Bechelany, M. Design of Halloysite-Based Nanocomposites by Electrospinning for Water Treatment. *Colloids Surfaces A Physicochem. Eng. Asp.* **2022**, *651*, 129696, doi:https://doi.org/10.1016/j.colsurfa.2022.129696.
142. Esposito, S. “Traditional” Sol-Gel Chemistry as a Powerful Tool for the Preparation of Supported Metal and Metal Oxide Catalysts. *Materials (Basel)*. **2019**, *12*.
143. Son, W.K.; Youk, J.H.; Lee, T.S.; Park, W.H. The Effects of Solution Properties and Polyelectrolyte on Electrospinning of Ultrafine Poly(Ethylene Oxide) Fibers. *Polymer (Guildf)*. **2004**, *45*, 2959–2966, doi:https://doi.org/10.1016/j.polymer.2004.03.006.
144. Zhang, H.; Li, S.; Branford White, C.J.; Ning, X.; Nie, H.; Zhu, L. Studies on Electrospun Nylon-6/Chitosan Complex Nanofiber Interactions. *Electrochim. Acta* **2009**, *54*, 5739–5745, doi:https://doi.org/10.1016/j.electacta.2009.05.021.
145. Zarei, M.; Samimi, A.; Khorram, M.; Abdi, M.M.; Golestaneh, S.I. Fabrication and Characterization of Conductive Polypyrrole/Chitosan/Collagen Electrospun Nanofiber Scaffold for Tissue Engineering Application. *Int. J. Biol. Macromol.* **2021**, *168*, 175–186, doi:https://doi.org/10.1016/j.ijbiomac.2020.12.031.
146. Cui, Z.; Zheng, Z.; Lin, L.; Si, J.; Wang, Q.; Peng, X.; Chen, W. Electrospinning and Crosslinking of Polyvinyl Alcohol/Chitosan Composite Nanofiber for Transdermal Drug Delivery. *Adv. Polym. Technol.* **2018**, *37*, 1917–1928, doi:https://doi.org/10.1002/adv.21850.
147. Ghadirian, S.; Karbasi, S. Evaluation of the Effects of Halloysite Nanotube on Polyhydroxybutyrate - Chitosan Electrospun Scaffolds for Cartilage Tissue Engineering Applications. *Int. J. Biol. Macromol.* **2023**, *233*, 123651, doi:https://doi.org/10.1016/j.ijbiomac.2023.123651.
148. Kuo, P.-C.; Sahu, D.; Yu, H.H. Properties and Biodegradability of Chitosan/Nylon 11 Blending Films. *Polym. Degrad. Stab.* **2006**, *91*, 3097–3102, doi:https://doi.org/10.1016/j.polymdegradstab.2006.07.025.

CHAPTER 3

FUNCTIONAL CELLULOSIC WATER-BASED BLEND MATERIALS FOR ELECTROSPUN NANOFIBER MEMBRANES AND HYBRID MAGNETIC COMPOSITES PREPARATION

The Third Chapter focuses initially on the recent progress regarding the development of high added value materials useful in water treatment and remediation, as obtained by starting from renewable and natural sources. The importance and properties of various micro- and nano-cellulosic derivatives obtained from secondary-raw materials have therefore been described, also focusing attention on various classes of sustainable doping agents for obtaining functional polymeric blends and advanced sustainable systems for the removal of contaminants from waters. In this context, the research activity focused on the use of waste bio-based materials and waterborne sources for the development of innovative cellulose-derived products, opportunely functionalized, which are employed as dopant agents for water-based polyvinyl alcohol solutions in order to obtain different electrospun nanofiber composite membranes. The so developed bio-based and eco-friendly membranes are tested in a dead-end filtration cell for the gravity-driven removal of two model organic dyes. A composite material with magnetic properties based on a cellulose derivative is also developed and tested for the sorption of organic dyes.

3.1. Secondary raw and natural-derived cellulose-based materials in environmental remediation

3.1.1. Plant-based cellulose derivatives in advanced materials development

Weeping willow, nettle, lucerne, balm-leaved archangel, and Spanish broom are among the wild plants found in continental and Mediterranean regions of Europe that are increasingly commonly studied as potential sources of cellulose fibers and for the development of useful cellulose derivatives [1]. The *Febacaea* family includes plants like the common broom (*Spartium junceum*), often known as Spanish broom. This latter is a perennial plant that is endemic to the Mediterranean region. Its long, green stems range in height from 0.5 to 3 meters. A sporadic foliage is present, and bright yellow blossoms are commonly visible at the ends of the branches. It may be found from South Europe to North Africa and up to the Middle East zones, as well as certain regions of Central and South America. It prospers in sunny sites with dry, sandy soils up to an altitude of 1200 m [2].

The Spanish broom has historically been extensively exploited as a source of raw materials for the production of ropes, sails, webs, bags, fine yarns, fabrics, and clothing, and today it is still used for a variety of purposes, including the extraction of yellow dye, decorative purposes, and the production of cellulose fibers [3]. Additionally, Spanish broom find interesting employments in the extraction of floral essences for perfume production, consolidation of steep slope terrains, and replanting of damaged regions.

In this regard, Spanish broom fibers might be used to make novel, environmentally friendly building materials based on concrete and cement mortar [4,5]. The residual properties of concrete reinforced with Spanish broom fibers are superior those of concrete reinforced with polypropylene fibers [6]. Researchers have also examined the usage of this broom for biomedical applications. To aid in the healing process and safeguard skin wounds, Spanish broom, flax, and hemp treatments infused with glycyrrhetic acid liposomes or hyalurosomes have been produced [7]. The preparation of novel skin wound dressings made from Spanish broom gauzes, filled with Vitamin E and *Lactobacillus plantarum* [8], has also been reported.

In the framework of the ongoing rise in environmental pollution due to widespread human activities in several sectors, including agriculture and manufacturing, Spanish broom is being studied as an adsorbent lignocellulosic material for mercury(II) removal from water with the aim of cleaning up pollution [2]. Furthermore, Spanish broom raw cellulose is also used to synthesize, by reaction with citric acid [9], cellulose citrate, a very effective and selective mercury(II) sorbent.

The textile industry uses a lot of organic dyes, which are a class of emerging contaminants that may be found into water bodies and pose a serious danger to both the environment and human health [10]. As a result, it is necessary to eliminate these pollutants from water sources. Their remediation has been accomplished using a variety of methods, including membrane filtration, flocculation, photocatalytic degradation, adsorption, electrochemistry, and biological therapy [11,12]. The sorption approach is a major and fascinating tactic that may be offered as a viable alternative among the ones previously addressed. For the effective and selective removal of this class of pollutants, several sorbing materials, composites, and hybrids based on carbon

nanotubes, reduced graphene oxide, micro-nano clays, and biopolymers have been continuously studied [13].

In particular, among other biodegradable and naturally generated polymers, cellulose-based materials and their derivatives are interesting sorbent systems, because of their relative availability and safety. In addition, these materials are efficient sorbents for many organic compounds, including pesticides, and are simple to functionalize due to the abundance of hydroxyl groups (-OH) on their surface [14].

The interaction of cellulose fibers with various matrices can also be improved by chemically functionalizing their surface [15]. Chemical or enzymatic techniques can be used to create various cellulose derivatives, including micro-nano cellulose, cellulose micro-nanocrystals, micro-nano fibrillated cellulose, and bacterial micro-nano cellulose [14]. In the production of bacterial nanocellulose by *Gluconacetobacter xylinus* (ATCC 700178), waste post-maceration liquid from Spanish broom enzymatic retting is used as a component [16].

3.1.2. Functionalization of cellulose derivatives for environmental remediation

Membrane filtering technologies are increasingly used to retain various pollutants from ground and wastewater as described in Chapter 2. It is feasible to create functional membranes for the effective and selective removal of specific water contaminants by readily combining polymers with functional additives,[17] like cellulosic derivatives, macrocycles and nanoclays showed in Figure 3.1 a–d and discussed below.

As an example, in a non-solvent induced phase separation process, a bio-based polylactide (PLA)/poly(butylene adipate-co-terephthalate) (PBAT) polymer blend is mixed with functionalized cellulose microfiber derived from empty fruit bunch and modified with maleic anhydride (MEFB). The produced PLA/PBAT-MEFB membrane demonstrated higher porosity and hydrophilicity. Furthermore, it has been investigated for the adsorption of the cationic dye methylene blue (MB) in batch and dynamic adsorption methods. Filtration studies demonstrated that the pure water flow is greater through the PLA/PBAT-MEFB membrane ($1214 \text{ L}\cdot\text{m}^{-2}\cdot\text{h}^{-1}$) than the PLA/PBAT pristine membrane ($371 \text{ L m}^{-2}\cdot\text{h}^{-1}$): the PLA/PBAT-MEFB membrane removed 97.2% of the MB, whereas the PLA/PBAT membrane retained just 58.7% [18].

Fibrous structures with nanoscale dimensions offer a number of exciting qualities, such as excellent mechanical behavior and large surface area to volume ratio, which makes them appealing for a wide range of applications [19]. Because of their large surface area, they may also be significantly and stably functionalized. Among the several methods for generating nanofibers, electrospinning is increasingly gaining popularity as a simple procedure that permits the construction of exceptionally porous structures of smooth non-woven nanofibers through careful control of operation parameters and polymer solution properties. When compared to typical phase inversion processes for membrane fabrication, electrospinning allows for the generation of interconnected pores with uniform pore size and porosities greater than 90% [20]. Electrospun membranes are being used in an increasing number of water purification processes, such as membrane distillation, feed pre-treatment prior to reverse osmosis or nanofiltration, to

remove divalent metal ions, oils, organic molecules, and other contaminants from the water source to be treated [21].

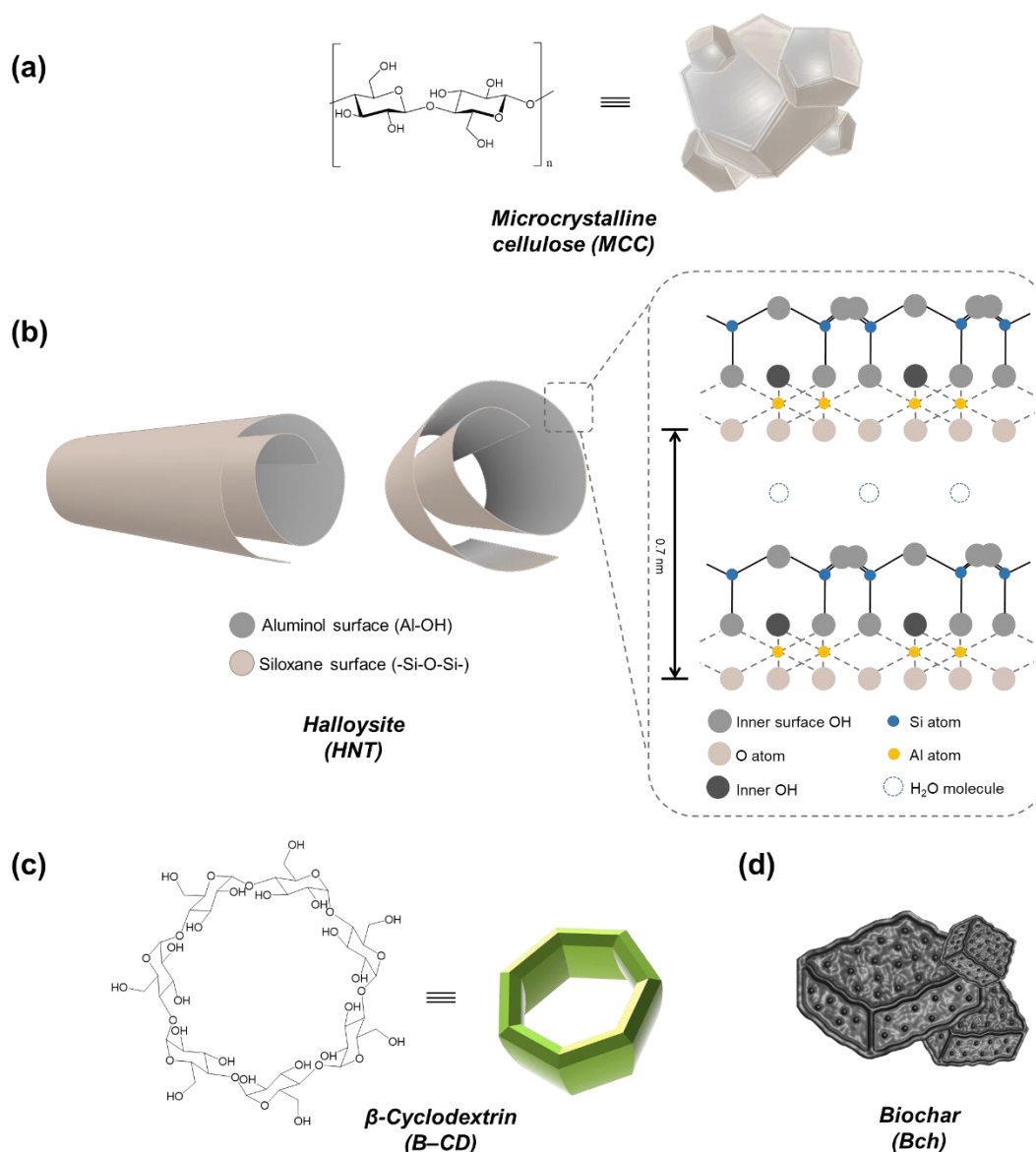


Figure 3.1. Graphical description of different eco-friendly additives, including microcrystalline cellulose (a), halloysite (b), β -cyclodextrin (c) and biochar (d), for the development of functional and advanced environmental remediation technologies.

Microcrystalline cellulose (MCC, see Figure 3.1 a), a cellulose derivative with particle sizes ranging from 10 to 200 μm , has been reported to have better mechanical qualities, surface area, functional groups, and other attributes compared to simple cellulose polymer [22,23].

The effect of cellulose whisker and microcrystals on the biocompatibility of cellulose-based electrospun scaffolds is studied in order to determine their potential usage in electrospun vascular tissue scaffolds. All experimental findings showed that they are promising dopant agents for improving scaffold biocompatibility [24].

Electrospun biocomposites, containing nanocellulose and chitosan entrapped within a poly(hydroxyalkanoate) (PHA) matrix, are being developed for the elimination of Congo red in

the field of environmental remediation. Electrospun bio composites comprising nanocellulose, chitosan, and PHA demonstrated to be excellent organic dye filtration systems. The dye removal of nanocellulose (30.9%) is 3-fold better than chitosan (10.5%) in PHA. To improve the adsorption of Congo red, nanocellulose and chitosan are added to the PHA mesh, which has a synergistic effect ranging from 2- to 7-fold when compared to separate bio adsorbents [25].

Eco-friendly mixed matrix membranes for the removal of MB dye over Congo red dye from simulated waste streams are also developed and evaluated. Hyacinth biomass is utilized as a raw material to extract nano activated carbon (NAC), which is then used as a filler to improve the performance of the blank cellulose acetate (CA) membrane for water treatment. The dye removal capabilities of the composite cast and electrospun CA/NAC are 52.7 and 70%, respectively. However, the pure cast and electrospun CA membranes only obtained 30 and 43.3%, respectively. The results revealed that electrospun membranes outperformed casted membranes [26].

On the other hand, the properties of halloysite (Figure 3.1 b) make it beneficial for a range of applications, including drug delivery, the development of anticorrosive and flame-resistant coatings, catalysis, and the removal of contaminants from water [27,28]. The combination of halloysite nanotubes and Fe_3O_4 nanoparticles improves heavy metal removal using electrospun membranes. Immobilizing halloysite nanotubes and Fe_3O_4 nanoparticles on polyethylene oxide/chitosan (PEO/CS) composite electrospun fibers results in magnetic nonwovens. The adsorbents have a homogenous structure, superior pore structure, high specific surface area, and superparamagnetic properties as a result of organic-inorganic hybridization. These nonwovens demonstrated good removal effectiveness of several heavy metal ions, with cadmium, copper, lead, and chrome adsorption capacity onto the nonwoven in the sequence $\text{Cr(VI)} < \text{Cd(II)} < \text{Cu(II)} < \text{Pb(II)}$ [29].

In recent years, cyclodextrin-based materials have garnered a lot of attention for eliminating dye pollutants from water among MCC and HNT adsorbents [30]. CDs (Figure 3.1 c) are cyclic oligosaccharides composed of (1,4)-linked glucopyranoside units with a hydrophobic interior cavity and a hydrophilic exterior surface. They are categorized based on the number of glucopyranoside units, which can be six, seven, or eight, resulting in α -, β -, and γ -cyclodextrins, respectively [31]. The capacity of CDs to create host-guest complexes with a wide range of compounds makes them excellent for applications in many areas such as pharmaceutical, biomedical, cosmetics, textiles, environmental, separation, and food [32–34]. β -CDs (Figure 3.1 b), as opposed to α - and γ -CDs, have piqued the interest of academics due to their low cost and ease of production.

In this regard, the development of electrospun fibers based on β -cyclodextrin has also been described in the literature. The resultant β -cyclodextrin electrospun nanofibers, obtained by using poly(acrylic acid) polymer and citric acid as cross-linking agents, need to undergo heat treatment to become stable and aqueous solution resistant, as well as to have a higher tensile strength. Because of the high β -cyclodextrin content and the presence of numerous carboxyl groups, the fibers exhibit remarkable adsorption and recyclable qualities towards the cationic dye MB. Dynamic filtering investigations indicate that the membranes can successfully separate

MB/MO mixture dyes at high flow rates of $150 \text{ mL}\cdot\text{min}^{-1}$ (volume 100 mL, MB concentration = $4.27 \text{ mg}\cdot\text{L}^{-1}$, MO concentration = $16.03 \text{ mg}\cdot\text{L}^{-1}$; ideal pH value of MB adsorption = 9) [35].

A practical approach for generating water-insoluble sericin/ β -cyclodextrin/PVA composite nanofibers (obtained by electrospinning technology with citric acid as the crosslinking agent) is discussed as well. In this instance, thermal crosslinking is also used. Because of the integration of β -CD and sericin, the composite nanofiber mat confirmed its applicability in aqueous solution media for MB removal, with a considerable increase in MB adsorption [36].

Biochar (Figure 3.1 d) produced from waste biomass has inspired considerable interest in the field of pollution reduction since it combines the benefits of "treating waste by waste" and limiting environmental effect, while achieving carbon capture and sequestration. Furthermore, the numerous functional groups, porosity, and stability of biochar all contribute to its catalytic and adsorption activity [37].

A tough portable water purification system has recently been developed using electrospun nanofibers. The device employs three distinct electrospun membranes. The first membrane is created by electrospinning a polyacrylonitrile/chitosan solution to function as an antibacterial membrane, the second membrane is created by immobilizing laccase onto an electrospun PAN/biochar mat to remove micropollutants, and the third membrane is created by electrospinning a PAN/biochar to operate as an adsorptive membrane. The applied approach eliminated over 99% of microorganisms, 83% of micropollutants, and more than 77% of turbidity in less than 5 minutes of contact time [38].

Zero-valent iron nanoparticles (NZVI) are widely employed in groundwater remediation due to their strong reactivity to a variety of pollutants [39,40]. On the other hand, NZVI particles are subject to aggregation, oxidation, and sedimentation. To overcome these problems, surfactants, suspending agents, and stabilizers are frequently employed [41]. If the NZVI particles are immobilized on a membrane or other surface with a large surface area, the possibility of secondary contamination may be reduced. Biochar can be used as a support for a variety of catalysts, including NZVI. This composite has piqued the interest because Fe(0)-NPs dispersed over biochar offers benefits such as in situ cleanup, decreased solid residue, organic compound decomposition, and ease of separation and reuse [37].

On this subject, one may consider that poly(vinyl alcohol) (PVA) is a hydrophilic polymer with minimal fouling potential and excellent film-forming properties [42] that may be used to electrospun nanofibers from water-based blends. A water-based PVA/starch hydrogel electrospun nanofiber membrane with a large surface area and three-dimensional structure represents an example. Following the thermal cross-linking procedure, the membrane is tested for filtration of 100 mL of MB/MO solution ($5 \text{ mg}\cdot\text{L}^{-1}$ for MB and $18.1 \text{ mg}\cdot\text{L}^{-1}$ for MO) at a flow rate of $180 \text{ mL}\cdot\text{min}^{-1}$. The MB adsorbs on the membrane after 54 seconds, and the MO flows through. With a dye separation efficiency of 99.6%, the MB content in the permeate decreased from 5 to $0.065 \text{ mg}\cdot\text{L}^{-1}$, whereas the MO concentration decreased from 18.1 to $17.5 \text{ mg}\cdot\text{L}^{-1}$ [11].

Considering all the shown examples, high value-added products, obtained from secondary raw materials and from renewable plant biomass, have therefore the potential to become a valid and concrete alternative for a sustainable modern industrial production and technology.

3.2. Microcrystalline cellulose and biochar from Spanish broom for eco-friendly PVA-based electrospun nanofiber composite membranes

3.2.1. Abstract

The approach of producing high-value-added materials from waste obtained from renewable plant biomass has the potential to become a key component of modern advanced manufacturing. In this regard, the goal of the present study was to create two cellulosic derivatives from Spanish broom (*Spartium junceum*), a common and plentiful broom found in the Mediterranean region. Microcrystalline cellulose and biochar were successfully obtained from this natural source and functionalized using simple, eco-friendly, one-step synthetic approaches with appropriate precursors and nanomaterials, such as (3-mercaptopropyl)trimethoxysilane, (3-glycidyloxypropyl)trimethoxy, citric acid, β -cyclodextrins, and halloysite nanotubes, to prepare green, hybrid, and cross-linked systems with specific designed properties (Figure 3.2).

The produced derivatives were characterized and used in the fabrication of eco-friendly water-based PVA nanofibers through electrospinning on non-woven glass microfiber substrate.

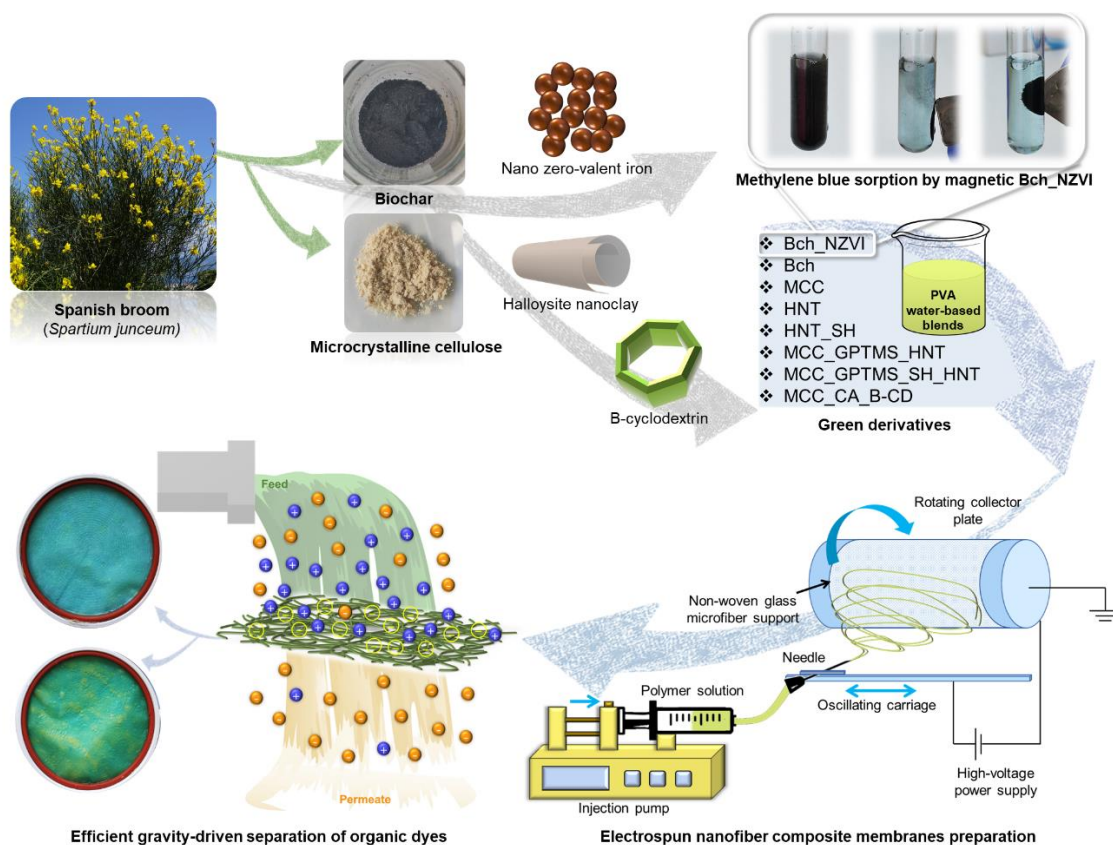


Figure 3.2. Illustration of microcrystalline cellulose and biochar from Spanish broom and their employment for the preparation of advanced electrospun nanofiber composite membranes for organic dyes removal.

The membranes demonstrated quite good mechanical tensile capabilities and were evaluated in a dead-end filtration cell for the removal of a methylene blue and methyl orange mixed solution, displaying good retention and separation performances towards the selected

cationic dye. In batch experiments, a biochar-supported nano zero-valent iron composite has been developed and evaluated for MB removal. The Langmuir adsorption isotherm model more accurately represents its sorption behavior, with a sorption capacity of $305.65 \text{ mg}\cdot\text{g}^{-1}$ ($C_0 = 100 \text{ mg}\cdot\text{L}^{-1}$, $\text{pH} = 7$, $T = 298 \text{ K}$). The whole research activity described in this Chapter refers to the content outlined in the article n.1 of the publication list.

3.2.2. Results and discussions

3.2.2.1 Extraction of microcrystalline cellulose and biochar from Spanish broom

Microcrystalline cellulose and biochar have been effectively obtained from Spanish broom and functionalized by means of appropriate precursors and nanomaterials to produce hybrid or cross-linked systems with specified characteristics. Spanish broom stems were cut into short slices and processed with maceration and trituration to make the cellulose more accessible. During the trituration process, two distinct portions were separated as powder fibers and straws with the use of an electric disintegrator. The straws were pyrolyzed to produce biochar, while the powder fibers were treated with sodium hydroxide to achieve hemicellulose and lignin solubilization, yielding alkali-treated fibers (pow_alk), and then oxidized in an acidic medium to produce bleached fibers (pow_bl) [43]. Finally, these latter were hydrolyzed with sulfuric acid and hydrochloric acid [44] to produce microcrystalline cellulose (Figure 3.3).

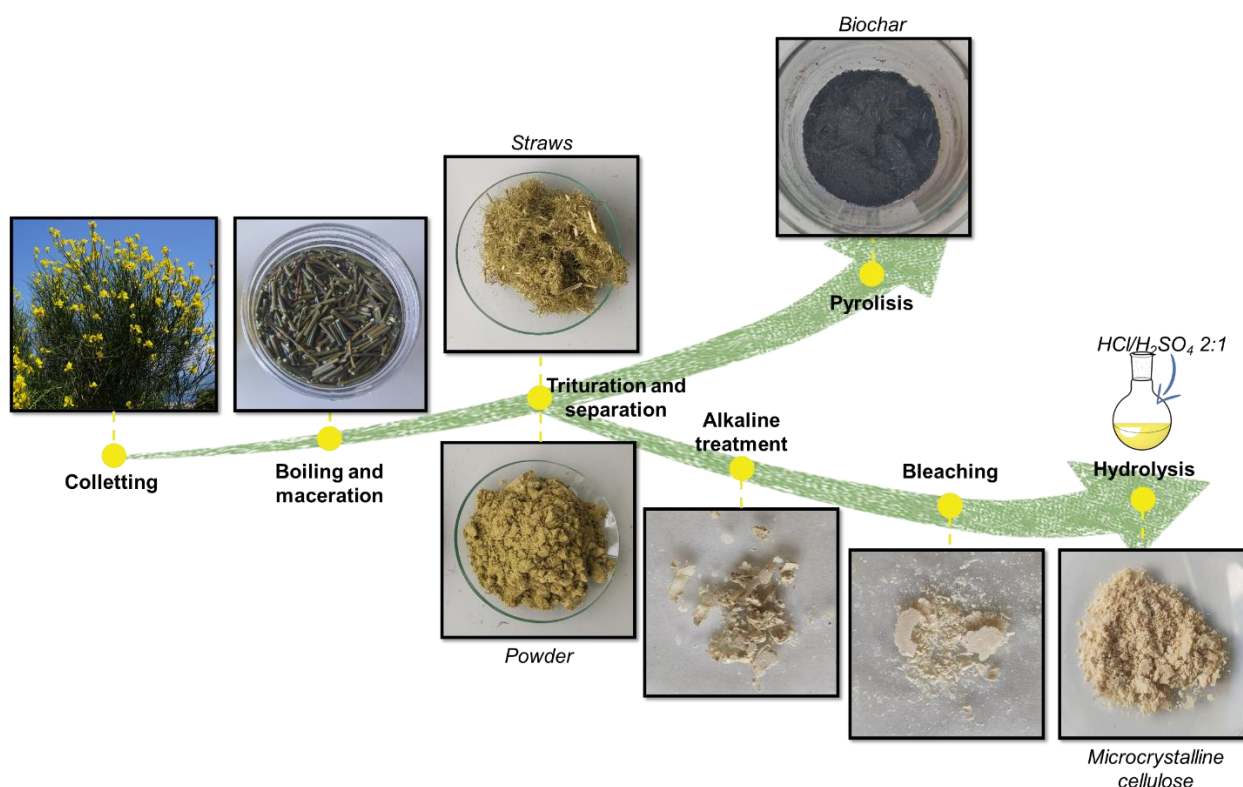


Figure 3.3. Step-ways schematization for the development of microcrystalline cellulose and biochar from *Spartium junceum*.

The starting materials and all derivatives were analyzed via ATR-FTIR technique (Figure 3.4). The FT-IR spectra of straws and powder fibers resulted quite similar. On the other hand, powder

fiber derivatives spectra show numerous changes following alkali and delignification treatments, demonstrating the efficient removal of lignin and hemicellulose [44]. CH₂ stretching signals are clearly visible for pow, pow_alk, and pow_bl samples at 2613 cm⁻¹ and 2545 cm⁻¹, with modest changes in intensity and ratio after each treatment.

Following hydrolysis, the CH₂ stretching signal emerges with a single band at 2594 cm⁻¹, which is due to the disappearance of hemicellulose CH₂ stretching vibration component [45]. Powder fibers provide a signal at 1731 cm⁻¹ that can be attributed to the hemicellulose acetyl groups or to the ester and carboxylic functionalities of phenolic acid acids from lignin and/or hemicellulose [46]. After alkali-treatment and bleaching, this last signal, as well as the bands at 1511 cm⁻¹ and 1237 cm⁻¹ relative to the C=C aromatic and C-O out of plane stretching vibration of the lignin aryl groups, respectively [47,48], are almost completely suppressed. Furthermore, a rise in the strength of the crystalline band at 1429 cm⁻¹ may suggest the existence of greater crystalline order in MCC [49].

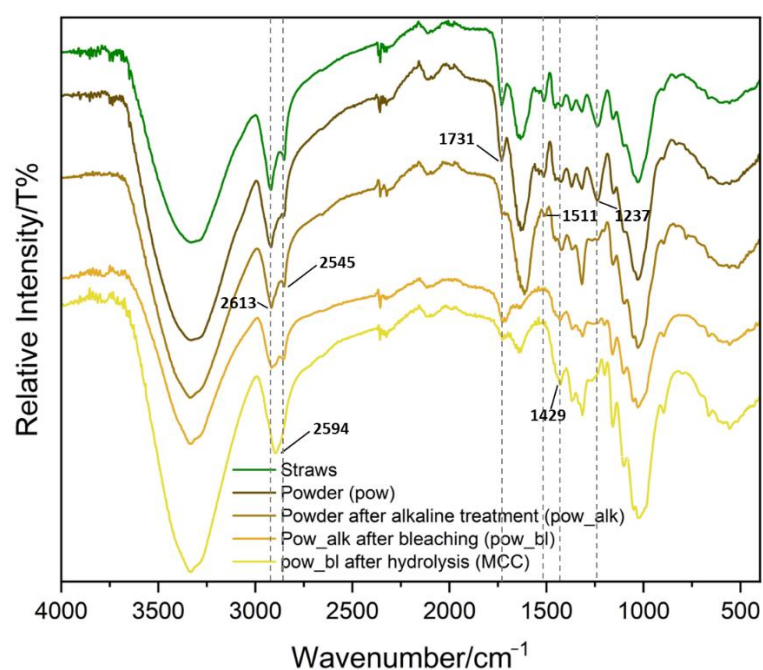


Figure 3.4. ATR-FTIR spectra of straws and powder from Spanish broom, as well as all powder intermediates and derivatives, obtained after each treatment for the production of MCC.

3.2.2.2 Microcrystalline cellulose and Biochar functionalization approaches

MCC and Bch may be functionalized using simple, eco-friendly, one-step synthetic techniques to produce a variety of green and sustainable derivatives. In particular, sol-gel technique, citric acid cross-linking, and liquid-phase chemical reduction were among the main procedures used. Sol-gel synthesis was used to create two distinct hybrid organic-inorganic compounds based on MCC and HNT along with (3-mercaptopropyl)trimethoxysilane (MPTES) and (3-glycidyloxypropyl)trimethoxysilane (GPTMS) silane precursors (Figure 3.5).

GPTMS sol-gel precursor has a bifunctional functionality due to the presence of a binding trimethoxysilyl group and an anchoring epoxy ring. Its polymerization begins with an epoxy-ring

opening reaction of the GPTMS molecules, followed by further processes of hydrolysis of the trimethoxysilyl group and condensation that lead to the subsequent alkoxy silane polymerization with formation of a 3D-polyethyleneoxide (PEO) matrix able to host by a chemical or a physical way functional nanofiller and molecules [51] (Figure 3.5 a).

The thiol group of MPTES, this latter employed to functionalize HNT and obtain the HNT_SH derivative, can react with the epoxy group of GPTMS. Furthermore, following a preliminary acidic hydrolysis phase, MPTES trimethoxysilane groups can react with the alkoxy silane ends of GPTMS, which may statistically bind each other, [52] boosting for example the reactivity of HNT_SH with GPTMS (Figure 3.5 b).

MCC_GPTMS_HNT and MCC_GPTMS_SH_HNT derivatives were obtained with the aim to exploit: (i) the organic functionalities of the hybrids for their well integration into the polymeric blends, (ii) the sorption properties of the functional halloysite nanotubes toward organic contaminants, (iii) the thiol-modified cross-linked matrix of (3-mercaptopropyl)trimethoxysilane functionalized HNT for improved affinity towards various water pollutants.

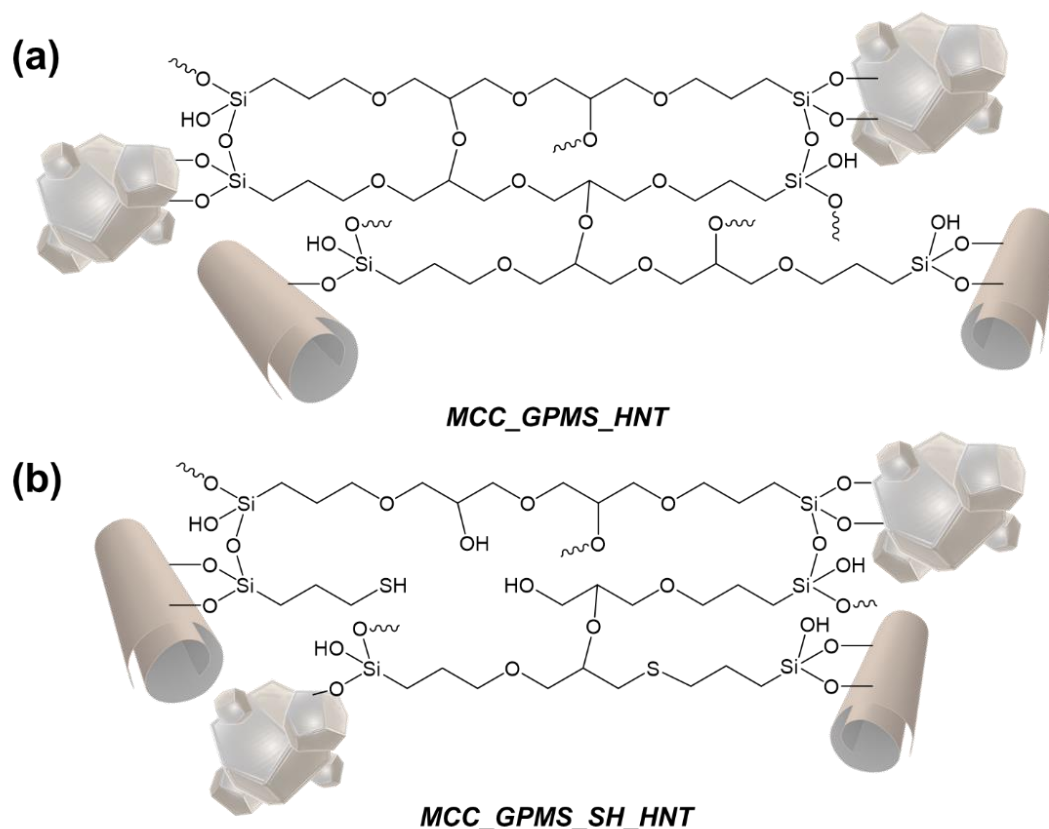


Figure 3.5. Illustration of MCC_GPTMS_HNT (a) and MCC_GPTMS_SH_HNT (b) hybrid derivatives.

Since cyclodextrins are extremely helpful in water remediation applications due to their ability to form inclusion complexes with organic molecules via weak interactions regulated by supramolecular chemistry [50], they were chosen as functional additives to be covalently and stably attached to MCC. A green synthesis was carried out using citric acid as a cross-linker for the surface functionalization of MCC, resulting in the MCC_CA_B-CD derivative (Figure 3.6).

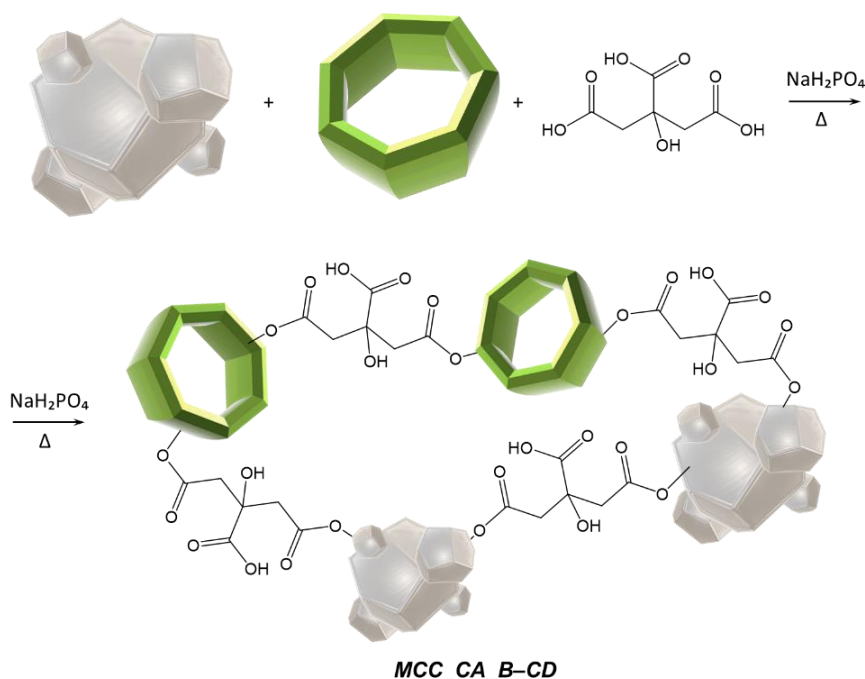


Figure 3.6. Illustration of MCC_CA_B-CD derivative.

Biochar was produced by a standard pyrolysis of Spanish broom straws. According to research on other natural derived products [51,52], a pyrolysis temperature of 400 °C is used with a residence period of 2 hours to create biochar to achieve the optimal chemical and morphological features (i.e. micro-porosity). In fact, the pyrolysis temperature and residence time have a significant influence on the chemical content and structure of the resulting biochar [53]. For example, an increasing charring temperature promote aromaticity and possibly recalcitrance [51].

Biochar-supported nano zero-valent iron composites were created by post-functionalizing biochar using a liquid-phase chemical reduction technique (see Equations 1 and 2 and Figure 3.7) [54,55]. Polyethylene glycol (PEG) was used as a stabilizer in the synthesis since it has been demonstrated that the addition of surfactants may coat micro zero-valent iron particles to improve their physical stability via steric stabilization [55].

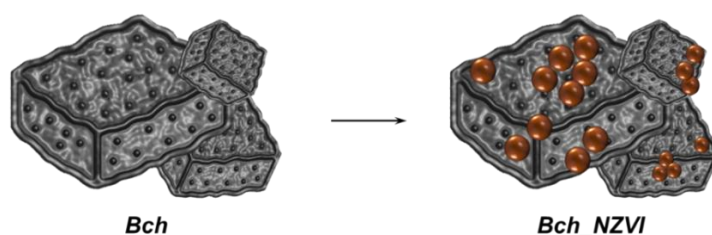
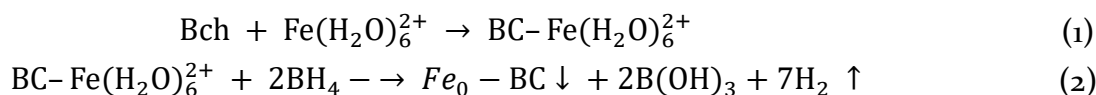


Figure 3.7. Illustration of Bch_NZVI derivative.

3.2.2.3 ATR-FTIR characterization of MCC and HNT nanofiller derivatives

The chemical composition of the functional derivatives produced from the modification of MCC and Bch with the specified nanomaterials and functional agents was studied using ATR-FTIR spectroscopy (Figure 3.8 a–d).

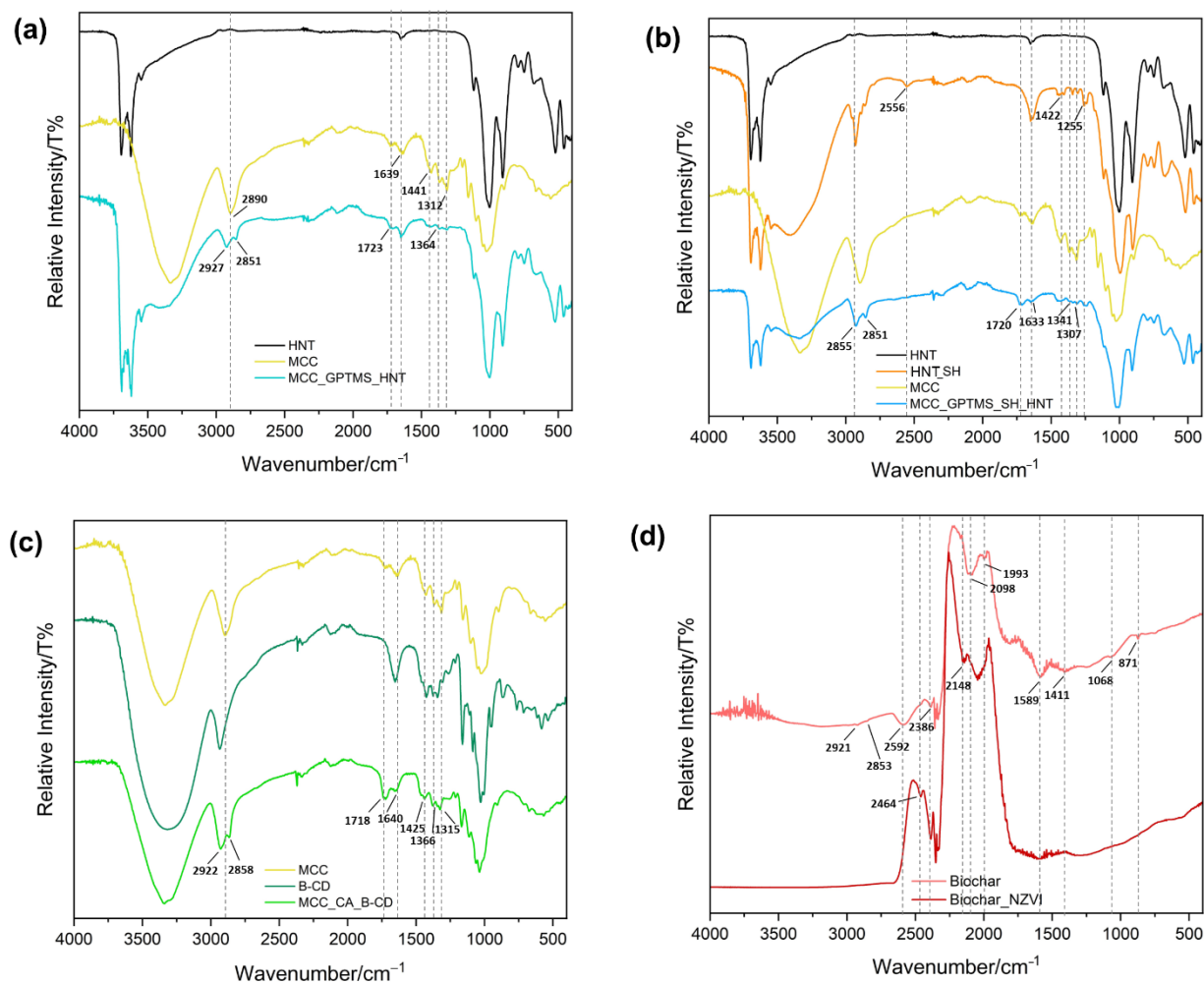


Figure 3.8. ATR-FTIR spectra of MCC and HNT (a), MCC and HNT_SH (b), MCC and B-CD (c), and Bch and Bch_NZVI (d).

The analysis of the signals reported in Table 3.1 demonstrate the effective gaining of final products.

In particular, MCC_GPTMS_HNT (Figure 3.8 a), MCC_GPTMS_SH_HNT (Figure 3.8 b) and MCC_CA_B-CD (Figure 3.8 c) FT-IR spectra display the characteristic signals of MCC related to C–H₂ stretching, C=O stretching, non-H-bonding and –COOH vibrations, C–O–C asymmetric vibration of the β -glycosidic linkage, C–O stretching and β -glycosidic C–H vibrations [43,56].

The MCC_GPTMS_HNT and MCC_GPTMS_SH_HNT spectra also reveal HNT-specific signals such as the inner-surface O–H stretching, inner O–H stretching, Si–O asymmetric stretching, Si–O stretching, Al–O–Si bending and Si–O–Si bending. Furthermore, they are identified by the presence of additional H–C–H stretching signals associated to the alkyl chains of the used alkoxy silanes precursors at 2927 and 2851 cm⁻¹ for MCC_GPTMS_HNT and 2855 and 2851 cm⁻¹ for MCC_GPTMS_SH_HNT [57–59].

Figure 3.8 d depicts the ATR-FT-IR of biochar and biochar-supported nano-zero valent iron, displaying signals associated with C–H stretching (aliphatic), C=C, –CH (terminal) groups and C≡C stretching, C=O stretching, C–N stretching, N–H bending, C=C stretching of aromatic C, C–O–C stretching and C–H bending aromatic CH out-of-plane deformation [54,55,60]. Furthermore, a wide signal from 1109 to 1397 cm^{-1} is found, which may be attributable to –COO bonds arising from the polyethylene glycol used in the manufacture of this derivative [54]. There are no observed peaks associated with the likely generation of iron oxides during the oxidation of Fe(0), but the poor definition of ATR-FTIR spectra of Bch and Bch_NZVI should be remarked.

Table 3.1. Main IR vibrations of pristine HNT, MCC, Bch, B-CD and all the obtained derivatives.

	HNT	MCC	MCC_GPTMS_HNT	Ref.
	<i>Wavenumber/cm⁻¹</i>			
Inner-surface O–H stretching	3696	n.r.	3691	[57,58]
Inner O–H stretching	3623	n.r.	3621	[57–59]
O–H stretching of water	3546	3062–3623	3548	[57–59]
C–H ₂ Asymmetric stretching	n.r.	2966–2806	2927	[57,58]
C–H ₂ Symmetric stretching	n.r.	2966–2806	2851	[58]
C=O str, non-H-bonding –COOH	n.r.	1716	1723	[43,56]
O–H deformation of water	1646	1639	1646	[43,57,59,61]
C–H Bending vibrations	n.r.	1420,1364, 1308	1441, 1364, 1312	[43,57,58]
C–O–C asymmetric vibration of the b- glycosidic linkage	n.r.	1099	1117	[43]
C–O stretching	n.r.	1023	-	[43]
β-glycosidic C–H vibrations	n.r.	896	-	[43,56]
Si–O asymmetric stretching	1118, 1000, 907	-	1118, 1002, 907	[57,59]
Si–O stretching	791,746	-	793, 750	[57–59,62]
Al–O–Si bending	678, 520	-	679, 524	[57,63]
Si–O–Si bending	457	-	459	[57,59]
	HNT_SH	MCC_GPTMS_SH_HNT	Ref.	
Inner-surface O–H stretching	3695		3695	[57,58]
Inner O–H stretching	3621		3621	[57–59]
O–H stretching of water	3542		3546	[43,57–59]
C–H ₂ Asymmetric stretching	2929		2855	[43,57,58]

C-H ₂ Symmetric stretching	2850	2851	[43,58]
S-H stretching	2556	n.r.	[64]
C=O str, non-H-bonding -COOH	n.r.	1720	[43,56]
O-H deformation of water	1642	1633	[43,57,59,61]
C-H Bending vibration	1422,1344, 1304	1439, 1341, 1307	[43,57,58]
Si-C bending	1255	1246	[64]
C-O-C asymmetric vibration of the β- glycosidic linkage	n.r.	1116	[43]
β-glycosidic C-H vibrations	n.r.	-	[43,56]
Si-O asymmetric stretching	1116, 992, 902	1113, 1112, 908	[57,59]
Si-O stretching	792,746	798,743	[57-59,62]
Al-O-Si bending	668, 520	676, 523	[57,63]
Si-O-Si bending	454	459	[57,59]
	B-CD	MCC_B-CD	Ref.
O-H stretching of water	3686-3031	3623-3062	[43,57-59]
C-H ₂ Asymmetric stretching	3007-2835	2922	[43,57,58]
C-H ₂ Symmetric stretching	3007-2835	2858	[43,58]
C=O str, non-H-bonding -COOH	-	1718	[43,56]
O-H deformation of water	1650	1640	[43,57,59,61]
C-H Bending vibration	1429, 1377, 1310	1425, 1366, 1315	[43,57,58]
C-O-C Asymmetric vibration of the β- glycosidic linkage	1090	1105	[43]
C-O stretching	1038	1032	[43]
β-glycosidic C-H vibrations	956	894	[43,56]
	Bch	Bch_NZVI	
C-H stretching (aliphatic)	2921, 2853	-	[55]
C=, -CH (terminal) groups and C≡C stretching	2592, 2386	2464, 2386	[55]
O-H deformation of water	2098	2148	[54]
C=O str	1993	2048-1965	[54]
C-N stretching and N-H bending	1589	1589	[54,55]
C=C stretching of aromatic C	1411	-	[60]
C-O-C stretching	1068	-	[60]

3.2.2.4 SEM characterizations of MCC and HNT nanofiller derivatives

The morphology of the MCC and Bch derivatives was studied using scanning electron microscopy (Figure 3.9 a–h').

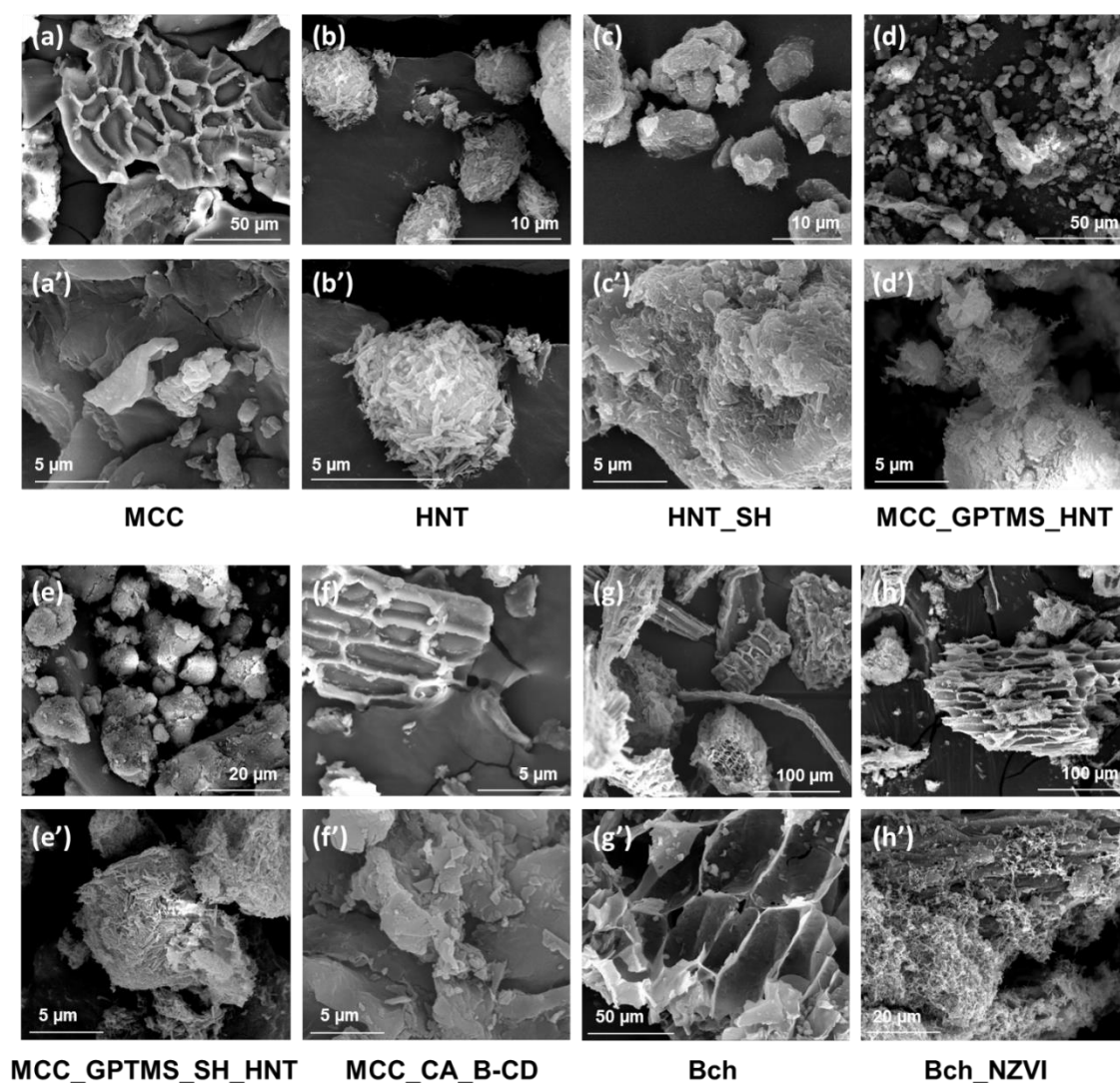


Figure 3.9. SEM images of the pristine MCC (a, a'), Bch (g, g'), and HNT (b, b') and functionalized HNT_SH (c, c'), MCC_GPTMS_HNT (d, d'), MCC_GPTMS_SH_HNT (e–e'), MCC_CA_B-CD (f, f') and Bch_NZVI (h, h') additives at different magnifications.

MCC and its derivatives have a non-fibrous shape, which can be attributed to the high cohesion of hydrogen bonding between cellulose small particles, resulting in aggregate formation [65,66]. SEM images results (Figure 3.9 a, a') verify the removal of lignin, hemicellulose, and other non-cellulosic components (i.e., contaminants) and effective separation of cellulose, correlating with the ATR-FTIR analyses. When compared to separate treatments, the combination of alkaline and acid oxidation treatments results in smoother

surfaces due to the removal of such components [44]. Meanwhile, hydrolysis produces defects and micro-sized fibrils with a slightly rough surface [66].

These outcomes agree with experimental results observed in the SEM images.

Because of the strong physical, hydrogen, and van der Waals bonding connections between their hydroxyl groups, pristine HNTs (Figure 3.9 b, b') have a distinct aggregated morphology [67]. Their long tubular and fibrous form, as well as their aggregated nature, are preserved even after the reaction with the two distinct cross-linkers and MCC (Figure 3.9 d-e'). In the case of the HNT_SH hybrid derivative (Figure 3.9 c,c'), the nanotubes appear to be bonded together with a rough surface, indicating the presence of an organic domain, a cross-linked matrix [68], and interactions between the functionalities. MCC aggregates are therefore visibly functionalized with HNTs with homogenous surface covering.

MCC_CA_B-CD micrographs (Figure 3.9 f, f') indicate a smoother morphology than pristine MCC due to its homogenous covering with cross-linked B-CDs. Furthermore, the incorporation of features that facilitate interactions between the components of the MCC derivative results in greater aggregation.

Biochar morphology is distinguished by a lamellar and irregular form with numerous big holes on its rough surface. Many regular particles with a uniform distribution may be seen on biochar after it has been modified with nano zero-valent iron. The inclusion of a PEG stabilizer promotes the effective dispersion of these particles on the surface of Bch [55].

3.2.2.5 MCC, HNT and Bch based electrospun composite nanofiber membranes

Distilled water was used to develop the PVA water-based solution (10% wt% g·ml⁻¹). The PVA solution was mixed with each dopant agent at a ratio of 3% (w/w nanofiller and PVA). After 30 minutes of mixing in an oil bath at 80°C, the mixture was cooled to room temperature before being electrospun.

Electrospinning was carried out at ambient temperature and humidity (30–40% RH). Each electrospun membrane is obtained using a voltage of 19 kV, a distance of 12 cm between the syringe needle tip and the metal collector, and a solution flow rate of 0.6 mL·h⁻¹, by collecting the nanofibers on a large rotating drum (at a velocity speed of 200 rpm) coated with aluminum foil and non-woven glass microfiber sheets. Two syringes were used simultaneously in an oscillating carriage, and the nanofibers were collected for a total of 5 hours for each membrane. Every composite membrane was dried overnight at 60 °C before being thermally treated for 8 hours at 180 °C [69]. Figure 3.10 a, b illustrates PVA-based electrospun composite nanofiber membranes doped with the functional derivatives described above, generated by electrospinning on a non-woven glass fiber substrate.

After heat treatment, the specimens have a brownish shade, which is typical of PVA-based nanofibers [69], and the electrospun nanofiber coating seems to be better attached to the substrate.

The average weight and thickness of the resulting PVA electrospun nanofiber composite membranes are shown in Table 3.2.



Figure 3.10. The appearance of the produced electrospun nanofiber composite membranes before (a) and after heat treatment b).

Table 3.2. Physical properties list of the developed PVA electrospun nanofiber composite membranes.

Name	Weight/mg·cm ⁻²	Average thickness/μm
Non-woven glass fiber support	2.94	0,085 ± 0,002
PVA	3.30	0,118 ± 0,003
PVA@MCC	3.27	0,124 ± 0,012
PVA@HNT	3.27	0,121 ± 0,001
PVA@HNT_SH	3.47	0,117 ± 0,006
PVA@MCC_GPTMS_HNT	3.29	0,115 ± 0,002
PVA@MCC_GPTMS_SH_HNT	3.04	0,118 ± 0,001
PVA@MCC_CA_B-CD	3.21	0,104 ± 0,001
PVA@Bch	3.52	0,132 ± 0,003
PVA@Bch_NZVI	2.94	0,113 ± 0,002

3.2.2.6 SEM characterizations of MCC, HNT and Bch based electrospun composite nanofiber membranes

SEM technique was used to investigate the shape and fiber diameter of the non-woven glass fiber support and the resultant electrospun nanofiber composite membranes (Figure 3.11, 3.12).

The SEM images show a pattern of thin mesh-like nanofibers with a high surface area-to-volume ratio.

Following the addition of the functional additives, the shape of the PVA nanofibers stays nearly unaltered. The manufactured nanofibers have a consistent diameter and a relatively smooth surface.

The existence of tiny spindle-like beads in PVA@MCC, PVA@MCC_GPTMS_HNT, PVA@MCC_GPTMS_SH_HNT, and PVA@MCC_CA_B-CD nanofibers is related to the influence of the viscosity of the PVA polymeric mix for the presence of the micro-nano fillers added [70,71].

The diameter and dispersion of PVA@Bch_NZVI nanofibers are inadequate. Because of the conductivity of the used Bch_NZVI dopant agent, the electrospinnability of this final mix requires additional study and testing to be properly optimized.

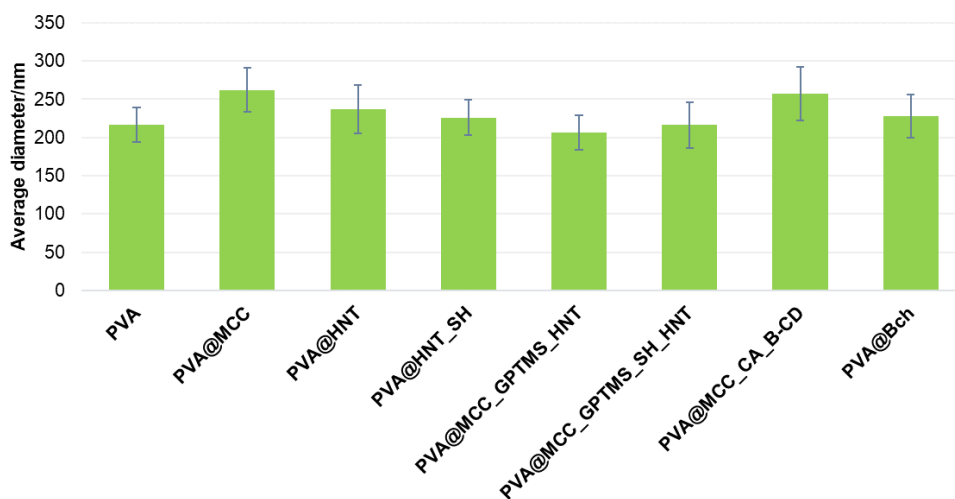


Figure 3.11. Histogram of the average diameter of the electrospun nanofibers after heat treatment.

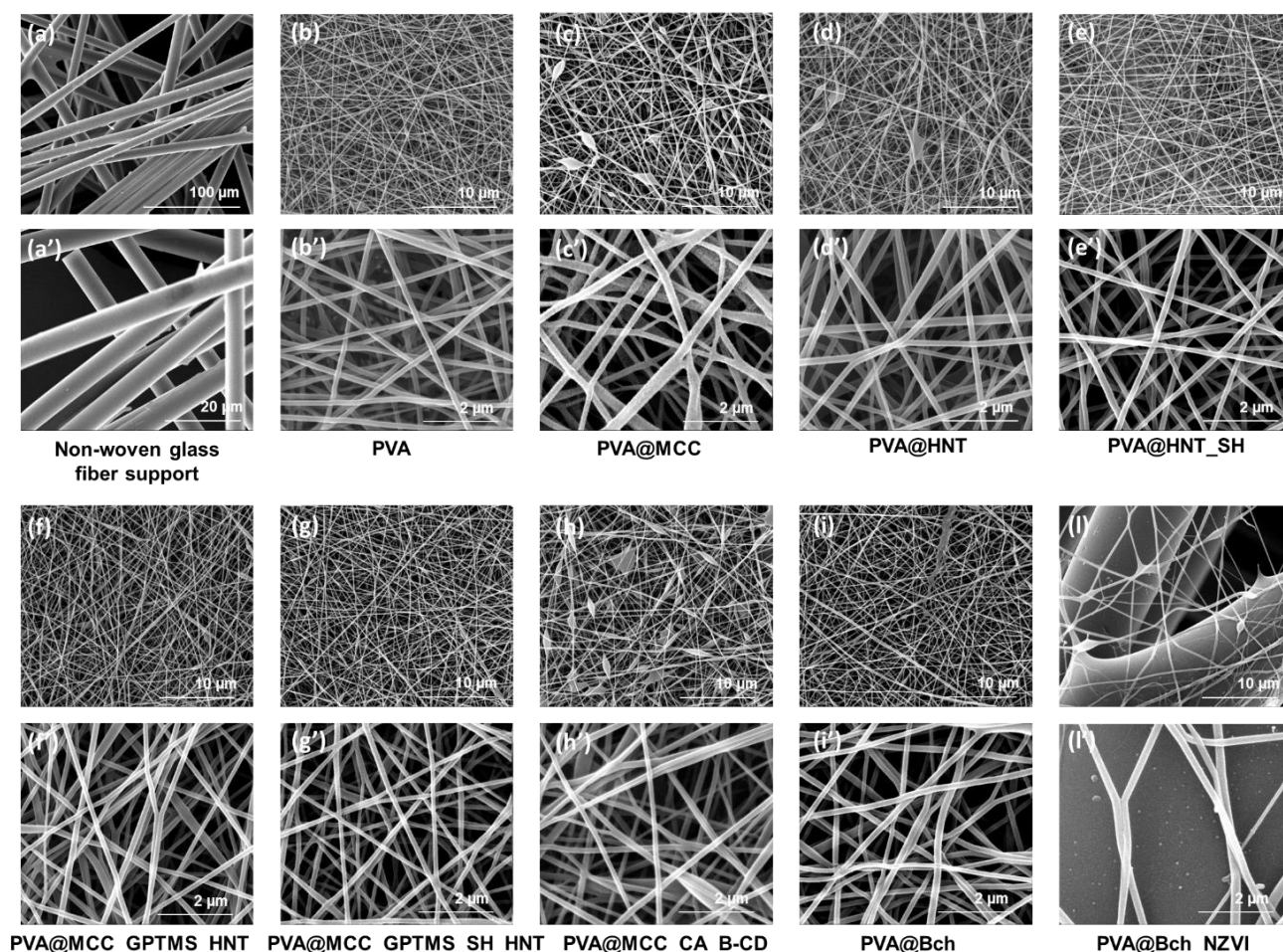


Figure 3.12. SEM images at two different magnifications (a-l and a'-l') of the pristine PVA and doped PVA-based electrospun nanofiber composite membranes, as well as the non-woven glass fiber used as support.

3.2.2.7 Water swelling of the developed electrospun nanofiber composite membranes

The swelling degree and mass loss (Figure 3.13 a,b) of the PVA electrospun nanofiber composite membranes before and after heat treatment were measured using the method

described by Hoang et al. [72] (see Chapter 6) to investigate the water resistance of the produced nanofibers.

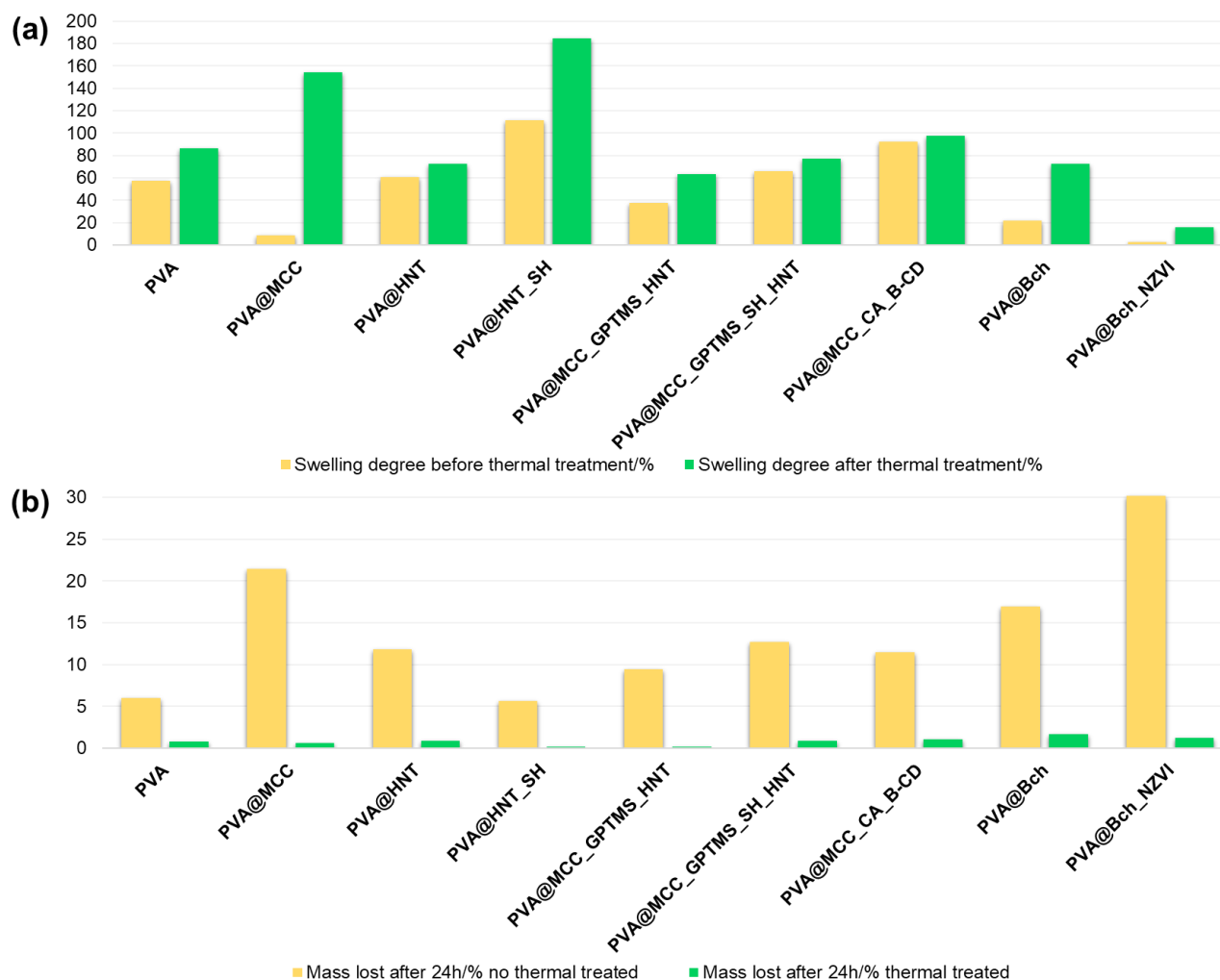


Figure 3.13. Histograms of the swelling degree of electrospun nanofiber composite membranes before and after heat treatment (a) and corresponding mass loss (b) after swelling experiment in water.

This value is significantly connected to hydrophilicity and crosslinking density, and it has a significant impact on dye retention performance.

Because of their partial water solubility, untreated PVA nanofibers lost weight after 24 hours of immersion. PVA@MCC and PVA@HNT_SH membranes display more swelling following heat treatment, indicating that they are more hydrophilic than the other membranes.

Furthermore, PVA@MCC_GPTMS_HNT, PVA@MCC_GPTMS_SH_HNT, PVA@MCC_CA_B-CD, and PVA@Bch nanofiber membranes exhibit lower water absorption values due to the formation of strong hydrogen interactions and a three-dimensional network through the functional additives used for the functionalization of PVA blends, resulting in high water resistance [73]. Within 24 hours, no loss of integrity is seen in thermal-treated PVA membranes. The acquired findings illustrate the effective integrity of the membranes exposed to water accomplished by thermal treatment and functionalization using the developed materials.

3.2.2.8 Tensile mechanical properties

The tensile stress-strain graphs of the produced PVA-based composite membranes, as well as the associated average maximum stress and elongation at break values, are shown in Figures 3.14 a,b.

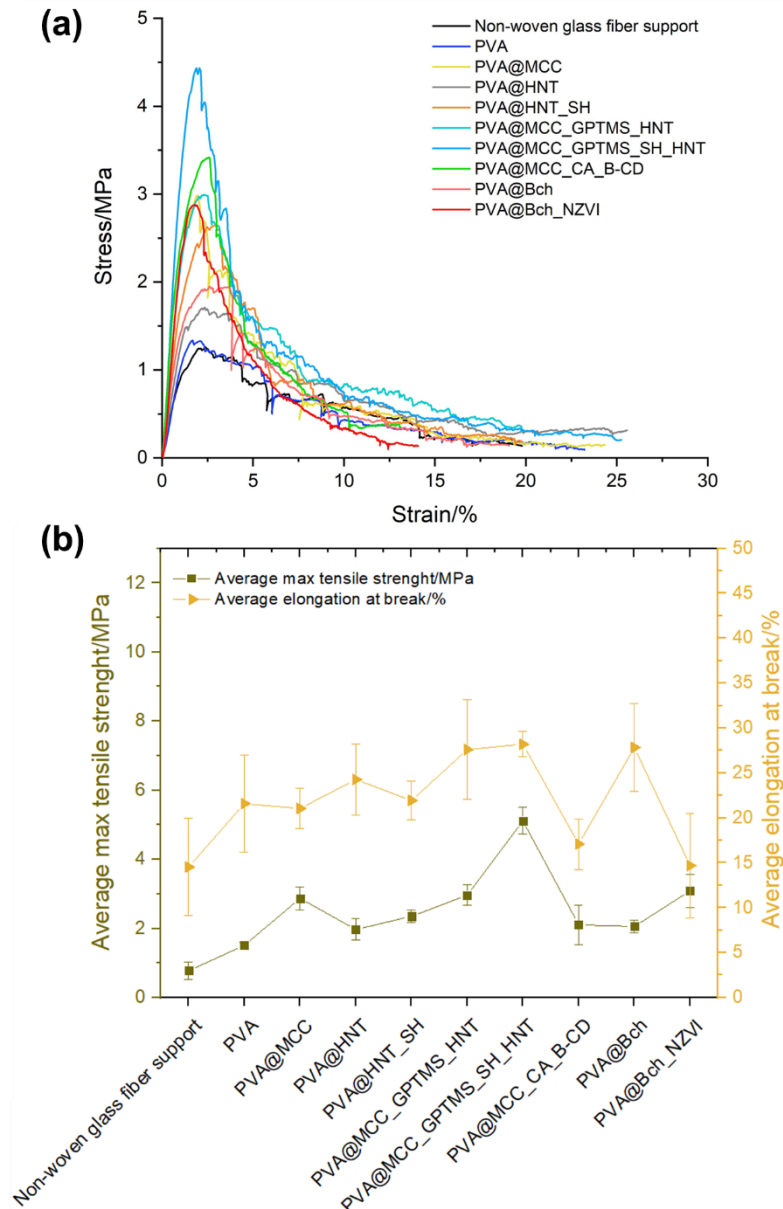


Figure 3.14. Representative tensile stress-strain curves of electrospun nanofiber composite membranes (a), with associated average maximum tensile strength and elongation at break values (b).

An increase of the average max strength is revealed for all the doped membranes (see Table 3.3). The PVA@MCC_GPTMS_HNT membrane performed best in terms of maximum stress and elongation at break value.

The solid form of HNT nanotubes may reduce the rigidity and stiffness of the resultant polymeric composite (i.e., with high concentration of HNTs) as well as nanofibers [74,75].

Table 3.3. Average maximum tensile strength and elongation at break values of the tested electrospun nanofiber composite membranes.

Name	Average max tensile strength/MPa	Average elongation at break/%
Non-woven glass fiber support	0.78 ± 0.24	14.52 ± 5.42
PVA	1.51 ± 0.08	21.58 ± 5.39
PVA@MCC	2.87 ± 0.34	21.05 ± 2.23
PVA@HNT	1.97 ± 0.31	24.27 ± 4.00
PVA@HNT_SH	2.35 ± 0.17	21.94 ± 2.11
PVA@MCC_GPTMS_HNT	2.96 ± 0.29	27.59 ± 5.54
PVA@MCC_GPTMS_SH_HNT	5.12 ± 0.39	28.19 ± 1.40
PVA@MCC_CA_B-CD	2.10 ± 0.57	17.08 ± 2.80
PVA@Bch	2.06 ± 0.18	27.84 ± 4.89
PVA@Bch_NZVI	3.09 ± 0.47	14.70 ± 5.79

The obtained results show an increase in tensile strength and elongation at break, which can be attributed to the non-woven glass fiber support on which the nanofibers are stable bridged, and the effective stress transfer from the PVA polymeric matrix to the hybrid dopant agents, due to the good affinity and the interfacial bonding between them, thus resulting in a reduction in the polymer chain mobility [67].

These studies led us to conclude that incorporating MCC into polymeric blends bring to an improvement in tensile strength and elongation at break of some nanocomposites, may be due to hydrogen bonding interactions between various cellulosic derivatives and the polymeric matrix, which increased the crystallization rate of the final nanocomposites, thus resulting in increased nanofiber stiffness and mechanical properties [76]. Furthermore, the heat treatment may induce fiber fusion and molecular entanglement, increasing the stiffness of the final membranes [77]. As a result, these experimental findings show that all of the produced membranes feature improved mechanical properties, making them appropriate for use in filtering systems.

3.2.2.9 Gravity-driven filtration tests for the removal of MB and MO

Various gravity-driven filtering experiments were performed to correlate the functionalities of the generated doped nanofibers, as well as their removal capacity and selectivity towards anionic and cationic organic dyes. The model molecules MB and MO are used to explore the factors influencing the removal of two distinct types of organic dyes from loaded and thermally treated composite ENMs.

After conditioning with distilled water, a gravity-driven filtration test of a mixture of both MO and MB ($[MO] = [MB] = 2.5 \text{ mg}\cdot\text{L}^{-1}$; $V_{\text{tot}} = 50 \text{ mL}$) was performed in a dead-end filtration cell. Table 3.4 displays the pure water and MO/MB flux data of the PVA-based electrospun nanofiber composite membranes, together with those of the support given as reference.

These findings demonstrate that the inclusion of hydrophilic hydroxyl-rich PVA polymer improved the hydrophilicity of various membranes when compared to non-woven glass fiber support [42,78]. Despite this, PVA@MCC_GPTMS_HNT, PVA@MCC_GPTMS_SH_HNT, PVA@MCC_CA_B-CD, and PVA@Bch membranes demonstrate a reduction in water

permeability when compared to pristine PVA samples, which is due to the presence of strong hydrogen interactions and a cross-linked system via the functional additives used and PVA polymer, as described in the previous paragraph [73].

Table 3.4. Pure water and MO/MB flux of the PVA-based electrospun nanofiber composite membranes.

Name	Pure water flux/ $L \cdot m^{-2} \cdot h^{-1}$	MO/MB flux/ $L \cdot m^{-2} \cdot h^{-1}$
Non-woven glass fiber support	597.3	404.6
PVA	696.9	597.3
PVA@MCC	533.8	501.7
PVA@HNT	725.1	603.1
PVA@HNT_SH	678.0	570.2
PVA@MCC_GPTMS_HNT	137.8	133.7
PVA@MCC_GPTMS_SH_HNT	241.2	142.5
PVA@MCC_CA_B-CD	205.6	147.6
PVA@Bch	252.9	199.1
PVA@Bch_NZVI	426.7	313.6

All of the membranes demonstrate selectivity for the elimination of the cationic dye MB (Figure 3.15 a,b and Table 3.5).

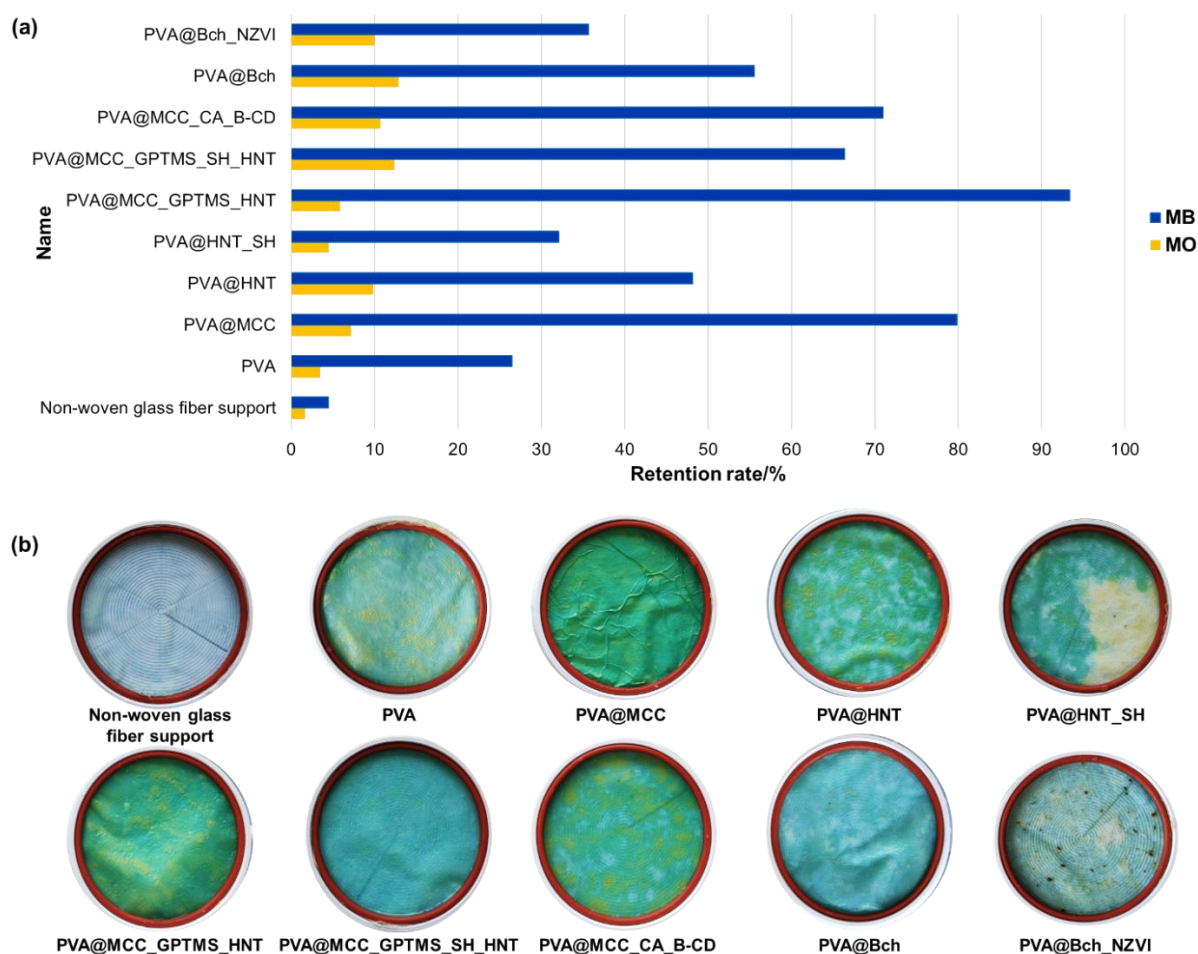


Figure 3.15. Retention rate percentage (a) for electrospun nanofiber composite membranes gravity driven dead-end filtration tests of a MO and MB mixed solution ($[MO] = [MB] = 5 \text{ mg} \cdot \text{L}^{-1}$; $V_{\text{tot}} = 50 \text{ mL}$), together with the final residue filtration membrane appearance (b).

PVA@MCC and PVA@MCC_GPTMS_HNT membranes have best performances, with retention rates of 93.4% and 79.9%, separation efficiencies of both dyes of 93.5% and 82.1%, and fluxes of 501.7 and 133.7 L·m⁻²·h⁻¹, respectively.

Due to the presence of many hydroxyl groups, electrostatic attraction and physical sorption are the primary sorption mechanisms between positively charged MB dye and negatively charged MCC-based dopant agents and the PVA membrane surface [79,80].

MCC_CA_B-CD additive exhibits the similar sorption behavior due to the carboxylic groups of the citric acid cross-linker and host-guest interactions between the cationic dye and β -cyclodextrins [36] (Figure 3.16).

Table 3.5. MB removal and separation efficiency achieved from gravity-driven filtration studies of MO/MB mixed solution.

Name	MB removal/%	Separation efficiency/%
Non-woven glass fiber support	4.5	49.7
PVA	26.5	58.2
PVA@MCC	79.9	82.1
PVA@HNT	48.2	64.8
PVA@HNT_SH	32.1	60.5
PVA@MCC_GPTMS_HNT	93.4	93.5
PVA@MCC_GPTMS_SH_HNT	66.4	72.1
PVA@MCC_CA_B-CD	71.0	75.4
PVA@Bch	55.6	64.7
PVA@Bch_NZVI	35.7	56.4

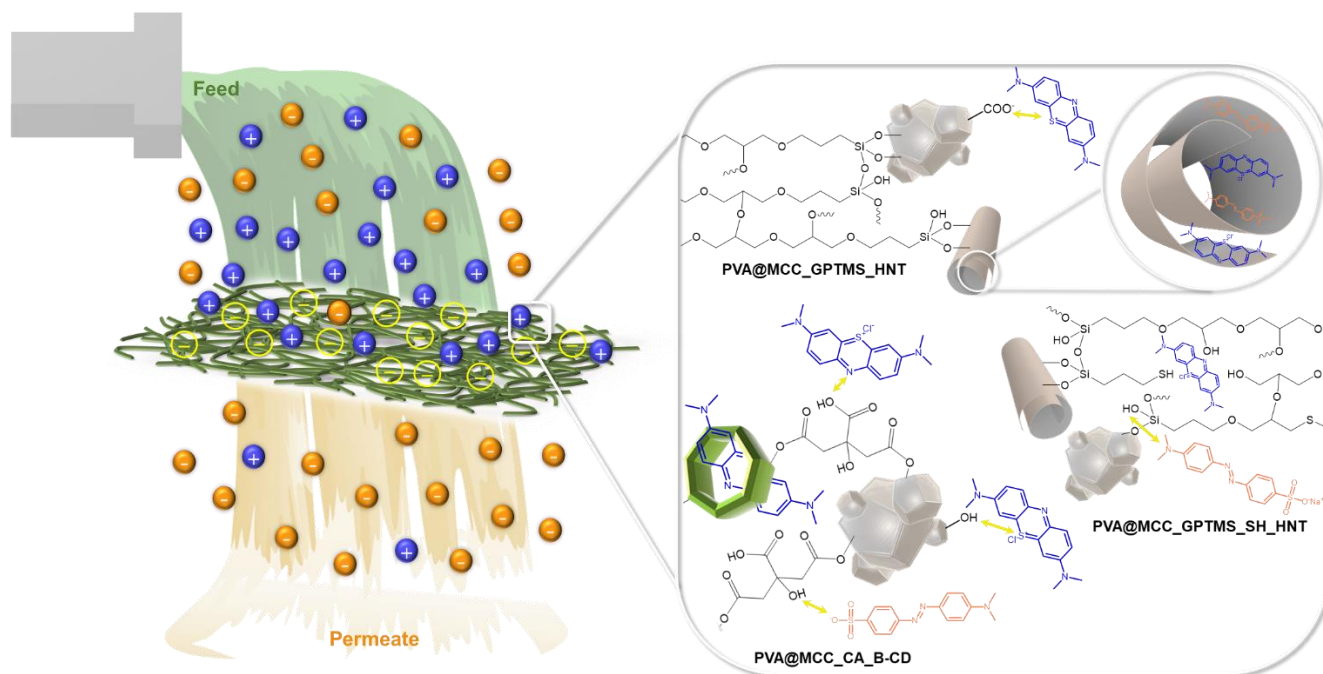


Figure 3.16. Illustration of the removal strategies involved in the filtration performances of the produced doped PVA-based electrospun nanofiber composite membranes.

Despite the strong sorption capabilities of HNT inorganic additives towards organic dyes [27], membranes doped with HNT and HNT_SH nanofillers display inferior performances

compared to MCC-based ones, demonstrating the effective contribution of MCC to the enhancement of filtering performances. The very porous and hydrophilic character of the PVA-based ENMs may also allow for greater interactions between the cationic and anionic MB and MO dyes and the functionalized nanofibers.

Figure 3.15 b shows a non-homogeneous distribution of dye on some membranes, resulting in a shade of color at the end of the filtration tests. The phenomenon may be related to the aggregation behavior of the dopant agents used during the electrospinning process as a result of hydrogen or electrostatic forces, as well as the high cross-linking density between the polymeric matrix and the functionally rich additives, which locally and not homogeneously may take place.

3.2.2.10 Biochar-supported nano-zero valent iron composite sorption study

The membranes based on nano zero-valent iron supported on Spanish broom derived biochar showed poor outcomes, owing to the need for optimization of the electrospinning settings and starting polymer formulation.

Batch sorptive removal studies with cationic MB dye as a model contaminant are provided for completeness and to demonstrate the sorption capabilities of this functional material (Figure 3.17 a–e).

The impact of the amount of Bch_NZVI on the elimination of MB was investigated (Figure 17 a,b). Bch_NZVI (5, 10, 20, 30, 50 mg) was poured into 20 mL of a 100 mg·L⁻¹ MB solution and allowed to sorb for 100 minutes.

The results showed that removal % rises with sorbent quantity, while sorption capacity reaches its maximum with 10 mg of Bch_NZVI at 117.87 mg·g⁻¹. The decrease in sorption capacity from 20 mg of sorbent is due to the presence of free accessible active sites for additional MB sorption, resulting in a relative drop in the number of MB molecules per unit of sorbent [81].

The impact of the initial MB concentration was investigated by immersing 20 mg of Bch_NZVI for 100 minutes in 20 mL MB solutions with concentrations of 5, 10, 50, 100, and 350 mg·L⁻¹. Figure 3.17 c,d shows how, at increasing MB concentrations, a removal percentage decrease owing to sorbent saturation and aggregation.

Furthermore, the sorption capacity increases with the growth of MB concentration. After 100 minutes of contact time with a 350 mg·L⁻¹ MB solution, a sorption capacity of 185.71 mg·g⁻¹ is reached.

Figure 3.17 e illustrates the impact of contact time between Bch_NZVI (20 mg) and 20 mL of a 100 mg·L⁻¹ MB solution. I removal percentage and sorption capacity rise with sorption time with a sigmoidal pattern. After 70 minutes of contact time, 99.8% MB removal is achieved with a sorption capacity of 98.66 mg·g⁻¹.

Internal diffusion resistance might cause a slower sorption rate in the beginning.

MB rapidly diffuses into the outer surface from the meso- and macro-pores of the Bch_NZVI nano sorbent in the first stage till saturation. Following that, MB molecules slowly penetrate the internal surface of Bch_NZVI meso-, macro-, and micro-cavities until equilibrium [37].

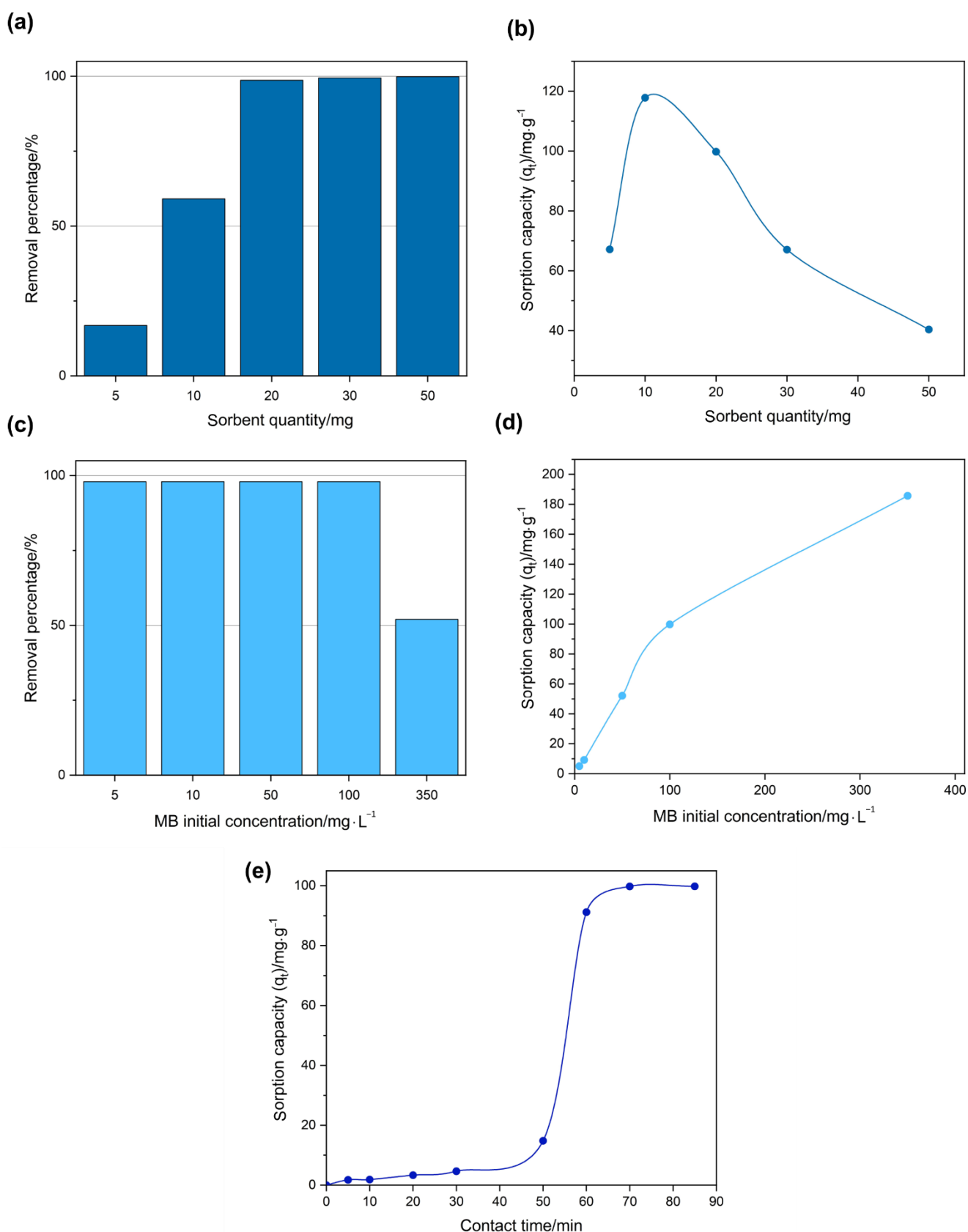


Figure 3.17. Plots related to the study of the impact of the amount of Bch_NZVI on the elimination of MB, in term of removal % (a,) and sorption capacity (b), of the initial MB concentration (c, d) and of contact time (e).

3.2.2.11 Biochar-supported nano-zero valent iron composite adsorption isotherms

Three non-linear adsorption isotherm models were examined to understand the sorbent/sorbate interactions and the conceptualization of the sorption system Bch_NZVI: the most often used Langmuir and Freundlich models, as well as the Temkin model. The Langmuir isotherm model describes the equilibrium between the sorbate and adsorbent systems, which involves the creation of a monolayer on the adsorption sites and is applicable to homogeneous surfaces. The Freundlich isotherm model, which assumes that multilayer sorption occurs on the surface of the adsorbent and that the sorption capacity increases continuously at high concentrations [82]. The Temkin isotherm model suggests a multilayer adsorption process and takes into account interactions between the sorbent and the adsorbate while discounting extremely low and extremely high concentration values [83].

According to the results reported in Figure 3.18 and Table 3.6, the Langmuir equation matches better the experimental adsorption data of the Bch_NZVI sorbent system with an R^2 of 0.9972. The results also agree well with the Freundlich isotherm calculations with an R^2 of 0.9822.

Table 3.6. Bch-NZVI adsorption equilibrium isotherm results.

Langmuir			Freundlich			Temkin		
$q_m/\text{mg}\cdot\text{g}^{-1}$	$K_L/\text{L}\cdot\text{mg}^{-1}$	R^2	$1/n$	$K_F/\text{L}\cdot\text{g}^{-1}$	R^2	B_T	$K_T/\text{L}\cdot\text{mg}^{-1}$	R^2
305.65	0.0044	0.9972	0.6343	4.5603	0.9822	41.4297	0.1394	0.9271

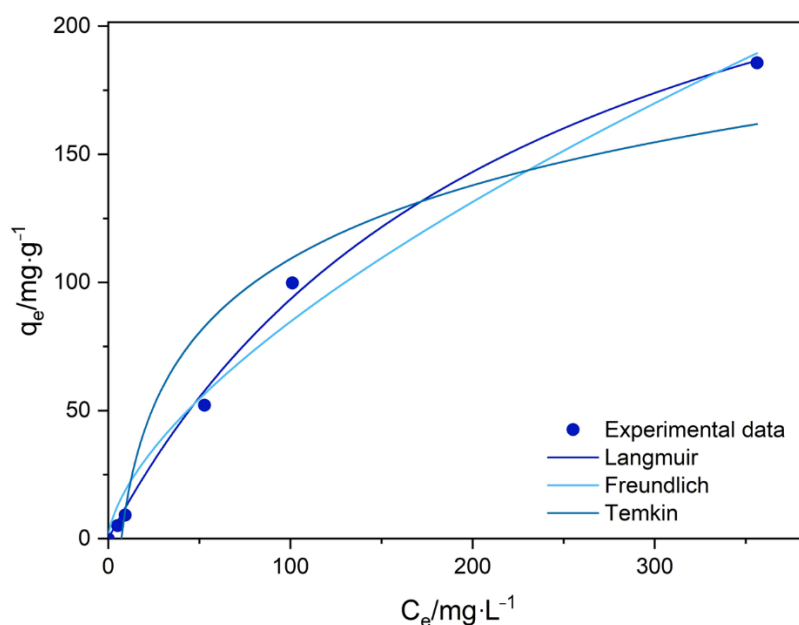


Figure 3.18. Bch-NZVI adsorption equilibrium isotherms together with different models fitting.

The determined high maximum sorption capacity (q_m) for MB in the developed Bch_NZVI composite is $305.65 \text{ mg}\cdot\text{g}^{-1}$ ($C_0 = 100 \text{ mg}\cdot\text{L}^{-1}$, $\text{pH} = 7$, $T = 298 \text{ K}$).

The value of $1/n$ from the Freundlich model reveals the nature of the process; $1/n$ values smaller than one are traditionally associated with excellent sorption [83]. Furthermore, $1/n > 1$ is

associated with a physical process, $1/n$ between 0.1 and 1 with a chemical process, and $1/n = 1$ with a linear process.

The value of $1/n$ is determined to be 0.6343, showing that the MB dye has strong chemical sorption on the Bch_NZVI surface [84,85].

Table 3.7 compares the sorption capacities of several biochar-based sorbents towards MB.

Table 3.7. The sorption capability of MB onto several reported biochar-based sorbents.

Type of sorbent	$q_m/\text{mg}\cdot\text{g}^{-1}$	Ref.
NZVI	208.33	[86]
Manganese-modified lignin biochar	248.96	[87]
Magnetic (Fe_3O_4) biochar composite	186.003	[88]
Hydrogen peroxide modified ball milled biochar	310	[89]
Banana pseudostem biochar	146.23	[90]
Reed biochar supported hydroxyapatite nanocomposite	21.1	[91]
Fe-sludge biochar	37.17	[85]
NZVI from Ricinus Communis Seeds Extract	61.37	[92]
Nano zero-valent iron supported-Spanish broom derived biochar	305.65	This work

The sorption behavior of MB onto Bch_NZVI may thus be characterized by the many main processes depicted in Figure 3.19.

Electrostatic and hydrogen bonding are the most prevalent interactions that may be exploited [93].

Furthermore, $n-\pi$ interaction via transfer of lone pairs of oxygen atoms from Bch_NZVI into the π orbital of the MB aromatic ring is feasible [94].

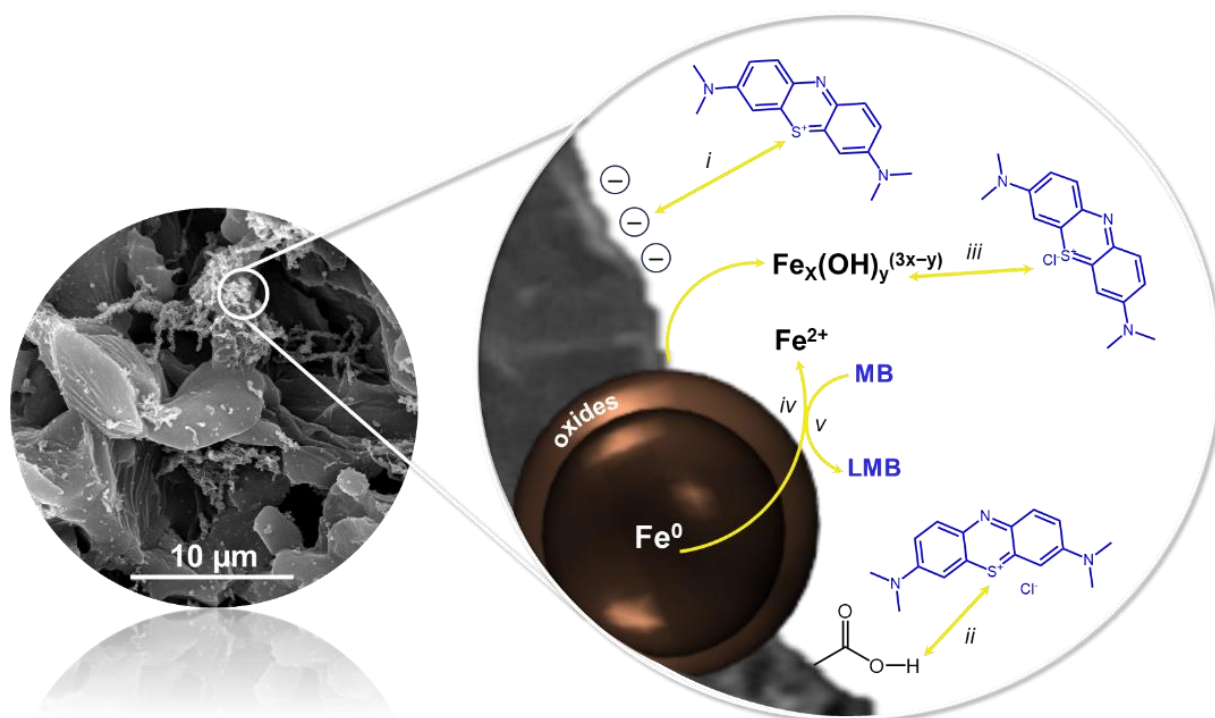


Figure 3.19. Illustration of the major processes involved in MB removal from Bch_NZVI sorbent (displayed in SEM micrograph) (i: hydrogen bonding, ii: electrostatic interactions, iii: flocculation, iv: oxidation, v: reduction).

Because of the nature of NZVI, the oxidation or corrosion of Fe^0 in the presence of water and oxygen during the synthetic process may result in the production of a unique core-shell structure.

As a result, the oxide shell that may form over the surface of Fe^0 might increase flocculation and complexation interactions with MB (see eq. 3) [95].



Another option is the reduction of MB to leucomethylene blue (a colourless derivative) by transferred electrons from Fe^0 (see equations 4 and 5) [96].



The magnetic characteristics of Bch_NZVI allow for its easy recovery using a magnet (Figure 3.20), in order to be subsequently regenerated and employed for another cycle of sorption.

Its recyclability cycles will be investigated in future tests.

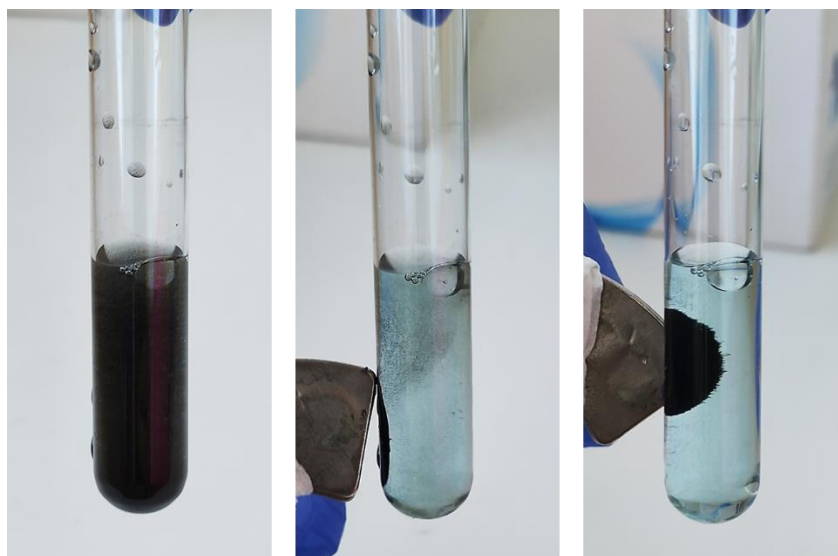


Figure 3.20. Bch_NZVI magnetic performances for simple recovery after MB sorption.

3.2.3. Conclusions

High-value-added products created from waste derived from renewable plant biomass have the potential to become a key element of modern advanced manufacturing, related in particular with (waste)water treatment and remediation. With this in mind, two derivatives of Spanish broom (*Spartium junceum*) were effectively produced. In particular, microcrystalline cellulose and biochar were developed from this natural source and modified through easy, eco-friendly and one-step synthetic methods using appropriate precursors and nanomaterials, i.e. (3-mercaptopropyl)trimethoxysilane, (3-glycidyloxypropyl)trimethoxy, citric acid, β -cyclodextrins and halloysite nanotubes, for the production of green hybrid and cross-linked systems showing specific and desired features.

ATR-FTIR spectroscopy and SEM microscopy were used to characterize the MCC, Bch, HNT_SH, MCC_GPTMS_HNT, MCC_GPTMS_SH_HNT, MCC_CA_B-CD, and BCH_NZVI derivatives. Electrospinning on non-woven glass microfiber support yields environmentally friendly water-based PVA composite nanofibers. SEM was used to morphologically characterize the membranes after heat treatment, and water swelling studies were used to investigate the hydrophilicity. Mechanical tensile characteristics showed improved results in terms of maximum stress and elongation at break value. All of the membranes were evaluated in a dead-end filtration cell with gravity-driven separation of a methylene blue and methyl orange mixed solution ($[MO] = [MB] = 2.5 \text{ mg}\cdot\text{L}^{-1}$; $V_{\text{tot}} = 50 \text{ mL}$), indicating selectivity for the removal of the cationic dye MB.

The top performing membranes are PVA@MCC and PVA@MCC_GPTMS_HNT, with retention rates of 93.4% and 79.9%, separation efficiencies of 93.5% and 82.1%, and fluxes of 501.7 and 133.7 $\text{L}\cdot\text{m}^{-2}\cdot\text{h}^{-1}$, respectively.

Biochar was functionalized with NZVI and examined in batch studies for MB removal. The Langmuir adsorption isotherm model, with a calculated high maximum sorption capacity (q_m) of 305.65 $\text{mg}\cdot\text{g}^{-1}$ for MB, better represents its sorption behavior. Because of the magnetic implemented characteristics of Bch_NZVI, it can be easily recovered and regenerated for another cycle of sorption. In future tests, this last characteristic will be thoroughly explored.

Finally, the extraction of two significant cellulose compounds derived from Spanish broom is reported. Various multi-functionalization procedures were used to create green functional additives used in the blending of PVA water-soluble polymer and the creation of new and sustainable membranes and sorbents. Their effective removal and separation capabilities of cationic dyes from water are proven, aiming to encourage the use of secondary-raw materials or biomasses for smart and sustainable environmental remediation technologies and either recyclable products.

References

1. Sfiligoj Smole, M.; Hribernik, S.; Kurečič, M.; Urbanek Krajnc, A.; Kreže, T.; Stana Kleinschek, K. Preparation of Cellulose Nanocrystals CNC from Nettle, Weeping Willow, Balm-Leaved Archangel, Lucerne and Spanish Broom BT - Surface Properties of Non-Conventional Cellulose Fibres. In: Sfiligoj Smole, M., Hribernik, S., Kurečič, M., Urbanek Krajnc, A., Kreže, T., Stana Kleinschek, K., Eds.; Springer International Publishing: Cham, 2019; pp. 73–86 ISBN 978-3-030-10407-8.
2. Arias Arias, F.E.; Beneduci, A.; Chidichimo, F.; Furia, E.; Straface, S. Study of the Adsorption of Mercury (II) on Lignocellulosic Materials under Static and Dynamic Conditions. *Chemosphere* **2017**, *180*, 11–23, doi:https://doi.org/10.1016/j.chemosphere.2017.03.137.
3. Gabriele, B.; Cerchiara, T.; Salerno, G.; Chidichimo, G.; Vetere, M.V.; Alampi, C.; Gallucci, M.C.; Conidi, C.; Cassano, A. A New Physical–Chemical Process for the Efficient Production of Cellulose Fibers from Spanish Broom (*Spartium Junceum* L.). *Bioresour. Technol.* **2010**, *101*, 724–729, doi:https://doi.org/10.1016/j.biortech.2009.08.014.
4. Juradin, S.; Jozić, D.; Netinger Grubeša, I.; Pamuković, A.; Čović, A.; Mihanović, F. Influence of Spanish Broom Fibre Treatment, Fibre Length, and Amount and Harvest Year on Reinforced Cement Mortar Quality. *Buildings* **2023**, *13*.
5. Juradin, S.; Boko, I.; Netinger Grubeša, I.; Jozić, D.; Mrakovčić, S. Influence of Different Treatment and Amount of Spanish Broom and Hemp Fibres on the Mechanical Properties of Reinforced Cement Mortars. *Constr. Build. Mater.* **2021**, *273*, 121702, doi:https://doi.org/10.1016/j.conbuildmat.2020.121702.
6. Juradin, S.; Vranješ, L.K.; Jozić, D.; Boko, I. Post-Fire Mechanical Properties of Concrete Reinforced with Spanish Broom Fibers. *J. Compos. Sci.* **2021**, *5*.
7. Abruzzo, A.; Cappadone, C.; Farruggia, G.; Luppi, B.; Bigucci, F.; Cerchiara, T. Glycyrrhetic Acid Liposomes and Hyalurosomes on Spanish Broom, Flax, and Hemp Dressings to Heal Skin Wounds. *Molecules* **2020**, *25*.
8. Cerchiara, T.; Giordani, B.; Melgoza, L.M.; Prata, C.; Parolin, C.; Dalena, F.; Abruzzo, A.; Bigucci, F.; Luppi, B.; Vitali, B. New Spanish Broom Dressings Based on Vitamin E and *Lactobacillus Plantarum* for Superficial Skin Wounds. *J. Drug Deliv. Sci. Technol.* **2020**, *56*, 101499, doi:https://doi.org/10.1016/j.jddst.2020.101499.
9. Tursi, A.; Gallizzi, V.; Olivito, F.; Algieri, V.; De Nino, A.; Maiuolo, L.; Beneduci, A. Selective and Efficient Mercury(II) Removal from Water by Adsorption with a Cellulose Citrate Biopolymer. *J. Hazard. Mater. Lett.* **2022**, *3*, 100060, doi:https://doi.org/10.1016/j.hazl.2022.100060.
10. Waheed, A.; Baig, N.; Ullah, N.; Falath, W. Removal of Hazardous Dyes, Toxic Metal Ions and Organic Pollutants from Wastewater by Using Porous Hyper-Cross-Linked Polymeric Materials: A Review of Recent Advances. *J. Environ. Manage.* **2021**, *287*, 112360, doi:https://doi.org/10.1016/j.jenvman.2021.112360.
11. Moradi, E.; Ebrahimzadeh, H.; Mehrani, Z.; Asgharinezhad, A.A. The Efficient Removal of Methylene Blue from Water Samples Using Three-Dimensional Poly (Vinyl Alcohol)/Starch Nanofiber Membrane as a Green Nanosorbent. *Environ. Sci. Pollut. Res.* **2019**, *26*, 35071–35081, doi:10.1007/s11356-019-06400-7.
12. Lan, D.; Zhu, H.; Zhang, J.; Li, S.; Chen, Q.; Wang, C.; Wu, T.; Xu, M. Adsorptive Removal of Organic Dyes via Porous Materials for Wastewater Treatment in Recent Decades: A Review on Species, Mechanisms and Perspectives. *Chemosphere* **2022**, *293*, 133464, doi:https://doi.org/10.1016/j.chemosphere.2021.133464.
13. Rando, G.; Sfameni, S.; Galletta, M.; Drommi, D.; Cappello, S.; Plutino, M.R. Functional Nanohybrids and Nanocomposites Development for the Removal of Environmental Pollutants and Bioremediation. *Mol.* **2022**, *27*.
14. Hassanisaadi, M.; Saberi Riseh, R.; Rabiei, A.; Varma, R.S.; Kennedy, J.F. Nano/Micro-Cellulose-Based Materials as Remarkable Sorbents for the Remediation of Agricultural Resources from Chemical Pollutants. *Int. J. Biol. Macromol.* **2023**, *246*, 125763, doi:https://doi.org/10.1016/j.ijbiomac.2023.125763.
15. Rol, F.; Belgacem, M.N.; Gandini, A.; Bras, J. Recent Advances in Surface-Modified Cellulose Nanofibrils. *Prog. Polym. Sci.* **2019**, *88*, 241–264, doi:https://doi.org/10.1016/j.progpolymsci.2018.09.002.
16. Infelise, L. Utilization of Post-Maceration Liquid from *Spartium Junceum* Enzymatic Retting in Biosynthesis of Bacterial Nanocellulose.
17. Rando, G.; Sfameni, S.; Plutino, M.R. Development of Functional Hybrid Polymers and Gel Materials for Sustainable Membrane-Based Water Treatment Technology: How to Combine Greener and Cleaner Approaches. *Gels* **2023**, *9*.
18. Chen, H.; Huang, M.; Liu, Y.; Meng, L.; Ma, M. Functionalized Electrospun Nanofiber Membranes for Water Treatment: A Review. *Sci. Total Environ.* **2020**, *739*, 139944, doi:https://doi.org/10.1016/j.scitotenv.2020.139944.
19. Fahimirad, S.; Fahimirad, Z.; Sillanpää, M. Efficient Removal of Water Bacteria and Viruses Using Electrospun Nanofibers. *Sci. Total Environ.* **2021**, *751*, 141673, doi:https://doi.org/10.1016/j.scitotenv.2020.141673.
20. Abd Halim, N.S.; Wirzal, M.D.H.; Hizam, S.M.; Bilad, M.R.; Nordin, N.A.H.M.; Sambudi, N.S.; Putra, Z.A.; Yusoff, A.R.M. Recent Development on Electrospun Nanofiber Membrane for Produced Water Treatment: A Review. *J. Environ. Chem. Eng.* **2021**, *9*, 104613, doi:https://doi.org/10.1016/j.jece.2020.104613.
21. Ahmed, F.E.; Lalia, B.S.; Hashaikeh, R. A Review on Electrospinning for Membrane Fabrication: Challenges and Applications. *Desalination* **2015**, *356*, 15–30, doi:https://doi.org/10.1016/j.desal.2014.09.033.
22. Abdul Khalil, H.P.S.; Bhat, A.H.; Ireana Yusra, A.F. Green Composites from Sustainable Cellulose Nanofibrils: A Review. *Carbohydr. Polym.* **2012**, *87*, 963–979, doi:https://doi.org/10.1016/j.carbpol.2011.08.078.
23. Ghasemi, S.; Tajvidi, M.; Bousfield, D.W.; Gardner, D.J. Reinforcement of Natural Fiber Yarns by Cellulose Nanomaterials: A Multi-Scale Study. *Ind. Crops Prod.* **2018**, *111*, 471–481, doi:https://doi.org/10.1016/j.indcrop.2017.11.016.
24. Jia, B.; Li, Y.; Yang, B.; Xiao, D.; Zhang, S.; Rajulu, A.V.; Kondo, T.; Zhang, L.; Zhou, J. Effect of Microcrystal Cellulose and Cellulose Whisker on Biocompatibility of Cellulose-Based Electrospun Scaffolds. *Cellulose* **2013**, *20*, 1911–1923, doi:10.1007/s10570-013-9952-0.
25. Soon, C.Y.; Rahman, N.A.; Tee, Y.B.; Talib, R.A.; Tan, C.H.; Abdan, K.; Chan, E.W.C. Electrospun Biocomposite:

- Nanocellulose and Chitosan Entrapped within a Poly(Hydroxyalkanoate) Matrix for Congo Red Removal. *J. Mater. Res. Technol.* **2019**, *8*, 5091–5102, doi:https://doi.org/10.1016/j.jmrt.2019.08.030.
26. Koriem, O.A.; Kamel, A.M.; Shaaban, W.; Elkady, M.F. Enhancement of Dye Separation Performance of Eco-Friendly Cellulose Acetate-Based Membranes. *Sustainability* **2022**, *14*.
 27. Danyliuk, N.; Tomaszewska, J.; Tatarchuk, T. Halloysite Nanotubes and Halloysite-Based Composites for Environmental and Biomedical Applications. *J. Mol. Liq.* **2020**, *309*, 113077, doi:https://doi.org/10.1016/j.molliq.2020.113077.
 28. Massaro, M.; Noto, R.; Riela, S. Past, Present and Future Perspectives on Halloysite Clay Minerals. *Molecules* **2020**, *25*.
 29. Li, L.; Wang, F.; Lv, Y.; Liu, J.; Zhang, D.; Shao, Z. Halloysite Nanotubes and Fe₃O₄ Nanoparticles Enhanced Adsorption Removal of Heavy Metal Using Electrospun Membranes. *Appl. Clay Sci.* **2018**, *161*, 225–234, doi:https://doi.org/10.1016/j.clay.2018.04.002.
 30. Kumari, P.; Singh, P.; Singhal, A.; A. Cyclodextrin-Based Nanostructured Materials for Sustainable Water Remediation Applications. *Environ. Sci. Pollut. Res.* **2020**, *27*, 32432–32448, doi:10.1007/s11356-020-09519-0.
 31. Liu, Z.; Ye, L.; Xi, J.; Wang, J.; Feng, Z. Cyclodextrin Polymers: Structure, Synthesis, and Use as Drug Carriers. *Prog. Polym. Sci.* **2021**, *118*, 101408, doi:https://doi.org/10.1016/j.progpolymsci.2021.101408.
 32. Matencio, A.; Navarro-Orcajada, S.; García-Carmona, F.; López-Nicolás, J.M. Applications of Cyclodextrins in Food Science. A Review. *Trends Food Sci. Technol.* **2020**, *104*, 132–143, doi:https://doi.org/10.1016/j.tifs.2020.08.009.
 33. Loftsson, T.; Duchêne, D. Cyclodextrins and Their Pharmaceutical Applications. *Int. J. Pharm.* **2007**, *329*, 1–11, doi:https://doi.org/10.1016/j.ijpharm.2006.10.044.
 34. Sharma, N.; Baldi, A. Exploring Versatile Applications of Cyclodextrins: An Overview. *Drug Deliv.* **2016**, *23*, 729–747, doi:10.3109/10717544.2014.938839.
 35. Zhao, R.; Wang, Y.; Li, X.; Sun, B.; Wang, C. Synthesis of β -Cyclodextrin-Based Electrospun Nanofiber Membranes for Highly Efficient Adsorption and Separation of Methylene Blue. *ACS Appl. Mater. Interfaces* **2015**, *7*, 26649–26657, doi:10.1021/acsami.5b08403.
 36. Zhao, R.; Wang, Y.; Li, X.; Sun, B.; Jiang, Z.; Wang, C. Water-Insoluble Sericin/ β -Cyclodextrin/PVA Composite Electrospun Nanofibers as Effective Adsorbents towards Methylene Blue. *Colloids Surfaces B Biointerfaces* **2015**, *136*, 375–382, doi:https://doi.org/10.1016/j.colsurfb.2015.09.038.
 37. Wu, Y.; Zhong, J.; Liu, B. Effective Removal of Methylene Blue with Zero-Valent Iron/Tea Residual Biochar Composite: Performance and Mechanism. *Bioresour. Technol.* **2023**, *371*, 128592, doi:https://doi.org/10.1016/j.biortech.2023.128592.
 38. Taheran, M.; Kumar, P.; Naghdi, M.; Brar, S.K.; Knystautas, E.J.; Verma, M.; Surampalli, R.Y. Development of an Advanced Multifunctional Portable Water Purifier. *Nanotechnol. Environ. Eng.* **2019**, *4*, 7, doi:10.1007/s41204-019-0054-6.
 39. Tosco, T.; Petrangeli Papini, M.; Cruz Viggi, C.; Sethi, R. Nanoscale Zerovalent Iron Particles for Groundwater Remediation: A Review. *J. Clean. Prod.* **2014**, *77*, 10–21, doi:https://doi.org/10.1016/j.jclepro.2013.12.026.
 40. Ren, J.; Woo, Y.C.; Yao, M.; Lim, S.; Tijjng, L.D.; Shon, H.K. Nanoscale Zero-Valent Iron (NZVI) Immobilization onto Graphene Oxide (GO)-Incorporated Electrospun Polyvinylidene Fluoride (PVDF) Nanofiber Membrane for Groundwater Remediation via Gravity-Driven Membrane Filtration. *Sci. Total Environ.* **2019**, *688*, 787–796, doi:https://doi.org/10.1016/j.scitotenv.2019.05.393.
 41. Hwang, Y.; Lee, Y.-C.; Mines, P.D.; Huh, Y.S.; Andersen, H.R. Nanoscale Zero-Valent Iron (NZVI) Synthesis in a Mg-Aminoclay Solution Exhibits Increased Stability and Reactivity for Reductive Decontamination. *Appl. Catal. B Environ.* **2014**, *147*, 748–755, doi:https://doi.org/10.1016/j.apcatb.2013.10.017.
 42. Li, M.; Li, J.; Zhou, M.; Xian, Y.; Shui, Y.; Wu, M.; Yao, Y. Super-Hydrophilic Electrospun PVDF/PVA-Blended Nanofiber Membrane for Microfiltration with Ultrahigh Water Flux. *J. Appl. Polym. Sci.* **2020**, *137*, 48416, doi:https://doi.org/10.1002/app.48416.
 43. Tarchoun, A.F.; Trache, D.; Klapötke, T.M.; Derradji, M.; Bessa, W. Ecofriendly Isolation and Characterization of Microcrystalline Cellulose from Giant Reed Using Various Acidic Media. *Cellulose* **2019**, *26*, 7635–7651, doi:10.1007/s10570-019-02672-x.
 44. Beroual, M.; Boumazza, L.; Mehelli, O.; Trache, D.; Tarchoun, A.F.; Khimeche, K. Physicochemical Properties and Thermal Stability of Microcrystalline Cellulose Isolated from Esparto Grass Using Different Delignification Approaches. *J. Polym. Environ.* **2021**, *29*, 130–142, doi:10.1007/s10924-020-01858-w.
 45. Kian, L.K.; Jawaid, M.; Ariffin, H.; Alothman, O.Y. Isolation and Characterization of Microcrystalline Cellulose from Roselle Fibers. *Int. J. Biol. Macromol.* **2017**, *103*, 931–940, doi:https://doi.org/10.1016/j.ijbiomac.2017.05.135.
 46. Flauzino Neto, W.P.; Silvério, H.A.; Dantas, N.O.; Pasquini, D. Extraction and Characterization of Cellulose Nanocrystals from Agro-Industrial Residue – Soy Hulls. *Ind. Crops Prod.* **2013**, *42*, 480–488, doi:https://doi.org/10.1016/j.indcrop.2012.06.041.
 47. El Achaby, M.; Fayoud, N.; Figueroa-Espinoza, M.C.; Ben youcef, H.; Aboulkas, A. New Highly Hydrated Cellulose Microfibrils with a Tendril Helical Morphology Extracted from Agro-Waste Material: Application to Removal of Dyes from Waste Water. *RSC Adv.* **2018**, *8*, 5212–5224, doi:10.1039/C7RA10239A.
 48. Ilyas, R.A.; Sapuan, S.M.; Ishak, M.R. Isolation and Characterization of Microcrystalline Cellulose from Sugar Palm Fibres (*Arenga Pinnata*). *Carbohydr. Polym.* **2018**, *181*, 1038–1051, doi:https://doi.org/10.1016/j.carbpol.2017.11.045.
 49. Hussin, M.H.; Pohan, N.A.; Garba, Z.N.; Kassim, M.J.; Rahim, A.A.; Brosse, N.; Yemloul, M.; Fazita, M.R.N.; Haafiz, M.K.M. Physicochemical of Microcrystalline Cellulose from Oil Palm Fronds as Potential Methylene Blue Adsorbents. *Int. J. Biol. Macromol.* **2016**, *92*, 11–19, doi:https://doi.org/10.1016/j.ijbiomac.2016.06.094.
 50. Romita, R.; Rizzi, V.; Gubitosa, J.; Gabaldón, J.A.; Fortea, M.I.; Gómez-Morte, T.; Gómez-López, V.M.; Fini, P.; Cosma, P. Cyclodextrin Polymers and Salts: An Eco-Friendly Combination to Modulate the Removal of Sulfamethoxazole from Water and Its Release. *Chemosphere* **2021**, *283*, 131238, doi:https://doi.org/10.1016/j.chemosphere.2021.131238.

51. Shaheen, S.M.; Mosa, A.; Natasha; Abdelrahman, H.; Niazi, N.K.; Antoniadis, V.; Shahid, M.; Song, H.; Kwon, E.E.; Rinklebe, J. Removal of Toxic Elements from Aqueous Environments Using Nano Zero-Valent Iron- and Iron Oxide-Modified Biochar: A Review. *Biochar* **2022**, *4*, 24, doi:10.1007/s42773-022-00149-y.
52. Zhao, B.; O'Connor, D.; Zhang, J.; Peng, T.; Shen, Z.; Tsang, D.C.W.; Hou, D. Effect of Pyrolysis Temperature, Heating Rate, and Residence Time on Rapeseed Stem Derived Biochar. *J. Clean. Prod.* **2018**, *174*, 977–987, doi:https://doi.org/10.1016/j.jclepro.2017.11.013.
53. Hasan Khan Tushar, M.S.; Mahinpey, N.; Khan, A.; Ibrahim, H.; Kumar, P.; Idem, R. Production, Characterization and Reactivity Studies of Chars Produced by the Isothermal Pyrolysis of Flax Straw. *Biomass and Bioenergy* **2012**, *37*, 97–105, doi:https://doi.org/10.1016/j.biombioe.2011.12.027.
54. Yildirim, G.M.; Bayrak, B. The Synthesis of Biochar-Supported Nano Zero-Valent Iron Composite and Its Adsorption Performance in Removal of Malachite Green. *Biomass Convers. Biorefinery* **2022**, *12*, 4785–4797, doi:10.1007/s13399-021-01501-1.
55. Wu, H.; Wei, W.; Xu, C.; Meng, Y.; Bai, W.; Yang, W.; Lin, A. Polyethylene Glycol-Stabilized Nano Zero-Valent Iron Supported by Biochar for Highly Efficient Removal of Cr(VI). *Ecotoxicol. Environ. Saf.* **2020**, *188*, 109902, doi:https://doi.org/10.1016/j.ecoenv.2019.109902.
56. Patterson, G.D.; McManus, J.D.; McSpedon, D.; Nazneen, S.; Wood, D.F.; Williams, T.; Hart-Cooper, W.M.; Orts, W.J. Garbage to Nanocellulose: Quantitative Isolation and Characterization of Steam-Treated Carboxymethyl Hemicellulose Nanofibrils from Municipal Solid Waste. *ACS Sustain. Chem. Eng.* **2023**, *11*, 2727–2736, doi:10.1021/acssuschemeng.2c05236.
57. Krishnaiah, P.; Ratnam, C.T.; Manickam, S. Development of Silane Grafted Halloysite Nanotube Reinforced Polylactide Nanocomposites for the Enhancement of Mechanical, Thermal and Dynamic-Mechanical Properties. *Appl. Clay Sci.* **2017**, *135*, 583–595, doi:https://doi.org/10.1016/j.clay.2016.10.046.
58. Yah, W.O.; Takahara, A.; Lvov, Y.M. Selective Modification of Halloysite Lumen with Octadecylphosphonic Acid: New Inorganic Tubular Micelle. *J. Am. Chem. Soc.* **2012**, *134*, 1853–1859, doi:10.1021/ja210258y.
59. Li, X.; Nikiforow, I.; Pohl, K.; Adams, J.; Johannsmann, D. Polyurethane Coatings Reinforced by Halloysite Nanotubes. *Coatings* **2013**, *3*, 16–25.
60. Wu, W.; Yang, M.; Feng, Q.; McGrouther, K.; Wang, H.; Lu, H.; Chen, Y. Chemical Characterization of Rice Straw-Derived Biochar for Soil Amendment. *Biomass and Bioenergy* **2012**, *47*, 268–276, doi:https://doi.org/10.1016/j.biombioe.2012.09.034.
61. Zhu, J.; Wang, F.; Li, D.; Zhai, J.; Liu, P.; Zhang, W.; Li, Y. Amine Functionalized Graphene Oxide Stabilized Pickering Emulsion for Highly Efficient Knoevenagel Condensation in Aqueous Medium. *Catal. Letters* **2020**, *150*, 1909–1922, doi:10.1007/s10562-020-03103-4.
62. Li, C.; Zhao, Y.; Zhu, T.; Li, Y.; Ruan, J.; Li, G. Effective Solvent-Free Oxidation of Cyclohexene to Allylic Products with Oxygen by Mesoporous Etched Halloysite Nanotube Supported Co₂+. *RSC Adv.* **2018**, *8*, 14870–14878, doi:10.1039/C7RA11245A.
63. Nohra, B.; Candy, L.; Blanco, J.-F.; Raoul, Y.; Mouloungui, Z. Synthesis of High-Molecular-Weight Multifunctional Glycerol Polyhydroxyurethanes PHUs. *Mol.* **2016**, *21*.
64. Senkevich, J.J.; Mitchell, C.J.; Yang, G.-R.; Lu, T.-M. Surface Chemistry of Mercaptan and Growth of Pyridine Short-Chain Alkoxy Silane Molecular Layers. *Langmuir* **2002**, *18*, 1587–1594, doi:10.1021/la01097of.
65. Xiu, H.; Ma, F.; Li, J.; Zhao, X.; Liu, L.; Feng, P.; Yang, X.; Zhang, X.; Kozliak, E.; Ji, Y. Using Fractal Dimension and Shape Factors to Characterize the Microcrystalline Cellulose (MCC) Particle Morphology and Powder Flowability. *Powder Technol.* **2020**, *364*, 241–250, doi:https://doi.org/10.1016/j.powtec.2020.01.045.
66. Beroual, M.; Trache, D.; Mehelli, O.; Boumaza, L.; Tarchoun, A.F.; Derradji, M.; Khimeche, K. Effect of the Delignification Process on the Physicochemical Properties and Thermal Stability of Microcrystalline Cellulose Extracted from Date Palm Fronds. *Waste and Biomass Valorization* **2021**, *12*, 2779–2793, doi:10.1007/s12649-020-01198-9.
67. Zhang, Y.; Meng, R.; Zhou, J.; Liu, X.; Guo, W. Halloysite Nanotubes-Decorated Electrospun Biobased Polyamide Scaffolds for Tissue Engineering Applications. *Colloids Surfaces A Physicochem. Eng. Asp.* **2022**, *648*, 129378, doi:https://doi.org/10.1016/j.colsurfa.2022.129378.
68. Massaro, M.; Colletti, C.G.; Lazzara, G.; Guernelli, S.; Noto, R.; Riela, S. Synthesis and Characterization of Halloysite-Cyclodextrin Nanosponges for Enhanced Dyes Adsorption. *ACS Sustain. Chem. Eng.* **2017**, *5*, 3346–3352, doi:10.1021/acssuschemeng.6b03191.
69. MirafTAB, M.; Saifullah, A.N.; Çay, A. Physical Stabilisation of Electrospun Poly(Vinyl Alcohol) Nanofibres: Comparative Study on Methanol and Heat-Based Crosslinking. *J. Mater. Sci.* **2015**, *50*, 1943–1957, doi:10.1007/s10853-014-8759-1.
70. Lee, J.S.; Choi, K.H.; Ghim, H. Do; Kim, S.S.; Chun, D.H.; Kim, H.Y.; Lyoo, W.S. Role of Molecular Weight of Atactic Poly(Vinyl Alcohol) (PVA) in the Structure and Properties of PVA Nanofabric Prepared by Electrospinning. *J. Appl. Polym. Sci.* **2004**, *93*, 1638–1646, doi:10.1002/app.20602.
71. Wu, X.-Q.; Mirza, N.R.; Huang, Z.; Zhang, J.; Zheng, Y.-M.; Xiang, J.; Xie, Z. Enhanced Desalination Performance of Aluminium Fumarate MOF-Incorporated Electrospun Nanofiber Membrane with Bead-on-String Structure for Membrane Distillation. *Desalination* **2021**, *520*, 115338, doi:https://doi.org/10.1016/j.desal.2021.115338.
72. Hoang, B.N.; Nguyen, T.T.; Bui, Q.P.T.; Bach, L.G.; Vo, D.-V.N.; Trinh, C.D.; Bui, X.-T.; Nguyen, T.D. Enhanced Selective Adsorption of Cation Organic Dyes on Polyvinyl Alcohol/Agar/Maltodextrin Water-Resistance Biomembrane. *J. Appl. Polym. Sci.* **2020**, *137*, 48904, doi:https://doi.org/10.1002/app.48904.
73. Azlin, M.N.M.; Sapuan, S.M.; Zuhri, M.Y.M.; Zainudin, E.S. Mechanical, Morphological and Thermal Properties of Woven Polyester Fiber Reinforced Poly(lactic Acid) (PLA) Composites. *Fibers Polym.* **2022**, *23*, 234–242, doi:10.1007/s12221-021-0139-2.

74. Karahan Toprakci, H.A.; Turgut, A.; Toprakci, O. Nailed-Bat like Halloysite Nanotube Filled Polyamide 6,6 Nanofibers by Electrospinning. *Polym. Technol. Mater.* **2021**, *60*, 522–535, doi:10.1080/25740881.2020.1819313.
75. HMTShirazi, R.; Mohammadi, T.; Asadi, A.A. Incorporation of Amine-Grafted Halloysite Nanotube to Electrospun Nanofibrous Membranes of Chitosan/Poly (Vinyl Alcohol) for Cd (II) and Pb(II) Removal. *Appl. Clay Sci.* **2022**, *220*, 106460, doi:https://doi.org/10.1016/j.clay.2022.106460.
76. Zhu, H.; Xie, Y. Hydrogen-Bonding Interaction Promoted Supercapacitance of Polylactic Acid-Graphene-Microcrystalline Cellulose/Polyaniline Nanofiber. *Mater. Today Chem.* **2023**, *30*, 101535, doi:https://doi.org/10.1016/j.mtchem.2023.101535.
77. Sanders, J.E.; Han, Y.; Rushing, T.S.; Gardner, D.J. Electrospinning of Cellulose Nanocrystal-Filled Poly (Vinyl Alcohol) Solutions: Material Property Assessment. *Nanomaterials* **2019**, *9*.
78. Huang, Z.; Yang, G.; Zhang, J.; Gray, S.; Xie, Z. Dual-Layer Membranes with a Thin Film Hydrophilic MOF/PVA Nanocomposite for Enhanced Antiwetting Property in Membrane Distillation. *Desalination* **2021**, *518*, 115268, doi:https://doi.org/10.1016/j.desal.2021.115268.
79. Tan, K.B.; Abdullah, A.Z.; Horri, B.A.; Salamatinia, B. Adsorption Mechanism of Microcrystalline Cellulose as Green Adsorbent for the Removal of Cationic Methylene Blue Dye. *J. Chem. Soc. Pakistan* **2016**, *38*.
80. Xiao, M.; Chery, J.; Frey, M.W. Functionalization of Electrospun Poly(Vinyl Alcohol) (PVA) Nanofiber Membranes for Selective Chemical Capture. *ACS Appl. Nano Mater.* **2018**, *1*, 722–729, doi:10.1021/acsanm.7b00180.
81. Zhang, P.; O'Connor, D.; Wang, Y.; Jiang, L.; Xia, T.; Wang, L.; Tsang, D.C.W.; Ok, Y.S.; Hou, D. A Green Biochar/Iron Oxide Composite for Methylene Blue Removal. *J. Hazard. Mater.* **2020**, *384*, 121286, doi:https://doi.org/10.1016/j.jhazmat.2019.121286.
82. Yu, K.L.; Lee, X.J.; Ong, H.C.; Chen, W.-H.; Chang, J.-S.; Lin, C.-S.; Show, P.L.; Ling, T.C. Adsorptive Removal of Cationic Methylene Blue and Anionic Congo Red Dyes Using Wet-Torrefied Microalgal Biochar: Equilibrium, Kinetic and Mechanism Modeling. *Environ. Pollut.* **2021**, *272*, 115986, doi:https://doi.org/10.1016/j.envpol.2020.115986.
83. Başar, C.A. Applicability of the Various Adsorption Models of Three Dyes Adsorption onto Activated Carbon Prepared Waste Apricot. *J. Hazard. Mater.* **2006**, *135*, 232–241, doi:https://doi.org/10.1016/j.jhazmat.2005.11.055.
84. Pandey, S.; Son, N.; Kang, M. Synergistic Sorption Performance of Karaya Gum Crosslink Poly(Acrylamide-Co-Acrylonitrile) @ Metal Nanoparticle for Organic Pollutants. *Int. J. Biol. Macromol.* **2022**, *210*, 300–314, doi:https://doi.org/10.1016/j.ijbiomac.2022.05.019.
85. Ahmad, A.; Singh, A.P.; Khan, N.; Chowdhary, P.; Giri, B.S.; Varjani, S.; Chaturvedi, P. Bio-Composite of Fe-Sludge Biochar Immobilized with Bacillus Sp. in Packed Column for Bio-Adsorption of Methylene Blue in a Hybrid Treatment System: Isotherm and Kinetic Evaluation. *Environ. Technol. Innov.* **2021**, *23*, 101734, doi:https://doi.org/10.1016/j.eti.2021.101734.
86. Arabi, S.; Sohrabi, M.R. Removal of Methylene Blue, a Basic Dye, from Aqueous Solutions Using Nano-Zerovalent Iron. *Water Sci. Technol. a J. Int. Assoc. Water Pollut. Res.* **2014**, *70*, 24–31, doi:10.2166/wst.2014.189.
87. Liu, X.-J.; Li, M.-F.; Singh, S.K. Manganese-Modified Lignin Biochar as Adsorbent for Removal of Methylene Blue. *J. Mater. Res. Technol.* **2021**, *12*, 1434–1445, doi:https://doi.org/10.1016/j.jmrt.2021.03.076.
88. Zeng, H.; Qi, W.; Zhai, L.; Wang, F.; Zhang, J.; Li, D. Magnetic Biochar Synthesized with Waterworks Sludge and Sewage Sludge and Its Potential for Methylene Blue Removal. *J. Environ. Chem. Eng.* **2021**, *9*, 105951, doi:https://doi.org/10.1016/j.jece.2021.105951.
89. Zhang, Y.; Zheng, Y.; Yang, Y.; Huang, J.; Zimmerman, A.R.; Chen, H.; Hu, X.; Gao, B. Mechanisms and Adsorption Capacities of Hydrogen Peroxide Modified Ball Milled Biochar for the Removal of Methylene Blue from Aqueous Solutions. *Bioresour. Technol.* **2021**, *337*, 125432, doi:https://doi.org/10.1016/j.biortech.2021.125432.
90. Liu, S.; Li, J.; Xu, S.; Wang, M.; Zhang, Y.; Xue, X. A Modified Method for Enhancing Adsorption Capability of Banana Pseudostem Biochar towards Methylene Blue at Low Temperature. *Bioresour. Technol.* **2019**, *282*, 48–55, doi:https://doi.org/10.1016/j.biortech.2019.02.092.
91. Li, Y.; Zhang, Y.; Zhang, Y.; Wang, G.; Li, S.; Han, R.; Wei, W. Reed Biochar Supported Hydroxyapatite Nanocomposite: Characterization and Reactivity for Methylene Blue Removal from Aqueous Media. *J. Mol. Liq.* **2018**, *263*, 53–63, doi:https://doi.org/10.1016/j.molliq.2018.04.132.
92. Abdelfatah, A.M.; Fawzy, M.; Eltaweil, A.S.; El-Khouly, M.E. Green Synthesis of Nano-Zero-Valent Iron Using Ricinus Communis Seeds Extract: Characterization and Application in the Treatment of Methylene Blue-Polluted Water. *ACS Omega* **2021**, *6*, 25397–25411, doi:10.1021/acsomega.1c03355.
93. Abd El-Monaem, E.M.; Omer, A.M.; El-Subruiti, G.M.; Mohy-Eldin, M.S.; Eltaweil, A.S. Zero-Valent Iron Supported-Lemon Derived Biochar for Ultra-Fast Adsorption of Methylene Blue. *Biomass Convers. Biorefinery* **2022**, doi:10.1007/s13399-022-02362-y.
94. Fan, S.; Wang, Y.; Wang, Z.; Tang, J.; Tang, J.; Li, X. Removal of Methylene Blue from Aqueous Solution by Sewage Sludge-Derived Biochar: Adsorption Kinetics, Equilibrium, Thermodynamics and Mechanism. *J. Environ. Chem. Eng.* **2017**, *5*, 601–611, doi:10.1016/j.jece.2016.12.019.
95. Zhu, K.; Chen, C. Chapter 6 - Application of NZVI and Its Composites into the Treatment of Toxic/Radioactive Metal Ions. In *Emerging Natural and Tailored Nanomaterials for Radioactive Waste Treatment and Environmental Remediation*; Chen, C.B.T.-I.S. and T., Ed.; Elsevier, 2019; Vol. 29, pp. 281–330 ISBN 1573-4285.
96. Trinh, B.-S.; Le, P.T.K.; Werner, D.; Phuong, N.H.; Luu, T.L. Rice Husk Biochars Modified with Magnetized Iron Oxides and Nano Zero Valent Iron for Decolorization of Dyeing Wastewater. *Processes* **2019**, *7*.

CHAPTER 4

SMART POLYMERIC BLENDS AND BEADS AS INNOVATIVE ADSORBENT SYSTEMS

The Fourth Chapter describes the importance of blending or functionalizing polymers for obtaining smart and functional systems to be applied for environmental remediation and water purification. In particular, the stimuli-responsive poly[2-(dimethylamino)ethylmethacrylate] (PDMAEMA) polymer and the class of pillararene macrocycles are described. The characteristics of these systems are of key importance for the design and development of new polyether sulfone blends reported in this research work. In particular, the synergic combination of polyether sulfone, with a new innovative smart polymer combining the responsiveness of PDMAEMA polymer and the host-guest properties of the covalently linked pillar[5]arene macrocycles, is described. The developed systems in the form of beads have been tested towards the selective adsorption of two model organic dyes, and adsorption kinetics and performances are shown.

4.1. Smart polymers and systems for water purification

4.1.1. Polyether sulfone based blends

The preservation and improvement of adequate water sources are becoming more crucial as global population development and associated anthropological activities are expanding. Unfortunately, the so-called “emerging contaminants” (such organic dyes, pharmaceuticals, etc.) that are now widely utilised in the textile, leather, paper, plastic, and cosmetic sectors are still not entirely eliminated by conventional techniques of wastewater treatment [1,2]. Due to their chemical persistence and toxicity, they really pose a concerning hazard to human health, which is why sustainable and innovative ways of waste water cleaning are now being researched [3–5].

Polyethersulfone (PES) is frequently utilised as an embedding polymer for the development of nano- and ultrafiltration membranes in the water purification, because of its good mechanical qualities and thermal and chemical stability [6]. Additionally, the development of functional PES-based systems by incorporation of additional polymers, cross-linkers, or nanofillers results in an enhancement of PES hydrophilicity, porosity, surface characteristics, and adsorption capabilities [7]. An innovative PES nanofiltration membrane with a rejection rate of more than 83% for the Lanazol blue 3R dye was produced by Amiri et al. using a combination of polyvinyl alcohol, graphene oxide, and sodium alginate [8].

In a different study, Athira et al. concentrated on the effective sulfonation of polyethersulfone polymer to produce sulfonated-polyethersulfone (SPES), as well as on the preparation of its blends with PES to develop cellulose acetate CA/PES blend membranes and SPES/PES blend membranes, the latter of which are distinguished by a significantly lower hydrophobicity than the other developed membranes [9].

The selectivity and anti-interference ability, the sensitivity, and the extraction/desorption dynamics are all greatly affected by the adsorbent system used to functionalize PES-based blends. All reported examples highlight the significance for developing membranes acting through selective adsorption mechanisms.

4.1.2. PDMAEMA stimuli-responsive polymer

Stimuli-responsive polymers constitute a class of valuable smart materials capable of adapting/reacting to the surrounding environment and they may be therefore used as efficient embedding systems. In this regard, poly[2-(dimethylamino)ethylmethacrylate] (PDMAEMA) is a polymer sensitive to external stimuli including temperature, pH, and ionic strength, and it had previously found uses in therapeutic/biomedical fields as well as nanotechnology [10].

PDMAEMA is a weak polybasic polymer with a pKa of approximately 7.5. Its polyelectrolyte behaviour derives from the tertiary amino group that may be protonated under acidic conditions and deprotonated at higher pH (Figure 4.1). PDMAEMA is also sensitive to temperature changes with a lower critical solution temperature (LCST) in the range of 32–53°C, depending on molecular weight, pH, and salt concentration. At low temperatures it shows a hydrophilic behaviour by creating hydrogen bonds with water, while at high temperatures it dehydrates and acquires hydrophobic properties [11].

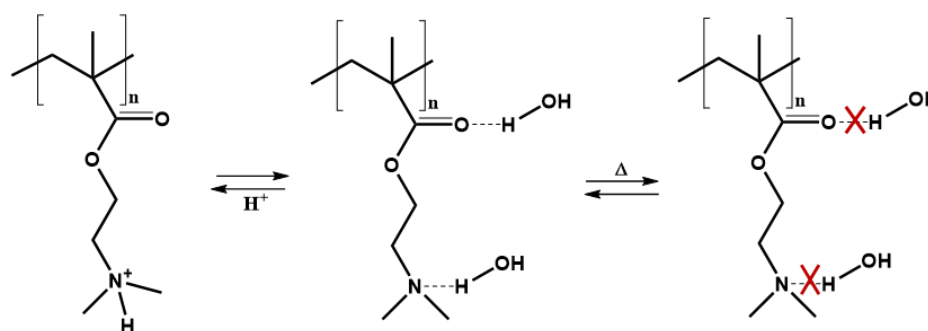


Figure 4.1. Schematization of the stimuli-responsive properties of PDMAEMA polymer.

A peculiar feature of PDMAEMA is the swelling property of its hydrogels. PDMAEMA gels show rapid expansion in water at pH values below 3, as the protonation of all tertiary amino groups increases the charge density on the network, while, at higher pHs, the gel is more compact. The ionic strength of the solution and the temperature also influence the swelling properties of PDMAEMA gels. In particular, at temperatures above 40 °C its swelling capacity decreases, as the hydrophobic interactions of the chains become stronger, making the gel more compact [12].

The influence of the pH on the equilibrium of swelling in water of PDMAEMA gel beads, cross-linked with N,N'-methylene-bis-acrylamide, is even more evident. These gel beads remain in their expanded state up to pH 7.7, while sharply collapsing into the hydrophobic state at pH 8 [13].

The amphiphilic character of PDMAEMA may be modulated by increasing the lipophilic portion of the polymer through the formation of copolymers (random [14] or block [15] copolymers), or through the quaternization of the amino groups with long-chain alkylating agents [16]. In this way, stimuli-responsive amphiphilic systems are obtained with interesting potential in the development of emulsifiers [17], or smart filter membranes [18].

The membrane, described by Cao et. al, obtained by coating a steel mesh with PDMAEMA hydrogel cross-linked with N,N'-methylene-bis-acrylamide, show super-hydrophilicity or super-lipophilicity, as a function of temperature and pH. The functionalized mesh can selectively separate water from oil/water mixtures and collect it separately by suitably regulating the temperature or pH. Subsequently, by increasing the temperature and the pH, the oil may permeate through the network and be collected in situ [18].

PDMAEMA is also commonly used in drug delivery [15] and in non-viral gene delivery [19], thanks to the fact that it has a pKa similar to the physiological pH, it is soluble in water and it has a high gene transfection efficiency. For example, micelles formed following the aggregation of polycaprolactone/PDMAEMA star-block copolymers (PCL-b-PDMAEMA) are able to encapsulate a poorly soluble drug, such as camptothecin (CPT), and to release it in vitro [15].

Like other cationic polymers [20], PDMAEMA in its protonated form or after quaternization with an alkylating agent is a bacterial growth inhibitor due to its interaction with negatively charged bacterial membranes. Both Gram-positive bacteria, such as *Escherichia coli*, and Gram-negative bacteria, such as *Staphylococcus epidermidis* and *Staphylococcus aureus*, growth are inhibited by bactericidal PDMAEMA. In particular, *Staphylococcus epidermidis* is more

susceptible to PDMAEMA being less hydrophobic and more negative than *Staphylococcus aureus* [21]. Since its bactericidal action takes place, PDMAEMA must come in contact with the bacterial cells, and in order to increase the contact surface, new biomaterials are obtained by depositing the polymer on nanomaterials, such as nanoparticles [22] or silicon nanowires [23].

It is possible to add more fascinating and functional characteristics to PDMAEMA by a variety of functionalization techniques. Using surface-initiated Activators Regenerated by Electron Transfer (ARGET) atom transfer radical polymerization (ATRP), Alotaibi et al. created magnetic mesoporous silica nanoparticles modified with PDMAEMA brushes ($\text{Fe}_3\text{O}_4@\text{MSN-PDMAEMA}$).

To develop cationic polymer chains ($\text{Fe}_3\text{O}_4@\text{MSN-QPDMAEMA}$) with a permanent positive charge, tertiary amines in the polymer chains were quaternized using 2-iodoethanol. It was explored if the synthetic materials might be used to remove the dyes methyl orange (MO) and sunset yellow (E110) from aqueous solutions. The outcomes demonstrated that, when the pH level is over 5, the $\text{Fe}_3\text{O}_4@\text{MSN-PDMAEMA}$ sample perform less well in terms of adsorption towards both dyes than the corresponding quaternary $\text{Fe}_3\text{O}_4@\text{MSN-QPDMAEMA}$ [24].

4.1.3. Pillar[n]arene-based adsorbent materials

The creation of novel, efficient adsorbents that use supramolecular techniques to remove target pollutants from a variety of matrices lately attract a lot of attention [25].

Supramolecular macrocycles with large recognition and hosting cavities play a significant role in host-guest chemistry. Examples include crown ethers, cyclodextrins, calixarenes, cucurbiturils, and pillararenes [25] (Figure 4.2).

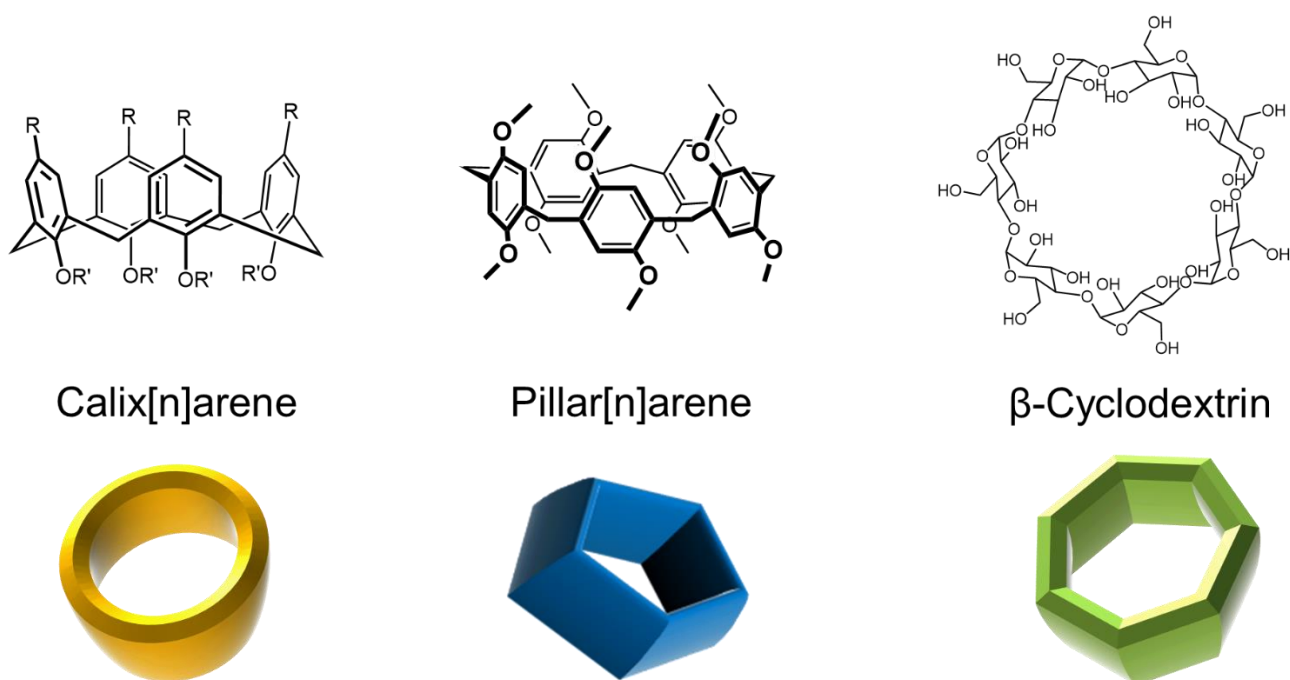


Figure 4.2. Graphical illustration of different examples of useful macrocyclic compounds.

This last is a subclass of cyclooligomers based on 1,4-dimethoxybenzene units joined together at the 2 and 5 positions by methylene bridges [26]. The cyclopentamer pillar[5]arene [27] in particular possesses two key properties: a hydrophobic and electron-rich cavity (with a diameter of around 5.5 Å), and a variety of phenolic oxygens ideal for functionalization. These characteristics allow pillar[5]arene derivatives to incorporate neutral and/or positively charged molecules (such as linear hydrocarbons, halogenalkanes, nitriles, amines, and viologens) through a variety of π interactions or charge transfer complexes [28].

In fact, this class of macrocycles has a number of promising applications in the fields of sensing [29,30], drug delivery [31], and catalysis [32]; new recent examples of their use in combination with polymers in the separation, filtration, and adsorption sectors are reported. This is made possible by their selectivity towards the inclusion of different target molecules [33,34].

By introducing hydrophilic groups at the edges of the pillararene structure (e.g. carboxylates), it is finally possible to solubilize these extraordinary molecular receptors in water, extending the molecular recognition towards molecules of biological origin or being pharmacologically active. These inclusion capabilities allow the application of pillararene systems also for sensing and recognizing polluting molecules, such as pesticides, dyes and herbicides (paraquat) [28,31].

The host-guest properties of macrocycles of synthetic origin have recently been combined with the physico-chemical properties of materials of organic or inorganic origin for the development of new materials with increased functionalities. In particular, the combination of the supramolecular chemistry of host macrocycles and the response to stimuli of Surface Plasmon Resonance (SPR) polymers represents an increasingly evolving field, considering the versatility of the functional applications that can derive from it. Polymer/macrocycle systems already find applications in the field of sensors for cations, anions, pH and temperature, in drug delivery, or in the preparation of self-healing materials [35].

Fu et al. described a novel luminescent elastomer based on the organic-inorganic hybrid polymer polydimethylsiloxane (PDMS). Following a hydrosilylation reaction with a decallyloxy-pillar[5]arene/fluorescent guest complex, a luminescent gel with double crosslinking is obtained: covalent and supramolecular [36].

The synthetic approach of Chang et al. instead envisaged the synthesis of a polymerizable pillararene monomer, thanks to the presence of a methacrylate group, to be used in the copolymerization reaction with methyl methacrylate. The polymer thus obtained has “pendant” pillaranes, which give rise to supramolecular cross-linking in the presence of a bifunctional guest. Such system is capable of responding to stimuli such as temperature increase; the insertion of a competitive host or guest molecule produces a sol for possible applications such as actuators and adaptive coatings [37].

The pillararene/PDMAEMA described by Wu et al. instead involve the synthesis of a pillararene derivative to be used as an initiator for the ATRP polymerization of DMAEMA. Then exploiting the pillar[5]arene/viologen affinity, a supramolecular block copolymer with a viologen-poly(N-isopropylacrylamide) (PNIPAM) guest polymer is prepared. This system is

capable of aggregating into stable supramolecular nanoparticles in aqueous solution at 40°C, which show excellent responsiveness to pH and temperature variations. These nanoparticles find application in the trapping of drugs such as photosensitizers for photodynamic therapies. The double response of the polymer to pH and temperature allows the release of the photosensitizing molecule and demonstrates the potential of smart polymers in one of the possible combinations with supramolecular hosts in drug delivery [38].

Moreover, inorganic or polymeric supports were used to produce and use various adsorbent materials that take advantage of the host-guest complexation of polluting dye molecules by macrocyclic compounds.

Examples of pillar[5]arenes-based adsorbent materials include:

- a quaternary cationic pillar[5]arene-modified zeolite with an 84% MO removal efficiency starting from an initial concentration of 100 mg·L⁻¹ after 12 hours [39];
- a pillar[5]arene-based 3D network polymer with a 95.2% uptake in 30 minutes of a 0.100 mM MO solution [40];
- a bi-pillar[5]arenes-based stimuli-responsive supramolecular polymeric network that uptakes 83.2% of MO in 30 minutes [41].

A new polymeric dye adsorbent obtained by using trimesoyl chloride as linkers to crosslink a bihydrazide-functionalized pillar[5]arene is developed by Zang et al. and represents one of the most recent achievements. In the selective adsorption and separation of tiny cationic dyes, like methylene blue and neutral red, the crosslinked polymeric material has shown excellent potentiality.

The results of the kinetic experiments demonstrate that the Freundlich isotherm model and the pseudo-second-order model both well predict the adsorption behaviours of the two dyes. Additionally, this newly created polymer adsorbent based on pillararene may be regenerated up to five times with essentially no decrease in adsorption efficiency [42].

4.2. Smart pillararene-based PES/PDMAEMA blends and beads for selective water contaminant adsorption

4.2.1. Abstract

The purpose of this research activity was to describe the synthesis of a novel smart polymer that combines the responsiveness of PDMAEMA polymer with the host-guest characteristics of covalently connected and opportunely functionalized pillar[5]arenes (Figure 4.3).

This polymer will be referred as P5-QPDMAEMA. The mixing of P5-QPDMAEMA with polyethersulfone resulted in the synthesis of functional beads, thanks to a conventional non-solvent induced phase separation (NIPS) method carried out at different coagulation pH, with the goal of testing them for the removal of organic dyes in water (Figure 4.4).

Specifically, adsorption experiments using methylene blue (MB), a typical cationic dye, and methyl orange (MO), a representative anionic dye, were performed on all the obtained beads.

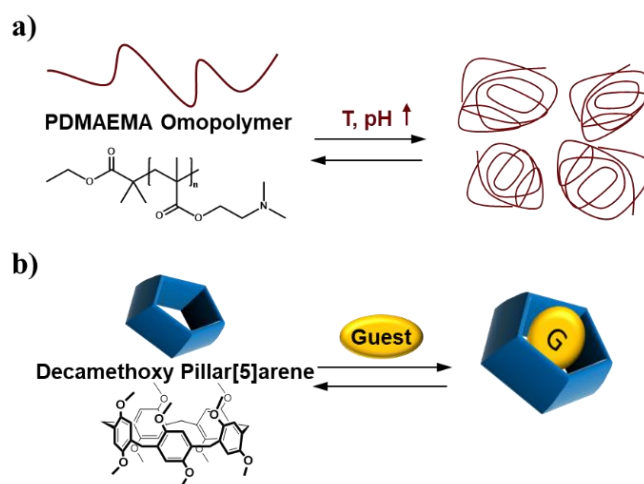


Figure 4.3. Graphical representation scheme of the stimuli-responsive features of PDMAEMA polymer (a) and host-guest properties of pillar[5]arenes (b).

The P5-QPDMAEMA based beads demonstrated the highest selectivity for the removal of the anionic dye and the best MO removal rate of 91.3% after 150 minutes beginning from a 20 mg·L⁻¹ solution. The pseudo-first order and Freundlich models were found to be the most appropriate to represent the MO adsorption behaviour based on the adsorption kinetics and isotherm calculations, achieving a maximum adsorption capacity of 21.54 mg·g⁻¹. Additionally, zwitterionic beads were created by post-functionalizing PDMAEMA and P5-QPDMAEMA based beads, and it is shown that they are capable to remove both cationic and anionic dyes.

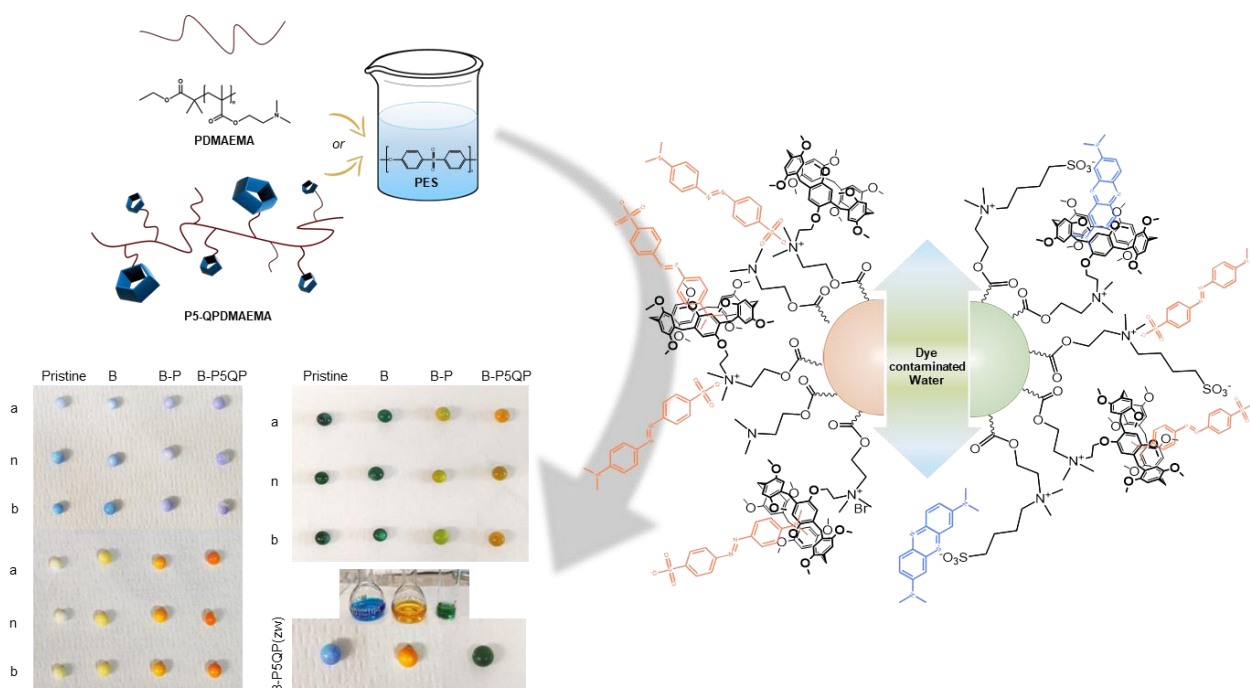


Figure 4.4. Graphical description of the development of smart pillar[5]arene-based PDMAEMA/PES blends for the production of functional beads and the smart adsorption of organic dyes.

The whole research activity described in this Chapter refers to the content outlined in the article n.4 of the publication list.

4.2.2. Results and discussions

4.2.2.1 P5-QPDMAEMA synthetic preparation and NMR characterization

A pillar[5]arene derivative (P5-Br) and PDMAEMA, both synthesised by using methods already described in literature [43–46], were the starting points for the synthesis of the designed smart polymer, P5-QPDMAEMA (Figure 4.5).

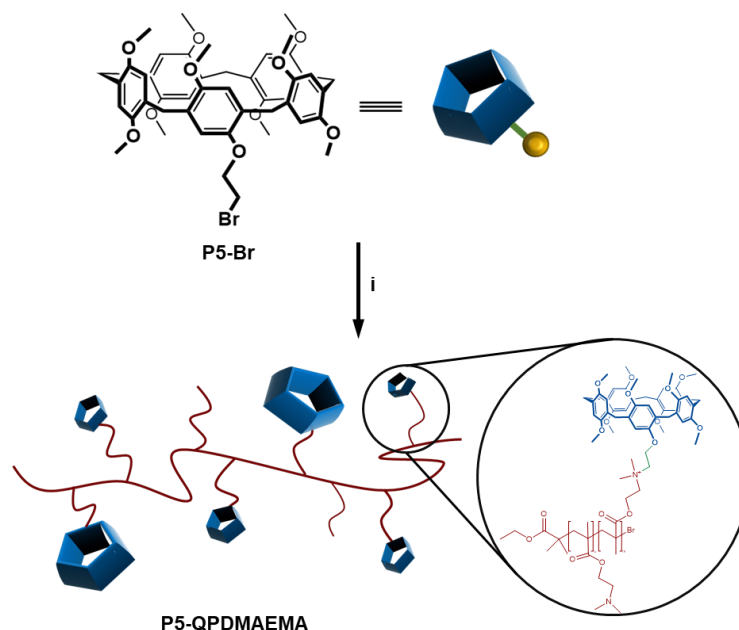


Figure 4.5. Illustration of the synthesis of P5-QPDMAEMA; (i) PDMAEMA, DMF, 323.15 K, 10 d).

In particular, the P5-Br derivative was produced by co-pillarizing 1,4-dimethoxybenzene and 1-(2-bromoethoxy)-4-methoxybenzene in accordance with the method outlined by Y. Zhou et al. [43]; meanwhile, the PDMAEMA polymer was synthesized by ARGET-ATRP of 2-(dimethylamino)ethyl methacrylate (DMAEMA) [44], by using the a monomer/catalyst/ligand/reducing agent molar ratios outlined by Willott et al. [45] and the catalyst/initiator molar ratio recommended by Keating et al. [46].

The P5-Br derivative was used as the alkylating agent during the last phase of the quaternarization process to alkylate the amino groups of PDMAEMA in order to produce the P5-QPDMAEMA polymer. For these purposes, a mole ratio of amino groups/P5-Br of 2:1 was used. Mole ratios of amino groups were calculated by dividing the weight of the polymer by the weight of the monomeric unit. They also refer to the number of dimethylaminoethyl groups present in the amount of PDMAEMA undergoing the alkylation reaction.

To examine and characterise the chemical structure of the finished polymer, ¹H NMR monodimensional experiments and Diffusion Ordered Spectroscopy (DOSY) NMR investigations were carried out (Figure 4.6).

Figure 4.6 a clearly shows both the aliphatic proton signals of PDMAEMA [47], as well as the distinctive aromatic proton signals associated to the pillararenic units [27].

Pillararene and PDMAEMA signals have the same diffusion coefficient ($D_{\text{obs}} = 3.52 \times 10^{-11} \text{ m}^2 \cdot \text{sec}^{-1}$), as shown by the DOSY plot in Figure 4.6 b, thus confirming the covalent functionalization of the polymer.

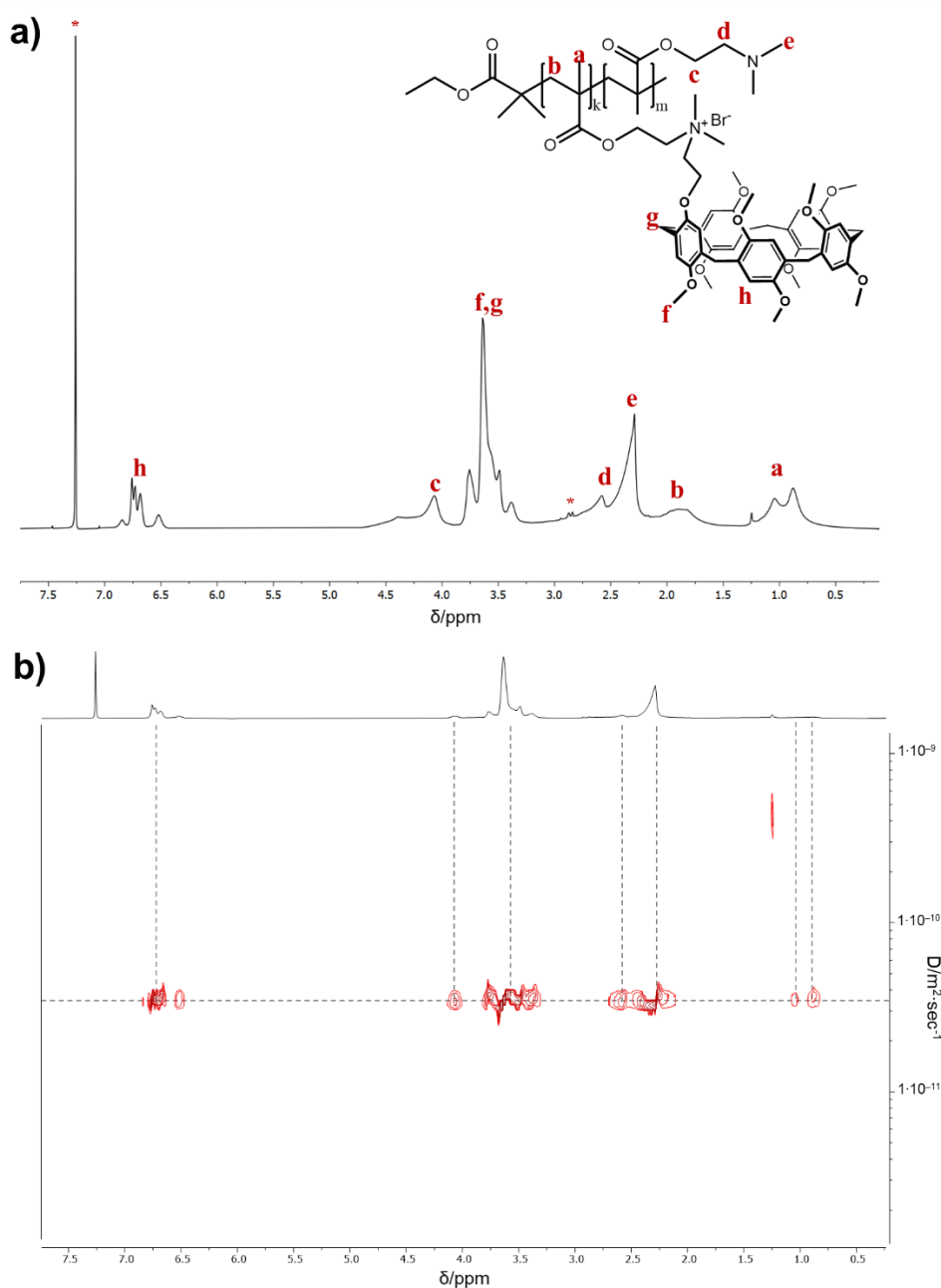


Figure 4.6. ^1H NMR (a) and DOSY spectra (b) of P5-QPDMAEMA (500 MHz, 298 K, CDCl_3). Asterisks correspond to residual solvent peaks.

The PDMAEMA backbone methyl groups and the aromatic resonances (resonances a in Figure 4.6 a) were carefully integrated to reveal that about one of every five monomeric units in the polymer are alkylated by P5-Br.

4.2.2.2 Smart polymeric blends development

Different types of beads based on blend polymers were developed by a conventional non-solvent induced phase separation (NIPS) procedure in order to generate simple to use adsorbent systems for the removal of target molecules from water [48].

Four different types of blends were produced by solubilizing polyethersulfone (PES), polyvinylpyrrolidone (PVP), as the pore former, and PDMAEMA or P5-QPDMAEMA in dimethylacetamide (DMAc), as the solvent (Figure 4.7).

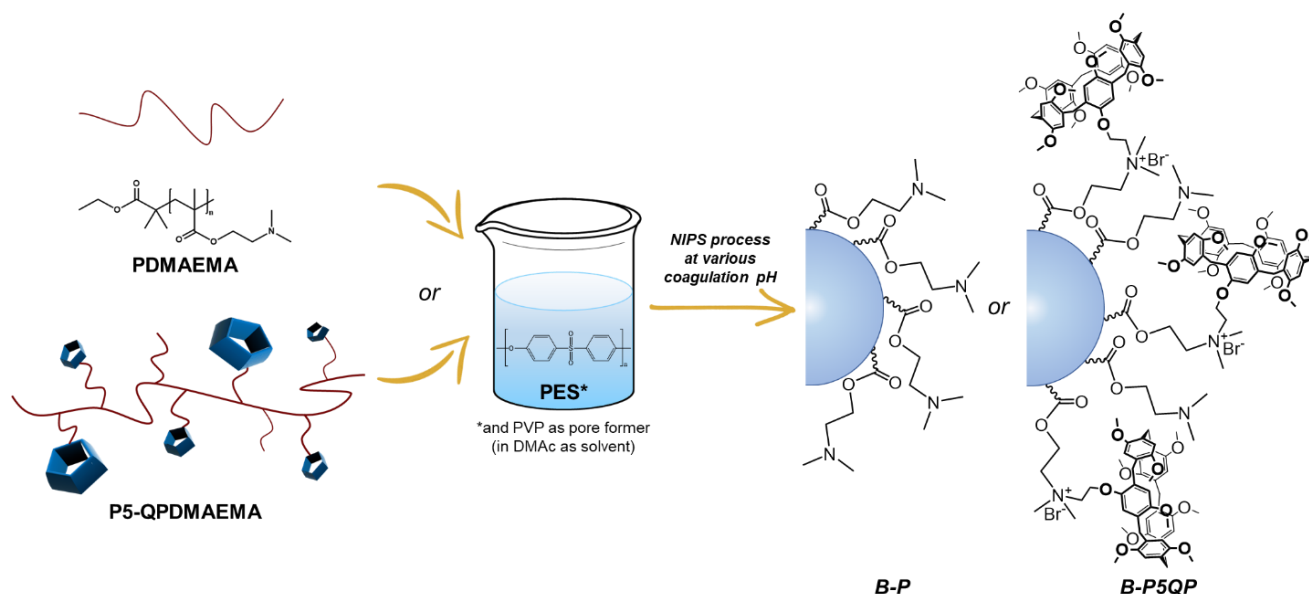


Figure 4.7. Graphical illustration of functional beads preparation.

To specifically take advantage of the pH-responsiveness of the PDMAEMA polymer the blends were dropped by the use of a syringe in three different coagulation baths (at different pH).

Table 4.1 contains a list for each developed bead, together with its composition and name.

Table 4.1. Proportion^{a)} of each agent used to make the beads.

Name	PES [%]	PVP [%]	PDMAEMA [%]	P5-QPDMAEMA [%]	DMAc [%]
Pristine	20	-	-	-	80
B ^{b)}	18	2	-	-	80
B-P	18	1	1	-	80
B-P5QP	18	1	-	1	80

a) Ratio w/w %; b) B=Blend, i.e. blend polymer based on PES and PVP; c) B-P, i.e. blend polymer based on PES, PVP and PDMAEMA; d) B-P5QP, i.e. blend polymer based on PES, PVP and P5-QPDMAEMA

The HCl (0.5 M), H₂O, and NaOH (0.5 M) solutions used for the coagulation baths are designated as (a), (n), and (b), thus indicating the employed acidic, neutral and basic reaction medium, respectively.

The beads were placed in the baths for 2 hours, removed, and then placed in water for 12 hours to completely coagulate.

Additionally, two zwitterionic beads known as B-P(zw) and B-P5QP(zw) were obtained by post-functionalizing [49] the B-P(b) and B-P5QP(b), using 1,4-butansultone in methanol (Figure 4.8). The functionalization percentage yields are 27.2% and 21.1%, respectively.

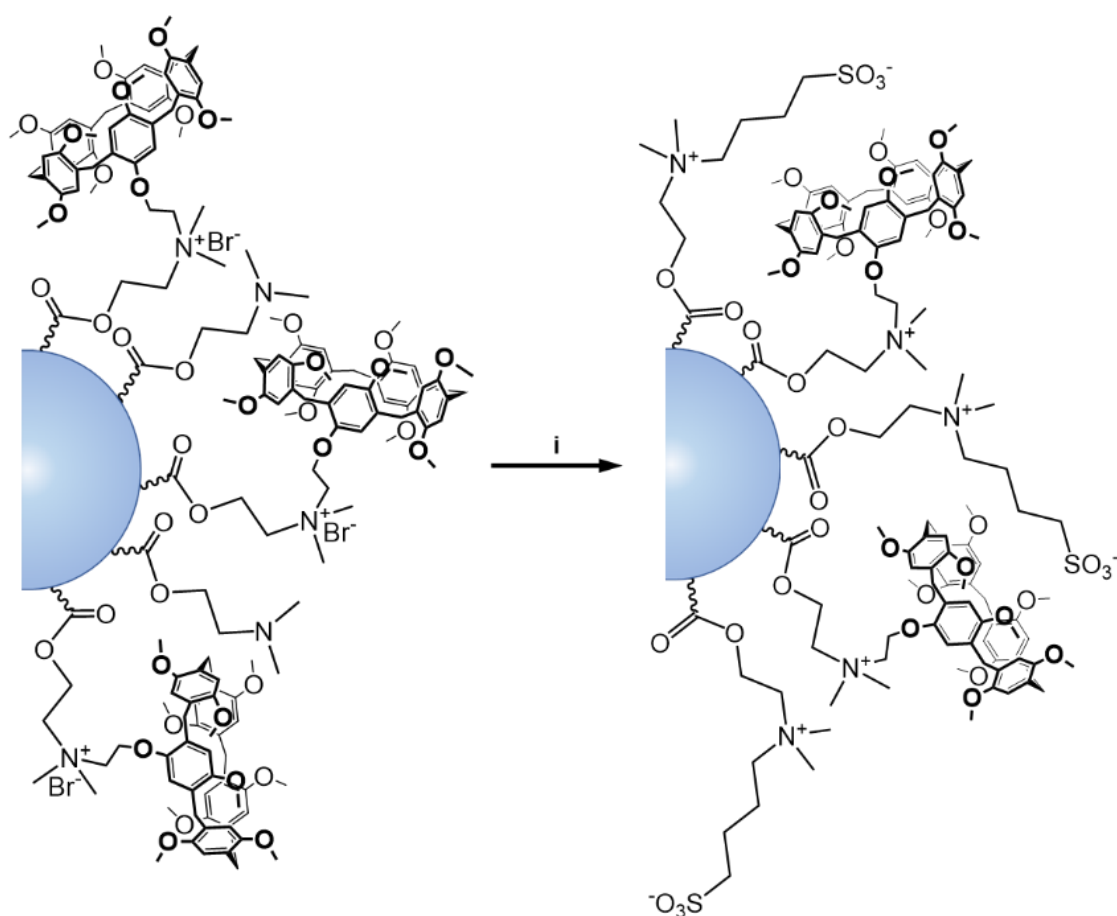


Figure 4.8. Graphic synthetic scheme for the formation of B-P5QP(zw) zwitterionic beads (i. 1,4-butansultone, CH_3OH , 313.15 K, 24h).

4.2.2.3 ATR-FTIR characterization of the functional beads

All the produced beads chemical composition was ascertained using attenuated total reflection infrared spectroscopy (ATR-FTIR), which also allowed us to verify their successful functionalization with the employed polymers (Figure 4.9 a, b).

The ATR-FT-IR spectra of the beads, as produced in neutral coagulation baths, are shown in Figure 4.9 a. The characteristic PES signals [50], such as those at 3095 cm^{-1} and 3067 cm^{-1} , relative to the presence of aromatic C–H groups [51], may be detected in all IR spectra. Signals for C–H alkyl groups at 2955 cm^{-1} and C=O amido groups at 1656 cm^{-1} occur by addition of PVP.

The distinctive signals of the PDMAEMA polymer in the B-P beads [52,53] are revealed at 2773 cm^{-1} and 2827 cm^{-1} , corresponding to C–H and $-\text{N}(\text{CH}_3)_2$ functionalities, as well as at 1725 cm^{-1} , related to the C=O of the ester group. The O–C groups of the pillararene units are responsible for the appearance of a new signal at 1038 cm^{-1} in the B-P5QP beads [54].

Figure 4.9 b show the comparison of the ATR-FT-IR spectra of B-P(b), B-P(zw), B-P5QP(b), and B-P5QP(zw) beads, revealing the appearance of additional signals in the zwitterionic beads at 1350 cm^{-1} , 909 cm^{-1} , and 781 cm^{-1} , corresponding to the S=O, S–O, and C–S groups, respectively, after the post-functionalization. In addition, a shift of the C=O vibration signal at 1671 cm^{-1} is observed.

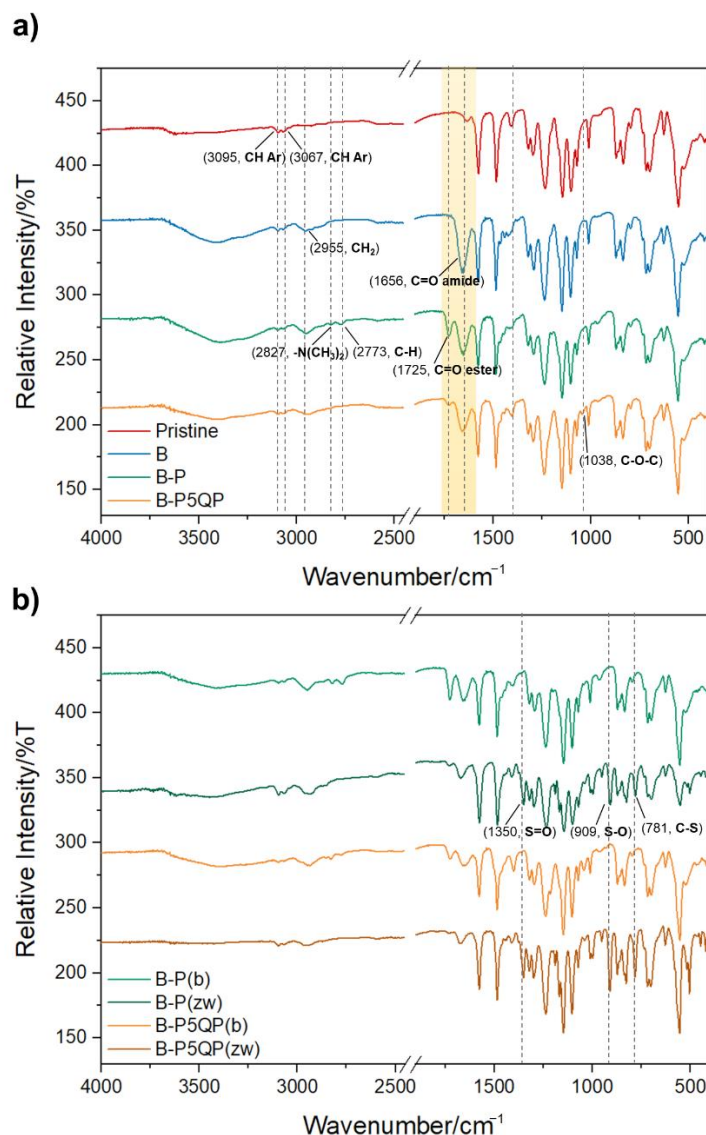


Figure 4.9. ATR-FTIR of beads prepared in neutral coagulation bath (a) and basic coagulation bath, before and after the post-functionalization with the 1,4-butanediol (b).

4.2.2.4 SEM characterization of the functional beads

Beads, cut into pieces using a fine scalpel and metallized with Au, were examined using scanning electron microscopy (SEM) to assess their bulk shape. The observed morphology (see Figure 4.10) match those often seen in previous PES-based systems as obtained by using the NIPS approach [48].

All beads have porous architectures in general, however those produced in basic coagulation baths differ from those produced at acidic pH because they possess a slightly less structural homogeneity and smaller average pores.

Smaller holes with a more homogenous distribution, regardless of pH synthetic condition, are characteristic of the bulk structure of P5-QPDMAEMA-based beads. This can be ascribed to a number of causes, including the original polymeric blend viscosity [55] or perhaps the

lower PDMAEMA pH sensitive amino groups, as a consequence of their partial replacement with pillararenic units, thus resulting in less morphological variations.

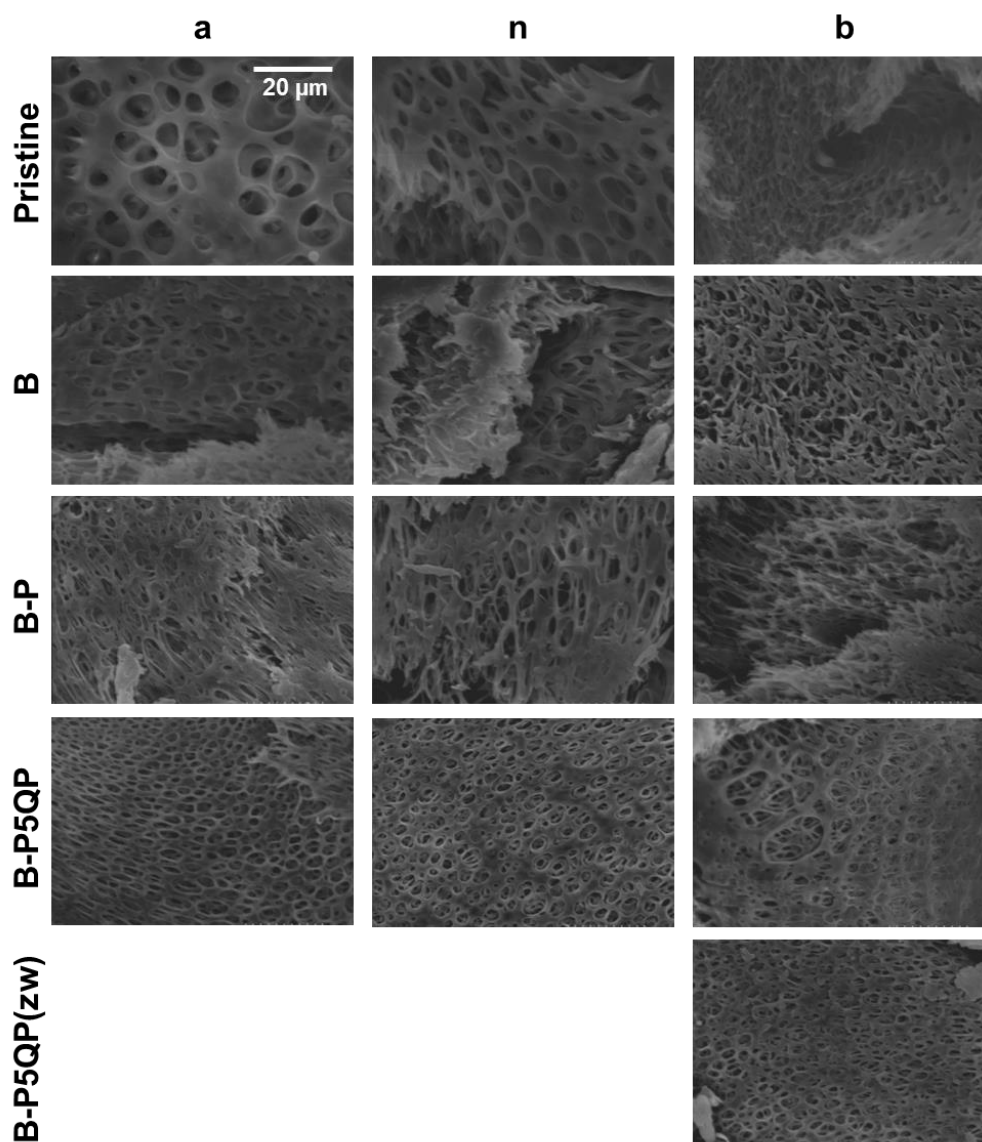


Figure 4.10. SEM images of the cross-sections of functional beads prepared at acidic (left column), neutral (central column) or basic pH (right column).

SEM examination was used to morphologically characterise the structure of B-P₅QP(zw), and the analysis results showed no appreciable morphological changes brought about by the post-functionalization procedure.

4.2.2.5 XPS characterization of the functional beads

An extremely surface-sensitive examination that can provide details about the oxidation state of the detected components is the X-ray photoelectron spectroscopy (XPS). The presence of C, O, S, and N is a defining characteristic of all studied samples. Depending on pH, Na and Cl are alternately identified in their normal oxidation states: Na⁺ ($BE_{(Na1s)} = 1071.5$ eV) and Cl⁻ ($BE_{(Cl2p)} = 199.5$ eV). Figure 4.11 a compares the C_{1s} spectra obtained from pristine samples at

various pH levels. The signals are shown to be characterised by three peaks by the peak fitting analysis, which are attributed to the C–C, C–O, and π - π^* shake-up satellites and located at BE = 285.0 eV, 286.5 eV, and 292.0 eV, respectively.

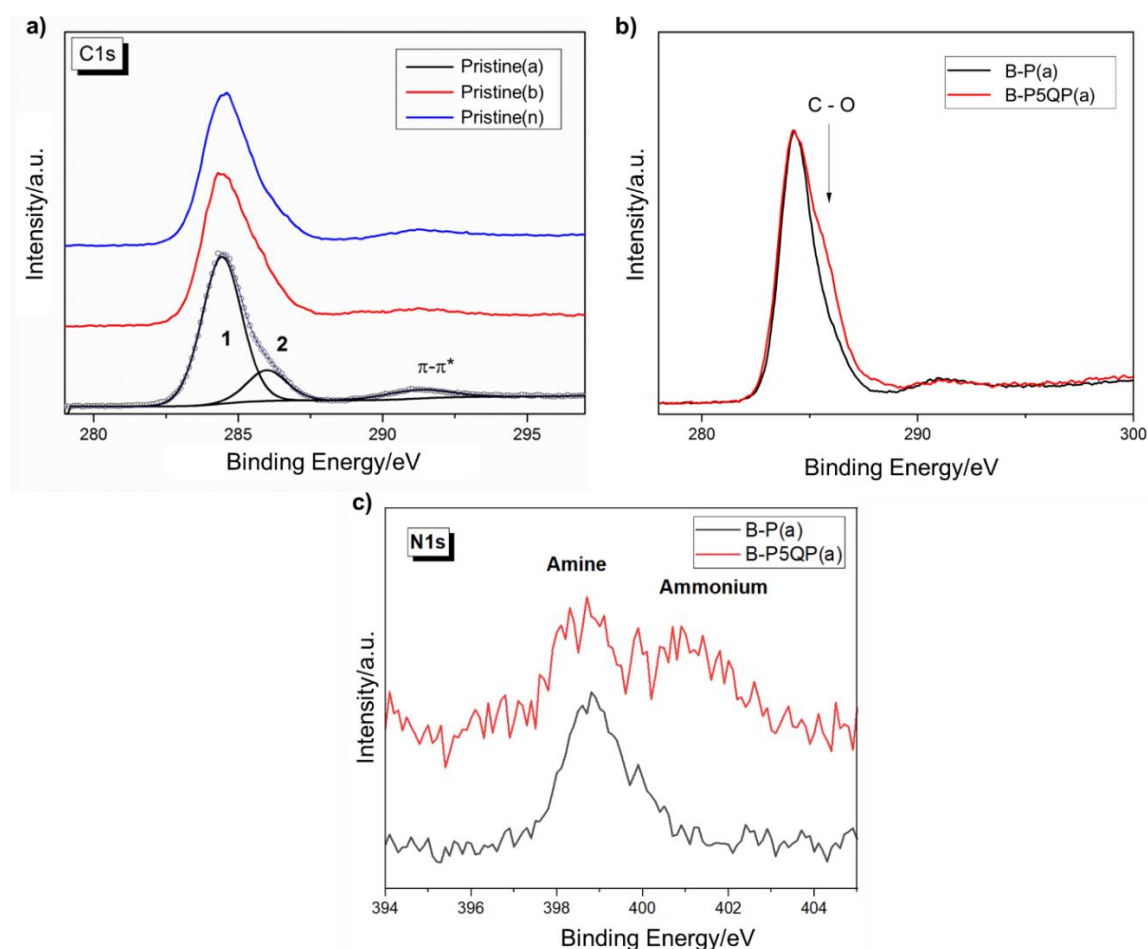


Figure 4.11. Comparison between the peaks associated with the C–C (1) and C–O (2) bonds and the C 1s signal obtained from the pristine samples a) and C 1s signal b) and N 1s signal c) of B-P(a) and B-P5QP(a) beads.

This last contribution is indicative of the PES aromatic structure [56]. Except for the appearance of the $-\text{COOH}(\text{R})$ contribution (BE = 290.0 eV) at basic pH levels, the structure of the C_{1s} signals remained mostly the same as pH is changed. The S_{2p} signal, which is recognised by its usual doublet S_{2p_{3/2}}-S_{2p_{1/2}} separated in energy by 1.2 eV and with the S_{2p_{3/2}} peak located at BE = 168.0 eV, is present, indicating the existence of the sulfonyl functional groups. A second peak identified as belonging to a sulphonate group occurred at BE = 168.7 eV when operating at basic pH levels.

The C 1s signal has the same structure in beads made from the mixture of PES and PVP, with an additional component at BE = 287.6 eV that is characteristic of the C=O (Figure 4.11 b) and, concurrently, a single N 1s peak at BE = 399.7 eV that is caused by the amidic group. The separation of the N 1s components, positioned at BE = 399.7 ÷ 399.8 eV and 402.0 ÷ 402.8 eV, attributed to amine and ammonium groups, respectively, is caused by the functionalization of the beads with PDMAEMA and P5-QPDMAEMA (Figure 4.11 c).

4.2.2.6 Organic dyes adsorption tests

Some preliminary batch tests were carried out to determine the applicability of the functionalized beads, as new useful systems with implemented properties compared to typical PES-based solutions in the separation of emerging pollutants from water.

A single bead (3 mg) was immersed in 2 mL of a 50 μ M water solution of each chosen dye as representative contaminants to perform qualitative preliminary adsorption tests. Particularly, MO was chosen as a representative anionic dye and MB as a reference cationic dye (Figure 4.12), of general small dimensions.

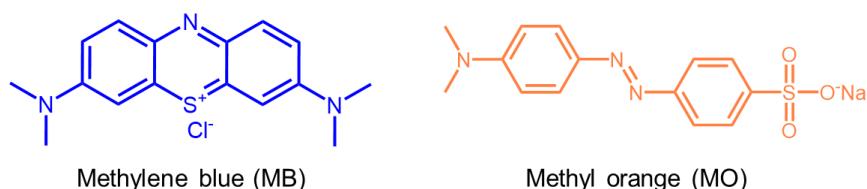


Figure 4.12. Chemical structures of MB and MO organic dyes.

Each bead was taken out of its individual solution after 24 hours at room temperature, rinsed with distilled water, and dried on filter paper (Figure 4.13). In Figure 4.13 a, the Pristine and B beads exhibit the highest levels of qualitative adsorption performance for the removal of MB, while the B-P and B-P5QP beads exhibit the highest levels of qualitative removal performance for MO.

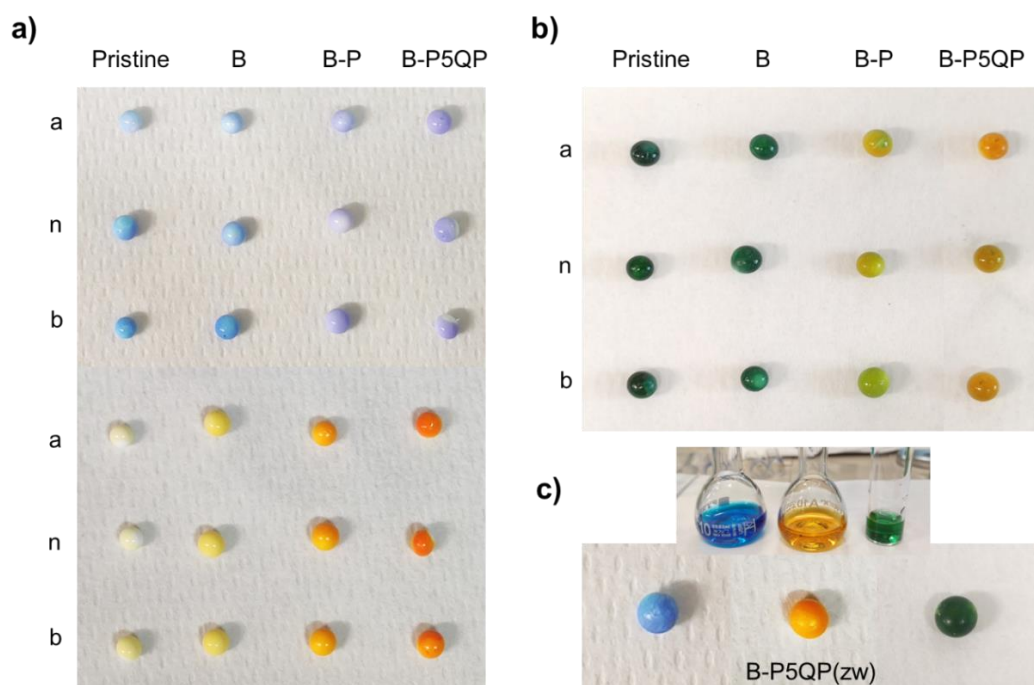


Figure 4.13. Qualitative beads adsorption tests of MB and MO (from top to bottom); each row refers to a bead produced at an acidic (a), neutral (n) or basic (b) coagulation bath (a); qualitative beads adsorption tests of 50 μ M of both MB and MO ($[MB] = [MO] = 50 \mu M$, $V_{tot} = 2 \text{ mL}$) (b); qualitative zwitterionic bead B-P5QP(zw) adsorption tests (from left to right) of MB and MO individual and mixed solutions (c).

The same adsorption test is conducted using an equimolar solution of MB and MO ($V_{\text{tot}} = 2$ mL total; $[\text{MB}] = [\text{MO}] = 50 \mu\text{M}$) to emphasise the selectivity of the beads. Figure 4.13 b demonstrates that the Pristine and B beads turn to a dark green colour after 24 hours, showing a non-selective adsorption of both dyes. The green colour decreases in the B-P beads and nearly vanishes entirely in the B-P5QP ones, suggesting a modest removal of MB, combined with a good MO adsorption.

Due to the higher number of protonated amino groups in the PDMAEMA chains and the possible host-guest interactions between the pillararenic units and the dye, the B-P5QP bead, produced in an acidic coagulation solution, exhibits the highest selectivity for removing the anionic dye MO.

The surface charge of each bead varies from the negatively charged Pristine and B beads (for the sulfonic acid groups of PES) [57] to the positively charged B-P and B-P5QP beads due to the partial or complete protonation/quaternarization of the amino groups present in the PDMAEMA chains. This variation is most likely the cause of the observed differences.

Finally, the P-B5QP(zw) bead adsorption test demonstrated the high capacity of this zwitterionic system towards the retention of both the two selected anionic and cationic dyes (Figure 4.13 c).

4.2.2.7 Adsorption performances of the beads

The removal percentage (%) and adsorption capacity ($q_t/\text{mg}\cdot\text{g}^{-1}$) of the functional beads were calculated in order to validate the affinity of the PDMAEMA-based beads (B-P and B-P5QP) towards the anionic MO dye (see eq. in Chapter 6). In order to do this, a comparison of the performances of various beads was carried out (Figure 4.14).

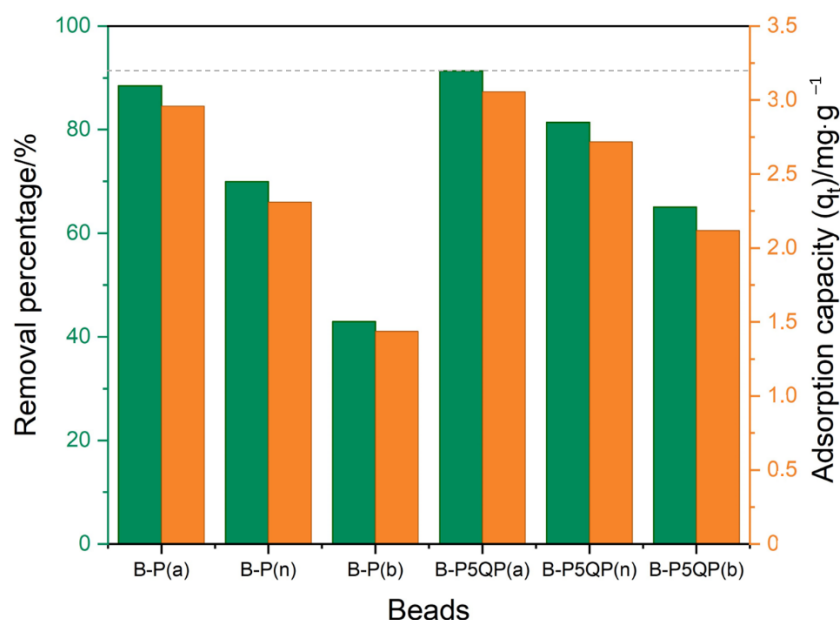


Figure 4.14. Histogram plot related to the removal percentage and adsorption capacity of different functional beads (contact time of 150 minutes; $20 \text{ mg}\cdot\text{L}^{-1}$ MO solution).

Each type of functional bead (≈ 60 mg) in 10 mL of a $20 \text{ mg}\cdot\text{L}^{-1}$ MO solution was left reacting for a total reaction time of 150 minutes. The B-P5QP(a) beads has the greatest removal rate (91.3%) and adsorption capacity ($3.06 \text{ mg}\cdot\text{g}^{-1}$) under these testing conditions, resulting in an almost complete discolouration of the solution.

4.2.2.8 Effect of adsorbent concentration

The effect of the adsorbent concentration variation was investigated in order to comprehend the adsorption behaviour of B-P5QP(a) beads, and the mechanism of their interaction with MO. Various amounts of B-P5QP(a) bead ($\approx 3, 10, 20, 35,$ and 60 mg) were added into a 10 mL of a $20 \text{ mg}\cdot\text{L}^{-1}$ MO solution, and stirred for 120 minutes (Figure 4.15).

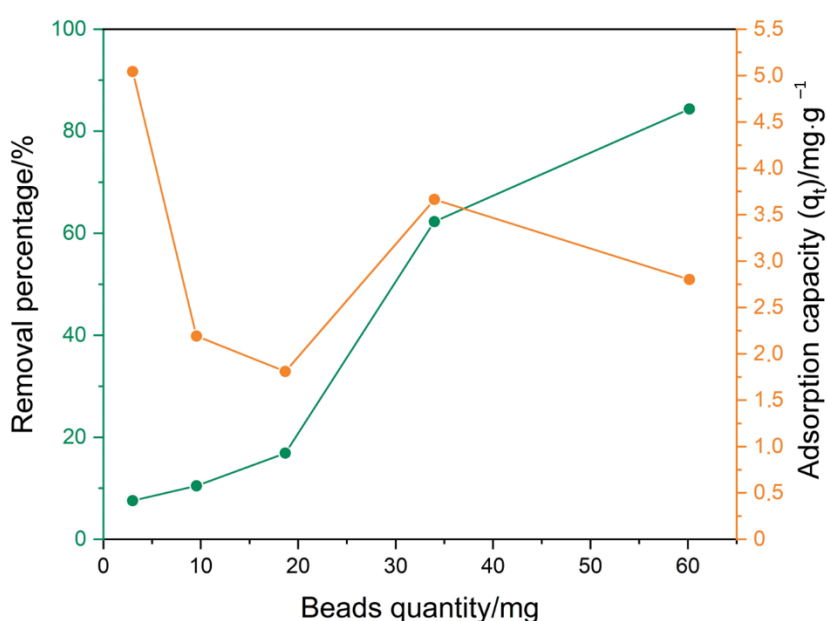


Figure 4.15. Plot showing the removal percentage and adsorption capacity as a function of B-P5QP(a) beads amount ($20 \text{ mg}\cdot\text{L}^{-1}$ MO solution; contact time of 120 minutes).

The experiment shows that the removal percentage increase with the increase of the beads quantity (green points), but the adsorption capacity (right side of the plot in Fig. 4.15) reaches its maximum at lower beads weights.

It is plausible that more active sites are engaged in the adsorption process at higher adsorbent concentrations. As a result, the diffusion resistance increases and a concentration gradient between the solution and the surface of the beads is promoted.

4.2.2.9 Effect of MO concentration

The effect of the initial MO concentration on a fixed quantity of B-P5QP(a) beads was investigated (Figure 4.16) by soaking ≈ 20 mg of B-P5QP(a) beads in 10 mL MO solutions at different concentrations (10, 20, 40, 80, 150, and $300 \text{ mg}\cdot\text{L}^{-1}$).

This experiment was performed to evaluate the mass transfer resistance from the solution to the solid phase that can affect the adsorption of the dye.

It is clear from the data shown in Figure 4.16 a, b that at higher MO concentrations, the removal % decreases as a result of the functional bead active sites becoming saturated.

In addition, after 24 hours at MO concentrations above 80 mg·L⁻¹, the adsorption capacity decreases for the rise in ionic strength between the beads.

Active sites are less accessible, and an equilibrium has been established [58].

After 5 hours of contact with a 300 mg·L⁻¹ MO solution, an adsorption capacity of 14.91 mg·g⁻¹ is attained.

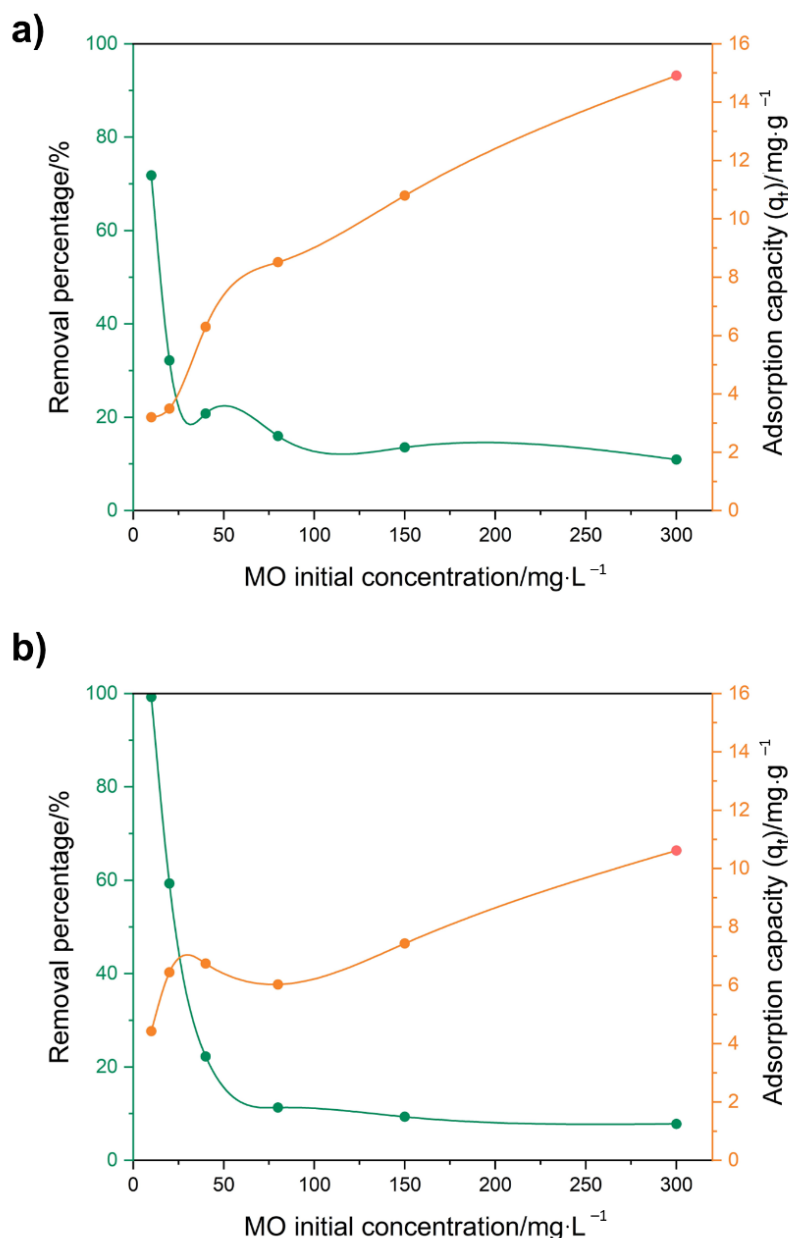


Figure 4.16. Plots of the removal percentage and adsorption capacity of B-P5QP(a) beads towards MO solutions at various concentrations after 5 hours (a) and 24 hours (b) of contact time.

4.2.2.10 Effect of contact time

Figure 4.17 illustrates the results of the study on the impact of the contact time between a $20 \text{ mg}\cdot\text{L}^{-1}$ MO solution (20 mL) and $\approx 20 \text{ mg}$ of B-P5QP(a) bead.

The graph shows that the removal percentage and adsorption capacity increase with the time. The 39% MO elimination with a $7.8 \text{ mg}\cdot\text{g}^{-1}$ adsorption capacity is achieved after 330 minutes of contact time. The initial slower adsorption rate may be caused by the internal diffusion resistance, as shown by the sigmoidal shape of the first data point trend (see inset in Figure 4.17), that also indicates an induction time for the adsorption/removal process. After 24 hours, the adsorption equilibrium is reached with a removal of 46.6% of MO at a rate of $9.7 \text{ mg}\cdot\text{g}^{-1}$.

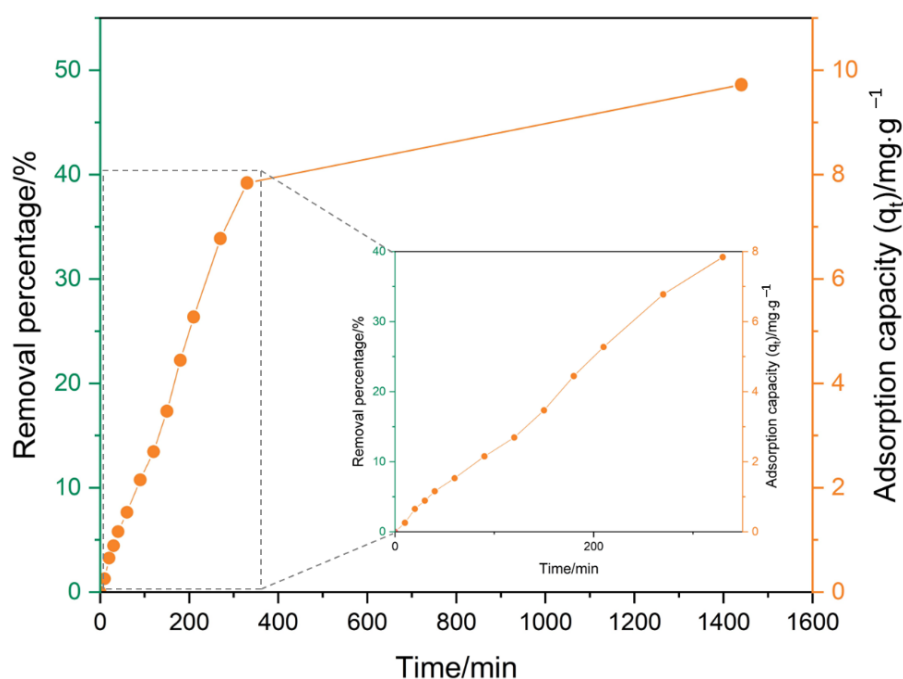


Figure 4.17. Plot showing the removal percentage and adsorption capacity variation of B-P5QP(a) beads and MO solution ($20 \text{ mg}\cdot\text{L}^{-1}$), as a function of time.

4.2.2.11 Adsorption kinetics

To assess the adsorption process for the adsorption of MO from the B-P5QP(a) bead, a detailed kinetic study was performed.

In this regard, four non-linear kinetic models were used (Table 4.2, Figure 4.18): pseudo-first order, pseudo-second order, intraparticle diffusion, and Elovich. In Chapter 6 all experimental details, together with the equations and the used methods, are given.

For the study of the adsorption behaviour of solid/liquid systems, pseudo-first order and pseudo-second order models are frequently used [59].

Additionally, the study of processes that might entail the mass transfer of adsorbate (film diffusion) and surface diffusion has made extensive use of the intra particle diffusion model for the evaluation of the rate-limiting phase of adsorption kinetics [60]. The Elovich model is the

final one used for this investigation; Zeldowitsch developed it to analyse the mass diffusion, surface diffusion, and activation, and deactivation energy to comprehend the chemisorption nature of adsorption [61].

According to the results, the pseudo-first order model correlation coefficient, $R^2=0.9762$, is the higher one. The degree of similarity between theoretical and experimental adsorption capabilities may also be used to assess how well the kinetic model fits the data. The pseudo-second-order model also shows a quite good correlation factor, indicating that this reaction model may take place in the rate-controlling step.

As a result, the physisorption or chemisorption adsorption processes might be difficult to distinguish in some circumstances and might even take place simultaneously [62].

Table 4.2. Adsorption kinetic rate constants and kinetic adopted models for MO adsorption by using B-P5QP(a) beads.

$q_{e,exp}/mg \cdot g^{-1}$	Pseudo-first order			Pseudo-second order		
	$q_e/mg \cdot g^{-1}$	k_1/min^{-1}	R^2	$q_e/mg \cdot g^{-1}$	$k_2/g \cdot mg^{-1} \cdot min^{-1}$	R^2
9.73	10.16	0.0034	0.9762	12.61	2.52	0.9582
	Intraparticle diffusion		Elovich			
	$k_{diff}/mg \cdot g^{-1} \cdot min^{-0.5}$		R^2	$\alpha/mg \cdot g^{-1} \cdot min^{-1}$	$\beta/g \cdot mg^{-1}$	R^2
	0.2982		0.8645	0.05	0.2881	0.9334

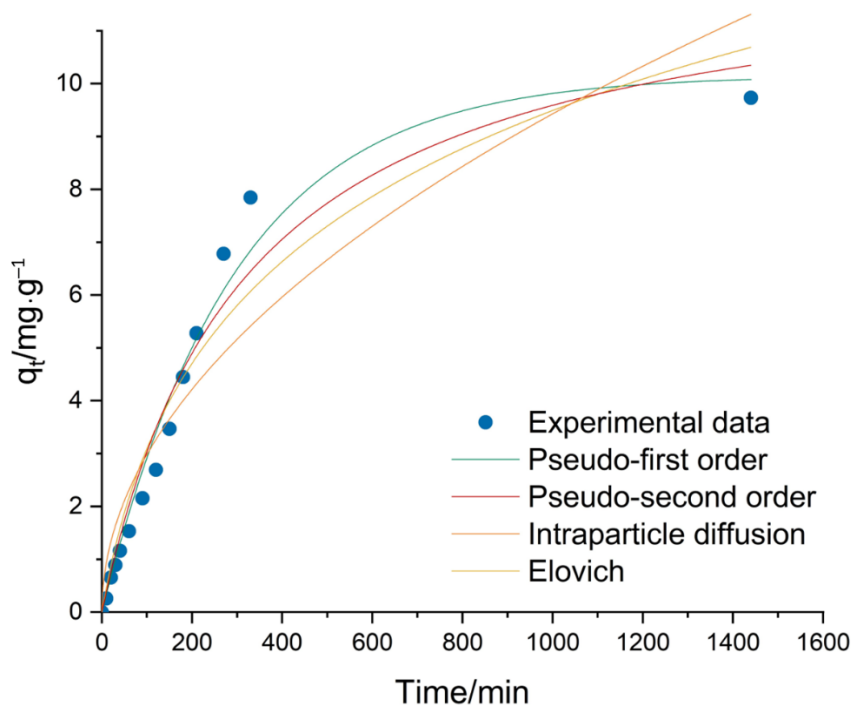


Figure 4.18. Plot of the adsorption capacity of MO by B-P5QP(a) beads as a function of time together with kinetic models fitting.

4.2.2.12 Adsorption isotherms

Three adsorption isotherm models, including the popular Langmuir and Freundlich models as well as the Temkin model, were employed in order to comprehend the adsorbent-adsorbate interactions and the design of the adsorption system B-P5QP(a) (Table 4.3 and Figure 4.19). Chapter 6 reports the followed equations and procedures.

The Langmuir isotherm model describes the equilibrium between the adsorbate and sorbent systems, which involves the creation of a monolayer on the sorption sites, and it is applicable to homogeneous surfaces. The Freundlich isotherm model assumes that multilayer adsorption occurs on the surface of the sorbent and that the adsorption capacity increases continuously at high concentrations [63]. The Temkin isotherm model suggests a multilayer adsorption process and takes into account interactions between the sorbent and the adsorbate, while discounting extremely low and extremely high concentration values [64].

Table 4.3. Isotherm equilibrium constants for different applied fitting models relative to the adsorption of MO by B-P5QP(a) beads.

Langmuir			Freundlich			Temkin		
$q_m / \text{mg} \cdot \text{g}^{-1}$	$k_L / \text{L} \cdot \text{mg}^{-1}$	R^2	$1/n$	$k_F / \text{L} \cdot \text{g}^{-1}$	R^2	B_T	$k_T / \text{L} \cdot \text{mg}^{-1}$	R^2
21.541	0.00812	0.9812	0.5199	0.8396	0.9988	3.780	0.141	0.9614

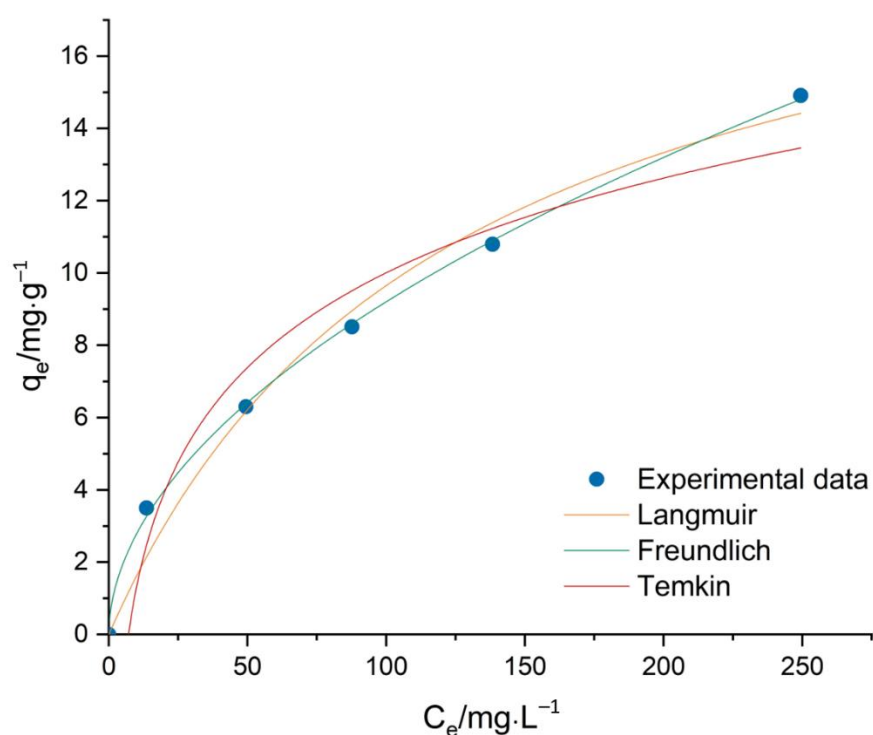


Figure 4.19. Plot showing the B-P5QP(a) bead adsorption capacities as a function of different MO equilibrium concentrations together with isotherm models fitting.

The Freundlich equation more closely approximates the actual adsorption data with an R^2 of 0.9988. According to the obtained experimental data, this model specifically predicts that the dye concentrations on the adsorbent will increase as long as the dye concentration increases [65], while the adsorption capacity exponentially decreases with the saturation of the reactive sorption sites of the adsorbent [66]. As previously indicated, this model also made reference to heterogeneous surfaces, making it relevant to systems in which monolayer (like chemisorption) and multilayer (like Van der Waals adsorption) adsorption processes occurs [60].

A chemisorption process is described for $1/n$ values, between 0.1 and 1, whereas a physisorption process is described for $1/n$ values greater than 1 [67]. The formation of chemical bonds, ion exchange, electrostatic interactions, van der Waals forces, hydrophobic attraction, hydrogen bonding, and physical adsorption are just a few of the numerous processes that might cause an adsorbent and an adsorbate to behave in an adsorption-like process [68]. In this regard, the B-P5QP(a) bead can exploit different mechanisms, due also possible to host-guest interactions between pillararenic units and dye molecules. In accordance with the Freundlich isotherm model, it is therefore conceivable to represent the adsorbent–adsorbate interactions between MO and B-P5QP(a) bead as a multilayer physio/chemisorption heterogeneous process.

4.2.2.13 Adsorption performances of zwitterionic beads

Finally, the ability of the B-P(zw) and B-P5QP(zw) zwitterionic beads to remove cationic MB and anionic MO dyes was examined. The adsorption properties of the zwitterionic beads were investigated using a 10 mL solution by addition of MB $20 \text{ mg}\cdot\text{L}^{-1}$ (5 mL) and MO $20 \text{ mg}\cdot\text{L}^{-1}$ (5 mL) (Figure 4.20 a,b).

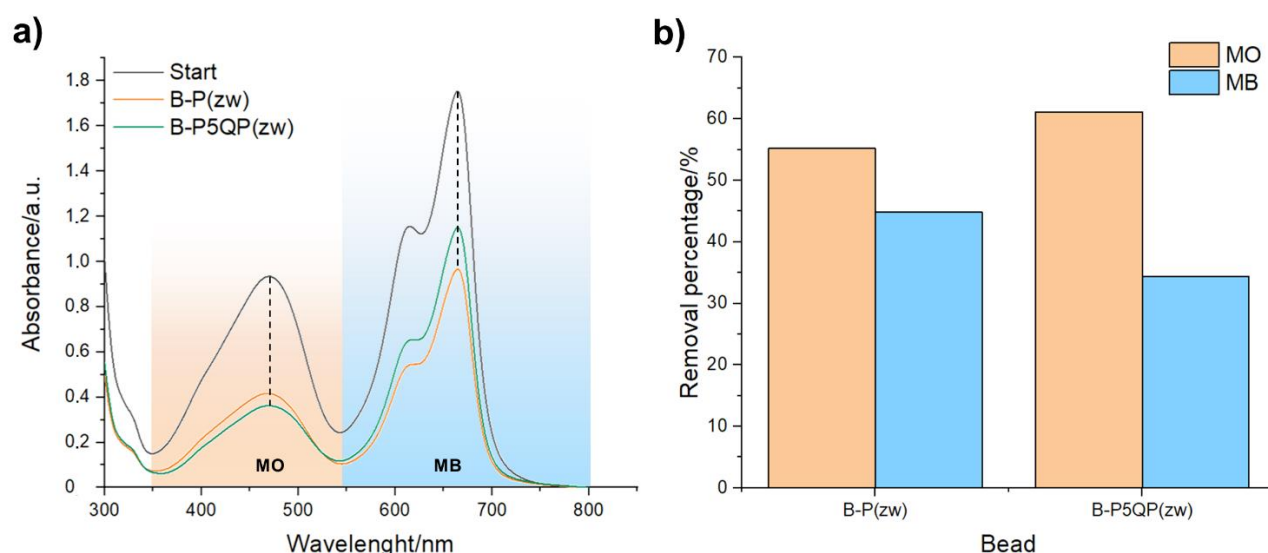


Figure 4.20. Adsorption spectra of MB+MO solution after 24 hours contact time with each B-P(zw) and B-P5QP(zw) of zwitterionic beads ($\approx 20 \text{ mg}$) (a); removal percentage of both cationic and anionic dyes (b).

The capacity to remove the tested anionic and cationic dyes from the solution is demonstrated by both zwitterionic beads. With a removal percentage of 44.9%, the B-P(zw)

beads in particular show the highest adsorption ability towards MB, whereas the B-P₅QP(zw) beads have a better adsorption of MO (61.1%). The dye adsorption behavior of the B-P(zw) beads may be ascribed to the presence of less permanent cationic functionalities due to the absence of P₅-Br units linked to the amino groups of PDMAEMA, as well as an increased number of negatively charged sites for a higher degree of functionalization with 1,4-butansultone, compared to the B-P₅QP(zw) beads.

However, the B-P₅QP(zw) beads combine the impact of more cationic charged sites, as well as of host-guest interactions with the pillararenic units for the adsorption of both dyes, featuring a greater adsorption towards the anionic MO. Figure 4.21 depicts a proposed scheme for the observed adsorption behavior. It is therefore possible to confirm that the post-functionalization enables the beads to concurrently remove both anionic and cationic dyes.

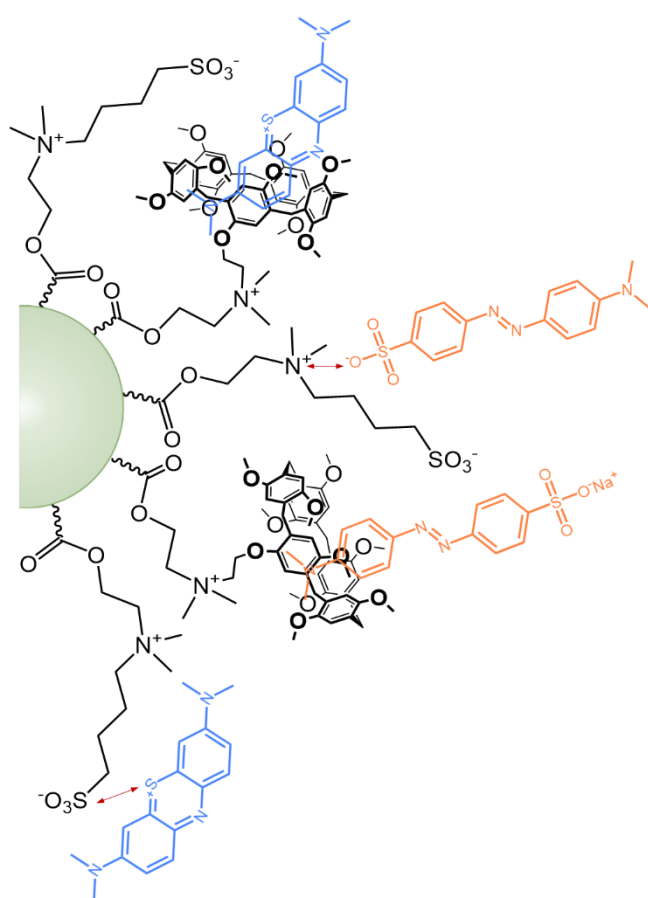


Figure 4.21. Illustration of MB and MO dye removal using the B-P₅QP(zw) bead.

The polymeric formulations described in the preceding paragraphs may open the way to the development of innovative and smart membranes for water filtration via the NIPS process.

Additionally, the employed post-functionalization technique with the 1,4-butansultone results in an alteration in the adsorption behavior of the initial beads and may be helpful in the production of zwitterionic antifouling materials and therefore corresponding membranes [69]. Nowadays, one of the major undesired problems with membrane-based filtration technology is

the growing fouling, which is affected by elements in wastewater such inorganic elements, bacteria, proteins, and other organic molecules [70].

Due to the reduced efficiency and longevity of the membranes caused by this issue, greater working pressures are needed, which increases energy consumption and the possibility of large economic losses. Even if the antifouling abilities of the B-P(zw) and B-P₅QP(zw) systems are actually under study, the results on amphiphilic antifouling coatings [71–73] or on zwitterionic membranes [71,74] will bring to assess the key-role of this peculiar feature in ongoing related investigations.

4.2.3. Conclusions

In order to create functional PES/PVP blended polymeric beads, a smart polymer P₅-QPDMAEMA, based on a pillar[5]arene and the stimuli-responsive polymer PDMAEMA, was successfully developed. The test removal of MB and MO from water using the beads, produced by a NIPS method, was first preliminary examined, with the P₅-QPDMAEMA based beads showing qualitatively not only the best MO removal, but also a strong selectivity towards the removal of the anionic dye.

The quasi-total discolouration of the solution is thus achieved after 150 minutes, which is further supported by studies that show the B-P₅QP(a) beads (≈ 60 mg) has removal rates and adsorption capacities of 91.3% and $3.06 \text{ mg}\cdot\text{g}^{-1}$, respectively, for 10 mL of a $20 \text{ mg}\cdot\text{L}^{-1}$ MO solution. An adsorption capacity of $14.91 \text{ mg}\cdot\text{g}^{-1}$ is attained after 5h of contact time with a $300 \text{ mg}\cdot\text{L}^{-1}$ MO solution. The effects of MO concentration, adsorbent amount, and contact time of B-P₅QP(a) bead were examined.

As a consequence, the pseudo-first order and Freundlich models are found to best describe the MO adsorption behaviour of B-P₅QP(a) bead in adsorption kinetics and isotherm calculations with a q_m of $21.54 \text{ mg}\cdot\text{g}^{-1}$. Its adsorption performance can be described through a physio/chemisorption process involving a multilayer heterogeneous surface. Additionally, the produced B-P(zw) and B-P₅QP(zw) zwitterionic beads showed a significant capacity for the removal of both the cationic and anionic tested dyes.

Finally, it is possible to conclude that those systems can represent valuable and innovative methods for selectively removing organic dyes from contaminated water; additionally, these polymeric blends can be used to create functional and smart membranes for wastewater filtration in textiles related sectors, with potential antifouling capabilities in the case of the employment of the zwitterionic B-P(zw) and B-P₅QP(zw) systems.

References

1. Tkaczyk, A.; Mitrowska, K.; Posyniak, A. Synthetic Organic Dyes as Contaminants of the Aquatic Environment and Their Implications for Ecosystems: A Review. *Sci. Total Environ.* **2020**, *717*, 137222, doi:https://doi.org/10.1016/j.scitotenv.2020.137222.
2. Trovato, V.; Mezzi, A.; Brucale, M.; Rosace, G.; Rosaria Plutino, M. Alizarin-Functionalized Organic-Inorganic Silane Coatings for the Development of Wearable Textile Sensors. *J. Colloid Interface Sci.* **2022**, *617*, 463–477, doi:https://doi.org/10.1016/j.jcis.2022.03.006.
3. Badawi, A.K.; Abd Elkodous, M.; Ali, G.A.M. Recent Advances in Dye and Metal Ion Removal Using Efficient Adsorbents and Novel Nano-Based Materials: An Overview. *RSC Adv.* **2021**, *11*, 36528–36553, doi:10.1039/D1RA06892J.
4. Ielo, L.; Giacobello, F.; Sfameni, S.; Rando, G.; Galletta, M.; Trovato, V.; Rosace, G.; Plutino, M.R. Nanostructured Surface Finishing and Coatings: Functional Properties and Applications. *Materials (Basel)*. **2021**, *14*, 1–41, doi:10.3390/ma14112733.
5. Rando, G.; Sfameni, S.; Galletta, M.; Drommi, D.; Cappello, S.; Plutino, M.R. Functional Nanohybrids and Nanocomposites Development for the Removal of Environmental Pollutants and Bioremediation. *Mol.* **2022**, *27*.
6. Wang, K.; Abdalla, A.A.; Khaleel, M.A.; Hilal, N.; Khraisheh, M.K. Mechanical Properties of Water Desalination and Wastewater Treatment Membranes. *Desalination* **2017**, *401*, 190–205, doi:https://doi.org/10.1016/j.desal.2016.06.032.
7. Otitoju, T.A.; Ahmad, A.L.; Ooi, B.S. Recent Advances in Hydrophilic Modification and Performance of Polyethersulfone (PES) Membrane via Additive Blending. *RSC Adv.* **2018**, *8*, 22710–22728, doi:10.1039/C8RA03296C.
8. Amiri, S.; Asghari, A.; Vatanpour, V.; Rajabi, M. Fabrication and Characterization of a Novel Polyvinyl Alcohol-Graphene Oxide-Sodium Alginate Nanocomposite Hydrogel Blended PES Nanofiltration Membrane for Improved Water Purification. *Sep. Purif. Technol.* **2020**, *250*, 117216, doi:https://doi.org/10.1016/j.seppur.2020.117216.
9. V. B., A.; Mohanty, S.; Nayak, S.K. Preparation and Characterization of Porous Polyethersulfone (PES) Membranes with Improved Biocompatibility by Blending Sulfonated Polyethersulfone (SPES) and Cellulose Acetate (CA) – A Comparative Study. *Mater. Today Commun.* **2020**, *25*, 101544, doi:https://doi.org/10.1016/j.mtcomm.2020.101544.
10. Wei, M.; Gao, Y.; Li, X.; Serpe, M.J. Stimuli-Responsive Polymers and Their Applications. *Polym. Chem.* **2017**, *8*, 127–143, doi:10.1039/C6PY01585A.
11. Bütün, V.; Armes, S.P.; Billingham, N.C. Synthesis and Aqueous Solution Properties of Near-Monodisperse Tertiary Amine Methacrylate Homopolymers and Diblock Copolymers. *Polymer (Guildf)*. **2001**, *42*, 5993–6008, doi:https://doi.org/10.1016/S0032-3861(01)00066-0.
12. Yanfeng, C.; Min, Y. Swelling Kinetics and Stimuli-Responsiveness of Poly(DMAEMA) Hydrogels Prepared by UV-Irradiation. *Radiat. Phys. Chem.* **2001**, *61*, 65–68, doi:https://doi.org/10.1016/S0969-806X(00)00374-1.
13. Orakdogan, N. Novel Responsive Poly(N,N-Dimethylaminoethyl Methacrylate) Gel Beads: Preparation, Mechanical Properties and PH-Dependent Swelling Behavior. *J. Polym. Res.* **2012**, *19*, 9914, doi:10.1007/s10965-012-9914-5.
14. Zheng, J.Y.; Tan, M.J.; Thoniyot, P.; Loh, X.J. Unusual Thermogelling Behaviour of Poly[2-(Dimethylamino)Ethyl Methacrylate] (PDMAEMA)-Based Polymers Polymerized in Bulk. *RSC Adv.* **2015**, *5*, 62314–62318, doi:10.1039/C5RA12816A.
15. Liu, Y.; Li, J.; Ren, J.; Lin, C.; Leng, J. Preparation and in Vitro PH-Responsive Drug Release of Amphiphilic Dendritic Star-Block Copolymer Complex Micelles. *Mater. Lett.* **2014**, *127*, 8–11, doi:https://doi.org/10.1016/j.matlet.2014.04.070.
16. Manouras, T.; Koufakis, E.; Anastasiadis, S.H.; Vamvakaki, M. A Facile Route towards PDMAEMA Homopolymer Amphiphiles. *Soft Matter* **2017**, *13*, 3777–3782, doi:10.1039/C7SM00365J.
17. Marchal, F.; Roudot, A.; Pantoustier, N.; Perrin, P.; Daillant, J.; Guenoun, P. Emulsion Stabilization and Inversion Using a PH- and Temperature-Sensitive Amphiphilic Copolymer. *J. Phys. Chem. B* **2007**, *111*, 13151–13155, doi:10.1021/jp0749827.
18. Cao, Y.; Liu, N.; Fu, C.; Li, K.; Tao, L.; Feng, L.; Wei, Y. Thermo and PH Dual-Responsive Materials for Controllable Oil/Water Separation. *ACS Appl. Mater. Interfaces* **2014**, *6*, 2026–2030, doi:10.1021/am405089m.
19. Mathew, A.; Cao, H.; Collin, E.; Wang, W.; Pandit, A. Hyperbranched PEGmethacrylate Linear PDMAEMA Block Copolymer as an Efficient Non-Viral Gene Delivery Vector. *Int. J. Pharm.* **2012**, *434*, 99–105, doi:https://doi.org/10.1016/j.ijpharm.2012.05.010.
20. Deka, S.R.; Sharma, A.K.; Kumar, P. Cationic Polymers and Their Self-Assembly for Antibacterial Applications. *Curr. Top. Med. Chem.* **2015**, *15*, 1179–1195, doi:10.2174/1568026615666150330110602.
21. Rawlinson, L.-A.B.; O’Gara, J.P.; Jones, D.S.; Brayden, D.J. Resistance of Staphylococcus Aureus to the Cationic Antimicrobial Agent Poly(2-(Dimethylamino Ethyl)Methacrylate) (PDMAEMA) Is Influenced by Cell-Surface Charge and Hydrophobicity. *J. Med. Microbiol.* **2011**, *60*, 968–976, doi:https://doi.org/10.1099/jmm.0.025619-0.
22. Song, J.; Jung, Y.; Lee, I.; Jang, J. Fabrication of PDMAEMA-Coated Silica Nanoparticles and Their Enhanced Antibacterial Activity. *J. Colloid Interface Sci.* **2013**, *407*, 205–209, doi:https://doi.org/10.1016/j.jcis.2013.06.016.
23. Stawski, D.; Rolińska, K.; Zielińska, D.; Sahariah, P.; Hjálmarsdóttir, M.Á.; Másson, M. Antibacterial Properties of Poly (N,N-Dimethylaminoethyl Methacrylate) Obtained at Different Initiator Concentrations in Solution Polymerization. *R. Soc. open Sci.* **2022**, *9*, 211367, doi:10.1098/rsos.211367.
24. Alotaibi, K.M.; Almethen, A.A.; Beagan, A.M.; Al-Swaidan, H.M.; Ahmad, A.; Bhawani, S.A.; Alswieleh, A.M. Quaternization of Poly(2-Diethyl Aminoethyl Methacrylate) Brush-Grafted Magnetic Mesoporous Nanoparticles Using 2-Iodoethanol for Removing Anionic Dyes. *Appl. Sci.* **2021**, *11*.
25. Ma, J.; Zhang, Y.; Zhao, B.; Jia, Q. Supramolecular Adsorbents in Extraction and Separation Techniques - A Review. *Anal. Chim. Acta* **2020**, *1122*, 97–113, doi:https://doi.org/10.1016/j.aca.2020.04.054.
26. Xue, M.; Yang, Y.; Chi, X.; Zhang, Z.; Huang, F. Pillararenes, A New Class of Macrocycles for Supramolecular Chemistry. *Acc. Chem. Res.* **2012**, *45*, 1294–1308, doi:10.1021/ar2003418.

27. Ogoshi, T.; Kanai, S.; Fujinami, S.; Yamagishi, T.; Nakamoto, Y. Para-Bridged Symmetrical Pillar[5]Arenes: Their Lewis Acid Catalyzed Synthesis and Host-Guest Property. *J. Am. Chem. Soc.* **2008**, *130*, 5022–5023, doi:10.1021/ja711260m.
28. Ogoshi, T.; Hashizume, M.; Yamagishi, T.; Nakamoto, Y. Synthesis, Conformational and Host-Guest Properties of Water-Soluble Pillar[5]Arene. *Chem. Commun.* **2010**, *46*, 3708–3710, doi:10.1039/CoCC00348D.
29. Ogoshi, T.; Yamagishi, T. Pillararenes: Versatile Synthetic Receptors for Supramolecular Chemistry. *European J. Org. Chem.* **2013**, *2013*, 2961–2975, doi:https://doi.org/10.1002/ejoc.201300079.
30. Pisagatti, I.; Crisafulli, D.; Pappalardo, A.; Trusso Sfrazzetto, G.; Notti, A.; Nastasi, F.; Parisi, M.F.; Micali, N.; Gattuso, G.; Villari, V. Photoinduced Electron Transfer in Host-Guest Interactions of a Viologen Derivative with a Didansyl-Pillar[5]Arene. *Mater. Today Chem.* **2022**, *24*, 100841, doi:https://doi.org/10.1016/j.mtchem.2022.100841.
31. Barbera, L.; Franco, D.; De Plano, L.M.; Gattuso, G.; Guglielmino, S.P.P.; Lentini, G.; Manganaro, N.; Marino, N.; Pappalardo, S.; Parisi, M.F.; et al. A Water-Soluble Pillar[5]Arene as a New Carrier for an Old Drug. *Org. Biomol. Chem.* **2017**, *15*, 3192–3195, doi:10.1039/C7OB00530J.
32. Wang, K.; Jordan, J.H.; Velmurugan, K.; Tian, X.; Zuo, M.; Hu, X.-Y.; Wang, L. Role of Functionalized Pillararene Architectures in Supramolecular Catalysis. *Angew. Chemie Int. Ed.* **2021**, *60*, 9205–9214, doi:https://doi.org/10.1002/anie.202010150.
33. Li, Z.; Yang, Y.-W. Macrocyclic-Based Porous Organic Polymers for Separation, Sensing, and Catalysis. *Adv. Mater.* **2021**, *n/a*, 2107401, doi:https://doi.org/10.1002/adma.202107401.
34. Ji, X.; Wang, H.; Wang, H.; Zhao, T.; Page, Z.A.; Khashab, N.M.; Sessler, J.L. Removal of Organic Micropollutants from Water by Macrocyclic-Containing Covalent Polymer Networks. *Angew. Chemie Int. Ed.* **2020**, *59*, 23402–23412, doi:https://doi.org/10.1002/anie.202009113.
35. Hu, J.; Liu, S. Engineering Responsive Polymer Building Blocks with Host-Guest Molecular Recognition for Functional Applications. *Acc. Chem. Res.* **2014**, *47*, 2084–2095, doi:10.1021/ar5001007.
36. Fu, R.; Zhang, J.; Liu, S.; Xu, X.-D.; Feng, S. Facile Construction of a Double Network Cross-Linked Luminescent Supramolecular Elastomer by Hydrosilylation and Pillar[5]Arene Host-Guest Recognition. *Chem. Commun.* **2020**, *56*, 6719–6722, doi:10.1039/DoCC02214D.
37. Chang, J.; Zhao, Q.; Kang, L.; Li, H.; Xie, M.; Liao, X. Multiresponsive Supramolecular Gel Based on Pillararene-Containing Polymers. *Macromolecules* **2016**, *49*, 2814–2820.
38. Wu, J.; Xia, L.; Liu, Z.; Xu, Z.; Cao, H.; Zhang, W. Fabrication of a Dual-Stimuli-Responsive Supramolecular Micelle from a Pillar[5]Arene-Based Supramolecular Diblock Copolymer for Photodynamic Therapy. *Macromol. Rapid Commun.* **2019**, *40*, 1900240, doi:https://doi.org/10.1002/marc.201900240.
39. Yang, Y.; Yang, J.; Du, Y.; Li, C.; Wei, K.; Lu, J.; Chen, W.; Yang, L. Preparation and Characterization of Cationic Water-Soluble Pillar[5]Arene-Modified Zeolite for Adsorption of Methyl Orange. *ACS Omega* **2019**, *4*, 17741–17751, doi:10.1021/acsomega.9b02180.
40. Shi, B.; Guan, H.; Shanguan, L.; Wang, H.; Xia, D.; Kong, X.; Huang, F. A Pillar[5]Arene-Based 3D Network Polymer for Rapid Removal of Organic Micropollutants from Water. *J. Mater. Chem. A* **2017**, *5*, 24217–24222, doi:10.1039/C7TA08894A.
41. Wei, T.-B.; Qi, L.-H.; Zhang, Q.-P.; Zhang, W.-H.; Yao, H.; Zhang, Y.-M.; Lin, Q. Stimuli-Responsive Supramolecular Polymer Network Based on Bi-Pillar[5]Arene for Efficient Adsorption of Multiple Organic Dye Contaminants. *New J. Chem.* **2020**, *44*, 12531–12537, doi:10.1039/DoN102524K.
42. Zhang, G.; Lou, X.-Y.; Li, M.-H.; Yang, Y.-W. A Pillar[5]Arene-Based Crosslinked Polymer Material for Selective Adsorption of Organic Dyes. *Dye. Pigment.* **2022**, *206*, 110576, doi:https://doi.org/10.1016/j.dyepig.2022.110576.
43. Zhou, Y.; Zhang, G.; Li, B.; Wu, L. Two-Dimensional Supramolecular Ionic Frameworks for Precise Membrane Separation of Small Nanoparticles. *ACS Appl. Mater. Interfaces* **2020**, *12*, 30761–30769, doi:10.1021/acsaami.0c05947.
44. Dong, H.; Matyjaszewski, K. ARGET ATRP of 2-(Dimethylamino)Ethyl Methacrylate as an Intrinsic Reducing Agent. *Macromolecules* **2008**, *41*, 6868–6870, doi:10.1021/ma8017553.
45. Willott, J.D.; Humphreys, B.A.; Murdoch, T.J.; Edmondson, S.; Webber, G.B.; Wanless, E.J. Hydrophobic Effects within the Dynamic PH-Response of Polybasic Tertiary Amine Methacrylate Brushes. *Phys. Chem. Chem. Phys.* **2015**, *17*, 3880–3890, doi:10.1039/C4CP05292G.
46. Keating IV, J.J.; Lee, A.; Belfort, G. Predictive Tool for Design and Analysis of ARGET ATRP Grafting Reactions. *Macromolecules* **2017**, *50*, 7930–7939, doi:10.1021/acs.macromol.7b01572.
47. Zhao, Q.; Ni, P. Synthesis of Well-Defined and near Narrow-Distribution Diblock Copolymers Comprising PMMA and PDMAEMA via Oxyanion-Initiated Polymerization. *Polymer (Guildf).* **2005**, *46*, 3141–3148, doi:https://doi.org/10.1016/j.polymer.2005.01.089.
48. Ho, C.-C.; Su, J.F. Boosting Permeation and Separation Characteristics of Polyethersulfone Ultrafiltration Membranes by Structure Modification via Dual-PVP Pore Formers. *Polymer (Guildf).* **2022**, *241*, 124560, doi:https://doi.org/10.1016/j.polymer.2022.124560.
49. Zhu, L.-J.; Zhu, L.-P.; Zhao, Y.-F.; Zhu, B.-K.; Xu, Y.-Y. Anti-Fouling and Anti-Bacterial Polyethersulfone Membranes Quaternized from the Additive of Poly(2-Dimethylamino Ethyl Methacrylate) Grafted SiO₂ Nanoparticles. *J. Mater. Chem. A* **2014**, *2*, 15566–15574, doi:10.1039/C4TA03199G.
50. Geng, Z.; Wang, X.; Jiang, H.; Zhang, L.; Chen, Z.; Feng, Y.; Geng, W.; Yang, X.; Huo, M.; Sun, J. High-Performance TiO₂ Nanotubes/Poly(Aryl Ether Sulfone) Hybrid Self-Cleaning Anti-Fouling Ultrafiltration Membranes. *Polym.* **2019**, *11*.
51. Hossain, M.A.; Elias, M.; Rahman, M.M.; Rahman, M.M.; Ali, M.S.; Razzak, M.A. Multi-Phenyl Structured Aromatic Hydrocarbon Polymer. **2020**, *55*, 139–146.
52. Zhou, Y.; Hu, Y.; Huang, W.; Cheng, G.; Cui, C.; Lu, J. A Novel Amphoteric β -Cyclodextrin-Based Adsorbent for Simultaneous Removal of Cationic/Anionic Dyes and Bisphenol A. *Chem. Eng. J.* **2018**, *341*, 47–57, doi:https://doi.org/10.1016/j.cej.2018.01.155.

53. Yang, L.-P.; Zou, P.; Pan, C.-Y. Preparation of Hierarchical Worm-like Silica Nanotubes. *J. Mater. Chem.* **2009**, *19*, 1843–1849, doi:10.1039/B814617A.
54. Liu, Y.; Lou, B.; Shangguan, L.; Cai, J.; Zhu, H.; Shi, B. Pillar[5]Arene-Based Organometallic Cross-Linked Polymer: Synthesis, Structure Characterization, and Catalytic Activity in the Suzuki–Miyaura Coupling Reaction. *Macromolecules* **2018**, *51*, 1351–1356, doi:10.1021/acs.macromol.7b02701.
55. Amirabedi, P.; Yegani, R.; Razavi Aghje, M.K. Experimental Design Applied to Fabrication of PSf Membranes via NIPS Method Part I: Influential Parameters on Membrane Porosity and Mechanical Strength. *J. Text. Polym.* **2013**, *1*, 24–30.
56. Gardella, J.A.; Ferguson, S.A.; Chin, R.L. $\pi^* \leftarrow \pi$ Shakeup Satellites for the Analysis of Structure and Bonding in Aromatic Polymers by X-Ray Photoelectron Spectroscopy. *Appl. Spectrosc.* **1986**, *40*, 224–232.
57. Breite, D.; Went, M.; Thomas, I.; Prager, A.; Schulze, A. Particle Adsorption on a Polyether Sulfone Membrane: How Electrostatic Interactions Dominate Membrane Fouling. *RSC Adv.* **2016**, *6*, 65383–65391, doi:10.1039/C6RA13787C.
58. Chen, J.; Tendeyong, F.; Yiaccoumi, S. Equilibrium and Kinetic Studies of Copper Ion Uptake by Calcium Alginate. *Environ. Sci. Technol.* **1997**, *31*, 1433–1439, doi:10.1021/es9606790.
59. Moussout, H.; Ahlafi, H.; Aazza, M.; Maghat, H. Critical of Linear and Nonlinear Equations of Pseudo-First Order and Pseudo-Second Order Kinetic Models. *Karbala Int. J. Mod. Sci.* **2018**, *4*, 244–254, doi:https://doi.org/10.1016/j.kijoms.2018.04.001.
60. Jasper, E.E.; Ajibola, V.O.; Onwuka, J.C. Nonlinear Regression Analysis of the Sorption of Crystal Violet and Methylene Blue from Aqueous Solutions onto an Agro-Waste Derived Activated Carbon. *Appl. Water Sci.* **2020**, *10*, 132, doi:10.1007/s13201-020-01218-y.
61. López-Luna, J.; Ramírez-Montes, L.E.; Martínez-Vargas, S.; Martínez, A.I.; Mijangos-Ricardez, O.F.; González-Chávez, M. del C.A.; Carrillo-González, R.; Solís-Domínguez, F.A.; Cuevas-Díaz, M. del C.; Vázquez-Hipólito, V. Linear and Nonlinear Kinetic and Isotherm Adsorption Models for Arsenic Removal by Manganese Ferrite Nanoparticles. *SN Appl. Sci.* **2019**, *1*, 950, doi:10.1007/s42452-019-0977-3.
62. Allen, S.J.; Gan, Q.; Matthews, R.; Johnson, P.A. Kinetic Modeling of the Adsorption of Basic Dyes by Kudzu. *J. Colloid Interface Sci.* **2005**, *286*, 101–109, doi:https://doi.org/10.1016/j.jcis.2004.12.043.
63. Yu, K.L.; Lee, X.J.; Ong, H.C.; Chen, W.-H.; Chang, J.-S.; Lin, C.-S.; Show, P.L.; Ling, T.C. Adsorptive Removal of Cationic Methylene Blue and Anionic Congo Red Dyes Using Wet-Torrefied Microalgal Biochar: Equilibrium, Kinetic and Mechanism Modeling. *Environ. Pollut.* **2021**, *272*, 115986, doi:https://doi.org/10.1016/j.envpol.2020.115986.
64. Başar, C.A. Applicability of the Various Adsorption Models of Three Dyes Adsorption onto Activated Carbon Prepared Waste Apricot. *J. Hazard. Mater.* **2006**, *135*, 232–241, doi:https://doi.org/10.1016/j.jhazmat.2005.11.055.
65. Nešić, A.R.; Veličković, S.J.; Antonović, D.G. Modification of Chitosan by Zeolite A and Adsorption of Bezactive Orange 16 from Aqueous Solution. *Compos. Part B Eng.* **2013**, *53*, 145–151, doi:https://doi.org/10.1016/j.compositesb.2013.04.053.
66. Crini, G. Kinetic and Equilibrium Studies on the Removal of Cationic Dyes from Aqueous Solution by Adsorption onto a Cyclodextrin Polymer. *Dye. Pigment.* **2008**, *77*, 415–426, doi:https://doi.org/10.1016/j.dyepig.2007.07.001.
67. Pandey, S.; Son, N.; Kang, M. Synergistic Sorption Performance of Karaya Gum Crosslink Poly(Acrylamide-Co-Acrylonitrile) @ Metal Nanoparticle for Organic Pollutants. *Int. J. Biol. Macromol.* **2022**, *210*, 300–314, doi:https://doi.org/10.1016/j.ijbiomac.2022.05.019.
68. Hou, N.; Wang, R.; Wang, F.; Bai, J.; Zhou, J.; Zhang, L.; Hu, J.; Liu, S.; Jiao, T. Fabrication of Hydrogels via Host–Guest Polymers as Highly Efficient Organic Dye Adsorbents for Wastewater Treatment. *ACS Omega* **2020**, *5*, 5470–5479, doi:10.1021/acsomega.0c00076.
69. AlSawaftah, N.; Abuwatfa, W.; Darwish, N.; Hussein, G. A Comprehensive Review on Membrane Fouling: Mathematical Modelling, Prediction, Diagnosis, and Mitigation. *Water* **2021**, *13*.
70. Guo, W.; Ngo, H.-H.; Li, J. A Mini-Review on Membrane Fouling. *Bioresour. Technol.* **2012**, *122*, 27–34, doi:https://doi.org/10.1016/j.biortech.2012.04.089.
71. Ielo, I.; Giacobello, F.; Castellano, A.; Sfameni, S.; Rando, G.; Plutino, M.R. Development of Antibacterial and Antifouling Innovative and Eco-Sustainable Sol–Gel Based Materials: From Marine Areas Protection to Healthcare Applications. *Gels* **2022**, *8*.
72. Sfameni, S.; Rando, G.; Marchetta, A.; Scolaro, C.; Cappello, S.; Urzì, C.; Visco, A.; Plutino, M.R. Development of Eco-Friendly Hydrophobic and Fouling-Release Coatings for Blue-Growth Environmental Applications: Synthesis, Mechanical Characterization and Biological Activity. *Gels* **2022**, *8*.
73. Sfameni, S.; Rando, G.; Galletta, M.; Ielo, I.; Brucale, M.; De Leo, F.; Cardiano, P.; Cappello, S.; Visco, A.; Trovato, V.; et al. Design and Development of Fluorinated and Biocide-Free Sol–Gel Based Hybrid Functional Coatings for Anti-Biofouling/Foul-Release Activity. *Gels* **2022**, *8*.
74. Hadidi, M.; Zydney, A.L. Fouling Behavior of Zwitterionic Membranes: Impact of Electrostatic and Hydrophobic Interactions. *J. Memb. Sci.* **2014**, *452*, 97–103, doi:https://doi.org/10.1016/j.memsci.2013.09.062.
1. Tkaczyk, A.; Mitrowska, K.; Posyniak, A. Synthetic Organic Dyes as Contaminants of the Aquatic Environment and Their Implications for Ecosystems: A Review. *Sci. Total Environ.* **2020**, *717*, 137222, doi:https://doi.org/10.1016/j.scitotenv.2020.137222.
2. Trovato, V.; Mezzi, A.; Brucale, M.; Rosace, G.; Rosaria Plutino, M. Alizarin-Functionalized Organic-Inorganic Silane Coatings for the Development of Wearable Textile Sensors. *J. Colloid Interface Sci.* **2022**, *617*, 463–477, doi:https://doi.org/10.1016/j.jcis.2022.03.006.
3. Badawi, A.K.; Abd Elkodous, M.; Ali, G.A.M. Recent Advances in Dye and Metal Ion Removal Using Efficient Adsorbents and Novel Nano-Based Materials: An Overview. *RSC Adv.* **2021**, *11*, 36528–36553, doi:10.1039/D1RA06892J.
4. Ielo, I.; Giacobello, F.; Sfameni, S.; Rando, G.; Galletta, M.; Trovato, V.; Rosace, G.; Plutino, M.R. Nanostructured Surface Finishing and Coatings: Functional Properties and Applications. *Materials (Basel)*. **2021**, *14*, 1–41, doi:10.3390/ma14112733.

5. Rando, G.; Sfamini, S.; Galletta, M.; Drommi, D.; Cappello, S.; Plutino, M.R. Functional Nanohybrids and Nanocomposites Development for the Removal of Environmental Pollutants and Bioremediation. *Mol.* **2022**, *27*.
6. Wang, K.; Abdalla, A.A.; Khaleel, M.A.; Hilal, N.; Khraisheh, M.K. Mechanical Properties of Water Desalination and Wastewater Treatment Membranes. *Desalination* **2017**, *401*, 190–205, doi:https://doi.org/10.1016/j.desal.2016.06.032.
7. Otitoju, T.A.; Ahmad, A.L.; Ooi, B.S. Recent Advances in Hydrophilic Modification and Performance of Polyethersulfone (PES) Membrane via Additive Blending. *RSC Adv.* **2018**, *8*, 22710–22728, doi:10.1039/C8RA03296C.
8. Amiri, S.; Asghari, A.; Vatanpour, V.; Rajabi, M. Fabrication and Characterization of a Novel Polyvinyl Alcohol-Graphene Oxide-Sodium Alginate Nanocomposite Hydrogel Blended PES Nanofiltration Membrane for Improved Water Purification. *Sep. Purif. Technol.* **2020**, *250*, 117216, doi:https://doi.org/10.1016/j.seppur.2020.117216.
9. V. B., A.; Mohanty, S.; Nayak, S.K. Preparation and Characterization of Porous Polyethersulfone (PES) Membranes with Improved Biocompatibility by Blending Sulfonated Polyethersulfone (SPES) and Cellulose Acetate (CA) – A Comparative Study. *Mater. Today Commun.* **2020**, *25*, 101544, doi:https://doi.org/10.1016/j.mtcomm.2020.101544.
10. Wei, M.; Gao, Y.; Li, X.; Serpe, M.J. Stimuli-Responsive Polymers and Their Applications. *Polym. Chem.* **2017**, *8*, 127–143, doi:10.1039/C6PY01585A.
11. Bütün, V.; Armes, S.P.; Billingham, N.C. Synthesis and Aqueous Solution Properties of Near-Monodisperse Tertiary Amine Methacrylate Homopolymers and Diblock Copolymers. *Polymer (Guildf).* **2001**, *42*, 5993–6008, doi:https://doi.org/10.1016/S0032-3861(01)00066-0.
12. Yanfeng, C.; Min, Y. Swelling Kinetics and Stimuli-Responsiveness of Poly(DMAEMA) Hydrogels Prepared by UV-Irradiation. *Radiat. Phys. Chem.* **2001**, *61*, 65–68, doi:https://doi.org/10.1016/S0969-806X(00)00374-1.
13. Orakdogan, N. Novel Responsive Poly(N,N-Dimethylaminoethyl Methacrylate) Gel Beads: Preparation, Mechanical Properties and PH-Dependent Swelling Behavior. *J. Polym. Res.* **2012**, *19*, 9914, doi:10.1007/s10965-012-9914-5.
14. Zheng, J.Y.; Tan, M.J.; Thoniyot, P.; Loh, X.J. Unusual Thermogelling Behaviour of Poly[2-(Dimethylamino)Ethyl Methacrylate] (PDMAEMA)-Based Polymers Polymerized in Bulk. *RSC Adv.* **2015**, *5*, 62314–62318, doi:10.1039/C5RA12816A.
15. Liu, Y.; Li, J.; Ren, J.; Lin, C.; Leng, J. Preparation and in Vitro PH-Responsive Drug Release of Amphiphilic Dendritic Star-Block Copolymer Complex Micelles. *Mater. Lett.* **2014**, *127*, 8–11, doi:https://doi.org/10.1016/j.matlet.2014.04.070.
16. Manouras, T.; Koufakis, E.; Anastasiadis, S.H.; Vamvakaki, M. A Facile Route towards PDMAEMA Homopolymer Amphiphiles. *Soft Matter* **2017**, *13*, 3777–3782, doi:10.1039/C7SM00365J.
17. Marchal, F.; Roudot, A.; Pantoustier, N.; Perrin, P.; Daillant, J.; Guenoun, P. Emulsion Stabilization and Inversion Using a PH- and Temperature-Sensitive Amphiphilic Copolymer. *J. Phys. Chem. B* **2007**, *111*, 13151–13155, doi:10.1021/jp0749827.
18. Cao, Y.; Liu, N.; Fu, C.; Li, K.; Tao, L.; Feng, L.; Wei, Y. Thermo and PH Dual-Responsive Materials for Controllable Oil/Water Separation. *ACS Appl. Mater. Interfaces* **2014**, *6*, 2026–2030, doi:10.1021/am405089m.
19. Mathew, A.; Cao, H.; Collin, E.; Wang, W.; Pandit, A. Hyperbranched PEGmethacrylate Linear PDMAEMA Block Copolymer as an Efficient Non-Viral Gene Delivery Vector. *Int. J. Pharm.* **2012**, *434*, 99–105, doi:https://doi.org/10.1016/j.ijpharm.2012.05.010.
20. Deka, S.R.; Sharma, A.K.; Kumar, P. Cationic Polymers and Their Self-Assembly for Antibacterial Applications. *Curr. Top. Med. Chem.* **2015**, *15*, 1179–1195, doi:10.2174/1568026615666150330110602.
21. Rawlinson, L.-A.B.; O’Gara, J.P.; Jones, D.S.; Brayden, D.J. Resistance of Staphylococcus Aureus to the Cationic Antimicrobial Agent Poly(2-(Dimethylamino Ethyl)Methacrylate) (PDMAEMA) Is Influenced by Cell-Surface Charge and Hydrophobicity. *J. Med. Microbiol.* **2011**, *60*, 968–976, doi:https://doi.org/10.1099/jmm.0.025619-0.
22. Song, J.; Jung, Y.; Lee, I.; Jang, J. Fabrication of PDMAEMA-Coated Silica Nanoparticles and Their Enhanced Antibacterial Activity. *J. Colloid Interface Sci.* **2013**, *407*, 205–209, doi:https://doi.org/10.1016/j.jcis.2013.06.016.
23. Stawski, D.; Rolińska, K.; Zielińska, D.; Sahariah, P.; Hjálmsarsdóttir, M.Á.; Másson, M. Antibacterial Properties of Poly (N,N-Dimethylaminoethyl Methacrylate) Obtained at Different Initiator Concentrations in Solution Polymerization. *R. Soc. open Sci.* **2022**, *9*, 211367, doi:10.1098/rsos.211367.
24. Alotaibi, K.M.; Almethen, A.A.; Beagan, A.M.; Al-Swaidan, H.M.; Ahmad, A.; Bhawani, S.A.; Alswieleh, A.M. Quaternization of Poly(2-Diethyl Aminoethyl Methacrylate) Brush-Grafted Magnetic Mesoporous Nanoparticles Using 2-Iodoethanol for Removing Anionic Dyes. *Appl. Sci.* **2021**, *11*.
25. Ma, J.; Zhang, Y.; Zhao, B.; Jia, Q. Supramolecular Adsorbents in Extraction and Separation Techniques - A Review. *Anal. Chim. Acta* **2020**, *1122*, 97–113, doi:https://doi.org/10.1016/j.aca.2020.04.054.
26. Xue, M.; Yang, Y.; Chi, X.; Zhang, Z.; Huang, F. Pillararenes, A New Class of Macrocycles for Supramolecular Chemistry. *Acc. Chem. Res.* **2012**, *45*, 1294–1308, doi:10.1021/ar2003418.
27. Ogoshi, T.; Kanai, S.; Fujinami, S.; Yamagishi, T.; Nakamoto, Y. Para-Bridged Symmetrical Pillar[5]Arenes: Their Lewis Acid Catalyzed Synthesis and Host-Guest Property. *J. Am. Chem. Soc.* **2008**, *130*, 5022–5023, doi:10.1021/ja711260m.
28. Ogoshi, T.; Hashizume, M.; Yamagishi, T.; Nakamoto, Y. Synthesis, Conformational and Host-Guest Properties of Water-Soluble Pillar[5]Arene. *Chem. Commun.* **2010**, *46*, 3708–3710, doi:10.1039/C0CC00348D.
29. Ogoshi, T.; Yamagishi, T. Pillararenes: Versatile Synthetic Receptors for Supramolecular Chemistry. *European J. Org. Chem.* **2013**, *2013*, 2961–2975, doi:https://doi.org/10.1002/ejoc.201300079.
30. Pisagatti, I.; Crisafulli, D.; Pappalardo, A.; Trusso Sfrassetto, G.; Notti, A.; Nastasi, F.; Parisi, M.F.; Micali, N.; Gattuso, G.; Villari, V. Photoinduced Electron Transfer in Host-Guest Interactions of a Viologen Derivative with a Didansyl-Pillar[5]Arene. *Mater. Today Chem.* **2022**, *24*, 100841, doi:https://doi.org/10.1016/j.mtchem.2022.100841.
31. Barbera, L.; Franco, D.; De Plano, L.M.; Gattuso, G.; Guglielmino, S.P.P.; Lentini, G.; Manganaro, N.; Marino, N.; Pappalardo, S.; Parisi, M.F.; et al. A Water-Soluble Pillar[5]Arene as a New Carrier for an Old Drug. *Org. Biomol. Chem.* **2017**, *15*, 3192–3195, doi:10.1039/C7OB00530J.
32. Wang, K.; Jordan, J.H.; Velmurugan, K.; Tian, X.; Zuo, M.; Hu, X.-Y.; Wang, L. Role of Functionalized Pillararene

- Architectures in Supramolecular Catalysis. *Angew. Chemie Int. Ed.* **2021**, *60*, 9205–9214, doi:https://doi.org/10.1002/anie.202010150.
33. Li, Z.; Yang, Y.-W. Macrocyclic-Based Porous Organic Polymers for Separation, Sensing, and Catalysis. *Adv. Mater.* **2021**, *n/a*, 2107401, doi:https://doi.org/10.1002/adma.202107401.
34. Ji, X.; Wang, H.; Wang, H.; Zhao, T.; Page, Z.A.; Khashab, N.M.; Sessler, J.L. Removal of Organic Micropollutants from Water by Macrocyclic-Containing Covalent Polymer Networks. *Angew. Chemie Int. Ed.* **2020**, *59*, 23402–23412, doi:https://doi.org/10.1002/anie.202009113.
35. Hu, J.; Liu, S. Engineering Responsive Polymer Building Blocks with Host-Guest Molecular Recognition for Functional Applications. *Acc. Chem. Res.* **2014**, *47*, 2084–2095, doi:10.1021/ar5001007.
36. Fu, R.; Zhang, J.; Liu, S.; Xu, X.-D.; Feng, S. Facile Construction of a Double Network Cross-Linked Luminescent Supramolecular Elastomer by Hydrosilylation and Pillar[5]Arene Host-Guest Recognition. *Chem. Commun.* **2020**, *56*, 6719–6722, doi:10.1039/DoCC02214D.
37. Chang, J.; Zhao, Q.; Kang, L.; Li, H.; Xie, M.; Liao, X. Multiresponsive Supramolecular Gel Based on Pillararene-Containing Polymers. *Macromolecules* **2016**, *49*, 2814–2820.
38. Wu, J.; Xia, L.; Liu, Z.; Xu, Z.; Cao, H.; Zhang, W. Fabrication of a Dual-Stimuli-Responsive Supramolecular Micelle from a Pillar[5]Arene-Based Supramolecular Diblock Copolymer for Photodynamic Therapy. *Macromol. Rapid Commun.* **2019**, *40*, 1900240, doi:https://doi.org/10.1002/marc.201900240.
39. Yang, Y.; Yang, J.; Du, Y.; Li, C.; Wei, K.; Lu, J.; Chen, W.; Yang, L. Preparation and Characterization of Cationic Water-Soluble Pillar[5]Arene-Modified Zeolite for Adsorption of Methyl Orange. *ACS Omega* **2019**, *4*, 17741–17751, doi:10.1021/acsomega.9b02180.
40. Shi, B.; Guan, H.; Shangguan, L.; Wang, H.; Xia, D.; Kong, X.; Huang, F. A Pillar[5]Arene-Based 3D Network Polymer for Rapid Removal of Organic Micropollutants from Water. *J. Mater. Chem. A* **2017**, *5*, 24217–24222, doi:10.1039/C7TA08894A.
41. Wei, T.-B.; Qi, L.-H.; Zhang, Q.-P.; Zhang, W.-H.; Yao, H.; Zhang, Y.-M.; Lin, Q. Stimuli-Responsive Supramolecular Polymer Network Based on Bi-Pillar[5]Arene for Efficient Adsorption of Multiple Organic Dye Contaminants. *New J. Chem.* **2020**, *44*, 12531–12537, doi:10.1039/DoNj02524K.
42. Zhang, G.; Lou, X.-Y.; Li, M.-H.; Yang, Y.-W. A Pillar[5]Arene-Based Crosslinked Polymer Material for Selective Adsorption of Organic Dyes. *Dye. Pigment.* **2022**, *206*, 110576, doi:https://doi.org/10.1016/j.dyepig.2022.110576.
43. Zhou, Y.; Zhang, G.; Li, B.; Wu, L. Two-Dimensional Supramolecular Ionic Frameworks for Precise Membrane Separation of Small Nanoparticles. *ACS Appl. Mater. Interfaces* **2020**, *12*, 30761–30769, doi:10.1021/acsaami.0c05947.
44. Dong, H.; Matyjaszewski, K. ARGET ATRP of 2-(Dimethylamino)Ethyl Methacrylate as an Intrinsic Reducing Agent. *Macromolecules* **2008**, *41*, 6868–6870, doi:10.1021/ma8017553.
45. Willott, J.D.; Humphreys, B.A.; Murdoch, T.J.; Edmondson, S.; Webber, G.B.; Wanless, E.J. Hydrophobic Effects within the Dynamic PH-Response of Polybasic Tertiary Amine Methacrylate Brushes. *Phys. Chem. Chem. Phys.* **2015**, *17*, 3880–3890, doi:10.1039/C4CP05292G.
46. Keating IV, J.J.; Lee, A.; Belfort, G. Predictive Tool for Design and Analysis of ARGET ATRP Grafting Reactions. *Macromolecules* **2017**, *50*, 7930–7939, doi:10.1021/acs.macromol.7b01572.
47. Zhao, Q.; Ni, P. Synthesis of Well-Defined and near Narrow-Distribution Diblock Copolymers Comprising PMMA and PDMAEMA via Oxyanion-Initiated Polymerization. *Polymer (Guildf.)* **2005**, *46*, 3141–3148, doi:https://doi.org/10.1016/j.polymer.2005.01.089.
48. Ho, C.-C.; Su, J.F. Boosting Permeation and Separation Characteristics of Polyethersulfone Ultrafiltration Membranes by Structure Modification via Dual-PVP Pore Formers. *Polymer (Guildf.)* **2022**, *241*, 124560, doi:https://doi.org/10.1016/j.polymer.2022.124560.
49. Zhu, L.-J.; Zhu, L.-P.; Zhao, Y.-F.; Zhu, B.-K.; Xu, Y.-Y. Anti-Fouling and Anti-Bacterial Polyethersulfone Membranes Quaternized from the Additive of Poly(2-Dimethylamino Ethyl Methacrylate) Grafted SiO₂ Nanoparticles. *J. Mater. Chem. A* **2014**, *2*, 15566–15574, doi:10.1039/C4TA03199G.
50. Geng, Z.; Wang, X.; Jiang, H.; Zhang, L.; Chen, Z.; Feng, Y.; Geng, W.; Yang, X.; Huo, M.; Sun, J. High-Performance TiO₂ Nanotubes/Poly(Aryl Ether Sulfone) Hybrid Self-Cleaning Anti-Fouling Ultrafiltration Membranes. *Polym.* **2019**, *11*.
51. Hossain, M.A.; Elias, M.; Rahman, M.M.; Rahman, M.M.; Ali, M.S.; Razzak, M.A. Multi-Phenyl Structured Aromatic Hydrocarbon Polymer. **2020**, *55*, 139–146.
52. Zhou, Y.; Hu, Y.; Huang, W.; Cheng, G.; Cui, C.; Lu, J. A Novel Amphoteric β -Cyclodextrin-Based Adsorbent for Simultaneous Removal of Cationic/Anionic Dyes and Bisphenol A. *Chem. Eng. J.* **2018**, *341*, 47–57, doi:https://doi.org/10.1016/j.cej.2018.01.155.
53. Yang, L.-P.; Zou, P.; Pan, C.-Y. Preparation of Hierarchical Worm-like Silica Nanotubes. *J. Mater. Chem.* **2009**, *19*, 1843–1849, doi:10.1039/B814617A.
54. Liu, Y.; Lou, B.; Shangguan, L.; Cai, J.; Zhu, H.; Shi, B. Pillar[5]Arene-Based Organometallic Cross-Linked Polymer: Synthesis, Structure Characterization, and Catalytic Activity in the Suzuki-Miyaura Coupling Reaction. *Macromolecules* **2018**, *51*, 1351–1356, doi:10.1021/acs.macromol.7b02701.
55. Amirabedi, P.; Yegani, R.; Razavi Aghje, M.K. Experimental Design Applied to Fabrication of PSf Membranes via NIPS Method Part: Influential Parameters on Membrane Porosity and Mechanical Strength. *J. Text. Polym.* **2013**, *1*, 24–30.
56. Gardella, J.A.; Ferguson, S.A.; Chin, R.L. $\Pi^* \leftarrow \pi$ Shakeup Satellites for the Analysis of Structure and Bonding in Aromatic Polymers by X-Ray Photoelectron Spectroscopy. *Appl. Spectrosc.* **1986**, *40*, 224–232.
57. Breite, D.; Went, M.; Thomas, I.; Prager, A.; Schulze, A. Particle Adsorption on a Polyether Sulfone Membrane: How Electrostatic Interactions Dominate Membrane Fouling. *RSC Adv.* **2016**, *6*, 65383–65391, doi:10.1039/C6RA13787C.
58. Chen, J.; Tendeyong, F.; Yiaccoumi, S. Equilibrium and Kinetic Studies of Copper Ion Uptake by Calcium Alginate. *Environ. Sci. Technol.* **1997**, *31*, 1433–1439, doi:10.1021/es960679o.

59. Moussout, H.; Ahlafi, H.; Aazza, M.; Maghat, H. Critical of Linear and Nonlinear Equations of Pseudo-First Order and Pseudo-Second Order Kinetic Models. *Karbala Int. J. Mod. Sci.* **2018**, *4*, 244–254, doi:<https://doi.org/10.1016/j.kijoms.2018.04.001>.
60. Jasper, E.E.; Ajibola, V.O.; Onwuka, J.C. Nonlinear Regression Analysis of the Sorption of Crystal Violet and Methylene Blue from Aqueous Solutions onto an Agro-Waste Derived Activated Carbon. *Appl. Water Sci.* **2020**, *10*, 132, doi:[10.1007/s13201-020-01218-y](https://doi.org/10.1007/s13201-020-01218-y).
61. López-Luna, J.; Ramírez-Montes, L.E.; Martínez-Vargas, S.; Martínez, A.I.; Mijangos-Ricardez, O.F.; González-Chávez, M. del C.A.; Carrillo-González, R.; Solís-Domínguez, F.A.; Cuevas-Díaz, M. del C.; Vázquez-Hipólito, V. Linear and Nonlinear Kinetic and Isotherm Adsorption Models for Arsenic Removal by Manganese Ferrite Nanoparticles. *SN Appl. Sci.* **2019**, *1*, 950, doi:[10.1007/s42452-019-0977-3](https://doi.org/10.1007/s42452-019-0977-3).
62. Allen, S.J.; Gan, Q.; Matthews, R.; Johnson, P.A. Kinetic Modeling of the Adsorption of Basic Dyes by Kudzu. *J. Colloid Interface Sci.* **2005**, *286*, 101–109, doi:<https://doi.org/10.1016/j.jcis.2004.12.043>.
63. Yu, K.L.; Lee, X.J.; Ong, H.C.; Chen, W.-H.; Chang, J.-S.; Lin, C.-S.; Show, P.L.; Ling, T.C. Adsorptive Removal of Cationic Methylene Blue and Anionic Congo Red Dyes Using Wet-Torrefied Microalgal Biochar: Equilibrium, Kinetic and Mechanism Modeling. *Environ. Pollut.* **2021**, *272*, 115986, doi:<https://doi.org/10.1016/j.envpol.2020.115986>.
64. Başar, C.A. Applicability of the Various Adsorption Models of Three Dyes Adsorption onto Activated Carbon Prepared Waste Apricot. *J. Hazard. Mater.* **2006**, *135*, 232–241, doi:<https://doi.org/10.1016/j.jhazmat.2005.11.055>.
65. Nešić, A.R.; Veličković, S.J.; Antonović, D.G. Modification of Chitosan by Zeolite A and Adsorption of Bezactive Orange 16 from Aqueous Solution. *Compos. Part B Eng.* **2013**, *53*, 145–151, doi:<https://doi.org/10.1016/j.compositesb.2013.04.053>.
66. Crini, G. Kinetic and Equilibrium Studies on the Removal of Cationic Dyes from Aqueous Solution by Adsorption onto a Cyclodextrin Polymer. *Dye. Pigment.* **2008**, *77*, 415–426, doi:<https://doi.org/10.1016/j.dyepig.2007.07.001>.
67. Pandey, S.; Son, N.; Kang, M. Synergistic Sorption Performance of Karaya Gum Crosslink Poly(Acrylamide-Co-Acrylonitrile) @ Metal Nanoparticle for Organic Pollutants. *Int. J. Biol. Macromol.* **2022**, *210*, 300–314, doi:<https://doi.org/10.1016/j.ijbiomac.2022.05.019>.
68. Hou, N.; Wang, R.; Wang, F.; Bai, J.; Zhou, J.; Zhang, L.; Hu, J.; Liu, S.; Jiao, T. Fabrication of Hydrogels via Host–Guest Polymers as Highly Efficient Organic Dye Adsorbents for Wastewater Treatment. *ACS Omega* **2020**, *5*, 5470–5479, doi:[10.1021/acsomega.0c00076](https://doi.org/10.1021/acsomega.0c00076).
69. AlSawafah, N.; Abuwatfa, W.; Darwish, N.; Hussein, G. A Comprehensive Review on Membrane Fouling: Mathematical Modelling, Prediction, Diagnosis, and Mitigation. *Water* **2021**, *13*.
70. Guo, W.; Ngo, H.-H.; Li, J. A Mini-Review on Membrane Fouling. *Bioresour. Technol.* **2012**, *122*, 27–34, doi:<https://doi.org/10.1016/j.biortech.2012.04.089>.
71. Ielo, I.; Giacobello, F.; Castellano, A.; Sfameni, S.; Rando, G.; Plutino, M.R. Development of Antibacterial and Antifouling Innovative and Eco-Sustainable Sol–Gel Based Materials: From Marine Areas Protection to Healthcare Applications. *Gels* **2022**, *8*.
72. Sfameni, S.; Rando, G.; Marchetta, A.; Scolaro, C.; Cappello, S.; Urzì, C.; Visco, A.; Plutino, M.R. Development of Eco-Friendly Hydrophobic and Fouling-Release Coatings for Blue-Growth Environmental Applications: Synthesis, Mechanical Characterization and Biological Activity. *Gels* **2022**, *8*.
73. Sfameni, S.; Rando, G.; Galletta, M.; Ielo, I.; Brucale, M.; De Leo, F.; Cardiano, P.; Cappello, S.; Visco, A.; Trovato, V.; et al. Design and Development of Fluorinated and Biocide-Free Sol–Gel Based Hybrid Functional Coatings for Anti-Biofouling/Foul-Release Activity. *Gels* **2022**, *8*.
74. Hadidi, M.; Zydney, A.L. Fouling Behavior of Zwitterionic Membranes: Impact of Electrostatic and Hydrophobic Interactions. *J. Memb. Sci.* **2014**, *452*, 97–103, doi:<https://doi.org/10.1016/j.memsci.2013.09.062>.

CHAPTER 5

CONCLUSIONS AND FINAL REMARKS

In conclusion, this PhD thesis provides an overview of the state of the art on innovative water treatment solutions for emerging contaminants, as well as to describe recent research studies focused on it.

In particular, Chapter 2 describes different polyamide 11-based electrospun nanofiber membranes doped hybrid halloysite derivatives. All the developed membranes show some promising improvements of the tensile mechanical features. After dead-end filtration experiments, PA₁₁@C₁₈_HNT_NH₂ and PA₁₁@HNT_N+C₁₈ 1-layer ENMs revealed a selectivity towards the removal of the cationic dye MB with a separation efficiency of 69.8 and 73.3 % respectively, at a constant flux of 10 mL·min⁻¹ (209 L·m⁻²·h⁻¹). Hence, PA₁₁@HNT_NH₂ 3-layer ENMs displayed the highest retention rate for MO and MB of 100 and 89.8%, respectively.

The morphology, wettability behavior, mechanical tensile and thermal properties of obtained pristine and doped PA₁₁ and PA₁₁/chitosan electrospun nanofiber composite membranes were also investigated, demonstrating a quite good improvement of characteristics via the synergistic effects of cationic and hydroxyl group rich chitosan biopolymer, good mechanical properties of PA₁₁ and PE support, and ultimately the functionalities of hybrid halloysite derivatives. All experimental findings also demonstrated a reduction in nanofiber quality and features with a larger chitosan ratio in the biopolymeric blend (70:30).

In Chapter 3 the development of innovative cellulose-derived conveniently functionalized products, which were employed as dopant agents for water-based polyvinyl alcohol solutions for different electrospun nanofiber composite membranes, is described. Mechanical tensile

characteristics showed improved results in terms of maximum stress and elongation at break value. All of the membranes were evaluated in a dead-end filtration cell with gravity-driven separation of a methylene blue and methyl orange mixed solution ($[MO] = [MB] = 2.5 \text{ mg}\cdot\text{L}^{-1}$; $V_{\text{tot}} = 50 \text{ mL}$), indicating selectivity for the removal of the cationic dye MB. The top performing membranes were PVA@MCC and PVA@MCC_GPTMS_HNT, with retention rates of 93.4% and 79.9%, separation efficiencies of 93.5% and 82.1%, and fluxes of 501.7 and 133.7 $\text{L}\cdot\text{m}^{-2}\cdot\text{h}^{-1}$, respectively. Biochar was functionalized with NZVI and examined in batch studies for MB removal. The Langmuir adsorption isotherm model, with a calculated high maximum sorption capacity (q_m) of 305.65 $\text{mg}\cdot\text{g}^{-1}$ for MB, better represented the sorption behaviour of the obtained magnetic composite that could be easily recovered and regenerated.

Chapter 4 reports the design and development of new polyether sulfone blends coupled with new innovative smart polymers combining the responsiveness of poly[2-(dimethylamino)ethyl methacrylate] polymer and the host-guest properties of the covalently linked pillararene macrocycles. Beads produced by a NIPS method starting from these polymeric blends, were first characterized and then tested for the removal of MB and MO from water. The P5-QPDMAEMA based beads showed qualitatively not only the best MO removal, but also a strong selectivity towards the removal of the anionic dye. B-P5QP(a) beads ($\approx 60 \text{ mg}$) were found to have removal rates and adsorption capacities of 91.3% and 3.06 $\text{mg}\cdot\text{g}^{-1}$, respectively, for 10 mL of a 20 $\text{mg}\cdot\text{L}^{-1}$ MO solution. An adsorption capacity of 14.91 $\text{mg}\cdot\text{g}^{-1}$ was attained after 5h of contact time with a 300 $\text{mg}\cdot\text{L}^{-1}$ MO solution. The effects of MO concentration, adsorbent amount, and contact time of B-P5QP(a) bead were examined. The pseudo-first order and Freundlich models were found to best describe the MO adsorption behaviour of B-P5QP(a) bead in adsorption kinetics and isotherm calculations with a q_m of 21.54 $\text{mg}\cdot\text{g}^{-1}$. Its adsorption performance can be described through a physio/chemisorption process involving a multilayer heterogeneous surface. With the aim to reduce the fouling problem in the filtration technology field, B-P(zw) and B-P5QP(zw) zwitterionic beads were produced. The latter showed a significant capacity for the removal of both cationic and anionic dyes. The assessment of the antifouling capability will be explored in future work.

Moreover, on the light of the showed experimental results achieved in this PhD thesis work, some observations and remarks can be outlined.

Recent nanotechnological and sustainable approaches in environmental remediation and treatment are the answers of researcher activities to the challenges of more efficient, green, and reusable water treatment procedures against common and new emerging contaminants.

As a matter of fact, nanotechnologies and novel nanomaterials are already being effectively used for water treatment in a wide range of industrial processes, thanks to their peculiar characteristics, including high surface area (surface/volume ratio), size effects, catalytic capability, and reactivity.

Moreover, nanomaterials may take advantages by:

- (i) tunable chemical modification and functionalization leading to new or implemented shapes and properties;
- (ii) their embedding in different (bio)polymers and matrices to produce (multi) functional hybrid materials or nanocomposites with even more enhanced physical, chemical, and mechanical properties when compared with the two separate starting

building blocks.

Nowadays many researcher efforts are devoted to the development of more and more sustainable and innovative products/technologies with potential application in interesting cross industrial sectors for human life, among them also environmental remediation and protection (Figure 5.1).

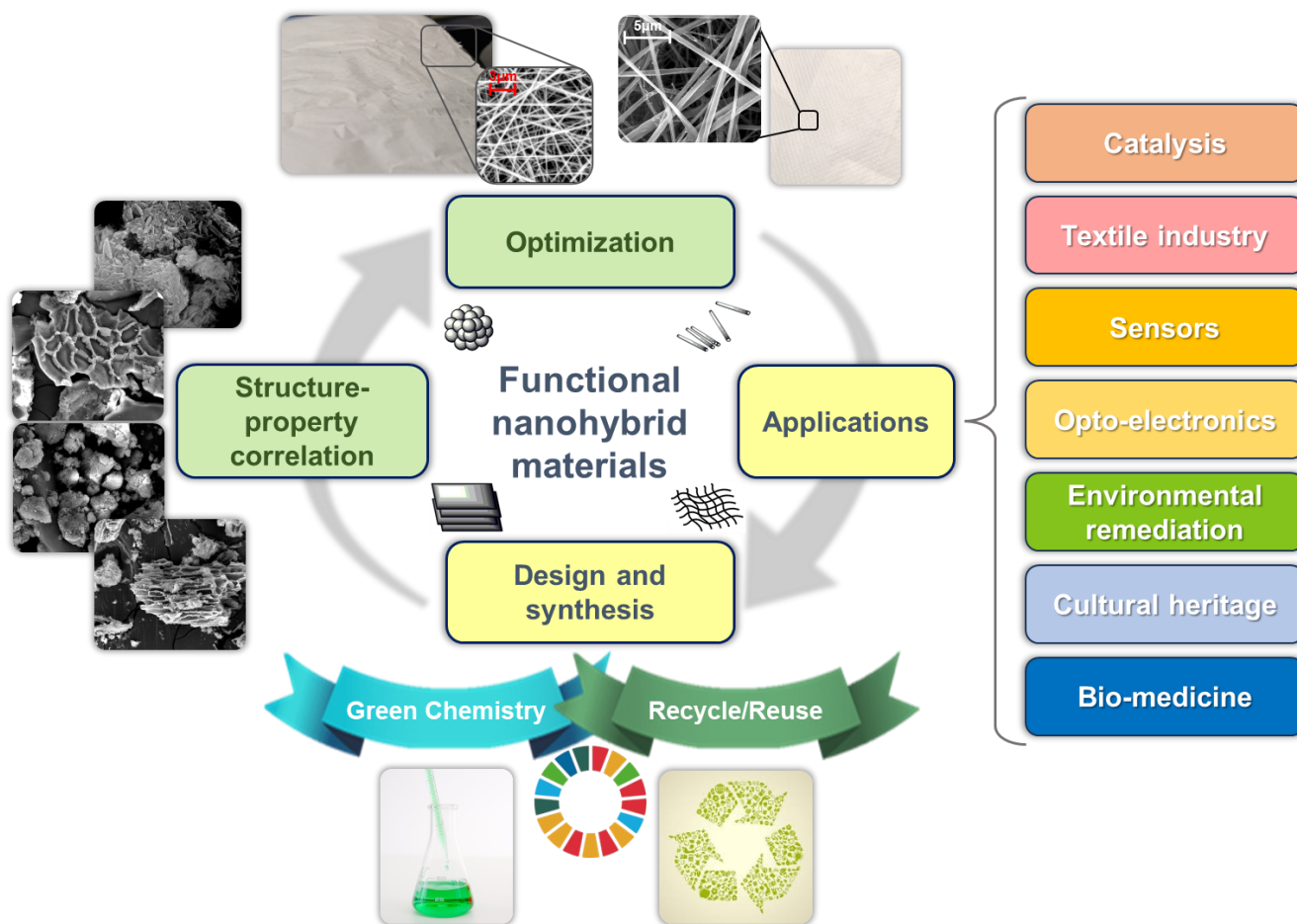


Figure 5.1. Graphical schematization of the development and application phases of functional hybrid materials.

In particular, functional nanohybrids and nanocomposites have shown several clear and distinct advantages (Figure 5.2), including:

- simple preparation using environmentally friendly methods;
- practically limitless functionalization possibilities;
- versatility in terms of shape and application forms;
- selectivity of adsorption;
- good stability;
- ability to be reused for numerous cycles of adsorption;
- possibility to be regenerated;
- applicability in bioremediation processes;
- ability to perform catalytic degradation processes;
- less hazardous than pure nanomaterials avoiding their dispersion.

In this regard, environmentally friendly membrane-based filtration technologies are explored and presented, along with it is well described how they may be modified through safe-by-design approaches and nanotechnology knowledge to control their hydrophilicity, porosity, mechanical and surface properties, and adsorption capabilities.

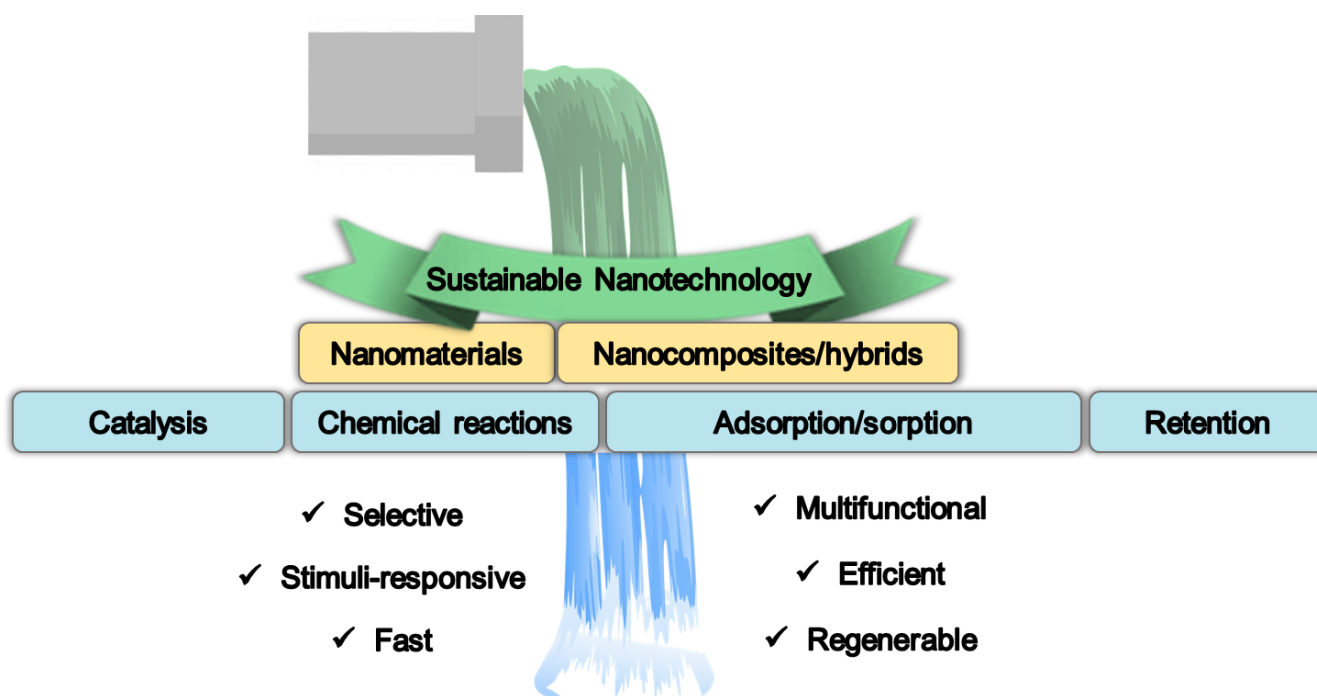


Figure 5.2. Advantages of nanocomposite/nanohybrid materials for water purification.

As a result, within the frame of the “RESTART” 2014-2020 PON-MIUR project, the synthetic steps starting by biopolymer-based or water-based blends are discussed, as well their functionalization with cross-linkers, nano/micro-fillers, stimuli-responsive polymers, or their preparation with innovative methods like electrospinning.

Two main sustainable approaches of electrospun membrane fabrication and functionalization with different additives (i.e., halloysite, microcrystalline cellulose and biochar derivatives) are presented to address the question of whether it is possible to combine greener and cleaner processes for eco-friendly water treatment technology, overcoming the limitations of waterborne (bio)polymers compared to fossil-based polymers.

In particular, some of the reported studies deal with the development of:

- different bio-polymer (polyamide 11 and chitosan) or waterborne doped polymer-based (polyvinyl alcohol) membranes prepared by the electrospinning technique;
- different functional electrospun nanofiber-based composite membranes prepared by electrospinning on selected supports (i.e., polyester calendared and non-woven glass fiber supports).

All experimental results emphasized some of the advantages of electrospun nanofiber membranes, as following:

- high tensile strength;
- high operational flux;

- high porosity;
- large specific surface area;
- modifiable functionalities;
- modifiable nanofiber dimensions;
- possible simple post-functionalization;
- long-lasting operations;
- the capacity to remove various contaminants from water;
- superior antibacterial/anti-fouling properties;
- ease of reusability;
- simplicity of management.

In particular, electrospun nanofiber composite membranes obtained on selected supports revealed advantages in term of easy of management and handling and increased mechanical properties and resistance making easier the possible scale up of the prototypal systems compared to not composite nanofiber membranes. Moreover, thanks to the innovative electrospinning production system employed, as the large rotating drum equipped with oscillating carriages, large membranes were developed make them suitable for the development of prototypes based on commercially available cartridges for wastewater remediation.

Another aspect that is object of the present PhD thesis concern the development of secondary-raw materials from natural and abundant bio-based resource as Spanish broom in order to reduce the use of critical raw-materials for a more sustainable production.

Microcrystalline cellulose and biochar were effectively obtained from this renewable source and modified according to easy, one-pot and sustainable procedures by means of alkoxysilane cross-linkers, halloysite, β -cyclodextrin, citric acid and nano zero-valent iron functional agents.

The obtained functional additives were embedded in water-based polyvinyl alcohol blends to obtain electrospun nanofiber composite membranes with excellent gravity-driven selective separation capabilities of cationic organic dyes. The features of the obtained membranes make them as good candidates, together with the previous described membranes, for the efficient purification of wastewaters from emerging contaminants.

Moreover, another study is focused on the development of a smart system based on a stimuli-responsive polymer (i.e., PDMAEMA) and a host-guest macrocyclic compound (i.e., pillar[5]arenes) by its blending in a polyether sulfone solution; these polymeric functional smart materials are investigated, thus demonstrating the effective formation of innovative polymeric beads, through the non-solvent induced phase separation process, suitable for the selective removal of anionic dyes from water. These systems in the form of beads could be employed for ex-situ remediation of polluted water by their dispersion in tanks containing the water to be treated for the adsorption of target contaminants. Their shape and form permit to be recovered for the possible regeneration and reuse for more cycle of adsorption. This feature will be studied in future experiments.

As a result, from all experimental evidence, it is possible to highlight that the rational design of initial polymeric and blends with appropriate nanofillers or functional agents is crucial to achieving membranes and systems with implemented mechanical, thermic, and chemical

resistance, as well as different pollutant retention properties.

Moreover, it is demonstrated how it is possible to develop innovative and sustainable solutions for the removal of common and emerging pollutants from contaminated water using safe-by-design functional composite and hybrid materials and technologies for more effective, low-consumption, and environmentally friendly treatment processes.

In particular, all experimental findings confirm that the use of bio-based or water-based polymeric formulations developed within this PhD thesis (funded by the “RESTART” 2014-2020 PON-MIUR project) may give raise to:

- an implementation of these environmentally friendly synthetic and treatment methods, on a large scale for the filtration of industrial, municipal, and agriculture (waste)waters or contaminated ground waters;
- rational and more efficient substitution of the traditional, more harmful fossil-based actually employed membrane technologies;
- moving towards a sustainable Industry 5.0.

In Figure 5.3 is illustrated the whole research activity.



Figure 5.3. Illustration of the whole research activity described within this PhD thesis as funded by the “RESTART” 2014-2020 PON-MIUR project.

To sum up, with these findings, we have only begun to discover the different possibilities of development and application of (multi)functional and (multi)component materials for the development of innovative and highly technological filtration systems based on membranes, and we will continue to work in this area by optimizing these systems also in the framework of ongoing funded projects.

CHAPTER 6

MATERIALS AND METHODS

6.1 Chapter 2: Experimental section¹

6.1.1. Materials

All materials and reagents were obtained from commercial suppliers for direct use unless mentioned. Halloysite, octadecylphosphonic acid, (3-aminopropyl)triethoxysilane, octyl/decyl glycidyl ether, dodecyl and tetradecyl glycidyl ethers, dimethyloctadecyl[3(trimethoxysilyl)propyl]ammoniumchloride (42 wt.% in methanol), polyamide 11, anisole, ethanol (absolute), formic acid and glacial acetic acid were all purchased from Sigma Aldrich at the highest purity level and used without any additional purification.

6.1.2. Synthetic procedures

6.1.2.1 *Halloysite functionalization with APTES (HNT-NH₂)*

(3-aminopropyl)triethoxysilane was employed to functionalize halloysite following a literature procedure [1] gaining the HNT-NH₂ derivative.

9 g of APTES were poured in 300 mL of EtOH (95%) and pH is adjusted between 4.5 and 5.5 (with 8 mL of glacial acetic acid).

¹ It refers to paragraph 2.2

Then, 30 g of HNT were added to this mixture. The system was left under stirring for two hours at 60°C before the product was recovered using Büchner filtration with a cellulose nitrate filter and washed with ethanol several times.

6.1.2.2 Halloysite functionalization with octadecylphosphonic acid and APTES (C18_HAL_NH₂)

Halloysite was dried out for 72 hours at 60°C. Following this, octadecylphosphonic acid (C18) was used to modify the HNT nanotube lumen in accordance with a method described in the literature [2]. For instance, 500 mg of halloysite was suspended in 500 mL of an EtOH/H₂O 4:1 v/v solution (pH 4 by acetic acid), along with 2 mmol of C18. The solution was allowed to get into the halloysite lumen by applying vacuum to the flask ten times with a water pump. The reaction was left to run for 7 days at room temperature with magnetic stirring. The product was dried at 60°C for 24 hours after being filtered through cellulose acetate filters on a Büchner filter.

The identical process outlined above was carried out to functionalize the C18_HNT with APTES (Figure 6.1). Then, 100 µL of APTES was reacted with 350 mg of C18_HNT in 5 mL of EtOH/H₂O 19:1 v/v (pH range of 4.5–5.5 for acetic acid). The reaction was allowed to proceed for 24 hours at 60°C. The product was then filtered using a Büchner filter on cellulose acetate filters, washed with ethanol, and left to dry for three days at 80°C in an oven.

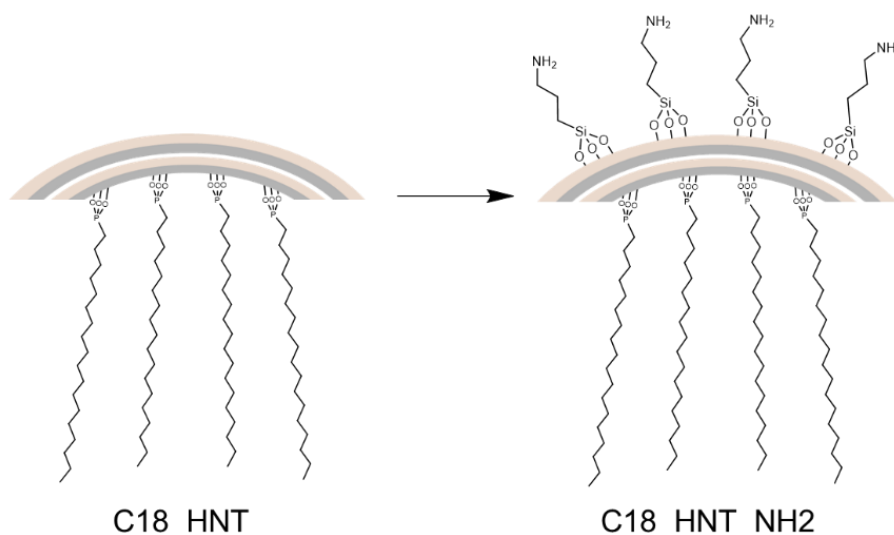


Figure 6.1. Graphical representation of C18_HNT and C18_HNT_NH₂ hybrid halloysite derivatives.

6.1.2.3 HNT_NH₂ functionalization with octyl/decyl glycidyl ether and dodecyl and tetradecyl glycidyl ethers (HNT_NH_C8-C10 and HNT_NH_C12-C14)

The derivative HNT_NH₂ was functionalized using octyl/decyl glycidyl ether and dodecyl and tetradecyl glycidyl ethers to generate the two hybrids HNT_NH_C8-C10 and HNT_NH_C12-C14 (Figure 6.2).

For each experiment, 10 g of HNT_NH₂ were combined with 3 mL of either C8-C10 or C12-C14 in a 100 mL H₂O/EtOH 10:1 v/v solution, and the mixture was stirred magnetically at 60 °C for five hours. The entire mixture was left three days to dry and curing in an oven set at 80°C.

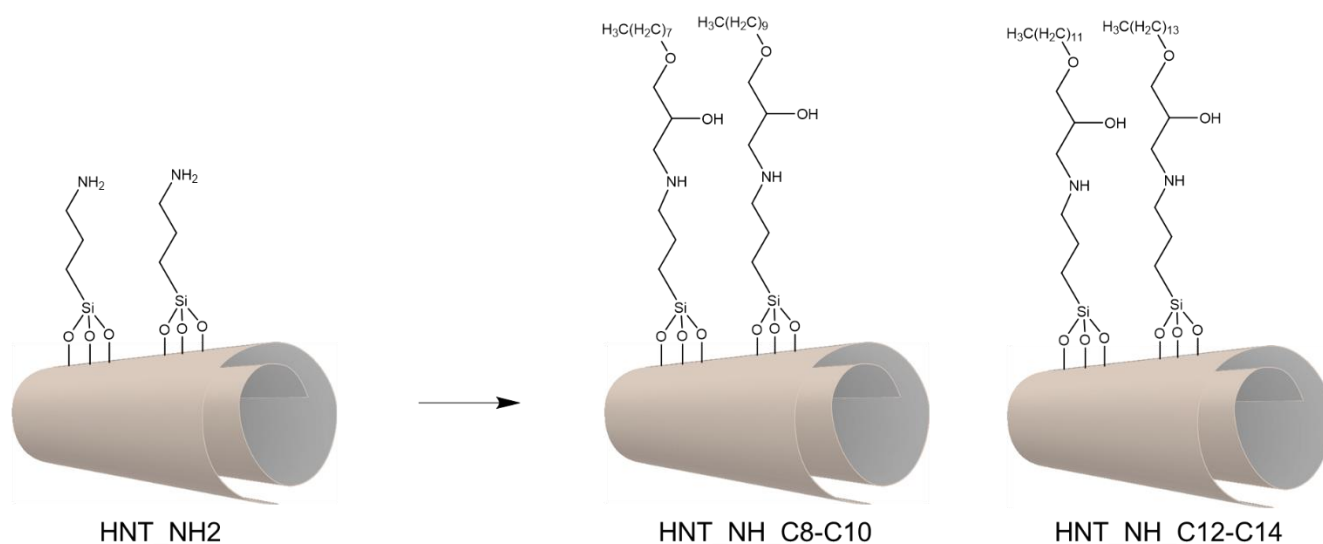


Figure 6.2. Graphical representation of HNT_NH_C8-C10 and HNT_NH_C12-C14 hybrid halloysite derivatives.

6.1.2.4 HNT functionalization with dimethyloctadecyl[3(trimethoxysilyl)propyl] ammoniumchloride (HNT_N+C18)

1.5 g of halloysite was mixed in 180 mL of an EtOH/H₂O 1:1 v/v solution for the functionalization of HNT with dimethyloctadecyl[3(trimethoxysilyl)propyl] ammoniumchloride solution (Figure 6.3). The mixture was stirred continuously for 24 hours at room temperature following the addition of 3 mL of N+C18 (2.2 mmol). The product was washed using a Büchner filter on cellulose acetate filters, then it was washed with ethanol and dried for three days at 80°C in an oven.

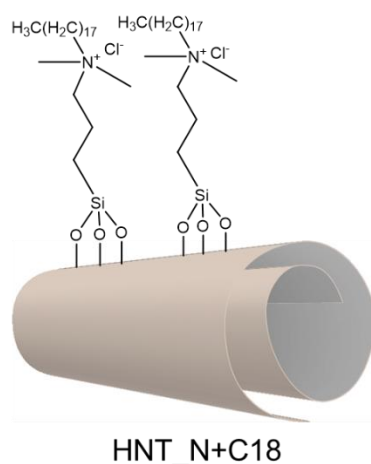


Figure 6.3. Graphical representation of HNT_N+C18 hybrid halloysite derivative.

6.1.3. Chemical-physical measurement and characterization

The chemical structure of the resulting hybrid materials was determined using Fourier transform infrared analysis (ATR FT-IR). FT-IR spectra were collected using a V-6600 Jasco Spectrometer (JASCO Europe s.r.l., Cremella, LC, Italy), equipped with the Spectra Manager™ Suite with integrated search software solution, KnowItAll® Informatics, and database JASCO

Edition (JASCO Europe s.r.l., Cremella, LC, Italy). Spectra were acquired at RT at a resolution of 4 cm^{-1} , employing a total of 32 scans per data set, and a range of $4000\text{--}500 \text{ cm}^{-1}$.

The structural data of the synthesized hybrid materials were studied by X-ray diffraction analysis (XRD) using the following parameters: 40 V, RT, 40 mA, range $10^\circ\text{--}80^\circ$ with a step of $0.2^\circ/\text{s}$. BrukerD8 Advance diffractometer (Bruker, Karlsruhe, Germany) with a Bragg–Brentano theta-2theta configuration and Cu K α radiation.

The morphology of pristine and hybrid halloysite derivatives and electrospun nanofiber membranes was studied by Scanning Electron Microscopy (SEM) employing a FEI Quanta 200 F SEM (Hillsboro, Oregon, USA) at an accelerating voltage of 20 kV.

A FEI Phenom XL tabletop SEM (Thermo Fisher Scientific, Massachusetts, United States) was also employed for the nanofiber diameters analysis with an at an accelerating voltage of 15 kV, using Phenom FiberMetric software. Prior to analysis, the samples were coated with gold using a sputter coater (LOT-Quantum Design). The average diameters and their standard deviations were expressed as $\sigma/2$ are based on at least 200 measurements per sample.

An Optical Contact Angle 25 setup from DataPhysics (Filderstadt, Germany) was used to study the static contact angles and wettability of the membranes. Droplets of $2 \mu\text{L}$ deionized water were dropped onto the membrane surface (25°C , $30 \pm 10\%$ relative humidity). Average initial contact angles and standard deviations (expressed as $\sigma/2$) were measured using the OCA 25 software.

A Dynamic mechanical analysis (DMA Q800 TA Instruments, New Castle, United States) was used to determine the mechanical tensile properties of the membranes performing three measurements for each sample (gauge length of $\sim 1 \text{ cm}$ and a width of $\sim 0.5 \text{ cm}$) with a strain rate of 5 \% min^{-1} . Standard deviations were expressed as $\sigma/2$. A high precision digital coating thickness gauge was used to measure the thickness of the membranes.

A Differential Scanning Calorimetry (DSC Q2000 TA Instruments, New Castle, United States) equipped with DSC Standard Cell RC and RCS 90 cooling unit, was used to study the thermal properties of the membranes performing a $20^\circ\text{C}\cdot\text{min}^{-1}$ heating ramp from 40 to 350°C , a $20^\circ\text{C}\cdot\text{min}^{-1}$ cooling until 40°C and a second heating ramp of $20^\circ\text{C}\cdot\text{min}^{-1}$ from 40 to 350°C . A T_{zero} aluminium pan and a nitrogen flow of $50.0 \text{ mL}\cdot\text{min}^{-1}$ were employed to perform three measurements for each sample. Standard deviations were expressed as $\sigma/2$.

6.1.4. Filtration studies

A dead-end filtration cell (Amicon Stirred Cell 200mL, Merck KGaA, Darmstadt, Germany) with a filtration area of 28.7 cm^2 was used to examine the filtering abilities of the nanofiber membranes. The ENMs underwent a pretreatment with 100 mL of deionized water before being tested for the elimination of the two target organic dyes. Then, MO and MB solutions were combined in the same ratio ($V_{\text{tot}} = 50 \text{ mL}$; $[\text{MB}] = [\text{MO}] = 2.5 \text{ mg}\cdot\text{L}^{-1}$) and the mixture was filtered at a constant rate of $10 \text{ mL}\cdot\text{min}^{-1}$ ($209 \text{ L}\cdot\text{m}^{-2}\cdot\text{h}^{-1}$) under nitrogen pressure. Following filtration, the UV-vis spectrophotometer was used to measure the organic dye concentrations, and equation 1 was used to compute the retention rates of the two tested organic dyes.

$$\text{Retention rate} = \frac{C_f - C_p}{C_f} \times 100 \quad (1)$$

Meanwhile the separation efficiency was determined by equation 2:

$$\text{Separation efficiency} = \frac{C_{MO_f}}{C_{MO_f} + C_{MB_f}} \times 100 \quad (2)$$

where C_f is the concentration of feed, and C_p is the concentration of permeate.

Measurements of UV-Vis spectroscopy were made using a Jasco V-770 UV-Vis spectrophotometer (JASCO Europe s.r.l., Cremella, LC, Italy) equipped with common measurement and analysis programmes and the Spectra Manager™ Suite Spectroscopy Software (JASCO Europe s.r.l., Cremella, Italy), at 25°C, in the spectral range of 300 to 800 nm.

6.2. Chapter 2: Experimental section²

6.2.1. Materials

All materials and reagents were obtained from commercial suppliers for direct use unless mentioned. (3-aminopropyl)triethoxysilane, octyl/decyl glycidyl ether, polyamide 11, ethanol, glacial acetic acid, anisole, dimethyloctadecyl[3(trimethoxysilyl)propyl]ammoniumchloride, formic acid were all purchased at the highest purity level at Sigma Aldrich and employed as received without any additional purification.

Chitosan (100.000–300.000 Da) was purchased at the highest purity level at Acros Organics and used as received without any further purification.

Polyester calendered fabrics (Fibertex VIGONIT 30), mass per unit area $30 \pm 3 \text{ g}\cdot\text{m}^2$, thickness 0.2 ± 0.1 were gently conferred from Fibertex Elephant España, S.L.U.

6.2.2. Synthetic procedures

6.2.2.1 *Synthesis of HNT_NH₂, HNT_NH_C8-C10, HNT_N+_C18 halloysite derivatives*

The three halloysite derivatives HNT_NH₂, HNT_NH_C8-C10, HNT_N+_C18 were synthesized according to the procedures described in paragraphs 6.1.2.1, 6.1.2.3 and 6.1.2.4, respectively.

6.2.3. Chemical-physical measurement and characterization

Scanning electron microscopy (SEM) was performed by the FEI Quanta 200 F SEM (Hillsboro, Oregon, USA) to analyse electrospun nanofiber composite membranes at a 20 kV accelerating voltage. A FEI Phenom XL tabletop SEM (Thermo Fisher Scientific, Massachusetts, United States) outfitted with Phenom FiberMetric software was used to measure the nanofiber diameter at a 15 kV accelerating voltage. Before analysis, the samples were coated with gold using a sputter coater (LOT-Quantum Design). For estimations of average diameter, at least 50 measurements of each sample were performed (standard deviations were denoted as $\sigma/2$).

² It refers to paragraph 2.3

A DataPhysics (Filderstadt, Germany) OCA 25 contact angle setup was used to test the wettability of the electrospun nanofiber membranes (without the PE support). For this analysis 2 μL of deionized water were poured to the nanofiber mat on the aluminium foil At room temperature (25 °C, 30% 10% relative humidity). The average contact angles and standard deviations, denoted as $\sigma/2$, were computed using the OCA 25 programme.

The tensile mechanical properties of the electrospun nanofiber composite membranes were analysed by a DMA Q800 (TA Instruments, New Castle, United States) performing three measurements for each sample (gauge length of ~ 1 cm and a width of ~ 0.5 cm) with a strain rate of 5 % min^{-1} (standard deviations were expressed as $\sigma/2$). A high accuracy digital coating thickness gauge was used to test the thickness of the membranes.

The thermal properties of the electrospun nanofiber composite membranes were determined with a DSC Q2000 (TA Instruments, New Castle, United States) equipped with DSC Standard Cell RC and RCS 90 cooling unit, performing a 20 °C $\cdot\text{min}^{-1}$ heating ramp from 40 to 350 °C, a 20 °C $\cdot\text{min}^{-1}$ cooling until 40 °C and a second heating ramp of 20 °C $\cdot\text{min}^{-1}$ from 40 to 350 °C. Measurements were performed using a T_{zero} aluminium pan and a nitrogen flow of 50.0 mL $\cdot\text{min}^{-1}$ (standard deviations were expressed as $\sigma/2$).

6.3. Chapter 3: Experimental section

6.3.1. Materials

All materials and reagents were obtained from commercial suppliers for direct use unless mentioned. (3-glycidyoxypropyl)trimethoxy silane, sodium dihydrogen phosphate monohydrate, citric acid, polyethylene glycol (PEG), halloysite, poly(vinyl alcohol) (Mw: 89,000-98,000, 99+% hydrolyzed), (3-mercaptopropyl)trimethoxysilane, iron(III) chloride, sodium borohydride, sodium hypochlorite (6-14% of active chlorine), sodium hydroxide, hydrochloric acid, ethanol (absolute), were all purchased at the highest purity level at Sigma Aldrich and used as received without any further purification.

The non-woven glass fiber support (30 g $\cdot\text{m}^{-2}$) was purchased from R&G Faserverbundwerkstoffe GmbH (Waldenbuch, Germany).

6.3.2. Synthetic procedures

6.3.2.1 *Spanish broom pre-treatment*

Spanish broom stems (*Spartium junceum* vermene) were collected in Messina, Sicily, Italy and sliced into 2 cm pieces. 100g of slices were boiled in 1L of distilled water for 1 hour, then placed in 500 mL of fresh water changed every day for 6 days. The macerated product was then dried at 60 °C for 24 hours before being triturated in a disintegrator for 15 minutes.

The resultant powder (10.2363 g) and straws (25.8568 g) were separated using a 200 m sieve (Figure 6.4).

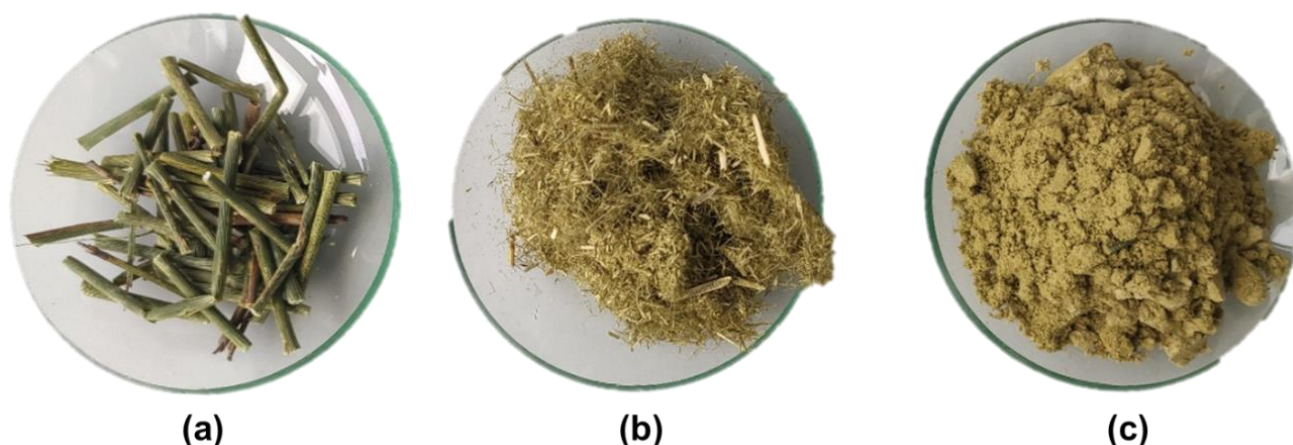


Figure 6.4. Digital photographs of Spanish broom stems after maceration and drying (a); straws (b) and powder (c) produced following disintegration and separation by sieving.

6.3.2.2 Microcrystalline cellulose preparation from Spanish broom powder

Alkali treatment. 20 g of powder was alkali treated with 800 mL ($40 \text{ mL}\cdot\text{g}^{-1}$) of 0.5 N NaOH for 1h at boiling temperature, in accordance with a process described in the literature [3]. The final product was centrifuged at 5000 rpm for five minutes before being repeatedly washed with distilled water to achieve pH neutrality. The powder was dried 12h at 60°C .

Bleaching. 15 g of alkali treated powder were poured in 600 mL of distilled water ($40 \text{ mL}\cdot\text{g}^{-1}$) with 30 g sodium hypochlorite ($2 \text{ g}\cdot\text{g}^{-1}$ of fibres) and 18 mL of acetic acid ($1.2 \text{ mL}\cdot\text{g}^{-1}$ of fibres) at 70°C for 3 h for the bleaching process. 30 g of sodium hypochlorite were added every hour to the mixture, for a total of 3 times. The mixture was kept reacting at 70°C for 15h. The final product was collected and centrifuged at 5000 rpm for 5 minutes. It was then repeatedly rinsed with distilled water until it reached a pH of 8, then dried for a whole night at 60°C .

Microcrystalline cellulose (MCC) preparation. MCC was produced employing an acid hydrolysis by HCl/H₂SO₄ (2:1, v/v), with a ratio of $20 \text{ mL}\cdot\text{g}^{-1}$. 1.6 g of cellulose obtained after bleaching were repulped under magnetic stirring in 26 mL of warm distilled water and with the help of ultrasonication. Then the acid mixture was added and kept reacting for 30 min at 100 C.

100 mL of distilled water were added in order to stop the reaction. The mixture was then centrifuged at 5000 rpm for five minutes, rinsed with distilled water until the pH is neutral, and dried in an oven at 60°C for 24 hours [4].

6.3.2.3 MCC functionalization with HNT (MCC_GPTMS_HNT)

MCC was functionalized by a reported procedure with some modifications employing GPTMS alkoxy silane precursor to be crosslinked to HNT (Figure 6.5) [5,6].

In particular, 100 mg of MCC were dispersed in 6 mL of an EtOH/H₂O (7:1 v/v) at pH 3 (1 droplet of HCl is added) and sonicated for 15 minutes. Then in another flask 100 mg of HNT were dispersed in 6 mL EtOH/H₂O (7:1 v/v) at pH 3 (1 droplet of HCl is added) and 200 mg of GPTMS were added.

The two solutions were combined and reflux-reacting for two hours while being magnetically stirred. The product was centrifuged for five minutes at 5000 rpm, rinsed many times in distilled water, and dried for two days at 60 °C.

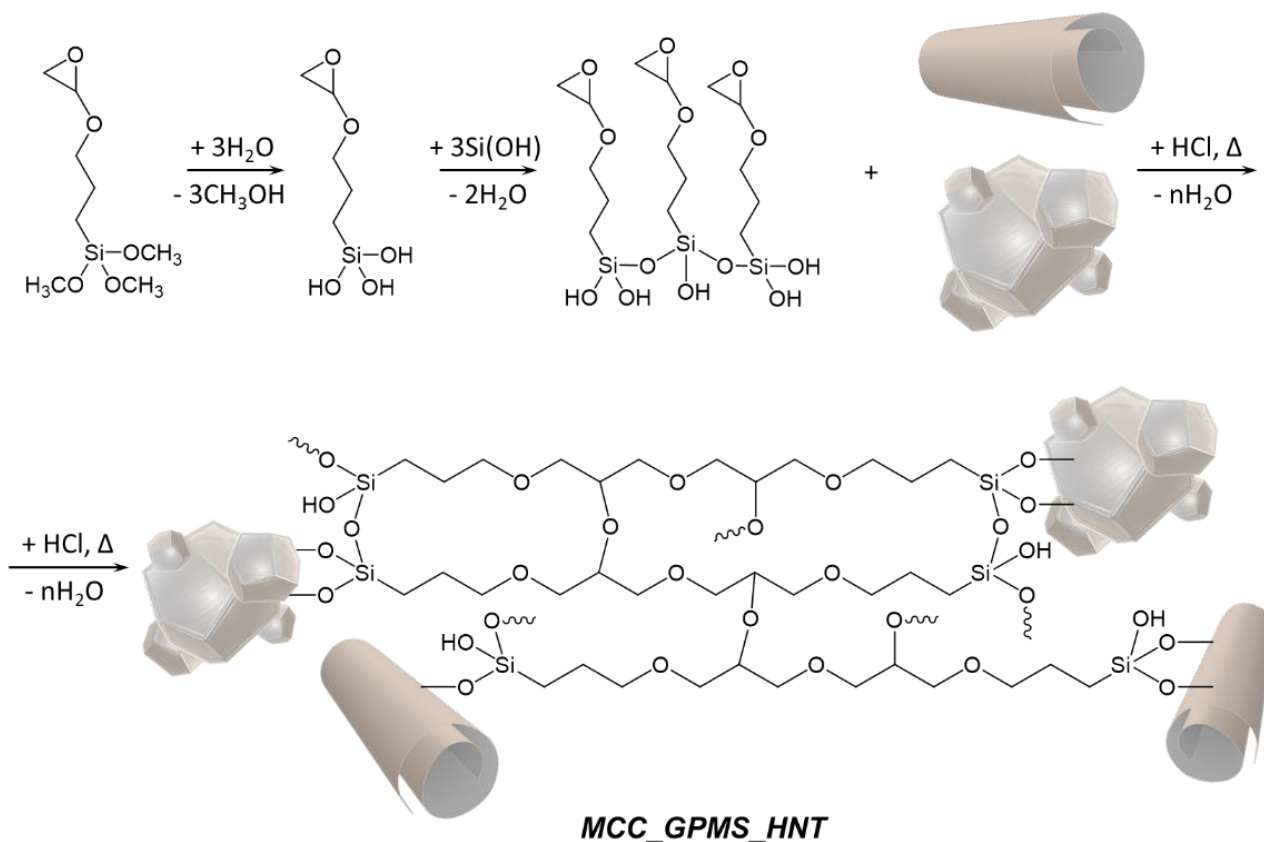


Figure 6.5. Graphical representation of the synthesis of MCC_GPTMS_HNT hybrid derivative.

6.3.2.4 Halloysite functionalization with (3-Mercaptopropyl)trimethoxysilane (HNT_SH)

A mixture of 2g of HNT, 200 mL of water, and 2g of (3-Mercaptopropyl)trimethoxysilane was kept at reflux for 24 hours to obtain the HNT_SH derivative. The product was centrifuged at 5000 rpm for five minutes, rinsed many times with distilled water, and dried at 60 °C for two days. [7].

6.3.2.5 MCC functionalization with HNT_SH (MCC_GPTMS_SH_HNT)

In order to obtain the MCC_GPTMS_SH_HNT derivative (Figure 6.6), 100 mg of MCC were dispersed in 12 mL of a EtOH/H₂O (7:1 v/v) solution with a pH of 3 and sonicated for 15 minutes.

The dispersion was then supplemented with 200 mg of GPTMS and refluxed for 30 minutes (under magnetic stirring).

100 mg of HNT_SH were then added to the mixture allowing to react at reflux for an additional 3 hours.

The product was centrifuged at 5000 rpm for five minutes, rinsed many times in distilled water, and dried at 60 °C for two days.

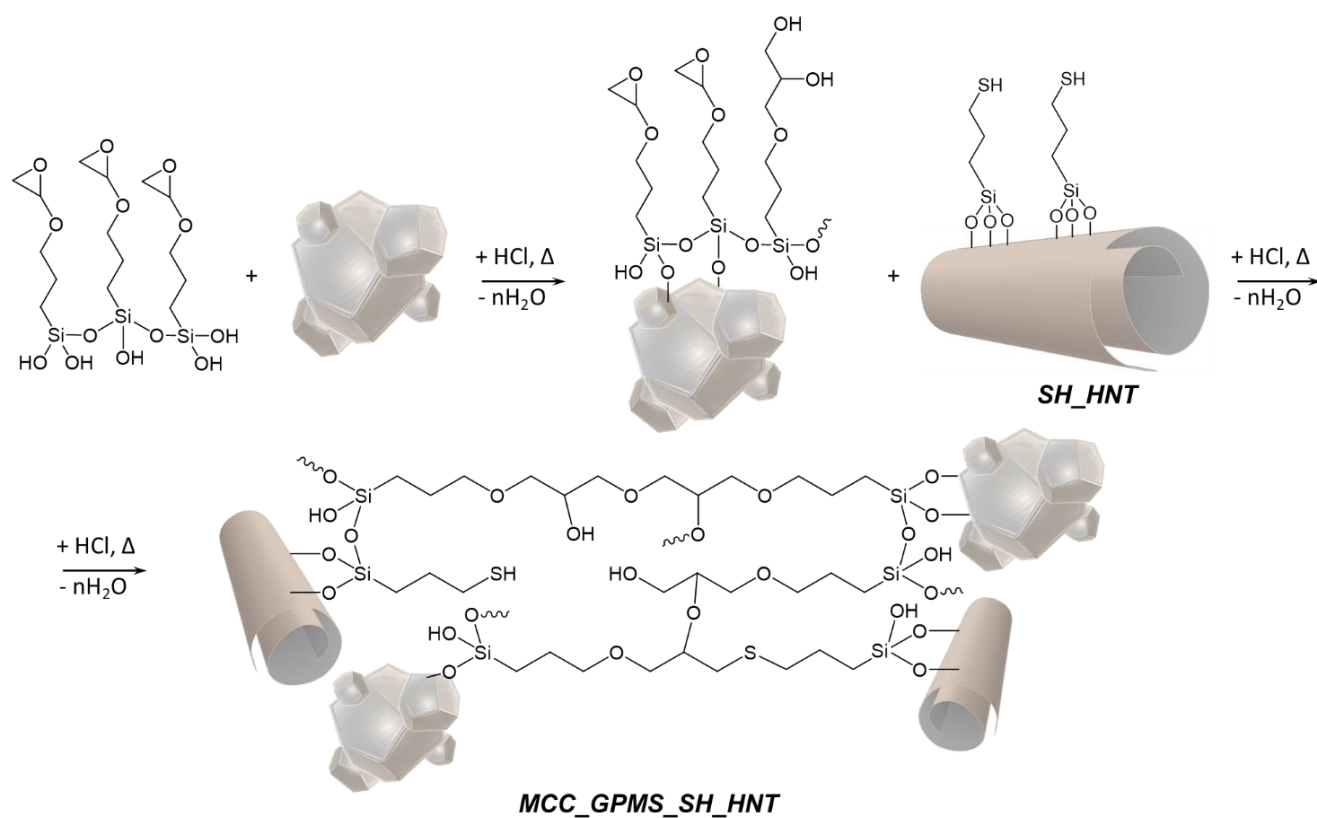


Figure 6.6. Graphical representation of the synthesis of MCC_GPTMS_SH_HNT hybrid derivative.

6.3.2.6 MCC functionalization with B-CD (MCC_CA_B-CD)

MCC_CA_B-CD system was obtained following some adapted literature approaches [8–11] (Figure 6.7).

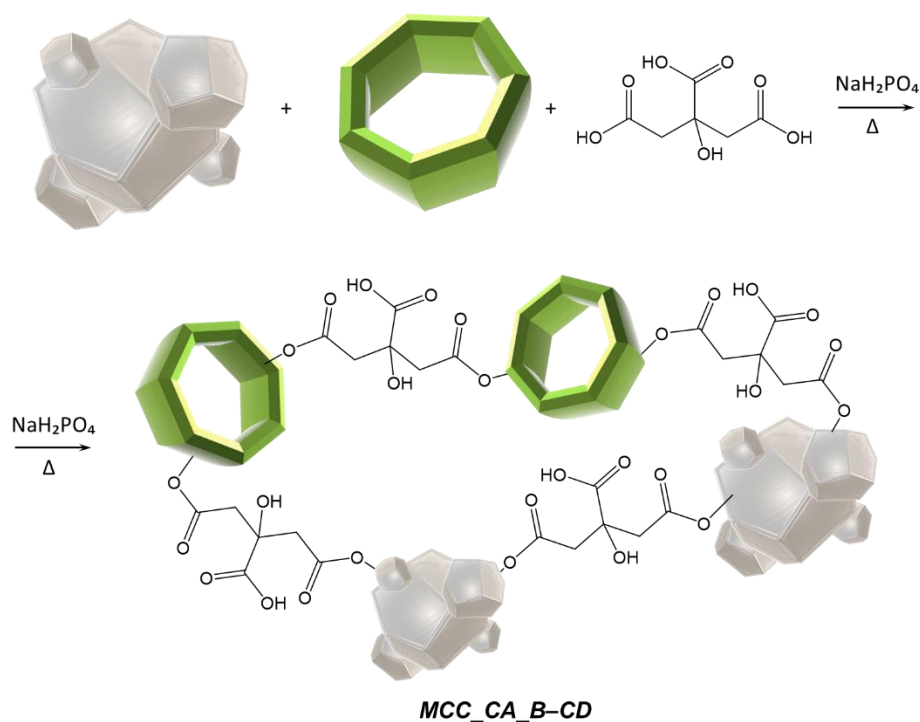


Figure 6.7. Graphical representation of the synthesis of MCC_CA_B-CD derivative.

Specifically, 5 mL of distilled water were combined with 100 mg of MCC, ultrasonicated for 15 minutes, and added with 100 mg of β -CD, 100 mg of citric acid, and 60 mg of sodium dihydrogen phosphate monohydrate.

50 mL of isopropanol were added after letting the mixture react for two hours at 80°C. The suspension was centrifuged at 5000 rpm for five minutes before being twice rinsed with distilled water and once with isopropanol.

The resulting powder was dried for 24 hours at 60°C.

6.3.2.7 Biochar preparation from spanish broom straws (Bch)

Spanish broom straws were pyrolyzed at 400°C for 2 h to produce the biochar (Bch) according some studies performed on other natural vegetable derived product [12]. 3.43 g of biochar were obtained from 10 g of straws.

6.3.2.8 Biochar modification with NZVI nanoparticles (Bch_NZVI)

A liquid-phase chemical reduction approach using some modified literature methodologies [13,14] was used to produce biochar-supported nano zero-valent iron composite (Figure 6.8). In specifically, 200mL of a 1/4 v/v ethanol/water solution were mixed with 3 g of PEG as a surfactant, and the mixture degassed under nitrogen and magnetic stirring for 30 minutes. Then 3 g of FeCl_3 were added into the mixture under the protection of nitrogen, and kept mixing for 30 min. After that 2 g of biochar were added. 100 mL of $1 \text{ mol}\cdot\text{L}^{-1}$ NaBH_4 EtOH solution, were put in the mixture drop by drop (with a speed of 1 drop per second) under nitrogen atmosphere and vigorous stirring. The mixture was stirred for a further 30 minutes under nitrogen and then filtered once the NaBH_4 solution has been entirely consumed. The resultant black solid was collected by centrifugation at 2000 rpm and repeatedly rinsed with water and EtOH.

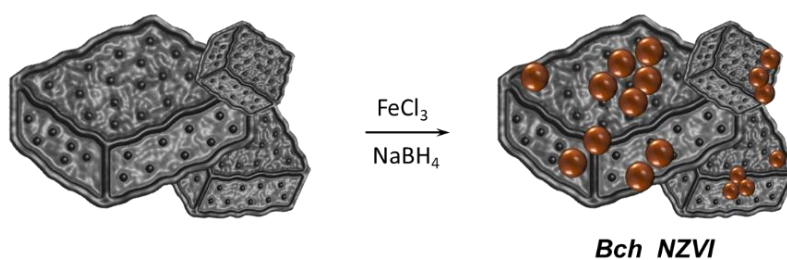


Figure 6.8. Graphical representation of the synthesis of Bch_NZVI derivative.

6.3.3. Chemical-physical measurement and characterization

The chemical structure of the developed additives was determined using Fourier transform infrared analysis (ATR FT-IR). FT-IR spectra were collected using a V-6600 Jasco Spectrometer (JASCO Europe s.r.l., Cremella, LC, Italy), equipped with the Spectra Manager™ Suite with integrated search software solution, KnowItAll® Informatics, and database JASCO Edition (JASCO Europe s.r.l., Cremella, LC, Italy). Spectra were acquired at RT at a resolution of 4 cm^{-1} , employing a total of 32 scans per data set, and a range of $4000\text{-}500 \text{ cm}^{-1}$.

Their morphology was investigated by a FEI Quanta 200 F SEM (Hillsboro, Oregon, USA) at an accelerating voltage of 20 kV.

The method described by Hoang et al. [16] was used to calculate the swelling degree of PVA electrospun nanofiber composite membranes both before and after heat treatment. The samples were first cut into small pieces (2 × 2 cm) and dried at 70 °C for 24 hours before being weighed on an analytical balance (Orma Scientific, Italy) with a precision of 0,0001 g to determine the original weight of the sample (m_i). The dried samples were then submerged for 24 hours in Milli-Q water at room temperature (25 °C). The wet membranes were weighted after being cleaned of extra water using cotton tissue paper (m_f). The specimen swelling was assessed using the following equation 3:

$$\text{Swelling degree (\%)} = \frac{m_f - m_i}{m_i} \times 100 \quad (3)$$

The mass loss after 24 hours was measured and represented as a percentage of the initial specimen mass (see equation 4) after drying the samples at 70 °C for 24 hours following the swelling test.

$$\text{Mass loss (\%)} = \frac{m_i - m_f}{m_f} \times 100 \quad (4)$$

An FEI Phenom XL tabletop SEM (Thermo Fisher Scientific, Massachusetts, United States) was used to investigate all composite electrospun nanofiber membranes at a 15 kV accelerating voltage. A sputter coater (LOT-Quantum Design) was used to coat the samples with gold prior to examination. The nanofiber diameters were measured using the programme Phenom FiberMetric. The average diameters and their standard deviations, which were denoted as $\sigma/2$, were based on at least 200 measurements per sample.

A DMA Q800 (TA Instruments, New Castle, United States) was used to study the mechanical tensile characteristics of the electrospun composite membranes. Three measurements were taken for each specimen at a strain rate of 1% min⁻¹ (gauge length of about ~1 cm and length of ~0.5 cm). The thickness of the samples was measured using a very accurate digital coating thickness gauge.

6.3.4. Filtration studies

A dead-end filtration cell was used to assess the filtration performance of the electrospun nanofiber composite membranes (Amicon Stirred Cell 200mL, Merck KGaA, Darmstadt, Germany) with a filtration area of 28.7 cm². The membranes were pre-treated with 100 mL of deionized water before testing. Subsequently 5 mg·L⁻¹ of MO and MB solutions were mixed in the same ratio for a total of 50 mL and gravity filtered. Following filtering, the organic dye concentrations were evaluated using a UV-vis spectrophotometer, and the retention rate of the two tested organic dyes was calculated using equation 5:

$$\text{Retention rate} = \frac{C_f - C_p}{C_f} \times 100 \quad (5)$$

Meanwhile the separation efficiency was determined by equation 6:

$$\text{Separation efficiency} = \frac{C_{MO_f}}{C_{MO_f} + C_{MB_f}} \times 100 \quad (6)$$

where C_f is the concentration of feed, and C_p is the concentration of permeate.

UV-Vis spectroscopy measurements were carried out at 25°C using a Jasco V-770 UV-Vis spectrophotometer (JASCO Europe s.r.l., Cremella, LC, Italy) equipped with standard measurement and analysis programs and the Spectra Manager™ Suite Spectroscopy Software (JASCO Europe s.r.l., Cremella, Italy).

6.3.5. Adsorption isotherm calculations

Removal efficiencies (%) of MB by the Bch_NZVI nanocomposite were calculated by the Equation 7:

$$\% = \frac{(C_0 - C_t)}{C_0} \times 100\% \quad (7)$$

where $C_0/\text{mg}\cdot\text{L}^{-1}$ and $C_t/\text{mg}\cdot\text{L}^{-1}$ are the dye concentrations at initial time and time t .

Sorption capacity ($q_t/\text{mg}\cdot\text{g}^{-1}$) was determined according to the Equation 8:

$$q_t = \frac{(C_0 - C_t)V}{W} \quad (8)$$

Adsorption isotherms were calculated from the graph of the adsorption capacity at the equilibrium ($q_e/\text{mg}\cdot\text{g}^{-1}$) vs the equilibrium dye concentration ($C_e/\text{mg}\cdot\text{L}^{-1}$).

In order to choose the model that fits the data the most accurately, regression coefficients (R^2) for all the various model types have been analysed.

Langmuir calculation (Equation 9) [17,18]:

$$q_e = \frac{q_m k_L C_e}{1 + k_L C_e} \quad (9)$$

where $C_e/\text{mg}\cdot\text{L}^{-1}$ is the equilibrium dye concentration in the solution, $k_L/\text{L}\cdot\text{mg}^{-1}$ is the Langmuir adsorption constant, and $q_m/\text{mg}\cdot\text{g}^{-1}$ is the theoretical maximum adsorption capacity.

Freundlich calculation (Equation 10) [17,19]:

$$q_e = k_F C_e^{1/n} \quad (10)$$

where $k_F/\text{L}\cdot\text{mg}^{-1}$ and n represent the Freundlich isotherm constants indicating the capacity and intensity of the adsorption, respectively.

Temkin calculation (Equation 11) [20,21]:

$$q_e = B_T \ln(k_T C_e) \quad (11)$$

Where $B_T/\text{J}\cdot\text{mol}^{-1}$ correspond to RT/b (T is the absolute temperature in K, R the universal gas constant) and $k_T/\text{L}\cdot\text{mg}^{-1}$ is the Temkin isotherm constant related to the heat of adsorption.

6.4. Chapter 4: Experimental section

6.4.1. Materials

All materials and reagents were obtained from commercial suppliers for direct use unless mentioned. 1,4-dimethoxy benzene, paraformaldehyde, ethyl α -bromoisobutyrate (EBiB), N, N, N', N'', N''' -pentamethyldiethylenetriamine (PMDETA), ascorbic acid, hydrochloric acid, sodium hydroxide, magnesium sulphate, polyethersulfone (PES), polyvinylpyrrolidone (PVP), methyl orange, methylene blue, the solvents methanol, dimethylformamide (DMF), dichloromethane, hexane, N,N-dimethylacetamide (DMAc) and deuterated solvent CDCl_3 , were acquired at most purity grade available from Sigma Aldrich and used as received. The monomer 2-(dimethylamino)ethyl methacrylate (DMAEMA) was purchased from Sigma Aldrich, and the hydroquinone monomethyl ether inhibitor was eliminated by passing it down a basic alumina column. When practicable, thin layer chromatography on silica gel plates with fluorescence indicator was used to monitor the synthesis processes. Chromophores were detected by UV light ($\lambda = 254 \text{ nm}$) or by treating the samples with acid dodeca-phosphomolybdic in ethanolic solution (5% w/v). The synthesis products were purified using column chromatography with 230–400 mesh silica gel as the stationary phase.

6.4.2. Synthetic procedures

6.4.2.1 *Synthesis of P5-Br*

The pillar[5]arene derivative was synthesized according to a literature method [22].

1,4-dimethoxy benzene (1.67 g, 12.1 mmol), paraformaldehyde (0.44 g, 14.6 mmol), 1-(2-bromoethoxy)-4-methoxy benzene (0.7 g, 3.0 mmol) and $[\text{BF}_3 \cdot \text{O}(\text{C}_2\text{H}_5)_2]$ (1.9 mL, 15.3 mmol) were mixed in 1,2-dichloroethane anhydrous (50 mL) and kept under stirring in an inert atmosphere (Ar). The reaction was stopped after 3.5 h at room temperature by adding a mixture of distilled water and methanol 2:1 v/v (150 mL) and kept stirring for 2 h. A sintered glass filter was used to filter the mixture, and the solvent was then evaporated. The dried solid was solubilized in CH_2Cl_2 (100 mL), washed with distilled H_2O ($2 \times 50 \text{ mL}$), dried with MgSO_4 and finally the solvent was evaporated. The reaction crude was purified by column chromatography (eluent mixture 1:3 hexane/ CH_2Cl_2), obtaining P5-Br as a white crystalline solid (1.25 g, 1.48 mmol, 50%).

$^1\text{H NMR}$ (500 MHz, CDCl_3): δ 6.80–6.76 (m, 9H, ArH), 6.70 (s, 1H, ArH), 4.04 (t, $J = 6.0 \text{ Hz}$, 2H, OCH_2), 3.81–3.77 (m, 10H, ArCH_2Ar), 3.68–3.64 (m, 27H, CH_3), 3.44 (t, $J = 6.0 \text{ Hz}$, 2H, BrCH_2) ppm.

6.4.2.2 *Synthesis of PDMAEMA*

Poly[2-(dimethylamino)ethyl methacrylate] (PDMAEMA) was synthesized by an ARGET-ATRP according to methods described by Willott et al. [23] and Keating et al. [24]

CuBr_2 (2.65 mg, 0.012 mmol), DMAEMA (5 mL, 30 mmol), PMDETA (25 μL , 0.12 mmol), EBiB (17 μL , 0.023 g, 0.12 mmol) and ascorbic acid (20.90 mg, 0.12 mmol) were added in chronological order to a degassed solution of methanol/ H_2O 9:1 v/v. The final ratio DMAEMA/ CuBr_2 /PMDETA /Ascorbic acid/EBiB was 2500:1:10:10:10 and DMAEMA/solvent ratio 1:1 v/v.

The reaction was left for 20 h at thermostatic bath at 35 °C under inert atmosphere (Ar). The reaction mixture was poured in H₂O at boiling temperature (150 mL), the precipitate recovered and dried under vacuum at 40 °C for 2 h. The solid product was dissolved in HCl (200 mL, 1 M) and precipitated with NaOH (150 mL, 2 M). The obtained precipitate was recovered and dissolved in CH₂Cl₂ (100 mL), the organic phase was washed with distilled water (3 × 20 mL), dried with MgSO₄ and finally the solvent was evaporated.

The obtained polymer was dissolved in CH₂Cl₂ (100 mL) and precipitated by adding hexane (80 mL). After eliminating the solvent, the polymer was washed with hexane and dried under vacuum at 40 °C for 2 h obtaining a transparent rubbery solid (3 g), stored at 4 °C.

¹H NMR (500 MHz, CDCl₃): δ 4.09 (br, 2H, CH₂OC=O), 2.62 (br, 2H, NCH₂), 2.32 (s, 6H, N(CH₃)₂), 1.84 (br, 2H, CH₂), 1.26 (s, CCH₃), 1.05–0.91 (br, 3H, CH₃) ppm.

6.4.2.3 Synthesis of P5-QPDMAEMA

PDMAEMA (100 mg) and P5-Br (257 mg, 0.3 mmol) were poured in DMF (5 mL) and keep reacting under stirring at 50 °C for 10 days. Subsequently CH₂Cl₂ (2 mL) and hexane (4 mL) were added to the reaction mixture and keep stirring until the formation of a precipitate.

The product was separated from the solvent and dried under vacuum obtaining a transparent glassy like product (243 mg).

¹H NMR (500 MHz, CDCl₃): δ 6.84–6.51 (m, 10H, ArH), 4.06 (br, 2H, CH₂OC=O), 4.06 (br, 2H, OCH₂), 3.75 (br, 10H, ArCH₂Ar), 3.63–3.49 (br, 27H, CH₃), 3.38 (br, 2H, BrCH₂), 2.58 (br, 2H, NCH₂), 2.28 (s, 6H, N(CH₃)₂), 1.88 (br, 2H, CH₂), 1.24 (s, CCH₃), 1.04–0.87 (br, 3H, CH₃) ppm.

6.4.3. Beads preparation

Polyethersulfone blends were prepared by mixing the polymers with a specific ratio (w/w) using DMAc as solvent and stirring for 12 h at RT. The casting solutions were subjected to an ultrasonic bath for 30 minutes before to the manufacture of the beads in order to eliminate bubbles.

The beads were prepared at various coagulation pH, thanks to a traditional non-solvent induced phase separation (NIPS) process. A 1 cc syringe (G26, 0.45 mm × 12 mm) and a 1.20 × 40 mm (18G × 1 1/2") needle, were placed at a distance of 5 cm from the coagulation bath. Three coagulation baths were used: i) HCl (50 mL, 0.5 M), ii) H₂O (50 mL), NaOH (50 mL, 0.5 M). Beads were left for 2 h in the coagulation baths and subsequently removed and left for 12 h in a H₂O bath (100 mL). After the coagulation beads were abundantly washed with H₂O and ethanol and dried at 50 °C for 24 h.

The post functionalization of B-P(b) and B-P5QP(b) beads was performed by the immersion of ≈145 mg of each kind of bead in 8 mL of MeOH with 0.8 g of 1,4-butansultone and keeping stirring at 40 °C for 24 h. The beads were subsequently washed with distilled water and ethanol and dried at 50 °C for 24h. The functionalization percentage was calculated gravimetrically with the Equation 12 [25]:

$$\text{Functionalization percentage \%} = \frac{W_f - W_i}{W_i} \times 100 \quad (12)$$

where W_f /mg is the final weight and W_i /mg is the initial weight.

6.4.4. Chemical-physical measurement and characterization

^1H NMR spectra were acquired at a temperature of 293 °K using a Varian 500 MHz spectrometer. The chemical shifts (δ) were reported in ppm with respect to the residual protiated signal of the solvent, while the values of the coupling constants (J) were reported in Hz.

Fourier transform infrared analysis (ATR-FT-IR) were acquired directly on a whole bead by using a V-6600 Jasco Spectrometer (JASCO Europe s.r.l., Cremella, LC, Italy), equipped with an attenuated Total Reflection accessory, including the Spectra Manager™ Suite with integrated search software solution, KnowItAll® Informatics and database JASCO Edition (JASCO Europe s.r.l., Cremella, LC, Italy). Spectra were recorded at room temperature, in the range of 4000–500 cm^{-1} acquiring 32 scans per data set with a resolution of 4 cm^{-1} .

UV-Vis spectroscopy measurements were performed at ~25 °C with a Jasco V-770 (JASCO Europe s.r.l., Cremella, LC, Italy) UV-Vis spectrophotometer equipped with standard measurement and analysis programs and the Spectra Manager™ Suite Spectroscopy Software (JASCO Europe s.r.l., Cremella, Italy).

A Hitachi S4000 SEM was employed for the morphology study of the beads operating at 15 kV. Beads were carefully sliced with a sharp scalpel to expose their cross-section. Thin slices were mounted onto an aluminium stub (PELCO) and metallized with a $\approx 10\text{nm}$ -thick 99.999% Au (Sigma-Aldrich) layer by means of a sputter coater (Quorum QR150R).

X-ray Photoelectron Spectroscopy (XPS) measurements, were performed using an ESCALAB 250Xi (Thermo Fisher Scientific Ltd., East Grinstead, UK) spectrometer, equipped with a monochromatized Al $K\alpha$ source ($h\nu = 1486.6 \text{ eV}$) and 6-channeltron as detection system. The tests were carried out with the constant pass energy (40 eV). The charge neutralization of the insulator samples was guaranteed by an electron flood gun during the measurements, operating at large spot area compensation mode. All spectra were registered and processed with Thermo Avatange software v5.979 (Thermo Fisher Scientific Ltd., East Grinstead, UK).

6.4.5. Adsorption kinetic studies and isotherm calculations

Calibration curves and adsorption measurements of MB and MO were obtained using a UV-Vis V-770, Jasco spectrophotometer (JASCO Europe s.r.l., Cremella, LC, Italy) at ~25°C. The concentration of MB was determined at $\lambda/\text{nm} = 664$, and MO at $\lambda/\text{nm} = 464$.

Removal efficiencies (%) of MB and MO by the different beads were calculated by the Equation 7.

Adsorption capacity ($q_t/\text{mg}\cdot\text{g}^{-1}$) was determined according to the Equation 8.

where $C_0/\text{mg}\cdot\text{L}^{-1}$ and $C_t/\text{mg}\cdot\text{L}^{-1}$ are the dye concentrations at initial time and time t ; V/L is the solution volume and W/g is the adsorbent mass.

In Figure 4.15–4.17 interpolate lines between experimental data points are qualitative and shown only to better visualize the process trend.

B-P5QP(a) bead ($\approx 20 \text{ mg}$) and $20 \text{ mg}\cdot\text{L}^{-1}$ MO solution (20 mL) was employed for the kinetic study. After each time interval, a portion of solution was taken out, the absorbance measured with the UV-Vis spectrophotometer at $\lambda/\text{nm} = 464$, ~25°C.

All the parameters were calculated from the graph of the adsorption capacity at time t ($q_t/\text{mg}\cdot\text{g}^{-1}$) vs. t/min .

Coefficients of regression (R^2) of all the different types of models have been evaluated and assessed to determine the best fit of the appropriate model.

For the pseudo-first order calculation the following equation 13 was employed [26,27]:

$$q_t = q_e(1 - e^{-k_1 t}) \quad (13)$$

where t/min is the contact time, $q_t/\text{mg}\cdot\text{g}^{-1}$ is the adsorption capacity at time t , $q_e/\text{mg}\cdot\text{g}^{-1}$ the adsorption at equilibrium, k_1/min^{-1} is the adsorption rate constants of pseudo-first order adsorption model.

For the pseudo-second order calculation the following Equation 14 was employed [26]:

$$q_t = \frac{q_e^2 k_2 t}{1 + q_e k_2 t} \quad (14)$$

where t/min is the contact time, $q_t/\text{mg}\cdot\text{g}^{-1}$ is the adsorption capacity at time t , $q_e/\text{mg}\cdot\text{g}^{-1}$ the adsorption capacity at equilibrium, $k_2/\text{g}\cdot\text{mg}^{-1}\cdot\text{min}^{-1}$ is the adsorption rate constants of pseudo-second-order adsorption model.

For the intraparticle diffusion calculation the following Equation 15 was employed [28,29]:

$$q_t = k_{diff} t^{1/2} + C \quad (15)$$

where t/min is the contact time, $q_t/\text{mg}\cdot\text{g}^{-1}$ is the adsorption capacity at time t , $k_{diff}/\text{mg}\cdot\text{g}^{-1}\cdot\text{min}^{-0.5}$ is the adsorption rate constants of intraparticle diffusion adsorption model and C is a constant.

For the Elovic calculation the following Equation 16 was employed [30,31]:

$$q_t = \frac{1}{\beta} \ln(\alpha\beta t + 1) \quad (16)$$

where t/min is the contact time, $q_t/\text{mg}\cdot\text{g}^{-1}$ is the adsorption capacity at time t , $\alpha/\text{mg}\cdot\text{g}^{-1}\cdot\text{min}^{-1}$ is the rate of adsorption, $\beta/\text{g}\cdot\text{mg}^{-1}$ is the desorption constant.

B-P5QP (a) beads (≈ 20 mg) and 20, 40, 80, 150 and 300 $\text{mg}\cdot\text{L}^{-1}$ MO solutions (10 mL) were employed for the adsorption isotherm study. A portion of solution was taken out after a contact time of 5h and the absorbance measured with the UV-Vis spectrophotometer at $\lambda/\text{nm} = 464$ ($T = 25$ °C).

All the parameters were calculated from the graph of the adsorption capacity at the equilibrium ($q_e/\text{mg}\cdot\text{g}^{-1}$) vs the equilibrium dye concentration $C_e/\text{mg}\cdot\text{L}^{-1}$.

Coefficients of regression (R^2) of all the different types of models have been evaluated and assessed to determine the best fit of the appropriate model.

The following adsorption isotherm models were evaluated:

- Langmuir model, Equation 7;
- Freundlich model, Equation 8;
- Temkin model, Equation 9.

References

1. Krishnaiah, P.; Ratnam, C.T.; Manickam, S. Development of Silane Grafted Halloysite Nanotube Reinforced Polylactide Nanocomposites for the Enhancement of Mechanical, Thermal and Dynamic-Mechanical Properties. *Appl. Clay Sci.* **2017**, *135*, 583–595, doi:<https://doi.org/10.1016/j.clay.2016.10.046>.
2. Yah, W.O.; Takahara, A.; Lvov, Y.M. Selective Modification of Halloysite Lumen with Octadecylphosphonic Acid: New Inorganic Tubular Micelle. *J. Am. Chem. Soc.* **2012**, *134*, 1853–1859, doi:[10.1021/ja210258y](https://doi.org/10.1021/ja210258y).
3. Couret, L.; Irle, M.; Belloncle, C.; Cathala, B. Extraction and Characterization of Cellulose Nanocrystals from Post-Consumer Wood Fiberboard Waste. *Cellulose* **2017**, *24*, 2125–2137, doi:[10.1007/s10570-017-1252-7](https://doi.org/10.1007/s10570-017-1252-7).
4. Tarchoun, A.F.; Trache, D.; Klapötke, T.M.; Derradji, M.; Bessa, W. Ecofriendly Isolation and Characterization of Microcrystalline Cellulose from Giant Reed Using Various Acidic Media. *Cellulose* **2019**, *26*, 7635–7651, doi:[10.1007/s10570-019-02672-x](https://doi.org/10.1007/s10570-019-02672-x).
5. Tang, G.; Ren, T.; Wang, Y.; Yan, Z.; Ma, L.; Hou, X.; Huang, X. Effect of Halloysite Nanotubes on Corrosion Protection Properties of the Self-Curing Epoxy Resin Coatings. *Pigment Resin Technol.* **2022**, *51*, 397–405, doi:[10.1108/PRT-04-2021-0041](https://doi.org/10.1108/PRT-04-2021-0041).
6. Rezaei-DashtArzhandi, M.; Sarrafzadeh, M.H.; Goh, P.S.; Lau, W.J.; Ismail, A.F.; Wong, K.C.; Mohamed, M.A. Enhancing the Desalination Performance of Forward Osmosis Membrane through the Incorporation of Green Nanocrystalline Cellulose and Halloysite Dual Nanofillers. *J. Chem. Technol. Biotechnol.* **2020**, *95*, 2359–2370, doi:<https://doi.org/10.1002/jctb.6455>.
7. Jlassi, K.; Chandran, S.; Mičušík, M.; Benna-Zayani, M.; Yagci, Y.; Thomas, S.; Chehimi, M.M. Poly(Glycidyl Methacrylate)-Grafted Clay Nanofiller for Highly Transparent and Mechanically Robust Epoxy Composites. *Eur. Polym. J.* **2015**, *72*, 89–101, doi:<https://doi.org/10.1016/j.eurpolymj.2015.09.004>.
8. Pirouzmand, M.; Sani, P.S.; Ghasemi, Z.; Azizi, S. Citric Acid-Crosslinked β -Cyclodextrin Supported Zinc Peroxide as a Biocompatible H₂O₂ Scavenger. *JBCJ. Biol. Inorg. Chem.* **2020**, *25*, 411–417, doi:[10.1007/s00775-020-01771-6](https://doi.org/10.1007/s00775-020-01771-6).
9. Jayaprabha, K.N.; Joy, P.A. Citrate Modified β -Cyclodextrin Functionalized Magnetite Nanoparticles: A Biocompatible Platform for Hydrophobic Drug Delivery. *RSC Adv.* **2015**, *5*, 22117–22125, doi:[10.1039/C4RA16044D](https://doi.org/10.1039/C4RA16044D).
10. Li, W.; Liu, H.; Li, L.; Liu, K.; Liu, J.; Tang, T.; Jiang, W. Green Synthesis of Citric Acid-Crosslinked β -Cyclodextrin for Highly Efficient Removal of Uranium(VI) from Aqueous Solution. *J. Radioanal. Nucl. Chem.* **2019**, *322*, 2033–2042, doi:[10.1007/s10967-019-06901-2](https://doi.org/10.1007/s10967-019-06901-2).
11. Castro, D.O.; Tabary, N.; Martel, B.; Gandini, A.; Belgacem, N.; Bras, J. Effect of Different Carboxylic Acids in Cyclodextrin Functionalization of Cellulose Nanocrystals for Prolonged Release of Carvacrol. *Mater. Sci. Eng. C* **2016**, *69*, 1018–1025, doi:<https://doi.org/10.1016/j.msec.2016.08.014>.
12. Wu, W.; Yang, M.; Feng, Q.; McGrouther, K.; Wang, H.; Lu, H.; Chen, Y. Chemical Characterization of Rice Straw-Derived Biochar for Soil Amendment. *Biomass and Bioenergy* **2012**, *47*, 268–276, doi:<https://doi.org/10.1016/j.biombioe.2012.09.034>.
13. Yıldırım, G.M.; Bayrak, B. The Synthesis of Biochar-Supported Nano Zero-Valent Iron Composite and Its Adsorption Performance in Removal of Malachite Green. *Biomass Convers. Biorefinery* **2022**, *12*, 4785–4797, doi:[10.1007/s13399-021-01501-1](https://doi.org/10.1007/s13399-021-01501-1).
14. Wu, H.; Wei, W.; Xu, C.; Meng, Y.; Bai, W.; Yang, W.; Lin, A. Polyethylene Glycol-Stabilized Nano Zero-Valent Iron Supported by Biochar for Highly Efficient Removal of Cr(VI). *Ecotoxicol. Environ. Saf.* **2020**, *188*, 109902, doi:<https://doi.org/10.1016/j.ecoenv.2019.109902>.
15. MirafTAB, M.; Saifullah, A.N.; Çay, A. Physical Stabilisation of Electrospun Poly(Vinyl Alcohol) Nanofibres: Comparative Study on Methanol and Heat-Based Crosslinking. *J. Mater. Sci.* **2015**, *50*, 1943–1957, doi:[10.1007/s10853-014-8759-1](https://doi.org/10.1007/s10853-014-8759-1).
16. Hoang, B.N.; Nguyen, T.T.; Bui, Q.P.T.; Bach, L.G.; Vo, D.-V.N.; Trinh, C.D.; Bui, X.-T.; Nguyen, T.D. Enhanced Selective Adsorption of Cation Organic Dyes on Polyvinyl Alcohol/Agar/Maltodextrin Water-Resistance Biomembrane. *J. Appl. Polym. Sci.* **2020**, *137*, 48904, doi:<https://doi.org/10.1002/app.48904>.
17. Yu, K.L.; Lee, X.J.; Ong, H.C.; Chen, W.-H.; Chang, J.-S.; Lin, C.-S.; Show, P.L.; Ling, T.C. Adsorptive Removal of Cationic Methylene Blue and Anionic Congo Red Dyes Using Wet-Torrefied Microalgal Biochar: Equilibrium, Kinetic and Mechanism Modeling. *Environ. Pollut.* **2021**, *272*, 115986, doi:<https://doi.org/10.1016/j.envpol.2020.115986>.
18. Langmuir, I. THE ADSORPTION OF GASES ON PLANE SURFACES OF GLASS, MICA AND PLATINUM. *J. Am. Chem. Soc.* **1918**, *40*, 1361–1403, doi:[10.1021/ja02242a004](https://doi.org/10.1021/ja02242a004).
19. Freundlich, H.M.F. Over the Adsorption in Solution. *J. Phys. Chem.* **1906**, *57*, 1100–1107.
20. Başar, C.A. Applicability of the Various Adsorption Models of Three Dyes Adsorption onto Activated Carbon Prepared Waste Apricot. *J. Hazard. Mater.* **2006**, *135*, 232–241, doi:<https://doi.org/10.1016/j.jhazmat.2005.11.055>.
21. Temkin, M.I. Kinetics of Ammonia Synthesis on Promoted Iron Catalysts. *Acta physiochim. URSS* **1940**, *12*, 327–356.
22. Zhou, Y.; Zhang, G.; Li, B.; Wu, L. Two-Dimensional Supramolecular Ionic Frameworks for Precise Membrane Separation

- of Small Nanoparticles. *ACS Appl. Mater. Interfaces* **2020**, *12*, 30761–30769, doi:10.1021/acsami.0c05947.
23. Willott, J.D.; Humphreys, B.A.; Murdoch, T.J.; Edmondson, S.; Webber, G.B.; Wanless, E.J. Hydrophobic Effects within the Dynamic PH-Response of Polybasic Tertiary Amine Methacrylate Brushes. *Phys. Chem. Chem. Phys.* **2015**, *17*, 3880–3890, doi:10.1039/C4CP05292G.
 24. Keating IV, J.J.; Lee, A.; Belfort, G. Predictive Tool for Design and Analysis of ARGET ATRP Grafting Reactions. *Macromolecules* **2017**, *50*, 7930–7939, doi:10.1021/acs.macromol.7b01572.
 25. Costamagna, V.; Wunderlin, D.; Larrañaga, M.; Mondragon, I.; Strumia, M. Surface Functionalization of Polyolefin Films via the Ultraviolet-Induced Photografting of Acrylic Acid: Topographical Characterization and Ability for Binding Antifungal Agents. *J. Appl. Polym. Sci.* **2006**, *102*, 2254–2263, doi:https://doi.org/10.1002/app.24165.
 26. Moussout, H.; Ahlafi, H.; Aazza, M.; Maghat, H. Critical of Linear and Nonlinear Equations of Pseudo-First Order and Pseudo-Second Order Kinetic Models. *Karbala Int. J. Mod. Sci.* **2018**, *4*, 244–254, doi:https://doi.org/10.1016/j.kijoms.2018.04.001.
 27. Lagergren, S.K. About the Theory of So-Called Adsorption of Soluble Substances. *Sven. Vetenskapskad. Handlingar* **1898**, *24*, 1–39.
 28. Jasper, E.E.; Ajibola, V.O.; Onwuka, J.C. Nonlinear Regression Analysis of the Sorption of Crystal Violet and Methylene Blue from Aqueous Solutions onto an Agro-Waste Derived Activated Carbon. *Appl. Water Sci.* **2020**, *10*, 132, doi:10.1007/s13201-020-01218-y.
 29. Weber Jr, W.J.; Morris, J.C. Kinetics of Adsorption on Carbon from Solution. *J. Sanit. Eng. Div.* **1963**, *89*, 31–59.
 30. López-Luna, J.; Ramírez-Montes, L.E.; Martínez-Vargas, S.; Martínez, A.I.; Mijangos-Ricardez, O.F.; González-Chávez, M. del C.A.; Carrillo-González, R.; Solís-Domínguez, F.A.; Cuevas-Díaz, M. del C.; Vázquez-Hipólito, V. Linear and Nonlinear Kinetic and Isotherm Adsorption Models for Arsenic Removal by Manganese Ferrite Nanoparticles. *SN Appl. Sci.* **2019**, *1*, 950, doi:10.1007/s42452-019-0977-3.
 31. Roginsky, S.; Zeldovich, Y.B. The Catalytic Oxidation of Carbon Monoxide on Manganese Dioxide. *Acta Phys. Chem. USSR* **1934**, *1*, 2019.

GLOSSARY

PDMAEMA	Poly[2-(dimethylamino)ethylmethacrylate]
P ₅	Pillar[5]arene
PES	Polyethersulfone
PVP	Polyvinylpyrrolidone
DMAc	Dimethylacetamide
NIPS	Non-solvent induced phase separation
HNT	Halloysite nanotube
PA ₁₁	Polyamide 11
Chi	Chitosan
PVA	Polyvinyl alcohol
PE	Polyester
APTES/NH ₂	(3-aminopropyl)triethoxysilane
GPTMS	(3-glycidyloxypropyl)trimethoxysilane
MPTES	(3-mercaptopropyl)trimethoxysilane
C8-C ₁₀	Octyl/decyl glycidyl ether
C ₁₂ -C ₁₄	Dodecyl and tetradecyl glycidyl ethers
N+C ₁₈ /N+_C ₁₈	Dimethyloctadecyl[3(trimethoxysilyl)propyl]ammoniumchloride
ENM	Electrospun nanofiber membrane
MMM	Mixed-matrix membrane
MCC	Microcrystalline cellulose
Bch	Biochar
NZVI	Nano zero-valent iron
B-CD	β-cyclodextrin
CA	Citric Acid
MO	Methyl orange
MB	Methylene blue
UV-Vis	Ultraviolet-Visible (UV-vis) Spectroscopy
WCA	Water contact Angle
ATR	Attenuated Total Reflection
FT-IR	Fourier-Transform Infrared Spectroscopy
SEM	Scanning Electron Microscope
XRD	X-Ray diffraction
XPS	X-ray photoelectron spectroscopy
NMR	Nuclear magnetic resonance
DOSY	Diffusion Ordered Spectroscopy
DMA	Dynamic mechanical analysis
DSC	Differential scanning calorimetry

La borsa di dottorato è stata cofinanziata con risorse del
Programma Operativo Nazionale Ricerca e Innovazione 2014-2020 (CCI 2014IT16M2OP005),
Fondo Sociale Europeo, Azione I.1 “Dottorati Innovativi con caratterizzazione Industriale”



UNIONE EUROPEA
Fondo Sociale Europeo

